An empirical calibration of the serpentine-water oxygen isotope fractionation at *T* = 25 to 100 °C

Maria Rosa Scicchitano[a,b,*], Juan Carlos de Obeso[c,1], Tyler B. Blum[b], John W. Valley[b], Peter B. Kelemen[d], William O. Nachlas[b], William Schneider[b], Michael J. Spicuzza[b], Franziska D.H. Wilke[a], Vladimir Roddatis[a]

[a]Deutsches GeoForschungsZentrum GFZ, Potsdam, D14473 Germany (maria.rosa.scicchitano@gfz-potsdam.de, fwilke@gfz-potsdam.de, vladimir.roddatis@gfz-potsdam.de)

[b]Department of Geoscience, University of Wisconsin, Madison, WI, 53706 USA (tbblum@wisc.edu, valley@geology.wisc.edu, nachlas@wisc.edu, wfschneider@wisc.edu, spicuzza@geology.wisc.edu)

[c]Department of Geoscience, University of Calgary, Calgary, T2N 1N4 Canada (JuanCarlos.deObeso@ucalgary.ca)

[d]Lamont-Doherty Earth Observatory, Columbia University, Palisades, NY, 10964 USA (peterk@ldeo.columbia.edu)

* Corresponding author. E-mail: maria.rosa.scicchitano@gfz-potsdam.de

[1] Present address: Department of Geology and Geophysics, University of Utah, Salt Lake City, UT, 84112 USA (juancarlos.deobeso@utah.edu)

Final Published Paper:

Scicchitano MR, de Obeso JC, Blum TB, Valley JW, Kelemen PB, Nachlas WO, Schneider W, Spicuzza MJ, Wilke FDH, Roddatis V (2023) An empirical calibration of the serpentine-water oxygen isotope fractionation at T = 25–100 C. Geochim Cosmochim Acta. 346:192-206.

Keywords: oxygen isotopes, equilibrium isotope fractionation, serpentine, Oman, SIMS

Abstract

The ability to precisely constrain the physical-chemical conditions of serpentinization, such as temperature and fluid source, is limited by the accuracy of calibrations for oxygen isotope fractionation between serpentine and water – i.e., 1000 $\ln\alpha_{(serpentine-water)}$ – which disagree by up to 20 ‰ when extrapolated to $T < 200$ °C. In this study, we present a new empirical calibration of 1000 $\ln\alpha_{(serpentine-water)}$ aiming to improve applications of oxygen isotope geochemistry to very low-T serpentinization ($T < 100$ °C).

We used the high-spatial resolution capabilities of Secondary Ion Mass Spectrometry (SIMS) to analyze oxygen isotope ratios in mineral pairs of calcite + serpentine, quartz + serpentine and talc + serpentine co-crystallized at scales ≤ 50 µm in six serpentinite samples from the Samail ophiolite (Oman). SIMS analysis shows that the mineral pairs are relatively homogenous in oxygen isotope ratios with variability in $\delta^{18}O$ values ≤ 2 ‰ (2s). Clumped isotope thermometry and petrological constraints indicate crystallization temperatures from 25 to 100 °C for the investigated samples. These independent constraints on temperature allowed us to derive 1000 $\ln\alpha_{(serpentine-water)}$ by combining $\Delta^{18}O_{(quartz-serpentine)}$, $\Delta^{18}O_{(talc-serpentine)}$ and $\Delta^{18}O_{(calcite-serpentine)}$ measured by SIMS in the investigated samples with $\Delta^{18}O_{(quartz-water)}$, $\Delta^{18}O_{(talc-water)}$ and $\Delta^{18}O_{(calcite-water)}$ calibrations available in the literature. Our empirical calibration of 1000 $\ln\alpha_{(serpentine-water)} = 1.04 \pm 0.20$ (2SE) $\times 10^6/T^2$ (T in K), from T = 25 to 100 °C, is within uncertainty of former high-temperature empirical calibrations extrapolated to $T < 100$ °C and matches experimental calibrations when extrapolated to $T = 250$ °C.

The new serpentine-water calibration enables more accurate reconstructions of fluid-rock interactions occurring during low-temperature serpentinization processes in various tectonic settings.

1. Introduction

Knowledge of the temperatures and fluid sources for serpentinization is fundamental to unravel the geodynamic settings and the complex reaction and tectonic histories recorded in serpentinites (e.g., Barnes et al., 2009; 2014; Deschamps et al., 2011; 2012; Scicchitano et al., 2022). Serpentinites can form at passive margins and oceanic settings due to interaction with seawater or evolved hydrothermal fluids (e.g., Skelton and Valley, 2000; Früh-Green et al., 2003; 2004; Ludwig et al., 2006; Barnes et al., 2009; Rouméjon and Cannat, 2014; Klein et al., 2015; Rouméjon et al., 2018), as well as in the forearc and mantle wedge of subduction zones due to interaction with metamorphic fluids released by dehydration of the subducting slab (e.g., Früh-Green et al., 2001; Scambelluri et al., 2004; Deschamps et al., 2010; John et al., 2011; Padrón-Navarta et al., 2011; Lafay et al., 2013; Cannaò et al., 2015; Kelemen et al., 2022), and on continents as a result of interaction with meteoric water (e.g., Wenner and Taylor, 1973; Barnes et al., 1978; Mayhew et al., 2013; Falk et al., 2016; Schwarzenbach et al., 2016; Ellison et al., 2021; Kelemen et al., 2021; Templeton et al., 2021). Nevertheless, due to the wide stability field of serpentine and to the paucity of suitable geothermobarometers in serpentinites (e.g., Mével, 2003; Evans, 2004), estimates of the *T*-*P* conditions of serpentinization using classic metamorphic equilibria are challenging. Alternatively, the temperature dependence of the $^{18}O/^{16}O$ equilibrium fractionation between mineral and fluids, first proposed by Urey (1947), has widely been used to reconstruct *T*-fluid paths in serpentinites (e.g., Wenner and Taylor, 1971; Früh-Green et al., 1990; 1996; 2001; Barnes et al., 2009; Schwarzenbach et al., 2013; Noël et al., 2018; Rouméjon et al., 2018; Scicchitano et al., 2022).

The basis for successful stable isotope thermometry is the attainment and preservation of isotopic equilibrium during a specific event; most often, this is applied where oxygen isotope compositions are fixed in the minerals at the time of crystallization and no subsequent resetting due to recrystallization or retrograde alteration occurs (e.g., Valley, 2001). The scale at which isotopic equilibrium can be characterized depends on the complexity of the metamorphic history and resultant rock microstructures, and can be established by analytical methods used for measuring oxygen isotope ratios with exceptionally high spatial resolution. Significant improvements with secondary ion mass spectrometers (SIMS) over the past decades allow the analysis of oxygen isotope ratios in a variety of minerals at scales < 50 μm and with precision better than 0.10 ‰, 1 standard deviation (1s; see Valley and Kita, 2009; Zhang et al., 2022). Recent SIMS studies of serpentinites from various tectonic environments have revealed oxygen isotope heterogeneities at the microscale, which show more complex fluid-rock interactions involving a wider variety of temperatures and fluid compositions than previously recognized through bulk isotope techniques (e.g., Scicchitano et al., 2018; 2021; 2022). Consequently, the ability to target by SIMS mineral pairs equilibrated at the microscale allows for more accurate reconstructions of *T*-fluid paths in rocks with complex metamorphic histories and multiple mineral generations and/or isotopic zoning, relative to analysis of mineral separates using bulk analytical techniques that yield average compositions over millimeter and larger length scales.

Another requirement for successful stable isotope thermometry is the knowledge of oxygen isotope equilibrium fractionation factors between mineral-mineral and mineral-fluid pairs. The accuracy of *T*-fluid estimates depends on how well such fractionation factors are constrained. Oxygen isotope fractionation factors between serpentine and water have been determined empirically (Wenner and Taylor, 1971; Früh-Green et al., 1996), using bond-strength methods (Savin and Lee, 1988; Zheng, 1993a), and based on experimental calibrations (Saccocia et al., 2009). Wenner and Taylor (1971) determined an approximate calibration of the oxygen isotope fractionation between serpentine-water and serpentine-magnetite by measuring oxygen isotopes in serpentine and magnetite separated from various oceanic and continental serpentinites. To construct a calibration curve from measured oxygen isotope fractionations, the temperature of equilibrium must be known. Wenner and Taylor (1971) assumed that serpentine and chlorite are isotopically indistinguishable and they calculated a temperature of formation for their serpentine-magnetite pairs between 100 and 450 °C by extrapolating measured $^{18}O/^{16}O$ fractionations between coexisting chlorites and Fe-Ti oxides in low-grade pelitic schist from various terranes (Garlick, 1969), where the O-isotope equilibration temperatures were determined by combining preliminary experimental calibrations of the oxygen isotope fractionation between quartz-water (later published in a revised version by Clayton et al., 1972) and muscovite-water (O´Neil and Taylor, 1969). Früh-Green et al. (1996) modified the calibration of Wenner and Taylor (1971) by replacing the experimental calibration of the quartz-water oxygen isotope fractionation with the empirical calibration of Sharp and Kirschner (1994), which resulted in a similar curve as the original one proposed by Wenner and Taylor (1971). The oxygen isotope fractionation between serpentine and water was calibrated experimentally by Saccocia et al. (2009) between 250 and 450 °C. In this temperature range, there is a good agreement within ± 2 ‰ between the experimental and empirical calibrations. Nevertheless, if these calibrations are extrapolated to lower temperatures assuming a linear dependence with $1/T^2$, a large discrepancy of up to 20 ‰ is observed. Because fractionation factors cannot be described with a simple function of temperature over a broad temperature range (Clayton, 1981), straight-line extrapolations of fractionation curves outside the investigated temperature range likely result in erroneous fractionation factors and should be avoided, particularly at low temperatures (Chacko et al., 2001). The only calibrations of the oxygen isotope fractionation between serpentine and water at $T <$ 100 °C available up to date are those based on semi-empirical bond-strength models by Savin and Lee (1988) and Zheng (1993a). Even though such calibrations are a useful first approximation when no experimental or empirical studies are available, their accuracy must be independently evaluated by other methods (Valley, 2001). In fact, while the increment method of Zheng (1993a; 1993b) is in good agreement with experimental calibrations for anhydrous silicates at 1000 K, a significant discrepancy is observed for apatite, oxides and hydrous silicates (Chacko et al., 2001), including serpentine at $T <$ 200 °C. The large uncertainty on the oxygen isotope fractionation between serpentine and water at $T <$ 200 °C prevents an accurate study of low temperature serpentinization and limits our understanding of some processes associated with low-temperature alteration of ultramafic rocks such as the production of hydrogen, sequestration of carbon, and the support of microbial activity (e.g. Kelemen et al., 2011; 2018; 2020; 2021; Mayhew et al., 2013; Miller et al., 2016; Ellison et al., 2021; Templeton et al., 2021), provided they are concomitant with serpentinization.

In this study we use the high spatial resolution of SIMS to measure oxygen isotope ratios in co-crystallized mineral pairs of serpentine + quartz, serpentine + talc and serpentine + calcite intergrown at the microscale in six serpentinites from the Samail ophiolite (Oman), whose temperature of crystallization was independently constrained in the range 25 to 100 °C by former studies (Falk and Kelemen, 2015; de Obeso and

Kelemen, 2018; Beinlich et al., 2020; Kelemen et al., 2021). This allows us to construct the first empirical calibration of the oxygen isotope fractionation between serpentine and water at $T < 100$ °C, and to evaluate the accuracy of bond-strength models as well as of extrapolations of experimental and former empirical calibrations at low temperatures.

2. The Samail ophiolite and sample selection

The Samail ophiolite in the Sultanate of Oman and United Arab Emirates (Fig. 1) is one of the largest (10,000 km^2) and best subaerially exposed ophiolitic terranes worldwide, consisting of a complete section composed of pelagic allochthonous sediments, pillow basalts, and a sheeted dike complex through to gabbro and upper mantle peridotite (Coleman and Hopson, 1981; Hopson et al., 1981; Lippard et al., 1986). The oceanic crust of the Samail ophiolite formed during the Cenomanian (96.5–95.5 Ma; Rioux et al., 2013) at a fast-spreading mid-ocean ridge or a suprasubduction zone spreading center (Glennie et al., 1974; Coleman, 1981; Searle and Cox, 1999). Initial thrusting over adjacent oceanic lithosphere soon after magmatic formation led to the formation of a high-grade metamorphic sole (peak P-T conditions of 700–900 °C and 0.8–1.4 GPa; Searle and Malpas, 1980; Hacker and Mosenfelder, 1996; Searle and Cox, 2002; Cowan et al., 2014; Soret et al., 2017), which consists of metasedimentary phyllite, greenschist facies metabasalt, and minor amphibolite of the Haybi Complex (Searle and Malpas, 1980). The metamorphic sole tectonically overlies Permian to Late Cretaceous distal to deep-sea sediments, meta-volcanic rocks, and shelf-facies limestone of the Hawasina Group, which are in turn overlying autochthonous Mesozoic to Proterozoic platform sediments of the Arabian continental margin (Coleman, 1981; Stanger, 1985; Nasir et al., 2007; Searle et al., 2015). Thrusting of the Samail ophiolite onto the Arabian continental margin was constrained between 95 and 80 Ma by U-Pb dating of magmatic zircon and $^{40}Ar/^{39}Ar$ ages of mica and hornblende from the metamorphic sole (e.g., Hacker et al., 1996; Warren et al., 2005; Rioux et al., 2012, 2013, 2016).

The mantle section of the ophiolite is 8–12 km thick and consists mainly of harzburgite, minor dunite (up to 15 %) and local lherzolite, which show a degree of hydration and carbonation varying from about 20 to 100 % resulting in the formation of serpentinite, carbonated serpentinite, listvenite and soapstone (e.g., Boudier and Coleman, 1981; Godard et al., 2000; 2021; Monnier et al., 2006; Hanghøj et al., 2010; de Obeso and Kelemen, 2018; Falk and Kelemen, 2015). Alteration spanned the history of the ophiolite and occurred in various tectonic settings and physical-chemical conditions: (i) from oceanic spreading ridges at $T < 400$ °C before obduction of the ophiolite due to interaction with seawater and/or evolved seawater (e.g., Dewandel et al., 2003; Boudier et al., 2010; Streit et al., 2012; Noël et al., 2018; Scicchitano et al., 2021); (ii) followed by alteration near the basal thrust during obduction (97 ± 29 Ma Rb-Sr isochron age of fuchsite in listvenite; Falk and Kelemen, 2015) at $T \approx 100$ °C (Falk and Kelemen, 2015; Beinlich et al., 2020; Kelemen et al., 2022) due to infiltration of fluids derived from dehydration of calc-silicate metasediments of the Hawasina Group (de Obeso et al., 2022); (iii) to present-day low-temperature ($T < 50$ °C) weathering and interaction with groundwater (e.g., Neal and Stanger, 1984; 1985; Streit et al., 2012; Falk et al., 2016; Miller et al., 2016; Noël et al., 2018; Kelemen et al., 2021; Scicchitano et al., 2021).

The samples chosen for this study (Table 1) come from outcrops in two different areas in the Samail ophiolite: "Ministry of Defense" (MoD) Mountain and Wadi Fins (Fig. 1). Different aliquots of the same samples were previously investigated by Falk and Kelemen (2015) and de Obeso and Kelemen (2018), who provided detailed petrographic, petrological, geochemical and bulk/mineral isotope characterization, and clumped isotope thermometry.

2.1. MoD Mountain: "high-temperature" samples

In the area of the MoD Mountain in Wadi Mansah (Fig. 1), discontinuous tabular lenses of listvenite, 10 to 200 m thick, are observed up to 300 m above the metamorphic sole, parallel to both the basal thrust of the ophiolite and banding in the partially serpentinized host peridotite (Falk and Kelemen, 2015; Kelemen et al., 2022). There is a gradational transition from listvenites to serpentinized peridotites characterized by the occurrence of the assemblage serpentine + quartz ± talc, which suggests an equilibrium crystallization temperature of 80 to 130 °C; the range of temperatures results from uncertainty related to thermodynamic parameters for minerals and poorly constrained crystallization pressures (Falk and Kelemen, 2015; Kelemen et al., 2020; 2022). X-ray diffraction (XRD) showed the occurrence of the three main serpentine polymorphs in the listvenite-serpentinite transition zone, with antigorite more abundant than chrysotile and lizardite (Falk and Kelemen, 2015). The petrological temperature estimates are in good agreement with the average clumped isotope temperature of 90 ± 15 °C measured in magnesite and dolomite from listvenites as well as with oxygen isotope thermometry in quartz and carbonate calculated assuming a water $\delta^{18}O$ value of 0 ‰ (Falk and Kelemen, 2015). Formation temperatures < 150 °C in the presence of an aqueous fluid are also suggested by the occurrence of quartz spherulites in listvenites, likely resulting from devitrification of opal (Falk and Kelemen, 2015), and by the lack of the magnesite + talc assemblage in the MoD Mountain listvenites (Kelemen et al., 2022). In 2017, the ICDP Oman

Drilling Project “Hole BT1B” (on the north side of Wadi Mansah, southeast of MoD Mountain; 23°21.861′N, 58°20.149′E) recovered a continuous, 300.1 m long drill core intersecting the serpentinized peridotite, listvenite, basal thrust and metamorphic sole (Kelemen et al., 2020). The occurrence of veins with intergrown amorphous carbon compounds and hematite sampled in the core are also consistent with temperatures lower than 200 °C (see Fig. 11 in Kelemen et al., 2022). Additionally, recent clumped isotope data in listvenites and carbonated serpentinites from the BT1B core yield an average temperature of 147 ± 58 °C (1s) (Beinlich et al., 2020; Kelemen et al., 2022). Compiling all clumped isotope temperatures calculated in outcrop (Falk and Kelemen, 2015) and core samples at MoD Mountain (Beinlich et al., 2020) yields an average temperature of 100 ± 46 °C (1s) (Kelemen et al., 2022).

For the purpose of this study, we characterized two outcrop samples (OM09-12 and OM10-02; Fig. S1-S2) equilibrated at $T \approx 100$ °C that were collected in the transition zone between listvenites and serpentinized peridotites by Falk and Kelemen (2015).

2.2. Wadi Fins: “low-temperature” samples

Mantle peridotites in Wadi Fins (Fig. 1) are exposed at the base of a water-carved canyon and are unconformably capped by up to 1.5 km of Late Cretaceous to Eocene marine limestones, which locally form dikes that intrude the underlying peridotite and extend approximately 10 m below the unconformity (de Obeso and Kelemen, 2018). Peridotites in Wadi Fins are intensely serpentinized and consist mainly of lizardite ± chrysotile (XRD, de Obeso and Kelemen, 2018; Raman spectroscopy, this study; Table S1) forming typical mesh textures, with rare relict olivine and pyroxene, crosscut by an extensive network of pure serpentine, carbonate and serpentine +

carbonate veins (Fig. S3-S7). Bulk $\delta^{13}C$ (–1.3 to +0.6 ‰, V-PDB) and $\delta^{18}O$ (22 to 28 ‰, V-SMOW) values as well as $^{87}Sr/^{86}Sr$ ratios (0.70778–0.70790) in calcite separated from veins are comparable, respectively, to those measured in Late Cretaceous limestones in the area and seawater at the Cretaceous-Paleogene boundary (de Obeso and Kelemen, 2018 and references therein). Isotopic data combined with reaction path modelling suggest that silica-bearing pore fluids in the Cretaceous-Paleogene limestones were responsible for alteration of the underlying peridotites and formation of various carbonate and serpentine veins at temperatures from about 20 to 60 °C, as determined by clumped isotope thermometry in the calcite veins (de Obeso and Kelemen, 2018).

For the purpose of this study, we chose five samples of carbonated serpentinites (OM13-1, OM13-11, OM13-13, OM13-14A and OM13-17A; Fig. S3-S7) previously characterized by de Obeso and Kelemen (2018), which equilibrated at T = 25 to 56 °C according to the calibration by Bristow et al. (2011) (Table 1 in de Obeso and Kelemen, 2018). The use of different calibrations for the calculation of clumped isotope temperatures (e.g., Ghosh et al., 2006; Dennis and Schrag, 2010) result in similar values within ± 10 °C at most (Table 1 in de Obeso and Kelemen, 2018).

3. Analytical methods

Polished rock billets with the desired target domains for SIMS analysis were cut and mounted in the central 15 mm of 25.4 mm epoxy discs along with grains of calcite (UWC-3; Kozdon et al., 2009), quartz (UWQ-1; Kelly et al., 2007) and antigorite (UWSrp-1; Scicchitano et al., 2021) reference materials. Epoxy discs were then (i) ground using a 6-μm fixed-diamond lapping pad, (ii) polished using 6-μm, 3-μm and 1-μm polycrystalline diamond suspensions, and (iii) cleaned with ethanol, concentrated liquid detergent and distilled water. They were dried in a vacuum oven for three hours before applying any conductive coating (see below). White-light interferometry confirmed that polishing relief across the mounts was ≤ 3 μm.

3.1. Scanning Electron Microscopy

The samples were imaged with a Hitachi S3400 Variable Pressure (VP) Scanning Electron Microscope (SEM) at the Department of Geoscience (University of Wisconsin-Madison, UW-Madison) operated at high vacuum in backscattered electron (BSE) and secondary electron (SE) modes. After SIMS analysis, each SIMS pit was imaged by SEM to check their geometry and ensure no contamination from surrounding phases. Analyses where pits were located on fractures, mixed domains or other features that could alter isotope ratios were rejected. Prior to SEM analysis, mounts were coated with 20 nm carbon. Images were acquired with accelerating voltage of 15 kV and working distance of 10 mm.

3.2. Electron Probe Microanalysis

Major and minor element composition of serpentine, talc and calcite from the investigated samples were analyzed using a CAMECA SXFive Field Emission Electron Probe Microanalyzer (EPMA) at the Department of Geoscience, UW-Madison. Analysis of serpentine and talc involved quantification of 12 elements (O, Na, Mg, Al, Si, K, Ca, Ti, Cr, Mn, Fe, Ni) measured at 15 kV and 10 nA with 2-5 μm beam diameter. All elements were measured using the Mean Atomic Number (MAN) technique for background regression (Donovan et al., 2019), except O which was measured using traditional off-peak background regression. Direct analysis of O using PC0 diffraction crystal was used to calculate OH content (wt. %) from excess O after apportioning to each measured cation. Serpentine analyses were normalized to 18 (O + OH) according to the general formula $Mg_6Si_4O_{10}(OH)_8$. Talc analyses were normalized to 12 (O + OH) according to the general formula $Mg_3Si_4O_{10}(OH)_2$. Analysis of calcite involved measurement of five elements (Ca, Mg, Fe, Mn, Sr) using MAN background regression at 15 kV and 10 nA with 5 μm diameter beam. A time-dependent intensity correction was applied to account for observed element migration during beam exposure. Calcite stoichiometry was calculated based on 1 C and 3 O according to the general formula $CaCO_3$ (Table S2).

3.3. Raman spectroscopy

Raman spectroscopy was completed following SIMS analysis for the purposes of identifying specific serpentine polymorphs. Prior to Raman analysis, conductive coatings (used for SIMS and EPMA analysis and SEM imaging) were removed using a 0.25 μm diamond suspension on a lapping pad, and sample surfaces were cleaned. Raman data were collected using a Horiba LabRAM-HR Evo, located in Nanoscale Imaging and Analysis Center at UW-Madison. Between one to three Raman analyses targeted regions within 10 μm of the SIMS pits to generate spectra for phase identification. Spectral acquisition utilized an excitation wavelength of 532 nm, a 1800 grove/mm grating, 100x objective in air, a confocal hole of 100 μm and a spectral slit of 100 μm. Each analysis consisted of spectra collection in two spectral ranges: 50-900 cm^{-1} and 3500-3800 cm^{-1}. Integration times at each spectral window ranged between 1-4 (x2) seconds, with two acquisitions used for spike correction. Integration times and laser intensity was adjusted to optimize spectra quality. The primary limiting factor on spectral quality was the presence of carbonate phases proximal to SIMS analyses. The presence of fluorescence in Raman spectra was highly variable from spot-to-spot and sample-to-sample, where presence was occasionally sufficient to obscure the Raman signal from targeted serpentine polymorphs.

3.4. Secondary Ion Mass Spectrometry

In situ oxygen isotope analyses of serpentine, talc, quartz and calcite were made using a CAMECA IMS-1280 large radius multicollector secondary ion mass spectrometer at the WiscSIMS laboratory, UW-Madison. A $^{133}Cs^{+}$ primary ion beam with an intensity of about 2 nA (silicates) and 1 nA (carbonates) was focused to a 10 μm diameter spot on the sample surface with a total impact energy of 20 keV, as described in details by previous studies (e.g., Kita et al., 2009; Śliwiński et al., 2016; Scicchitano et al., 2021). A normal incidence electron gun was used for charge compensation and a gold coating (60 nm) was applied to ensure electrical conductivity (Kita et al., 2009). Secondary ions were collected with Faraday cup detectors (L′2–$^{16}O^{-}$, H1–$^{18}O^{-}$, FC2–$^{16}O^{1}H^{-}$); typical count rates on $^{16}O^{-}$ were on the order of 2.2–2.9 × 10^{9} cps (silicates) and 1.6–2.1 × 10^{9} cps (carbonates). The mass resolution of the SIMS was set at $M/\Delta M \approx 4800$ (10 % of peak height) to resolve the $^{16}O^{1}H^{-}$ and $^{17}O^{-}$ mass peaks. Analyses lasted 3.5 minutes including pre-sputtering (10 s), automated centering of the secondary ion beam into the field aperture (120 s) and data collection (80 s).

The instrumental mass fractionation (IMF), drift and repeatability throughout the analytical session were monitored by bracketing 10-20 unknown analyses with at least eight analyses of the reference material located in the same mount (Table S1-S2). A suite of seven antigorite reference materials was analyzed at the start, throughout and at the end of the analytical session (Table S3) to monitor and quantify matrix effects related to variations in Mg/Fe ratios in serpentine, by constructing calibration curves as described in Scicchitano et al. (2021). These calibration curves were then used to correct $\delta^{18}O$ values measured in serpentine from the Oman samples. Bias between different serpentine polymorphs was estimated as in Scicchitano et al. (2021). The repeatability in each mount varied between ± 0.16 to ± 0.23 ‰ (1s) in UWQ-1, ± 0.13 to ± 0.24 ‰ in UWSrp-1 and ± 0.14 to ± 0.27 ‰ in UWC-3. An unnoticed increase throughout the whole session of the pre-amplifier vacuum pressure (from 1×10^{-3} to 1×10^{-1} mbar; Fig. S8) might have caused instability in the signal and explain the occasional lower (but acceptable) repeatability observed throughout the session. Because of crystal orientation effects in chrysotile (Scicchitano et al., 2021), we estimate that the total analytical uncertainty on individual analyses performed in this polymorph (or mixtures containing it) are on the order of ± 1 ‰ (1s), while total analytical uncertainties on antigorite and lizardite are better than ± 0.5 ‰ (1s). For the latter, the main source of uncertainty is the accuracy of the calibration curves for the correction of Mg/Fe matrix effects (Table S3-2).

Because isotope ratios measured by SIMS are affected by instrumental mass fractionation depending on the targeted matrix, reference materials should have the same crystal structure and chemical composition as the minerals to be analyzed in natural samples (e.g., Valley and Kita, 2009). Consequently, the analysis of oxygen isotope ratios in talc from the Oman serpentinites required the development of an appropriate talc reference material. A detailed characterization of the chemical (SEM, EPMA, X-ray mapping) and isotopic compositions (gas source mass spectrometry and SIMS) of a talc sample (UWT-1) from the Mineralogical Collection at the Department of Geoscience (UW-Madison) is presented in the Supplementary Material.

4. Results

4.1. Textures and major mineral compositions

Sample ***OM09-12*** analyzed in this study consists mainly of antigorite (as documented by Raman and in agreement with previous XRD analyses by Falk and Kelemen, 2015; Table S1) intergrown with quartz and minor dolomite, magnesite and talc (Fig. 2a-c). The matrix consists of several crosscutting veins of dolomite, serpentine, magnesite, talc, Fe-oxide and disseminated Cr-spinel (Fig. 2d, S1). Antigorite has homogenous major element chemical composition with an average Mg# of 96 mole % [Mg# = 100 × Mg / (Mg + Fe) on a molar basis, with Fe = Fe total] (Table S1). Sample ***OM10-02*** consists mainly of a sheared matrix of chrysotile + magnesite + talc with relict chromite (Fig. S2), which is crosscut by veins of chrysotile + talc + Fe-oxide (Fig. 2e-f). Chrysotile and talc show uniform compositions and have an average Mg# of 97 and 95 mole %, respectively (Table S1). The mineral pairs antigorite + quartz and chrysotile + talc, which equilibrated at $T \approx$ 100 °C, were targeted by SIMS.

Carbonated serpentinites from Wadi Fins have complex textures and careful evaluation of the mineral assemblages observed in veins was required in order to target by SIMS the serpentine + calcite equilibrium assemblage. In all samples, different generations of serpentine and calcite were identified texturally (Fig. 3, S3-S7). In ***OM13-1***, the vein consists of at least three generations of serpentine + calcite with intergrown dolomite and blocks of serpentinites showing complex textures (Fig. S3). In ***OM13-11***, the targeted vein consists mainly of calcite + lizardite/chrysotile (Cal_1 + Lz_1), which includes blocks of the host serpentinite as well as domains of calcite + serpentine fragments (Cal_2 + Srp_2; Fig. 3a-b, S4). Lizardite (Lz_1) in textural equilibrium with calcite (Cal$_1$) appears as elongated grains as opposed to serpentine fragments (Srp$_2$) and serpentinite blocks, which show complex textures (Fig. S4); additionally, it is crosscut by a second generation of calcite (calcite vein in Fig. 3a, S4b). Fine-grained dolomite is sometimes observed between serpentine and calcite domains or interspersed within the calcite matrix (Fig. 3a-b). In ***OM13-13***, the targeted vein consists of a calcite + lizardite/chrysotile assemblage (Cal$_1$ + Lz$_1$) that is crosscut by a later calcite + dolomite vein (Cal$_2$ + Dol); various fragments of serpentinite and lizardite ± chrysotile (Srp$_2$) are also found in the vein (Fig. 3c-d, S5). The latter are not in textural equilibrium with calcite as evidenced by crosscutting relationships and relict mesh textures (Fig. S5c). In ***OM13-14A***, the host serpentinite is crosscut by a complex vein consisting of a calcite + lizardite/chrysotile assemblage (Cal$_1$ + Lz$_1$) that appears in textural equilibrium and by a domain in which fragments of serpentine and serpentinite do not appear to be precipitated together with the surrounding calcite (Cal$_2$ + Srp$_2$) (Fig. 3e-f, S6). In ***OM13-17A***, a large symmetric vein consisting of a calcite + chrysotile/lizardite assemblage on the outer edges (Cal$_1$ + Ctl$_1$), a second calcite generation not coexisting with serpentine (Cal$_2$) and a second chrysotile generation not coexisting with carbonate in the center (Ctl$_2$) was targeted by SIMS (Fig. 3g-h, S7). Only the first assemblage is in textural equilibrium. The equilibrium calcite + serpentine assemblages (Cal$_1$ + Lz$_1$) in all samples, which equilibrated at T = 25–56 °C (clumped isotope thermometry; de Obeso and Kelemen, 2018), were considered as the main target for SIMS.

Serpentine intergrown with calcite in the veins crosscutting serpentinites in Wadi Fins consists of a mixture between lizardite and chrysotile, as evidenced by Raman spectroscopy (Table S1) and in agreement with previous XRD characterizations by de Obeso and Kelemen (2018). It has uniform major element compositions within a single sample and has an average Mg# varying from 94 to 96 mole % between different samples (Table S1). In some samples, fringes of more Fe-rich serpentine (Mg# = 93 mole %) are observed surrounding serpentine intergrown with calcite. Calcite in veins shows uniform Fe (FeO ≤ 0.4 wt. %) and Mn contents (MnO < 0.7 wt. %), whereas Mg content varies mostly between 0.3 to 2.1 wt. % and occasionally up to 4.5 wt. % (Table S2). However, no correlation is observed with textures and across different samples.

4.2. SIMS oxygen isotope ratios

The oxygen isotope ratios measured by SIMS in the selected samples are shown in the supplementary Tables S1 (silicates) and S2 (calcite), and the average $\delta^{18}O$ values for each mineral pair in textural equilibrium are shown in Table 1. In the MoD samples ***OM09-12*** and ***OM10-02***, antigorite, quartz, chrysotile and talc are homogeneous in oxygen isotope ratios at a sub-1 ‰ level having a variability of ≤ ± 0.4 ‰ (1s). In all samples from Wadi Fins except for ***OM13-1***, serpentine (Srp_1) and calcite (Cal_1) in textural equilibrium have oxygen isotope ratios that vary by ± 0.3 to ± 0.7 ‰ (1s) and by ± 0.5 to ± 1.1 ‰ (1s), respectively. In sample ***OM13-1***, while serpentine in the different textural locations has a variability better than ± 0.8 ‰ (1s), calcite is highly heterogeneous in oxygen isotope ratios (variability of ± 2.6 to ± 3.9 ‰, 1s). Consequently, sample ***OM13-1*** is not suitable for the purpose of this study and is not further discussed.

SIMS analysis in the samples from Wadi Fins highlighted significant variations in the oxygen isotope ratios of different generations of calcite and serpentine. In sample ***OM13-11***, Cal_2 and the calcite vein crosscutting the Srp_1 + Cal_1 assemblage have average $\delta^{18}O$ values of 18.0 ± 0.1 ‰ (1s, n = 2) and 20.7 ± 1.1 ‰ (1s, n = 4), respectively, which are significantly lower compared to Cal_1 ($\delta^{18}O$ = 27.6 ± 0.5 ‰, 1s, *n* = 37). Similarly, calcite in equilibrium with dolomite in sample ***OM13-13*** (Cal_2) has an average $\delta^{18}O$ value that is about 5 ‰ lower compared to calcite in equilibrium with serpentine (Cal_1) – i.e., 21.4 ± 2.8 (1s, *n* = 8) versus 26.1 ± 1.0 ‰ (1s, *n* = 30). On the contrary, Lz_1 and Srp_2 differ by less than 1 ‰. In sample ***OM13-14A***, Cal_1 and Cal_2 have similar oxygen isotope ratios ($\delta^{18}O$ = 27.3 ± 1.1, 1s, *n* = 15, versus 27.7 ± 0.6 ‰, 1s, *n* = 4), while Lz_2 has an average $\delta^{18}O$ value that is about 2 ‰ lower compared to Lz_1 (12.1 ± 0.4, 1s, *n* = 11, versus 14.3 ± 0.3 ‰, 1s, *n* = 3). Finally, the calcite not intergrown with serpentine in sample ***OM13-17A*** (Cal_2) has an average $\delta^{18}O$ value of 24.1 ± 0.7 ‰ (1s, *n* = 16), which is about 3 ‰ lower compared to Cal_1 intergrown with chrysotile Ctl_1 ($\delta^{18}O$ = 27.3 ± 0.7 ‰, 1s, *n* = 29). SIMS analysis of the second chrysotile generation not intergrown with calcite (Ctl_2) in sample ***OM13-17A*** resulted in very low secondary ion yields that can be attributed to the high porosity of this serpentine generation, hence these data are inaccurate and not further discussed.

5. Discussion

Provided isotopic equilibrium is reached and preserved and the oxygen isotope fractionation between mineral-mineral or mineral-fluid are known, then analysis of co-crystallized minerals enables determination of equilibration temperatures. The inverse is also true, in that if the temperature of equilibration is independently constrained, then analysis of oxygen isotopes in mineral pairs co-crystallized over a given range of temperatures provides an empirical calibration of mineral-mineral and/or mineral fluid oxygen isotope fractionation factors as well as the ability to estimate fluid compositions. The variation of $^{18}O/^{16}O$ fractionation (1000 lnα)

between two minerals or a mineral-fluid pair (*a* and *b*) equilibrated over a temperature range (*T* in Kelvin) often shows a linear correlation with $1/T^2$ (Chacko et al., 2001; Valley, 2001):

$$1000 \ln \alpha \,(a-b) = \frac{A\,(a-b)\times 10^6}{T^2} \qquad (1)$$

Where α (*a*–*b*) is the fractionation factor at a given temperature *T*, and A (*a*–*b*) is a constant referred to as the A-factor. Values of 1000 lnα (*a*–*b*) can be approximated by the relation (Hoefs, 2018):

$$1000 \ln \alpha \,(a-b) \approx \Delta\,(a-b) = \delta(a) - \delta(b) \qquad (2)$$

Where δ(*a*) and δ(*b*) are oxygen isotope values measured in two different phases.

Equilibrium is difficult to prove and rocks often preserve complex textures suggesting multiple metamorphic or crystallization events at different *P*-*T*-time-deformation-X_{fluid}, which indicate the lack of equilibration at least at the scale of the hand-specimen. Nevertheless, many rocks preserve evidence of equilibration at the microscale (i.e., local equilibrium) and high-spatial resolution microanalytical techniques such as SIMS, combined with detailed petrographic observations, provide constraints on the thermometric conditions recorded by minerals constituting a given local equilibrium assemblage. Evidences of disequilibrium, such as zoning in the oxygen isotope composition of minerals at the microscale, can also be identified through SIMS analysis. Consequently, oxygen isotope fractionation factors measured by SIMS in co-crystallized minerals from rocks with complex textures and metamorphic histories can be more accurate than those determined using bulk techniques on mineral separates, which average the oxygen isotope ratios of different mineral generations.

5.1. Equilibrium temperatures

Estimation of crystallization temperatures in serpentinites is difficult due to the lack or paucity of suitable geothermometers. Clumped isotope thermometry in carbonated serpentinites is, therefore, a powerful alternative method when petrological estimates are not possible. Nevertheless, temperatures derived from clumped isotope techniques may represent average estimates if multiple carbonate generations crystallized over a range of temperatures are analyzed. Clumped isotope thermometry cannot be performed at the high-spatial resolution of SIMS, but such method can be used in tandem with SIMS to establish the degree of homogeneity in $\delta^{18}O$ of different carbonate generations at the microscale, hence supporting the use of a bulk approach for clumped isotope thermometry.

Temperature estimates for the MoD samples characterized in this study were made by Falk and Kelemen (2015) and Beinlich et al. (2020), and they are reviewed in detail by Kelemen et al. (2022). Merging all clumped isotope temperatures calculated in outcrop (Falk and Kelemen, 2015) and core samples at MoD Mountain (Beinlich et al., 2020) yields an average temperature of 100 ± 46 °C (1s) in agreement with petrological estimates (Kelemen et al., 2022). We consider this to be the best estimate of the crystallization temperature and respective uncertainty for the antigorite + quartz and talc + chrysotile assemblages in samples OM09-12 and OM10-02.

Clumped isotope temperatures for the carbonate + serpentine veins in carbonated serpentinites from Wadi Fins were determined by de Obeso and Kelemen (2018) following calibrations by Bristow et al. (2011), Dennis and Schrag (2010), and Ghosh et al. (2006) (Table 1 in de Obeso and Kelemen, 2018). As in de Obeso and Kelemen (2018), the temperatures derived from the calibration of Bristow et al. (2011), which range between 25 ± 4 and 50 ± 3 °C in the investigated samples, are considered for discussions in the current study. The uncertainty deriving from the choice of different calibrations for calculating clumped isotope temperatures is on the order of ± 8 °C at most in the targeted samples. SIMS analyses in the Wadi Fins samples show, however, the occurrence of different calcite generations in the veins, characterized by lower oxygen isotope ratios relative to the low temperature calcite in equilibrium with serpentine (i.e., $Cal_1 + Srp_1$). Lower $\delta^{18}O$ values can be the result of higher crystallization temperatures, lower $\delta^{18}O$ fluids or a combination of both. Nevertheless, only in sample OM13-11 do the two calcite generations have $\delta^{18}O$ values that differ significantly from each other (about 9 ‰, resulting in ΔT of about 60 °C at constant water $\delta^{18}O$), whereas in all other samples the variation is lower than 5 ‰ (resulting in $\Delta T < 30$ °C at constant water $\delta^{18}O$). Because of the larger sampling scale of clumped isotope techniques relative to SIMS, we cannot exclude that mixing of different carbonate generations might have affected the corresponding thermometric estimates resulting in larger uncertainties on the calculation of equilibrium temperatures. In fact, temperatures calculated from SIMS $\delta^{18}O$ values in Cal_1 ($\delta^{18}O_{calcite}$ = 26.1 to 27.6 ‰; Table S2) assuming precipitation from pure seawater ($\delta^{18}O_{water}$ = –1 ‰) are up to 20 °C lower (T = 24 to 32 °C; calcite-water fractionation factors after O´Neil et al., 1969) relative to clumped isotope temperatures (T = 25 to 50 °C). Consequently, we estimate that the uncertainty on the clumped isotope temperatures of the Wadi Fins samples is on the order of ± 20 °C (1s).

5.2. Disequilibrium effects

SEM imaging coupled with *in situ* analysis of oxygen isotopes by SIMS show that the investigated samples, particularly those from Wadi Fins, have complex textures and consist of multiple generations of serpentine + calcite with different $\delta^{18}O$ values (Fig. 3, S3-S7; Table S1-S2). This suggests that the different mineral pairs likely equilibrated at different temperatures and/or with different $\delta^{18}O$ fluids. SEM imaging and EPMA analysis of the mineral pairs constituting the equilibrium assemblages (i.e., Cal_1 + Srp_1 in the Wadi Fins samples, Atg + Qtz and Tlc + Ctl in the MoD samples) show, however, that all phases are homogeneous in their major cation chemical composition within a single sample suggesting compositional equilibrium. Additionally, SIMS analyses in such mineral pairs show that the variability in oxygen isotope ratios at the microscale is up to about ± 1 ‰ (1s) at most (Fig. 4, 5), which is larger than the typical repeatability measured by SIMS in homogeneous reference materials or minerals equilibrated at high temperature (i.e., 1s of 0.1 ‰; e.g., Valley and Kita, 2009; Zhang et al., 2022), and might suggest disequilibrium effects that are likely at such low temperatures. Nevertheless, given that these assemblages formed at very low temperatures (T < 100 °C) and that the uncertainty deriving from extrapolation to lower temperatures of empirical and experimental calibrations of the oxygen isotope fractionation is on the order of about 20 ‰, we consider satisfactory the variability of ± 1 ‰ measured in the investigated mineral pairs. At such low temperatures, the effects of diffusion processes, which would be deleterious for thermometry, are also negligible and can be ignored. Consequently, for the purpose of this study, we treat the targeted antigorite + quartz, chrysotile + talc and $calcite_1$ + $serpentine_1$ as homogeneous in oxygen isotope ratios and we assume that such assemblages record the equilibrium composition at the time of precipitation from a fluid with a constant $\delta^{18}O$ value.

5.3. Empirical calibration of $\Delta^{18}O$(Serpentine-H_2O)

Multiple analyses of oxygen isotope ratios by SIMS in antigorite + quartz, chrysotile + talc and serpentine + calcite in six samples from the Oman ophiolite allowed us to calculate the following oxygen isotope fractionations: $\Delta^{18}O_{(quartz\text{-}antigorite)} = 15.0 \pm 0.3$ ‰ (2SE) at 100 °C (sample OM09-12), $\Delta^{18}O_{(talc\text{-}chrysotile)} = 3.8 \pm 0.3$ ‰ at 100 °C (sample OM10-02), $\Delta^{18}O_{(calcite\text{-}serpentine)} = 13.2 \pm 0.3$ to 16.6 ± 0.3 ‰ in the *T* range of 25 to 50 °C (samples OM13-11 to OM13-17A) (Table 1). The uncertainty of average mineral-serpentine fractionation values measured by SIMS is expressed as the standard error (2SE), which depends on the number of mineral pairs analyzed in each sample. Given that the temperature of crystallization is known, the mineral-serpentine oxygen isotope fractionations measured by SIMS can be combined with available calibrations of oxygen isotope fractionation between quartz-water (Clayton et al., 1972; Friedman and O´Neil, 1977; Matsuhisa et al., 1979; Matthews and Backinsale, 1979; Ligang et al., 1989; Zheng, 1993b; Hu and Clayton, 2003; Pollington et al., 2016; Sharp et al., 2016), talc-water (Savin and Lee, 1988; Zheng, 1993a) and calcite-water (O´Neil et al., 1969; Golyshev et al., 1981; Kim and O´Neil, 1997) in order to calculate the A-factor for the serpentine-water fractionation (see Table S4 for details on calculations). In the choice of mineral-fluid calibrations, we favored experimental over empirical and theoretical calibrations if laboratory experiments were made at temperatures relevant for our study – that is $T < 200$ °C. This is the case for the calcite-water system (O´Neil et al., 1969; Golyshev et al., 1981; Kim and O´Neil, 1997), while all experiments for the quartz-water system were made at $T > 250$ °C. In the latter case, in addition to experimental calibrations made at T = 250 to 500 °C, we also considered empirical and theoretical calibrations extending to lower temperatures. For the talc-water system, only bond-strength model calibrations are considered. The following mineral-water fractionation values are averages of multiple calibrations available in the literature (Tables S1 and S4): $\Delta^{18}O_{(talc-water)}$ = 13.5 ± 0.1 ‰ (1SE) for sample OM10-02, $\Delta^{18}O_{(quartz-water)}$ = 20.9 ± 0.8 ‰ (1SE) for sample OM09-12, and $\Delta^{18}O_{(calcite-water)}$ = 23.5 ± 0.3 ‰ (1SE) to 28.1 ± 0.3 ‰ (1SE) for the Wadi Fins sample. Water $\delta^{18}O$ values of –2 to +4 ‰ are calculated to be in equilibrium with calcite and serpentine in the Wadi Fins samples, which is consistent with a progressive equilibration of Cretaceous seawater trapped in pore spaces with authigenic calcite (e.g., Falk and Kelemen, 2015). The quartz-water and talc-water fractionation factors predict water $\delta^{18}O$ values of +3.6 and –0.6 ‰ to be in equilibrium with quartz, talc and serpentine in the MoD samples. Such compositions are similar to the values of –1 ± 3 ‰ (at T = 80 °C) and 5 ± 3 ‰ (at T = 130 °C) calculated by Falk and Kelemen (2015) and they are consistent with fluids derived from subducted metasediments (Falk and Kelemen, 2015). Combining such mineral-water fractionations with our new SIMS data, oxygen isotope fractionation between serpentine and water at T = 25 to 100 °C can be described as follows (Fig. 6):

$$1000 \ln \alpha \text{ (serpentine – water)} = \frac{1.04 \times 10^6}{T^2} \qquad (3)$$

Yielding an A-factor of 1.04 ± 0.20 (2SE) and assuming zero fractionation at infinite temperature (i.e., forcing the intercept to zero; Table S4). The slope of the fit would not change significantly if the intercept is not forced to zero, and the resulting A-factor would be within 2SE uncertainty of the one shown in equation (3). The uncertainty of average serpentine-water fractionation values in each sample were calculated by propagation of the 2SE value of the average $\Delta^{18}O$(mineral-serpentine) measured by SIMS and the 2SE value of the average mineral-water fractionation factors resulting from multiple calibrations (Table 1). The large uncertainty on the fit ($R^2 = 0.47$) results from the relatively large variability in $\delta^{18}O$ values of the targeted equilibrium mineral pairs and large uncertainty on clumped isotope equilibrium temperatures, which are perhaps unavoidable at such low temperatures, as well as from the uncertainty on the mineral-water fractionation factors used to calculate serpentine-water oxygen isotope fractionations. Despite the large uncertainty on the fit, our empirical calibration is within uncertainty of former high-temperature empirical calibrations of the oxygen isotope fractionation (Wenner and Taylor, 1971; Früh-Green et al., 1996), when these are extrapolated to $T < 200$ °C, as well as with the experimental fractionation of Saccocia et al. (2009) if our calibration is extrapolated to $T = 250$ °C (Fig. 7). However, the new calibration predicts $\Delta^{18}O_{(serpentine-water)}$ up to 8 ‰ lower compared to the bond-strength methods of Savin and Lee (1988) and Zheng (1993a), and 18 ‰ lower compared to the experimental calibration of Saccocia et al. (2009) if the latter is extrapolated to $T = 25$ °C.

5.4. The effect of pressure

The clumped isotope temperatures of 25 to 60 °C measured in carbonate + serpentine veins from the carbonated serpentinites at Wadi Fins suggest that alteration occurred near the surface (de Obeso and Kelemen, 2018). Given that carbonated serpentinites at Wadi Fins are capped by 1.5 km limestones (Nolan et al., 1990; Racey, 1995; Wyns et al., 1992), it is inferred that vein formation occurred at moderate pressures ($P < 0.05$ GPa) (de Obeso and Kelemen, 2018). In contrast, the depth (hence pressure) at which listvenites and transitional lithologies at MoD formed is more difficult to constrain due to discrepancies between the peak pressure recorded in the metamorphic sole (generally, maximum $P \approx 1.2$ GPa; in drill core from MoD, $P \approx 0.7$ to 1 GPa corresponding to 25 to 40 km depth; Kotowski et al. 2021) and the total structural thickness of the ophiolite measured perpendicularly to the paleo-seafloor or to the crust-mantle transition zone (i.e., 30 km corresponding to $P < 0.8$ GPa; Boudier and Coleman, 1981; Nicolas et al., 1996; 2000; Kelemen et al., 2022). Independently of the reasons for such discrepancies (see Kelemen et al., 2022 for more details), the samples used in this study to build an empirical calibration of the serpentine-water oxygen isotope fractionation formed at pressures that differ by 1.2 GPa at most. For most isotope exchange reactions, except for D/H between hydrous minerals and water (e.g., Polyakov and Kharlashina 1994; Mineev and Grinenko, 1996; Horita et al., 1999; 2002), the volume change (ΔV^0_R) is small resulting in small pressure effects on the stable isotope fractionation (Chacko et al., 2001). At $T > 500$ °C and for $\Delta P < 2$ GPa, pressure effects on oxygen isotope fractionation for all investigated minerals are, in fact, close to or within analytical uncertainty (≤ 0.2 ‰) (Horita, 2005). Even though the difference in pressure at which the investigated samples formed is < 2 GPa, crystallization temperatures are much lower ($T = 25$ to 100 °C). Nevertheless, it is unlikely that such low temperatures persist at depths of 40 km. Consequently, the $\Delta P = 1.2$ GPa is an extreme upper limit and we exclude any significant pressure effect on the serpentine-water oxygen isotope fractionation at $T < 100$ °C.

5.5. The effect of mineral composition

Significant compositional effects up to 1.3 ‰ at 1000 K on the oxygen isotope fractionation have been observed in silicates, particularly due to Al^{3+} substitutions in the tetrahedral site of plagioclases (O´Neil and Taylor, 1967; Matsuhisa et al., 1979; Kieffer, 1982; Clayton et al., 1989) and in the octahedral site of jadeite-diopside (Matthews et al., 1983; Chacko et al., 2001), as well as due to $Fe^{3+} \leftrightarrow Al^{3+}$ substitutions in garnet (e.g., Kieffer, 1982; Kohn and Valley, 1998). The new empirical calibration proposed in this study is built using oxygen isotope fractionations measured between quartz-antigorite, talc-chrysotile, and calcite-lizardite±chrysotile. While quartz, calcite and talc do not show significant variations in their major element chemical composition, serpentine in natural samples often has variable Mg/Fe ratios (typical Mg# = 78 to 99 mole %; Evans et al., 2009; 2012; Mayhew and Ellison, 2020) and it incorporates variable amounts of Al^{3+} (up to 3.6 wt. % Al_2O_3 at 2 GPa–650 °C and 4.5 wt. % Al_2O_3 at 0.3 GPa–560 °C; Padrón-Navarta et al., 2013) and Fe^{3+} (0.16 to 1.94 wt. % Fe_2O_3; Evans et al., 2012) through Tschermak substitutions (e.g., Evans, 2004; Evans et al., 2012; Padrón-Navarta et al., 2013; Debret et al., 2015). Hence, the effects of chemical variations in serpentine on the oxygen isotope fractionation must be evaluated.

In the investigated samples, the Mg# of serpentine varies on average from 94 to 97 mole % (Table S1-2). Such variation should not cause significant oxygen isotope fractionation, as experimental and theoretical data in other silicates suggest that the effects of $Fe^{2+} \leftrightarrow Mg^{2+}$ substitutions in the octahedral site are negligible (< 0.1 ‰) at least at high temperature (T > 500 °C) (e.g., Matthews et al., 1983). Trivalent cations (Al^{3+}, Fe^{3+}, Cr^{3+}) are commonly incorporated in serpentine through a Tschermak exchange reaction between serpentine-amesite (${}^{VI}Mg^{2+}\_{}^{IV}Si^{4+} \leftrightarrow {}^{VI}Al^{3+}\_{}^{IV}Al^{3+}$) and serpentine-cronstedtite (${}^{VI}Mg^{2+}\_{}^{IV}Si^{4+} \leftrightarrow {}^{VI}Fe^{3+}\_{}^{IV}Fe^{3+}$) endmembers (e.g., Evans et al., 2012). Given no experimental calibrations on the effect of Tschermak substitutions on the oxygen isotope fractionation, it is possible to quantify it approximately by combining the effects of plagioclase substitutions (i.e., Al^{3+} exchange in the tetrahedral site between albite and anorthite, which results in lower $\delta^{18}O$ values with increasing Al^{3+} in the IV site) and jadeite-diopside substitutions (i.e., Al^{3+} exchange in the octahedral site between jadeite and diopside, which results in higher $\delta^{18}O$ values with increasing Al^{3+} in the VI site). These effects act to nearly cancel each other and thus have an opposite effect on oxygen isotope fractionation (Chacko et al., 2001 and references therein). Using the approach described in Kohn and Valley (1998), we estimate that the effect of Tschermak substitutions in the serpentine-amesite system is a depletion in ^{18}O of about 0.3 ‰ at 575 °C. To the best of our knowledge, no experimental calibrations of the effect of cation substitutions on oxygen isotope fractionations were made at $T < 100$ °C. Consequently, such effects cannot be accurately estimated at low temperature due to the uncertainty deriving from the extrapolation of high temperature experimental calibrations to low temperature.

5.6. The salt effect

According to de Obeso and Kelemen (2018), the carbonate + serpentine veins crosscutting the serpentinites in Wadi Fins probably precipitated from pore fluids in equilibrium with the limestones capping the ultramafic rocks, which likely had chemical compositions similar to Cretaceous seawater as suggested by the bulk $\delta^{13}C$ (–1.3 to +0.6 ‰) and $\delta^{18}O$ (22 to 28 ‰) values as well as $^{87}Sr/^{86}Sr$ ratios (0.70778–0.70790) in calcite separated from the veins (see Table 2 in de Obeso and Kelemen, 2018). In contrast, listvenites and transitional lithologies at MoD precipitated from a

CO_2- and Sr-rich fluid derived from dehydration of calc-silicate metasediments from the Hawasina Group (Falk and Kelemen, 2015; Kelemen et al., 2022; de Obeso et al., 2022; see Supplementary Table 2 in Kelemen et al., 2022). Such fluids may differ significantly in their assumed content of dissolved species, for example in modeled concentrations of Na^+ (10667 vs 2989 mg/kg H_2O in Wadi Fins and MoD, respectively), Ca^{2+} (2774 vs 98 mg/kg H_2O), K^+ (383 vs 782 mg/kg H_2O), $SiO_{2(aq)}$ (7 vs 10214 mg/kg H_2O), Fe^{2+} (0.0001 vs 0.0011 mg/kg H_2O) and Al^{3+} (0.001 vs 19 mg/kg H_2O). Consequently, possible variations of the oxygen isotope fractionation between serpentine and aqueous fluids due to the occurrence of variable amount of dissolved salts (i.e., salt effect; e.g., Horita, 2005 and reference therein) should be evaluated. In general, experiments performed at low temperatures (T < 100 °C) using single-salt solutions (e.g., NaCl, KCl, $MgCl_2$, $CaCl_2$, $MgSO_4$, Na_2SO_4) show that the salt effect on $^{18}O/^{16}O$ fractionation highly depends on cation type and charge, and is almost independent of anion type and charge (Horita, 2005 and reference therein). Additionally, the isotopic effect is negligible for monovalent cations (e.g., Na^+, K^+) at T < 100 °C, and it becomes significant for high-valence cations (e.g., Mg^{2+}, Ca^{2+}, Al^{3+}) with increasing concentration (Horita, 2005). Considering the differences in the assumed salt concentrations of the fluids in equilibrium with the samples investigated in this study, we estimate that the salt effect would not exceed 1 ‰, which is within the uncertainty related to variability in $\delta^{18}O$ of the targeted mineral assemblages.

5.7. Implications

Our new calibration allows the physical and chemical conditions of serpentinization to be constrained more accurately at very low temperatures (T < 100 °C) and has important implications for recognizing modern alteration of mantle peridotite at low temperature due to interaction with groundwater as well as for understanding associated processes such as carbon sequestration and biogeochemical activity. For instance, observations performed at the Oman Drilling Project `Batin Alteration`(BA) sites show various evidence of near-surface serpentinization and carbonation of mantle peridotite such as: (i) the occurrence of young (20-52 ky) calcite veins mutually cross-cutting (and therefore presumed cogenetic) waxy serpentine veins in the upper 100 m of the drill cores, (ii) oxidation of the matrix with abundant formation of Fe-oxy-hydroxides in the upper 30 m of the drill cores, (iii) sampling of highly alkaline and reduced fluids in the boreholes (Kelemen et al., 2021). Scicchitano et al. (2021) showed that the oxygen isotope composition recorded at the microscale in two serpentinite samples from the BA1B core are indeed consistent with different stages of hydrothermal alteration, which started in an oceanic setting and continued in a continental setting due to low-temperature (T < 50 °C) interaction with groundwater having different $\delta^{18}O$ values. Nevertheless, Scicchitano et al. (2021) calculated alteration temperatures by extrapolating to T < 100 °C the empirical calibration by Früh-Green et al. (1996) because it is the only one predicting temperatures that are consistent with the modern alteration inferred at BA sites. In contrast, experimental and semi-empirical calibrations (Savin and Lee, 1988; Zheng, 1993a; Saccocia et al., 2009) predict temperatures higher than 100 °C, hence lack of modern alteration at BA sites. The new empirical calibration presented in the current study confirms that the temperatures calculated by Scicchitano et al. (2021) are accurate and therefore that low-temperature, near-surface alteration of peridotite is active at BA sites in the Oman ophiolite.

6. Summary

This study presents the first empirical calibration of the oxygen isotope fractionation between serpentine and water at T = 25 to 100 °C by combining the high-spatial resolution of SIMS with detailed petrological, geochemical, and thermometric characterizations of six serpentinite samples from the Oman ophiolite. The new empirical calibration – $1000 \ln\alpha_{(serpentine\text{-}water)} = 1.04 \pm 0.20$ (2SE) $\times 10^6/T^2$ (T in K) – is within uncertainty of former high temperature empirical calibrations, when these are extrapolated to T < 200 °C, as well as with experimental calibrations at T = 250 °C. It allows more accurate estimates of serpentinization temperatures and fluid oxygen isotope compositions during alteration of ultramafic rocks at T < 100 °C compared to calibrations based on the bond-strength method and the experimental calibration, if the latter is extrapolated to T < 200 °C. Considering the variability in $\delta^{18}O$ values measured by SIMS in the targeted mineral pairs, no significant effects of pressure, mineral and fluid compositions are predictable on the equilibrium oxygen isotope fractionation between serpentine and water at T < 100 °C.

Acknowledgments

We thank Noriko Kita and Kouki Kitajima for assistance with SIMS analyses, and Drae Rogers (UW-Madison) and Nicolai Klitscher (GFZ) for assistance with sample preparation. We also thank two anonymous reviewers for improving the quality of the manuscript with their valuable comments, and Stefano Bernasconi for editorial handling. This study was supported by the U.S. Department of Energy, Office of Science, Office of Basic Energy Sciences under Award Number DE-FG02-93ER14389. WiscSIMS is supported by NSF (EAR2004618) and the University of Wisconsin-Madison. Kelemen and de Obeso's effort on this manuscript was supported by Kelemen's Arthur D. Storke Chair at Columbia University. Sample collection, clumped isotope analyses, and petrological estimates of pressure and temperature in samples from the Samail ophiolite used in this study were supported by NSF Research Grant EAR-1516300 and Alfred P. Sloan Foundation Grant 2014-3-01, to Columbia University, both with Kelemen as PI, and the International Continental Drilling Program's "Oman Drilling Project", with Kelemen as co-PI with Jürg Matter and Damon Teagle.

Supplementary Material

Supplementary Material A. UWT-1: a talc reference material for SIMS

Supplementary Material B. Supplementary Figures

Table S1. SIMS oxygen isotope (S1-1) and EPMA major chemical element compositions (S1-2) in silicates from the investigated samples of the Samail ophiolite. Representative Raman spectra of serpentine targeted by SIMS in the various samples are shown in S1-3.

Table S2. SIMS oxygen isotope (S2-1) and EPMA major chemical element compositions (S2-2) in calcite from the investigated samples of the Samail ophiolite.

Table S3. SIMS oxygen isotope compositions of serpentine and talc reference materials along with the calibration of matrix effects in serpentine (S3-1 to S3-3) and EPMA major chemical element compositions of the UWT-1talc reference material (S3-4).

Table S4. Calculation of serpentine-water fractionation factors.

References

Barnes, I., O´Neil, J.R., Trescases, J.J., 1978. Present day serpentinization in New Caledonia, Oman and Yugoslavia. Geochimica et Cosmochimica Acta 42, 144–145.

Barnes, J.D., Beltrando, M., Lee, C.T.A., Cisneros, M., Loewy, S., Chin, E., 2014. Geochemistry of Alpine serpentinites from rifting to subduction: A view across paleogeographic domains and metamorphic grade. Chemical Geology 389, 29–47.

Barnes, J.D., Paulick, H., Sharp, Z.D., Bach, W., Beaudoin, G., 2009. Stable isotope ($\delta^{18}O$, δD, $\delta^{37}Cl$) evidence for multiple fluid histories in mid-Atlantic abyssal peridotites (ODP Leg 209). Lithos 110, 83–94.

Beinlich, A., Plümper, O., Boter, E., Müller, I.A., Kourim, F., Ziegler, M., Harigane, Y., Lafay, R., Kelemen, P.B., 2020. Ultramafic Rock Carbonation: Constraints From Listvenite Core BT1B, Oman Drilling Project. Journal of Geophysical Research: Solid Earth 125.

Boudier, F., Baronnet, A., Mainprice, D., 2010. Serpentine mineral replacements of natural olivine and their seismic implications: Oceanic lizardite versus subduction-related antigorite. Journal of Petrology 51, 495–512.

Boudier, F., Coleman, R.G., 1981. Cross section through the peridotite in the Semail ophiolite. Journal of Geophysical Research 86, 2573–2592.

Bristow, T.F., Bonifacie, M., Derkowski, A., Eiler, J.M., Grotzinger, J.P., 2011. A hydrothermal origin for isotopically anomalous cap dolostone cements from south China. Nature 474 (7349), 68–71.

Cannaò, E., Agostini, S., Scambelluri, M., Tonarini, S., Godard, M., 2015. B, Sr and Pb isotope geochemistry of high-pressure Alpine metaperidotites monitors fluidmediated element recycling during serpentinite dehydration in subduction mélange (Cima di Gagnone, Swiss Central Alps). Geochimica et Cosmochimica Acta 163, 80–100.

Chacko, T., Cole, D.R., Horita, J., 2001. Equilibrium oxygen, hydrogen and carbon isotope fractionation factors applicable to geologic systems. Reviews in Mineralogy and Geochemistry, 43, 1–81.

Clayton, R.N., 1981. Isotopic thermometry. In: Newton, R.C., Navrostky, A., Wood, B.J. (eds), The thermodynamics of minerals and melts. Springer-Verlag, Berlin, p. 85–109.

Clayton, R.N., Goldsmith, J.R., Mayeda, T.K., 1989. Oxygen isotope fractionation in quartz, albite, anorthite, and calcite. Geoch. Cosmoch. Acta 53, 725–733.

Clayton, R.N., O´Neil, J.R., Mayeda, T.K., 1972. Oxygen isotope exchange between quartz and water. J. Geophys. Res. 77, 3057–3067.

Coleman, R. G., 1981. Tectonic setting for ophiolite obduction in Oman. Journal of Geophysical Research, 86, 2497–2508.

Coleman, R.G., Hopson, C.A., 1981. Introduction to the Oman Ophiolite special issue. J. Geophys. Res. Solid Earth 86 (B4), 2495–2496.

Cowan, R.J., Searle, M.P., Waters, D.J., 2014. Structure of the metamorphic sole to the Oman ophiolite, Sumeini window and Wadi Tayyin: Implications for ophiolite obduction processes. Geological Society, London, Special Publications, 392, 155–175.

Debret, B., Bolfan-Casanova, N., Padrón-Navarta, J.A., Martin-Hernandez, F., Andreani, M., Garrido, C.J., López, S.-V., Gómez-Pugnaire, M.T., Muñoz, M., Trcera, N., 2015. Redox state of iron during high-pressure serpentinite dehydration. Contributions to Mineralogy and Petrology, 169, 1–18.

Dennis, K.J., Schrag, D.P., 2010. Clumped isotope thermometry of carbonatites as an indicator of diagenetic alteration. Geochim. Cosmochim. Acta 74 (14), 4110–4122.

de Obeso, J.C., Kelemen, P.B., 2018. Fluid rock interactions on residual mantle peridotites overlain by shallow oceanic limestones: Insights from Wadi Fins, Sultanate of Oman. Chemical Geology 498, 139–149.

de Obeso, J.C., Kelemen, P.B., Leong, J.M., Menzel, M.D., Manning, C.E., Godard, M., Cai, Y., Bolge, L., 2022. Deep Sourced Fluids for Peridotite Carbonation in the Shallow Mantle Wedge of a Fossil Subduction Zone: Sr and C Isotope Profiles of OmanDP Hole BT1B. Journal of Geophysical Research: Solid Earth 127.

Deschamps, F., Godard, M., Guillot, S., Chauvel, C., Andreani, M., Hattori, K., Wunder, B., France, L., 2012. Behavior of fluid-mobile elements in serpentines from abyssal to subduction environments: Examples from Cuba and Dominican Republic. Chemical Geology 312–313, 93–117.

Deschamps, F., Guillot, S., Godard, M., Andreani, M., Hattori, K., 2011. Serpentinites act as sponges for fluid-mobile elements in abyssal and subduction zone environments. Terra Nova 23, 171–178.

Deschamps, F., Guillot, S., Godard, M., Chauvel, C., Andreani, M., Hattori, K., 2010. In situ characterization of serpentinites from forearc mantle wedges: Timing of serpentinization and behavior of fluid-mobile elements in subduction zones. Chemical Geology 269, 262–277.

Dewandel, B., Boudier, F., Kern, H., Warsi, W., Mainprice, D., 2003. Seismic wave velocity and anisotropy of serpentinized peridotite in the Oman ophiolite. Tectonophysics 370, 77–94.

Donovan, J.J., Kremser, D., Fournelle, J., Goemann, K., 2019. Probe for EPMA – User's guide and reference manual. Probe Software Inc. (Eugene), 429pp.

Ellison, E.T., Templeton, A.S., Zeigler, S.D., Mayhew, L.E., Kelemen, P.B., Matter, J.M., 2021. Low-Temperature Hydrogen Formation During Aqueous Alteration of Serpentinized Peridotite in the Samail Ophiolite. Journal of Geophysical Research: Solid Earth 126.

Evans, B.W., 2004. The Serpentinite Multisystem Revisited: Chrysotile Is Metastable. International Geology Review 46, 479–506.

Evans, B.W., Dyar, M.D., Kuehner, S.M., 2012. Implications of ferrous and ferric iron in antigorite. American Mineralogist, 97, 184–196.

Evans, B.W., Kuehner, S.M., Chopelas, A., 2009. Magnetite-free, yellow lizardite serpentinization of olivine websterite, Canyon Mountain complex, N.E. Oregon. American Mineralogist, 94, 1731–1734.

Falk, E.S., Guo, W., Paukert, A.N., Matter, J.M., Mervine, E.M., Kelemen, P.B., 2016. Controls on the stable isotope compositions of travertine from hyperalkaline springs in Oman: Insights from clumped isotope measurements. Geochimica et Cosmochimica Acta 192, 1–28.

Falk, E.S., Kelemen, P.B., 2015. Geochemistry and petrology of listvenite in the Samail ophiolite, Sultanate of Oman: Complete carbonation of peridotite during ophiolite emplacement. Geochimica et Cosmochimica Acta 160, 70–90.

Friedman, I., O´Neil, J.R., 1977. Compilation of stable isotope fractionation factors of geochemical interest. U.S. Geol. Surv. Prof. Paper 440–KK, Washington, D.C. (67 pp.).

Früh-Green, G.L., Connolly, J.A.D., Plas, A., Kelley, D.S., Grobéty, B., 2004. Serpentinization of oceanic peridotites: implications for geochemical cycles and biological activity. In: Wilcock, W.S.D., Delong, E.F., Kelley, D.S., Baross, J.A., Cary, S.C. (Eds.), The Subseafloor Biosphere at Mid-Ocean Ridges, Geophysical Monograph Series 144, pp. 119–136.

Früh-Green, G.L., Kelley, D.S., Bernasconi, S.M., Karson, J.A., Ludwig, K.A., Butterfield, D.A., Boschi, C., Proskurowski, G., 2003. 30,000 Years of hydrothermal activity at the Lost City vent field. Science 301, 495–498.

Früh-Green, G.L., Plas, A., Lécuyer, C., 1996. Petrologic and stable isotope constraints on hydrothermal alteration and serpentinization of the EPR shallow mantle at Hess Deep (site 895). In: Mével, C., Gillis, K.M., Allan, J.F., Meyer, P.S. (Eds.), Proceedings of the Ocean Drilling Program, Scientific Results 147, 255–291.

Früh-Green, G.L., Scambelluri, M., Vallis, F., 2001. O-H isotope ratios of high pressure ultramafic rocks: Implications for fluid sources and mobility in the subducted hydrous mantle. Contributions to Mineralogy and Petrology 141, 145–159.

Früh-Green, G.L., Weissert, H., Bernoulli, D., 1990. A multiple fluid history recorded in Alpine ophiolites. Journal of the Geological Society of London 147, 959–970.

Garlick, G.D., 1969. The stable isotopes of oxygen. Handbook of geochemistry (ed. K. Wedehohl, p. 1–27. Berlin-Heidelberg-New York: Springer 1969.

Ghosh, P., Adkins, J., Affek, H., Balta, B., Guo, W., Schauble, E.A., Schrag, D., Eiler, J.M., 2006. ^{13}C-^{18}O bonds in carbonate minerals: a new kind of paleothermometer. Geochim. Cosmochim. Acta 70 (6), 1439–1456.

Glennie, K.W., Boeuf, M.G.A., Hughes-Clarke, M.W., Moody-Stuart, M., Pilaar, W.F.H., Reinhardt, B.M., 1974. Geology of the Oman Mountains.

Verhandelingen Koninklijk Nederlands Geologisch-Mijnbouwkundig Genootschap, 31, 1–423.

Godard, M., Carter, E.J., Decrausaz, T., Lafay, R., Bennett, E., Kourim, F., de Obeso, J. -C., Michibayashi, K., Harris, M., Coggon, J.A., Teagle, D.A.H., Kelemen, P.B., 2021. Geochemical Profiles Across the Listvenite-Metamorphic Transition in the Basal Megathrust of the Semail Ophiolite: Results From Drilling at OmanDP Hole BT1B. Journal of Geophysical Research: Solid Earth 126(12).

Godard, M., Jousselin, D., Bodinier, J.-L., 2000. Relationships between geochemistry and structure beneath a palaeo-spreading centre: A study of the mantle section in the Oman ophiolite. Earth and Planetary Science Letters, 180(1–2), 133–148.

Golyshev, S.I., Padalko, N.L., Pechenkin, S.A., 1981. Fractionation of stable isotopes in carbonate systems. Geochem. Int'l. 18(5), 85–99

Hacker, B.R., Mosenfelder, J.L., 1996. Metamorphism and deformation along the emplacement thrust of the Samail ophiolite, Oman. Earth and Planetary Science Letters, 144, 435–451.

Hacker, B.R., Mosenfelder, J.L., Gnos, E., 1996. Rapid emplacement of the Oman ophiolite: Thermal and geochronologic constraints. Tectonics, 15, 1230–1247.

Hanghøj, K., Kelemen, P.B., Hassler, D., Godard, M., 2010. Composition and Genesis of Depleted Mantle Peridotites from the Wadi Tayin Massif, Oman Ophiolite; Major and Trace Element Geochemistry, and Os Isotope and PGE Systematics. Journal of Petrology, 51(1–2), 201–227.

Hoefs, J., 2018. Stable isotope geochemistry (8th edition). Springer (Berlin), 437pp.

Hopson, C.A., Coleman, R.G., Gregory, R.T., Pallister, J.S., Bailey, E.H., 1981. Geologic section through the Samail Ophiolite and associated rocks along a

Muscat-Ibra Transect, southeastern Oman Mountains. Journal of Geophysical Research: Solid Earth, 86(B4), 2527–2544.

Horita, J., 2005. Stable isotope thermometry: there is more to it than temperature. Geoch. Journal 39, 481–496.

Horita, J., Cole, D.R., Polyakov, V.B., Driesner, T., 2002. Experimental and theoretical study of pressure effects on hydrogen isotope fractionation in the system brucite-water at elevated temperatures. Geochim. Cosmochim. Acta 66, 3769–3788.

Horita, J., Driesner, T., Cole, D.R., 1999. Pressure effect on hydrogen isotope fractionation between brucite and water at elevated temperatures. Science 286, 1545–1547.

Hu, G., Clayton, R.N., 2003. Oxygen isotope salt effects at high pressure and high temperature and the calibration of oxygen isotope geothermometers. Geoch. Cosmoch. Acta 67(17), 3227–3246.

John, T., Scambelluri, M., Frische, M., Barnes, J.D., Bach, W., 2011. Dehydration of subducting serpentinite: Implications for halogen mobility in subduction zones and the deep halogen cycle. Earth and Planetary Science Letters 308, 65–76.

Kelemen, P.B., Aines, R., Bennett, E., Benson, S.M., Carter, E., Coggon, J.A., de Obeso, J.C., Evans, O., Gadikota, G., Dipple, G.M., Godard, M., et al., 2018. In situ carbon mineralization in ultramafic rocks: Natural processes and possible engineered methods. Energy Procedia 146, 92–102.

Kelemen, P.B., de Obeso, J.C., Leong, J.A., Godard, M., Okazaki, K., Kotowski, A. J., et al., 2022. Listvenite Formation During Mass Transfer into the Leading Edge of the Mantle Wedge: Initial Results from Oman Drilling Project Hole BT1B. Journal of Geophysical Research: Solid Earth, 127(2), 1–38.

Kelemen, P.B., Leong, J.A., de Obeso, J.C., Matter, J.M., Ellison, E.T., Templeton, A., et al., 2021. Initial results from the Oman Drilling Project Multi-Borehole Observatory: Petrogenesis and ongoing alteration of mantle peridotite in the weathering horizon. Journal of Geophysical Research: Solid Earth, 1–52.

Kelemen, P.B., Matter, J., Streit, E.E., Rudge, J.F., Curry, W.B., Blusztajn, J., 2011. Rates and mechanisms of mineral carbonation in peridotite: natural processes and recipes for enhanced, in situ CO_2 capture and storage. Annual Review of Earth and Planetary Sciences 39, 545–576.

Kelemen, P.B., Matter, J.M., Teagle, D.A.H., Coggon, J.A., and the Oman Drilling Science Team, 2020. Proceedings of the Oman Drilling Project: College Station, TX (International Ocean Discovery Program). doi:10.14379/Oman.ph1-2.proc.2020, and specific chapters therein. 2020 (4+1+3+2 +3 …).

Kelly, J.L., Fu, B., Kita, N.T., Valley, J.W., 2007. Optically continuous silcrete quartz cements of the St. Peter Sandstone: High precision oxygen isotope analysis by ion microprobe. Geochimica et Cosmochimica Acta 71, 3812–3832.

Kieffer, S.W., 1982. Thermodynamic and lattice vibrations of minerals: 4. Application to phase equilibria, isotope fractionation, and high pressure thermodynamics properties. Rev. Geophys. Space Phys. 20, 827–849.

Kim, S.-T., O´Neil, J.R., 1997. Equilibrium and nonequilibrium oxygen isotope effects in synthetic carbonates. Geoch. Cosmoc. Acta 61, 3461–3475

Kita, N.T., Ushikubo, T., Fu, B., Valley, J.W., 2009. High precision SIMS oxygen isotope analysis and the effect of sample topography. Chemical Geology 264, 43–57.

Klein, F., Humphris, S.E., Guo, W., Schubotz, F., Schwarzenbach, E.M., Orsi, W.D., 2015. Fluid mixing and the deep biosphere of a fossil Lost City-type hydrothermal system at the Iberia Margin. Proceedings of the National Academy of Sciences of the United States of America 112(39), 12036–12041.

Kohn, M.J., Valley, J.W., 1998. Effect of cation substitution in garnet and pyroxene on equilibrium oxygen isotope fractionation. J. Metam. Geol. 16, 625–639.

Kotowski, A.J., Cloos, M., Stockli, D.F. and Bos Orent, E., 2021. Structural and thermal evolution of an infant subduction shear zone: Insights from sub-ophiolite metamorphic rocks recovered from Oman Drilling Project Site BT-1B. Journal of Geophysical Research: Solid Earth, 126(12), e2021JB021702

Kozdon, R., Ushikubo, T., Kita, N.T., Spicuzza, M., Valley, J.W., 2009. Intratest oxygen isotope variability in the planktonic foraminifer N. pachyderma: Real vs. apparent vital effects by ion microprobe. Chemical Geology 258, 327–337.

Lafay, R., Deschamps, F., Schwartz, S., Guillot, S., Godard, M., Debret, B., Nicollet, C., 2013. High-pressure serpentinites, a trap-and-release system controlled by metamorphic conditions: Example from the Piedmont zone of the western Alps. Chemical Geology 343, 38–54.

Ligang, Z., Jingxiu, L., Huanbo, Z., Zhensheng, C., 1989. Oxygen isotope fractionation in the quartz-water-salt system. Economic Geology 84(6), 1643–1650

Lippard, S.J., Shelton, A.W., Gass, I.G., 1986. The ophiolite of the Northern Oman. Geological Society, London, Memoirs, 11(1), 1–16.

Ludwig, K.A., Kelley, D.S., Butterfield, D.A., Nelson, B.K., Früh-Green, G., 2006. Formation and evolution of carbonate chimneys at the Lost City Hydrothermal Field. Geochimica et Cosmochimica Acta 70, 3625–3645.

Matsuhisa, Y., Goldsmith, J.R., Clayton, R.N., 1979. Oxygen isotopic fractionation in the system quartz-albite-anorthite-water; Geochim. Cosmochim. Acta 43, 1131–1140.

Matthews, A., Backinsale, R.D., 1979. Oxygen isotope equilibration systematics between quartz and water. Am. Mineral. 64(1–2), 232–240

Matthews, A., Goldsmith, J.R., Clayton, R.N., 1983. Oxygen isotope fractionations involving pyroxenes: the calibration of mineral-pair geothermometers. Geoch. Cosmoch. Acta 47, 631–644.

Mayhew, L.E., Ellison, E.T., 2020. A synthesis and meta-analysis of the Fe chemistry of serpentinites and serpentine minerals. Phil. Trans. R. Soc. A 378: 20180420.

Mayhew, L.E., Ellison, E.T., McCollom, T.M., Trainor, T.P., Templeton, A.S., 2013. Hydrogen generation from low-temperature water-rock reactions. Nature Geoscience 6, 478–484.

Menzel, M.D., Urai, J.L., de Obeso, J.C., Kotowski, A., Manning, C.E., Kelemen, P.B., Kettermann, M., Jesus, A.P., Harigane, Y., 2020. Brittle Deformation of Carbonated Peridotite—Insights From Listvenites of the Samail Ophiolite (Oman Drilling Project Hole BT1B). Journal of Geophysical Research: Solid Earth 125.

Mével, C., 2003. Serpentinization of abyssal peridotites at mid-ocean ridges. C.R. Geoscience 335, 825–852.

Miller, H.M., Matter, J.M., Kelemen, P., Ellison, E.T., Conrad, M.E., Fierer, N., Ruchala, T., Tominaga, M., Templeton, A.S., 2016. Modern water/rock reactions in Oman hyperalkaline peridotite aquifers and implications for microbial habitability. Geochimica et Cosmochimica Acta 179, 217–241.

Mineev, S.D., Grinenko, V.A., 1996. The pressure influence on hydrogen isotopes fractionation in the serpentine-water system. V M Goldschmidt Conf. Abstract 1, 404.

Monnier, C., Girardeau, J., Le Mée, L., Polvé, M., 2006. Along-ridge petrological segmentation of the mantle in the Oman ophiolite. Geochemistry, Geophysics, Geosystems, 7(11), 1–51.

Nasir, S., Al Sayigh, A.R., Al Harthy, A., Al-Khirbash, S., Al-Jaaidi, O., Musllam, A., et al., 2007. Mineralogical and geochemical characterization of listwaenite from the Semail ophiolite, Oman. Geochemistry, 67(3), 213–228.

Neal, C., Stanger, G., 1984. Calcium and magnesium hydroxide precipitation from alkaline groundwaters in Oman, and their significance to the process of serpentinization. Mineralogical Magazine, 48, 237–241.

Neal, C., Stanger, G., 1985. Past and present serpentinisation of ultramafic rocks: An example from the Semail ophiolite nappe of northern Oman. The Chemistry of Weathering, 149, 249–275.

Nicolas, A., Boudier, F., Ildefonse, B., 1996. Variable crustal thickness in the Oman ophiolite: Implication for oceanic crust. Journal of Geophysical Research: Solid Earth, 101(B8), 17941–17950.

Nicolas, A., Boudier, F., Ildefonse, B., Ball, E., 2000. Accretion of Oman and United Arab Emirates ophiolite: Discussion of a new structural map. Marine Geophysical Research, 21, 147–179.

Noël, J., Godard, M., Oliot, E., Martinez, I., Williams, M., Boudier, F., Rodriguez, O., Chaduteau, C., Escario, S., Gouze, P., 2018. Evidence of polygenetic carbon trapping in the Oman Ophiolite: Petro-structural, geochemical, and carbon and oxygen isotope study of the Wadi Dima harzburgite-hosted carbonates (Wadi Tayin massif, Sultanate of Oman). Lithos 323, 218–237.

Nolan, S.C., Skelton, P.W., Clissold, B.P., Smewing, J.D., 1990. Maastrichtian to early Tertiary stratigraphy and palaeogeography of the Central and Northern Oman Mountains. Geol. Soc. Lond., Spec. Publ. 49 (1), 495–519.

O´Neil, J.R., Taylor, H.P. Jr., 1967. The oxygen isotope and cation exchange chemistry of feldspars. J. Geophys. Res. 74, 6012-6022

O´Neil, J.R., Taylor, H.P. Jr., 1969. Oxygen isotope equilibrium between muscovite and water. Am. Mineral. 52, 1414-1437.

O´Neil, J.R., Clayton, R.N., Mayeda, T.K., 1969. Oxygen isotope fractionation in divalent metal carbonates. Journal of Chemical Physics, 51, 5547–5558.

Padrón-Navarta, J.A., Sánchez-Vizcaíno, V.L., Garrido, C.J., Gómez-Pugnaire, M.T., 2011. Metamorphic record of high-pressure dehydration of antigorite serpentinite to chlorite harzburgite in a subduction setting (Cerro del Almirez, Nevado-Filábride complex, Southern Spain). Journal of Petrology 52(10), 2047–2078.

Padrón-Navarta, J.A., Sánchez-Vizcaíno, Hermann, J., Connolly, J.A.D., Garrido, C.J., Gómez-Pugnaire, M.T., Marchesi, C., 2013. Tschermak´s substitution in antigorite and consequences for phase relations and water liberation in high-grade serpentinites. Lithos 178, 186–196.

Pollington, A.D., Kozdon, R., Anovitz, L.M., Georg, R.B., Spicuzza, M.J., Valley, J.W., 2016. Experimental calibration of silicon and oxygen isotope fractionations between quartz and water at 250 °C by in situ microanalysis of experimental products and application to zoned low δ^{30}Si quartz overgrowths. Chemical Geology 421, 127–142

Polyakov, V.B., Kharlashina, N.N., 1994. Effect of pressure on equilibrium isotopic fractionation. Geoch. Cosmoch. Acta 58, 4739–4750.

Racey, A., 1995. Lithostratigraphy and larger foraminiferal (Nummulitid) biostratigraphy of the Tertiary of northern Oman. Micropaleontology 41, 1–123.

Rioux, M., Bowring, S., Kelemen, P., Gordon, S., Dudás, F., Miller, R., 2012. Rapid crustal accretion and magma assimilation in the Oman-U.A.E. ophiolite: High precision U-Pb zircon geochronology of the gabbroic crust. Journal of Geophysical Research, 117, B07201.

Rioux, M., Bowring, S., Kelemen, P., Gordon, S., Miller, R., Dudás, F., 2013. Tectonic development of the Samail ophiolite: High-precision U-Pb zircon geochronology and Sm-Nd isotopic constraints on crustal growth and emplacement. Journal of Geophysical Research: Solid Earth 118, 2085–2101.

Rioux, M., Garber, J., Bauer, A., Bowring, S., Searle, M., Kelemen, P., Hacker, B., 2016. Synchronous formation of the metamorphic sole and igneous crust of the Semail ophiolite: New constraints on the tectonic evolution during ophiolite formation from high-precision U–Pb zircon geochronology. Earth and Planetary Science Letters, 451, 185–195.

Rouméjon, S., Cannat, M., 2014. Serpentinization of mantle-derived peridotites at mid-ocean ridges: Mesh texture development in the context of tectonic exhumation. Geochemistry, Geophysics, Geosystems 15, 2354–2379.

Rouméjon, S., Williams, M.J., Früh-Green, G.L., 2018. In-situ oxygen isotope analyses in serpentine minerals: Constraints on serpentinization during tectonic exhumation at slow- and ultraslow-spreading ridges. Lithos 323, 156–173.

Saccocia, P.J., Seewald, J.S., Shanks, W.C., 2009. Oxygen and hydrogen isotope fractionation in serpentine-water and talc-water systems from 250 to 450 °C, 50 MPa. Geochimica et Cosmochimica Acta 73, 6789–6804.

Savin, S.M., Lee, M., 1988. Isotopic studies of phyllosilicates. In: Bailey S.W. (ed.), Hydrous phyllosilicates. Reviews in Mineralogy, 19, 189–223.

Scambelluri, M., Fiebig, J., Malaspina, N., Müntener, O., Pettke, T., 2004. Serpentinite Subduction: Implications for Fluid Processes and Trace-Element Recycling. International Geology Review 46, 595–613.

Schwarzenbach, E.M., Früh-Green, G.L., Bernasconi, S.M., Alt, J.C., Plas, A., 2013. Serpentinization and carbon sequestration: A study of two ancient peridotite-hosted hydrothermal systems. Chemical Geology 351, 115–133.

Schwarzenbach, E.M., Gill, B.C., Gazel, E., Madrigal, P., 2016. Sulfur and carbon geochemistry of the Santa Elena peridotites: Comparing oceanic and continental processes during peridotite alteration. Lithos 252–253, 92–108.

Scicchitano, M.R., Lafay, R., Valley, J.W., Kita, N.T., Nachlas, W.O., 2022. Protracted hydrothermal alteration recorded at the microscale in the Chenaillet ophicarbonates (Western Alps): Insights from in situ $\delta^{18}O$ thermometry in serpentine, carbonate and magnetite. Geochimica et Cosmochimica Acta 318, 144–164.

Scicchitano, M.R., Rubatto, D., Hermann, J., Shen, T., Padrón-Navarta, J.A., Williams, I.S., Zheng, Y.-F., 2018. Oxygen isotopes analysis of serpentine minerals by SHRIMP: analytical developments and geological applications. Geostandards and Geoanalytical Research 42, 459–479.

Scicchitano, M.R., Spicuzza, M.J., Ellison, E.T., Tuschel, D., Templeton, A.S., Valley, J.W., 2021. In Situ Oxygen Isotope Determination in Serpentine

Minerals by SIMS: Addressing Matrix Effects and Providing New Insights on Serpentinisation at Hole BA1B (Samail ophiolite, Oman). Geostandards and Geoanalytical Research 45, 161–187.

Searle, M., Cox, J., 1999. Tectonic setting, origin, and obduction of the Oman ophiolite. Geological Society of America Bulletin 111(1), 104–122.

Searle, M., Cox, J., 2002. Subduction zone metamorphism during formation and emplacement of the Semail ophiolite in the Oman Mountains. Geological Magazine, 139, 241–255.

Searle, M.P., Malpas, J., 1980. The structure and metamorphism of rocks beneath the Semail ophiolite of Oman and their significance in ophiolite obduction. Transactions of the Royal Society of Edinburgh: Earth Sciences, 71(4), 247–262.

Searle, M.P., Waters, D.J., Garber, J.M., Rioux, M., Cherry, A.G., Ambrose, T.K., 2015. Structure and metamorphism beneath the obducting Oman ophiolite: Evidence from the Bani Hamid granulites, northern Oman mountains. Geosphere, 11(6), 1812–1836.

Sharp, Z.D., Gibbons, J.A., Maltsev, O., Atudorei, V., Pack, A., Sengupta, S., Shock, E.L., Knauth, L.P., 2016. A calibration of the triple oxygen isotope fractionation in the SiO_2–H_2O system and applications to natural samples. Geoch. Cosmoch. Acta 186, 105–119.

Sharp, Z., Kirschner, D., 1994. Quartz-calcite oxygen isotope thermometry: a calibration based on natural isotopic variations. Geochim. Cosmochim. Acta, 58, 4491–4501.

Skelton, A.D.L., Valley, J.W., 2000. The relative timing of serpentinisation and mantle exhumation at the ocean-continent transition, Iberia: constraints from oxygen isotopes. Earth and Planetary Science Letters 178, 327–338.

Śliwiński, M.G., Kitajima, K., Kozdon, R., Spicuzza, M.J., Fournelle, J.H., Denny, A., Valley, J.W., 2016. Secondary Ion Mass Spectrometry Bias on Isotope Ratios in Dolomite–Ankerite, Part I: $\delta^{18}O$ Matrix Effects. Geostandards and Geoanalytical Research 40, 157–172.

Soret, M., Agard, P., Dubacq, B., Plunder, A., Yamato, P., 2017. Petrological evidence for stepwise accretion of metamorphic soles during subduction infancy (Semail ophiolite, Oman and UAE). Journal of Metamorphic Geology, 35(9), 1051–1080.

Stanger, G., 1985. Silicified serpentinite in the Semail nappe of Oman. Lithos, 18, 13–22.

Streit, E., Kelemen, P., Eiler, J., 2012. Coexisting serpentine and quartz from carbonate-bearing serpentinized peridotite in the Samail Ophiolite, Oman. Contributions to Mineralogy and Petrology 164, 821–837.

Templeton, A.S., Ellison, E.T., Glombitza, C., Morono, Y., Rempfert, K.R., Hoehler, T.M., Zeigler, S.D., Kraus, E.A., Spear, J.R., Nothaft, D.B., Fones, E.M., Boyd, E.S., Munro-Ehrlich, M., Mayhew, L.E., Cardace, D., Matter, J.M., Kelemen, P.B., 2021. Accessing the Subsurface Biosphere Within Rocks Undergoing Active Low-Temperature Serpentinization in the Samail Ophiolite (Oman Drilling Project). Journal of Geophysical Research: Biogeosciences 126(10), e2021JG006315.

Urey, H.C., 1947. The thermodynamic properties of isotopic substances. J. Chem. Soc. (London), p. 562-581.

Valley, J. W., 2001. Stable isotope thermometry at high temperatures. Reviews in Mineralogy and Geochemistry, 43, 365–413.

Valley, J.W., Kita, N.T., 2009. In situ oxygen isotope geochemistry by ion microprobe. Mineralogical Association of Canada Shortcourse Series 41, 19–63.

Warren, C.J., Parrish, R.R., Waters, D.J., Searle, M.P., 2005. Dating the geologic history of Oman's Semail ophiolite: Insights from U-Pb geochronology. Contributions to Mineralogy and Petrology, 150(4), 403–422.

Wenner, D.B., Taylor, H.P., 1971. Temperatures of serpentinization of ultramafic rocks based on O^{18}/O^{16} fractionation between coexisting serpentine and magnetite. Contributions to Mineralogy and Petrology, 32, 165–185.

Wenner, D.B., Taylor, H.P., 1973. Oxygen and hydrogen isotope studies of the serpentinization of ultramafic rocks in oceanic environments and continental ophiolite complexes. American Journal of Science, 273, 207–239.

Wyns, R., Bechennec, F., Le Meteour, J., Roger, J., 1992. Explanatory Notes to the Geological Map of the Tiwi Quadrangle, Sultanate of Oman. Geoscience Map, Scale 1:100,000, Sheet NF 40-8B. Ministry of Petroleum and Minerals, Directorate General of Minerals, Sultanate of Oman.

Zhang, M., Fukuda, K., Spicuzza, M.J., Siron, G., Heimann, A., Kita, N.T., Ushikubo, T., Valley, J.W., 2022. SIMS matrix effects in oxygen isotope analysis of olivine and pyroxene: Application to Acfer 094 chondrite chondrules and the primitive chondrule minerals (PCM) line. Chem Geol. 608, 121016.

Zheng, Y.-F., 1993a. Calculation of oxygen isotope fractionation in hydroxyl-bearing silicates. Earth and Planetary Science Letters 121, 247–263.

Zheng, Y.-F., 1993b. Calculation of oxygen isotope fractionation in anhydrous silicate minerals. Geoch. Cosmoch. Acta 57, 1079–1091.

Tables

Table 1

Summary of SIMS data measured in the investigated mineral pairs and calculated oxygen isotope fractionations.

Sample ID	Locality	*T* (°C)*	$\delta^{18}O_{V\text{-}SMOW}$ (‰) calcite			$\delta^{18}O_{V\text{-}SMOW}$ (‰) serpentine			$\delta^{18}O_{V\text{-}SMOW}$ (‰) quartz			$\delta^{18}O_{V\text{-}SMOW}$ (‰) talc		
			average	*n*	2s	average	*n*	2s	average	*n*	2s	average	*n*	2s
OM13-13	Wadi Fins	25	26.1	30	2.0	12.6	14	0.7	-	-	-	-	-	-
OM13-17A	Wadi Fins	41	27.3	29	1.3	10.5	25	0.9	-	-	-	-	-	-
OM13-14A	Wadi Fins	44	27.3	15	2.2	12.1	11	0.7	-	-	-	-	-	-
OM13-11	Wadi Fins	50	27.6	37	0.9	13.8	26	1.5	-	-	-	-	-	-
OM09-12	MoD	100	-	-	-	9.4	18	0.8	24.5	20	0.7	-	-	-
OM10-02	MoD	100	-	-	-	9.0	16	0.7	-	-	-	12.9	10	0.8

* Temperature estimates are calculated from clumped isotope thermometry in de Obeso and Kelemen (2018) for the Wadi Fins samples (see their Table 1, after Bristow et al. 2011), and a compilation of clumped isotope data from Falk and Kelemen (2015) and Beinlich et al. (2020) for the MoD samples (see Kelemen et al., 2022).

Oxygen isotopes in calcite, serpentine, talc, and quartz are averages from SIMS data (complete dataset shown in Tables S1 to S3). Oxygen isotope fractionations between serpentine-talc, serpentine-quartz and serpentine-calcite are calculated from SIMS data.

Oxygen isotope fractionations between calcite-water (OM13-13, OM13-17A, OM13-14A and OM13-11), quartz-water (OM09-12) and talc-water (OM10-02) are average from multiple calibrations available in the literature (see Table S4 for details).

Serpentine-water oxygen isotope fractionations are calculated combining the mineral-serpentine fractionations measured by SIMS with the mineral-water fractionations available in the literature (see text and Table S4 for more details). The best fit of such data yields an A-factor of 1.04±0.2 (2SE) as a function of $1/T^2$ (Fig. 6).

Table 1.

Continue.

Sample ID	1000 ln $\alpha^{18}O_{(Mineral\text{-}Serpentine)}$ (‰)			1000 ln $\alpha^{18}O_{(Mineral\text{-}Water)}$ (‰)			1000 ln $\alpha^{18}O_{(Serpentine\text{-}Water)}$ (‰)		
	average	2s	2SE	average	2s	2SE	average	2s	2SE
OM13-13	13.2	1.0	0.3	28.1	0.5	0.3	14.7	1.1	0.4
OM13-17A	16.6	1.7	0.3	25.0	0.5	0.3	8.3	1.8	0.4
OM13-14A	15.0	1.3	0.4	24.5	0.5	0.3	9.3	1.4	0.5
OM13-11	13.6	0.9	0.2	23.5	0.5	0.3	9.8	1.0	0.3
OM09-12	15.0	1.1	0.3	20.9	2.5	0.8	5.8	2.7	0.8
OM10-02	3.8	0.9	0.3	13.5	0.2	0.1	9.6	0.9	0.3

Figure captions

Fig. 1. Simplified geological map of the Samail ophiolite in Oman and the United Arab Emirates (UAE). Samples for this study come from Wadi Fins (red star) and MoD Mountain (red square). Modified after Nicolas et al. (2009).

Fig. 2. SEM-BSE images of representative textures in samples OM09-12 (a-d) and OM10-02 (e-f) from MoD, Oman. Location of SIMS pits (white circles) and corresponding $\delta^{18}O$ values (‰, V-SMOW) are shown in (a), (e) and (f). Crossed circles are outliers. Atg–antigorite, Qtz–quartz, Dol–dolomite, Fe-Ox–Fe-oxide, Mgs–magnesite, Tlc–talc, Srp–serpentine, Ctl–chrysotile.

Fig. 3. SEM-BSE images of representative textures in samples OM13-11 (a-b), OM13-13 (c-d), OM13-14A (e-f) and OM13-17A (g-h) from Wadi Fins, Oman. Location of SIMS pits (white circles) and corresponding $\delta^{18}O$ values (‰, V-SMOW) are shown. Crossed circles are outliers. Dol–dolomite, Srp–serpentine, Ctl–chrysotile, Lz–lizardite, Cal–calcite.

Fig. 4. Oxygen isotopes measured by SIMS (expressed on the V-SMOW scale) in co-crystallized pairs of serpentine + quartz (a) and serpentine + talc (b) in MoD samples (Oman ophiolite). The average oxygen isotope fractionation values ($\Delta^{18}O$) are also shown (yellow circle and solid line). Error bars are 2σ values (Table S1).

Fig. 5. Oxygen isotopes measured by SIMS (expressed on the V-SMOW scale) in co-crystallized pairs of serpentine + calcite in four samples from Wadi Fins (Oman

ophiolite). The average oxygen isotope fractionation values ($\Delta^{18}O$) are also shown (yellow circle and solid line). Error bars are 2σ values for serpentine (Table S1) and 2s for calcite (Table S2).

Fig. 6. Oxygen isotope fractionations between serpentine and water calculated combining the average $\Delta^{18}O$(mineral-serpentine) measured by SIMS (shown in Fig. 4 and 5) with mineral-water fractionations available in the literature (Table S4). The large horizontal error bars are due to the large uncertainties on temperature (i.e., ± 46 °C for MoD and ± 20 °C for Wadi Fins). The vertical error bars are calculated by propagating the 2SE of the average $\Delta^{18}O$(mineral-serpentine) measured by SIMS and the 2SE of the average mineral-water fractionation factors resulting from multiple calibrations (Table 1).

Fig. 7. Comparison of different calibrations of the oxygen isotope fractionation between serpentine and water. The orange boxes indicate the range in serpentine-water fractionation factors (see Table S4) and temperature (including the uncertainties of ± 46 °C for MoD and ± 20 °C for Wadi Fins) for the two sets of samples investigated in this study.

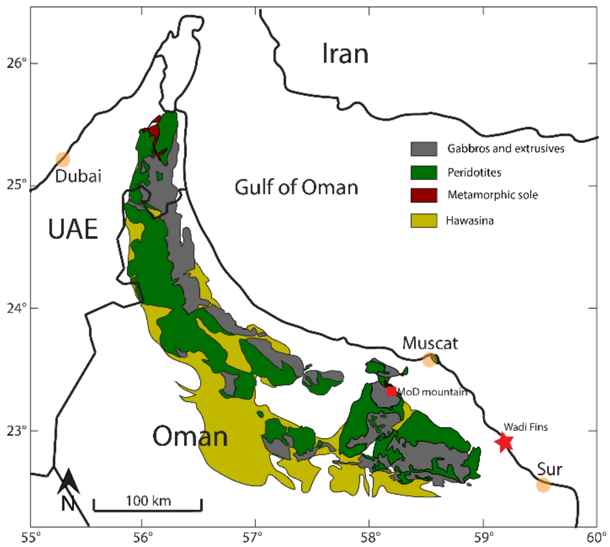

Fig. 1. Simplified geological map of the Samail ophiolite in Oman and the United Arab Emirates (UAE). Samples for this study come from Wadi Fins (red star) and MoD Mountain (red square). Modified after Nicolas et al. (2009).

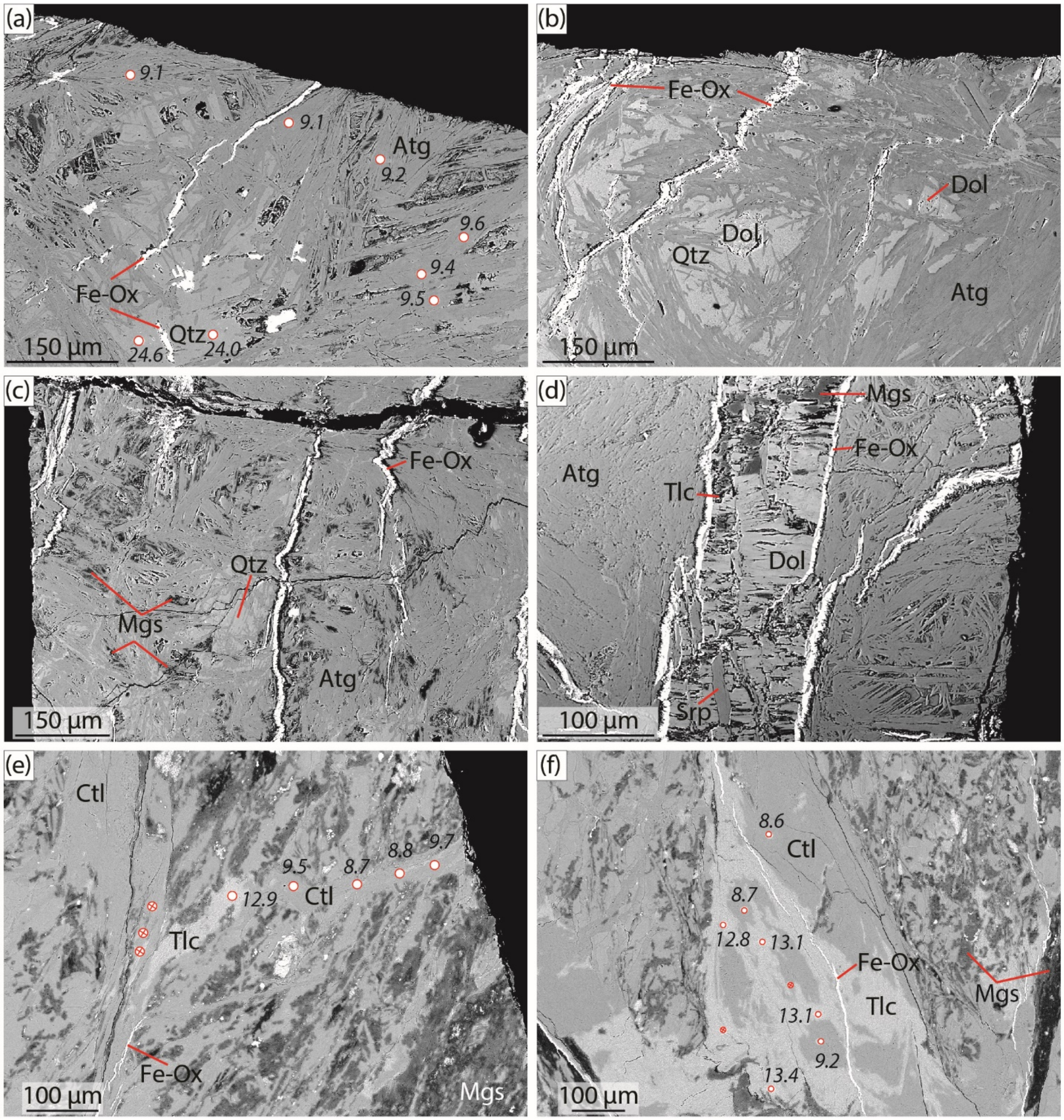

Fig. 2. SEM-BSE images of representative textures in samples OM09-12 (a-d) and OM10-02 (e-f) from MoD, Oman. Location of SIMS pits (white circles) and corresponding $\delta^{18}O$ values (‰, V-SMOW) are shown in (a), (e) and (f). Crossed circles are outliers. Atg–antigorite, Qtz–quartz, Dol–dolomite, Fe-Ox–Fe-oxide, Mgs–magnesite, Tlc–talc, Srp–serpentine, Ctl–chrysotile.

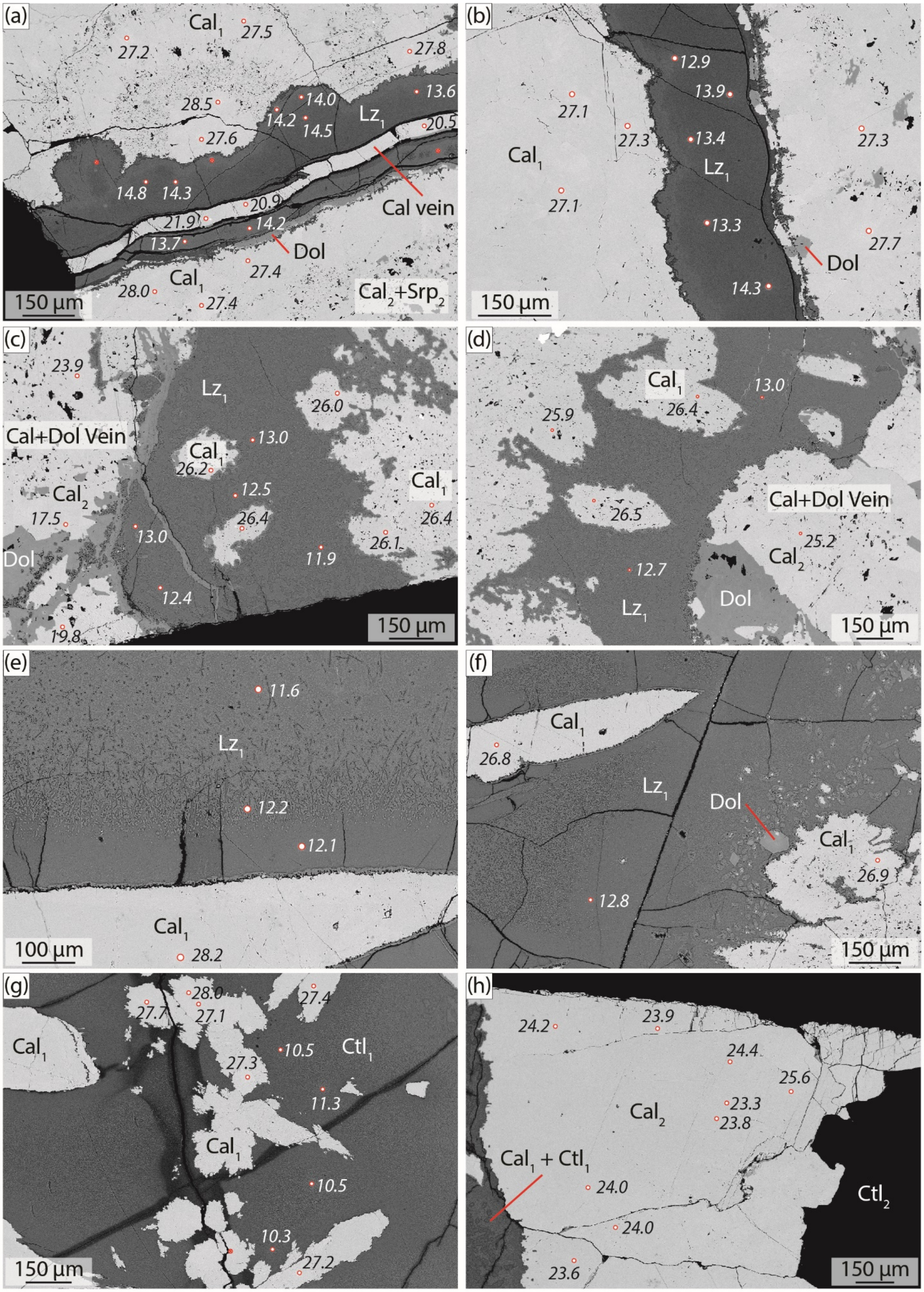
(a)
Cal1
27.5
27.2
27.8
28.5
14.0
13.6
14.2
14.5
Lz1
20.5
27.6
14.8
14.3
Cal vein
20.9
21.9
14.2
13.7
Dol
27.4
Cal1
28.0
27.4
Cal2+Srp2
150 µm
(b)
12.9
13.9
27.1
27.3
13.4
27.3
Cal1
Lz1
27.1
13.3
27.7
Dol
14.3
150 µm
(c)
23.9
Lz1
26.0
Cal+Dol Vein
13.0
Cal1
26.2
Cal2
12.5
Cal1
26.4
17.5
13.0
26.4
26.1
11.9
Dol
12.4
150 µm
19.8
(d)
Cal1
13.0
26.4
25.9
Cal+Dol Vein
26.5
25.2
Cal2
12.7
Lz1
Dol
150 µm
(e)
11.6
Lz1
12.2
12.1
Cal1
100 µm
28.2
(f)
Cal1
26.8
Lz1
Dol
Cal1
26.9
12.8
150 µm
(g)
28.0
27.4
27.7
27.1
Cal1
10.5
Ctl1
27.3
11.3
Cal1
10.5
10.3
27.2
150 µm
(h)
24.2
23.9
24.4
25.6
Cal2
23.3
23.8
Cal1 + Ctl1
24.0
Ctl2
24.0
23.6
150 µm

Fig. 3. SEM-BSE images of representative textures in samples OM13-11 (a-b), OM13-13 (c-d), OM13-14A (e-f) and OM13-17A (g-h) from Wadi Fins, Oman. Location of SIMS pits (white circles) and corresponding $\delta^{18}O$ values (‰, V-SMOW) are shown. Crossed circles are outliers. Dol–dolomite, Srp–serpentine, Ctl–chrysotile, Lz–lizardite, Cal–calcite.

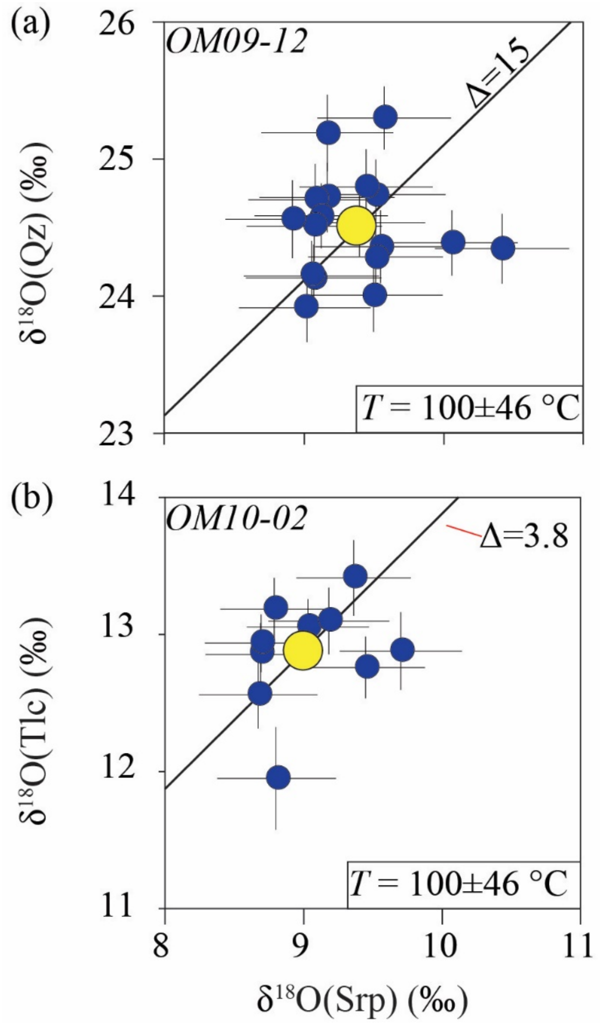

Fig. 4. Oxygen isotopes measured by SIMS (expressed on the V-SMOW scale) in co-crystallized pairs of serpentine + quartz (a) and serpentine + talc (b) in MoD samples (Oman ophiolite). The average oxygen isotope fractionation values ($\Delta^{18}O$) are also shown (yellow circle and solid line). Error bars are 2σ values (Table S1).

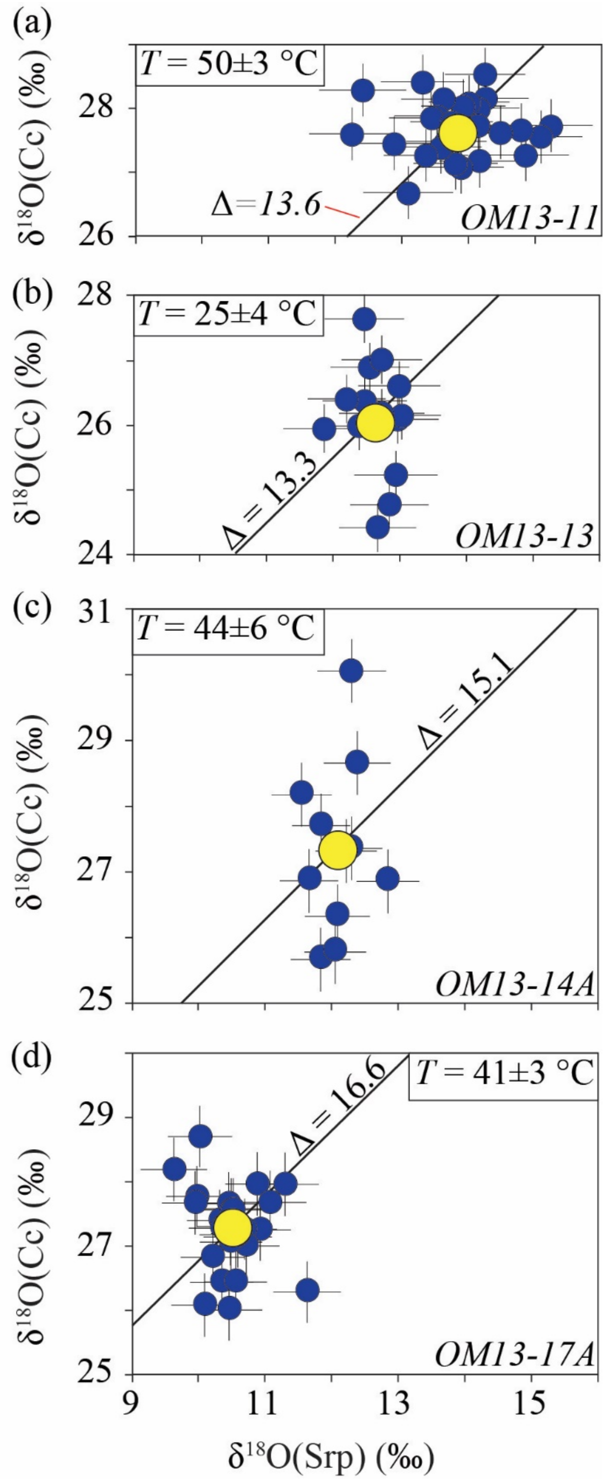

Fig. 5. Oxygen isotopes measured by SIMS (expressed on the V-SMOW scale) in co-crystallized pairs of serpentine + calcite in four samples from Wadi Fins (Oman ophiolite). The average oxygen isotope fractionation values ($\Delta^{18}O$) are also shown (yellow circle and solid line). Error bars are 2σ values for serpentine (Table S1) and 2s for calcite (Table S2).

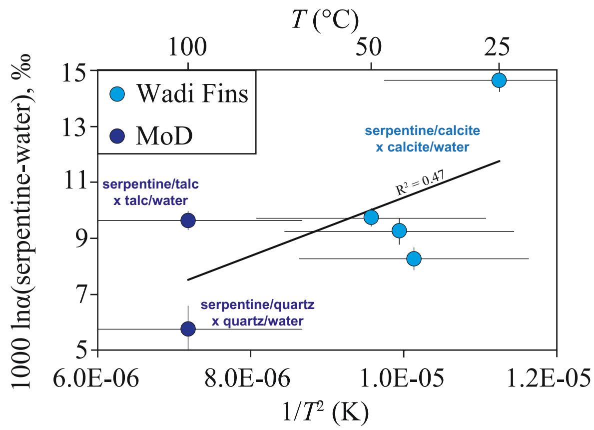

Fig. 6. Oxygen isotope fractionations between serpentine and water calculated combining the average $\Delta^{18}O$(mineral-serpentine) measured by SIMS (shown in Fig. 4 and 5) with mineral-water fractionations available in the literature (Table S4). The large horizontal error bars are due to the large uncertainties on temperature (i.e. ±46 °C for MoD and ±20 °C for Wadi Fins). The vertical error bars are calculated by propagating the 2SE of the average $\Delta^{18}O$(mineral-serpentine) measured by SIMS and the 2SE of the average mineral-water fractionation factors resulting from multiple calibrations (Table 1).

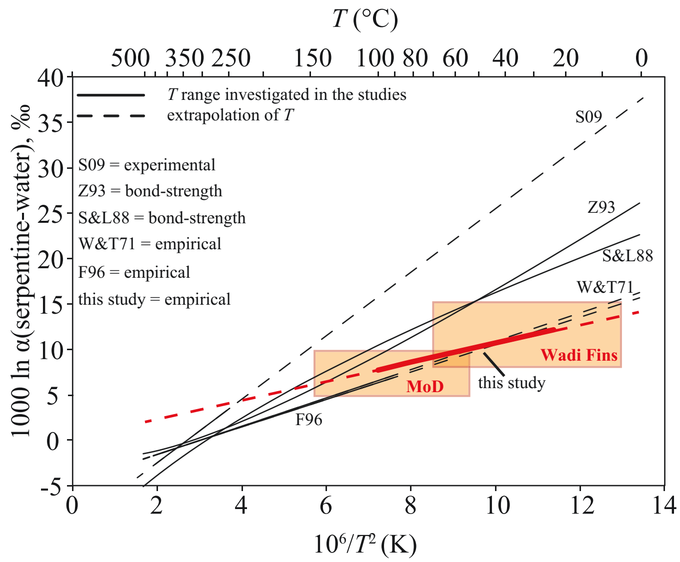

Fig. 7. Comparison of different calibrations of the oxygen isotope fractionation between serpentine and water. The orange boxes indicate the range in serpentine-water fractionation factors (see Table S4) and temperature (including the uncertainties of ±46 °C for MoD and ±20 °C for Wadi Fins) for the two sets of samples investigated in this study.

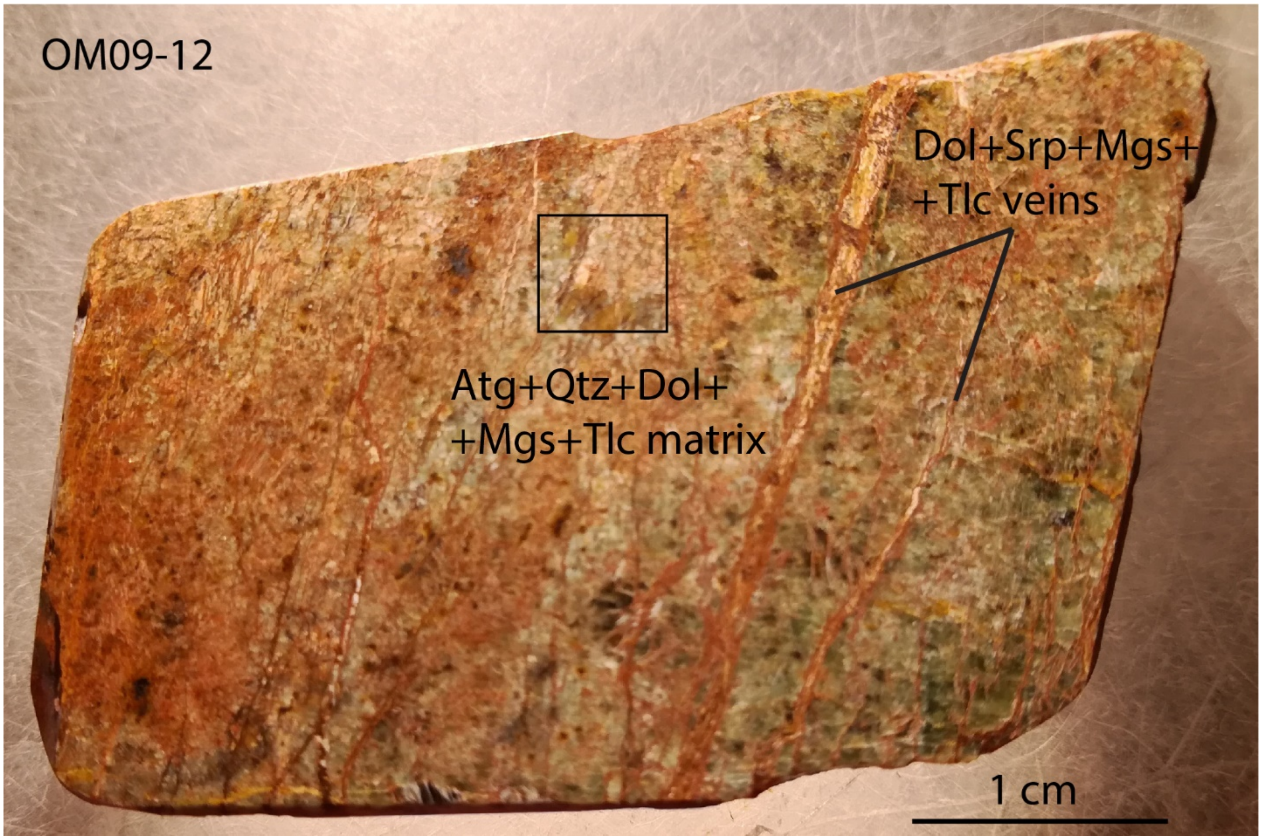

Fig. S1. Reflected light image of sample OM09-12 (MoD, Wadi Mansah, Oman). The square indicates the area targeted by SIMS. Atg–antigorite, Qtz–quartz, Dol–dolomite, Mgs–magnesite, Tlc–talc, Srp–serpentine.

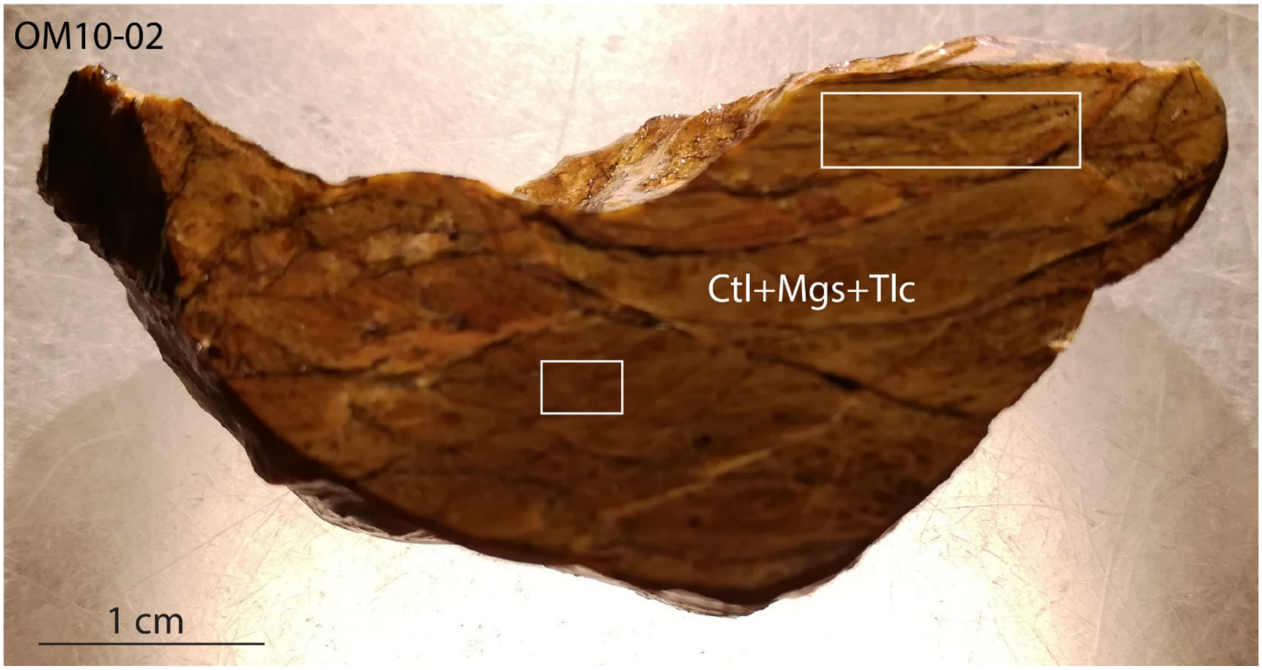

Fig. S2. Reflected light image of sample OM10-02 (MoD, Wadi Mansah, Oman). The squares indicate the areas targeted by SIMS. Mgs–magnesite, Tlc–talc, Ctl–chrysotile.

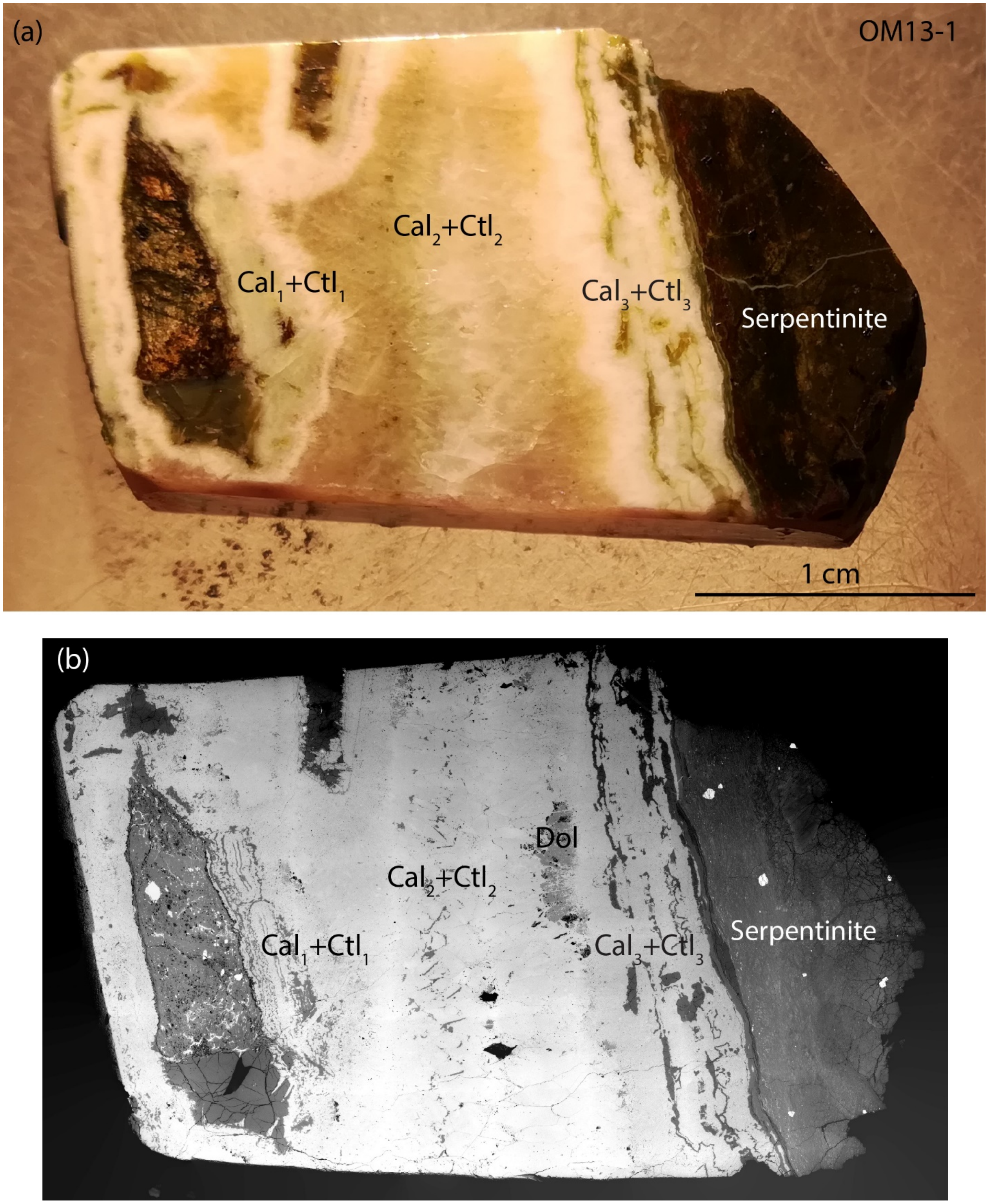

Fig. S3. (a) Reflected light and (b) SEM-BSE images of sample OM13-1 (Wadi Fins, Oman) showing different generations of calcite + serpentine in the vein. Cal–calcite, Ctl–chrysotile, Dol–dolomite.

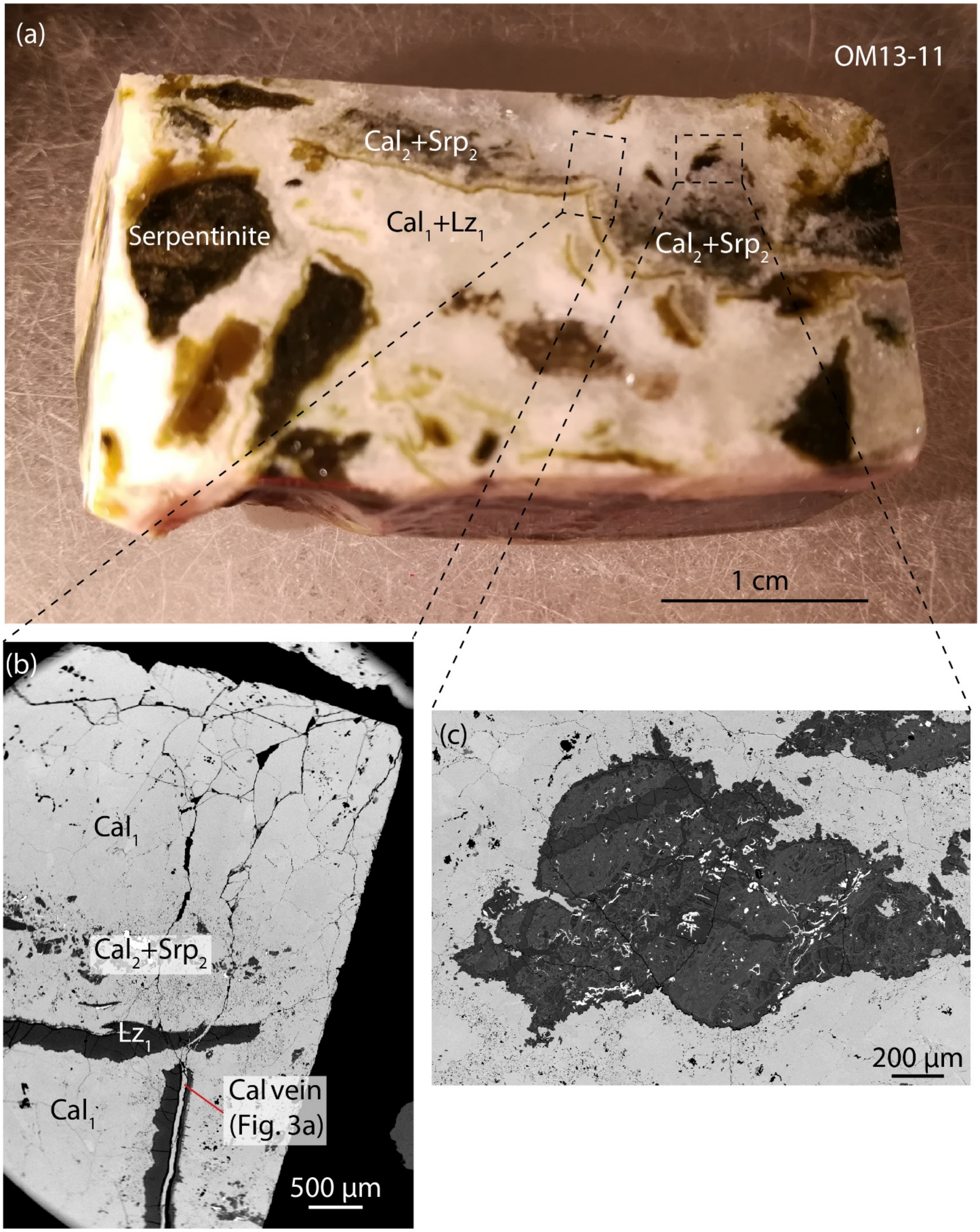

Fig. S4. (a) Reflected light and (b, c) SEM-BSE images of sample OM13-11 (Wadi Fins, Oman). Lizardite (Lz_1) in textural equilibrium with calcite (Cal_1) is crosscut by later calcite veins and appears as elongated grains as opposite to serpentine fragments (Cal_2+Srp_2) (b) or serpentinite blocks with complex mesh textures (c). Cal–calcite, Lz–lizardite, Srp–serpentine. The SEM-BSE image in (b) is rotated 90° relative to the higher resolution image shown in Fig. 3a.

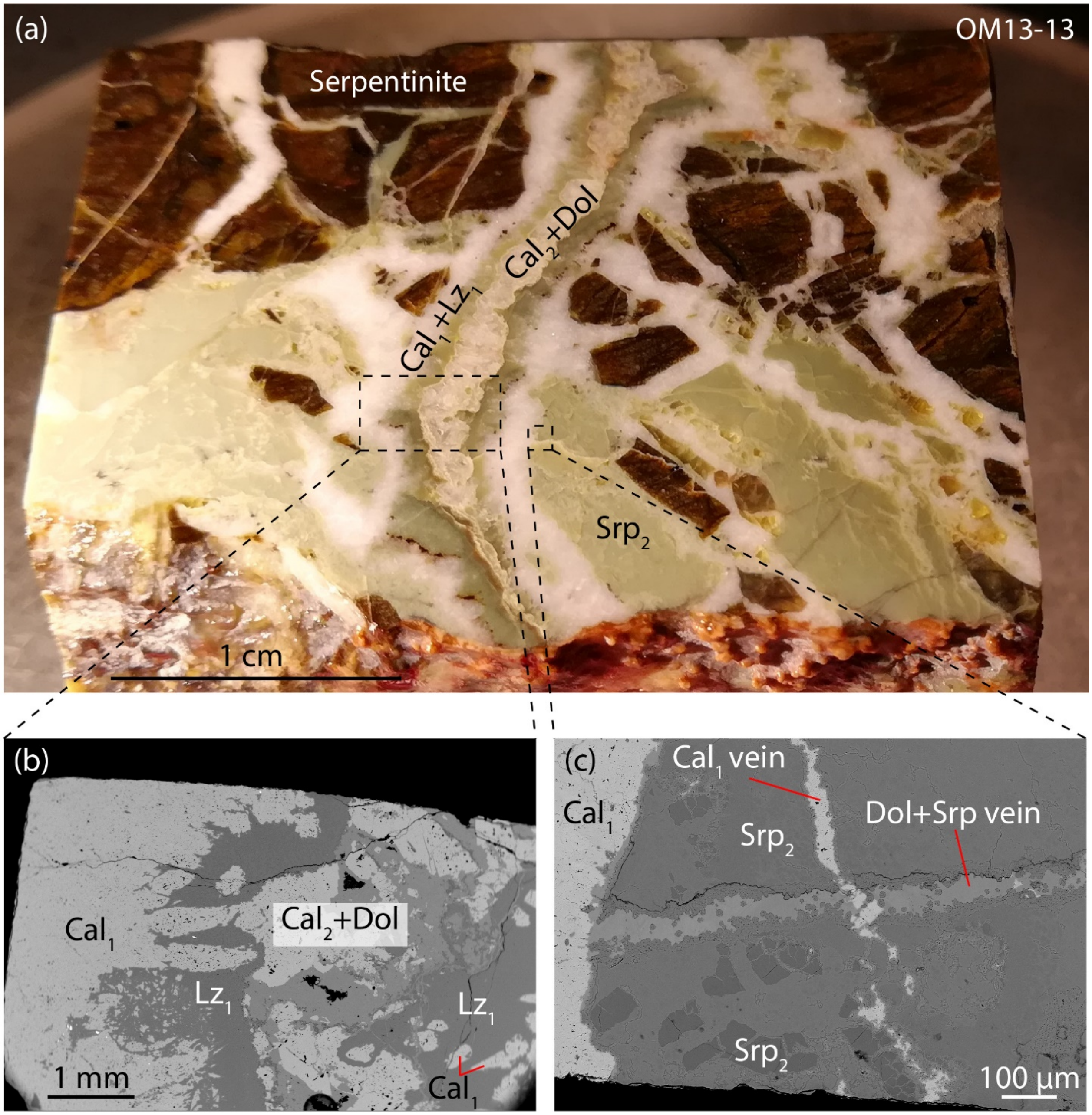

Fig. S5. (a) Reflected light and (b, c) SEM-BSE images of sample OM13-13 (Wadi Fins, Oman). Lizardite + calcite in textural equilibrium (Cal_1+Lz_1) is crosscut by a later calcite + dolomite vein (Cal_2+Dol). Serpentine fragments (Lz_2) are not in textural equilibrium with calcite (Cal_1) as evidenced by crosscutting relationships and relict of complex textures (c). Cal–calcite, Lz–lizardite, Dol–dolomite, Srp–serpentine.

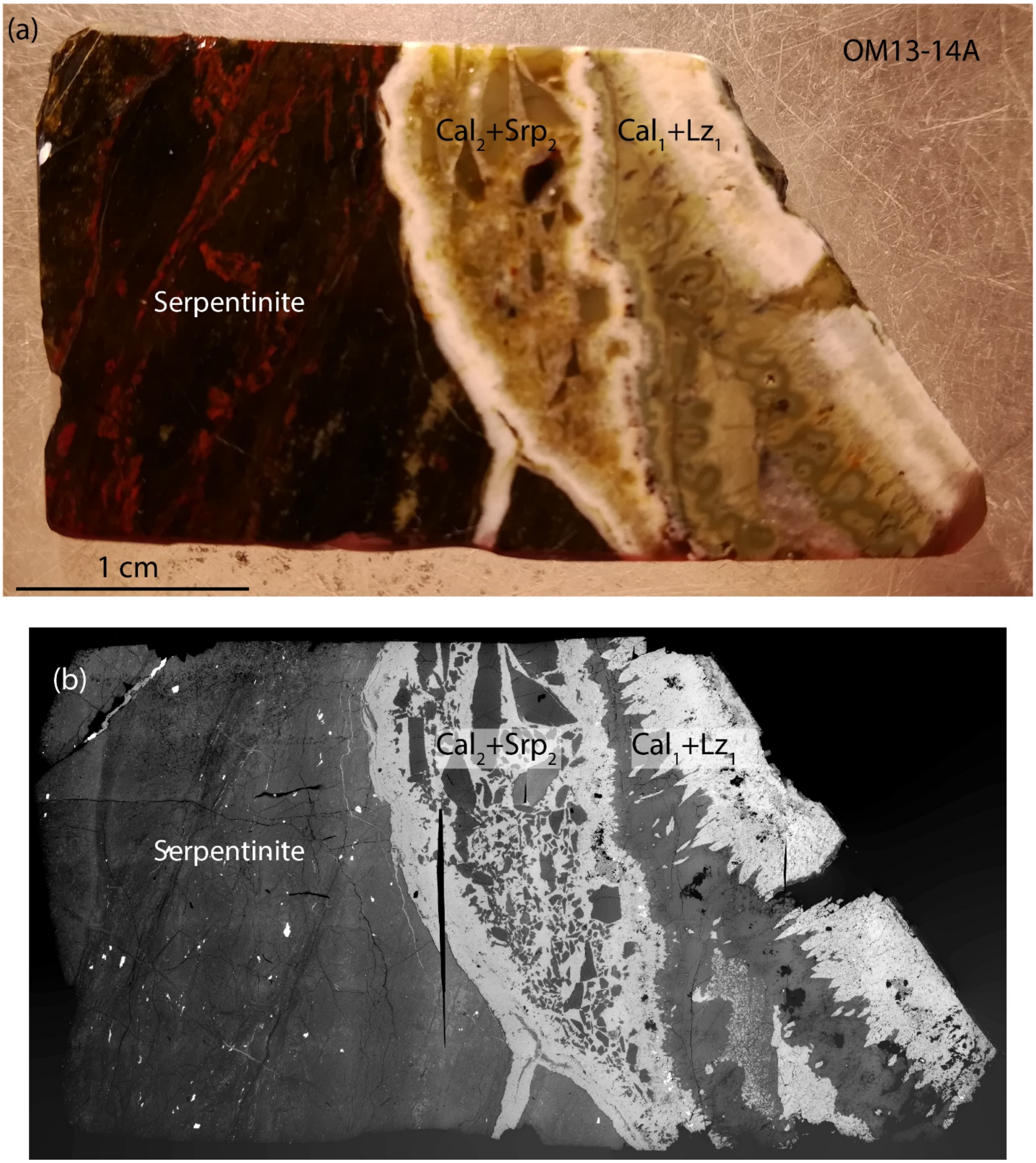

Fig. S6. (a) Reflected light and (b) SEM-BSE images of sample OM13-14A (Wadi Fins, Oman). Cal_1+Lz_1 are in textural equilibrium as opposite to Cal_2+Srp_2. Cal–calcite, Lz–lizardite, Srp–serpentine.

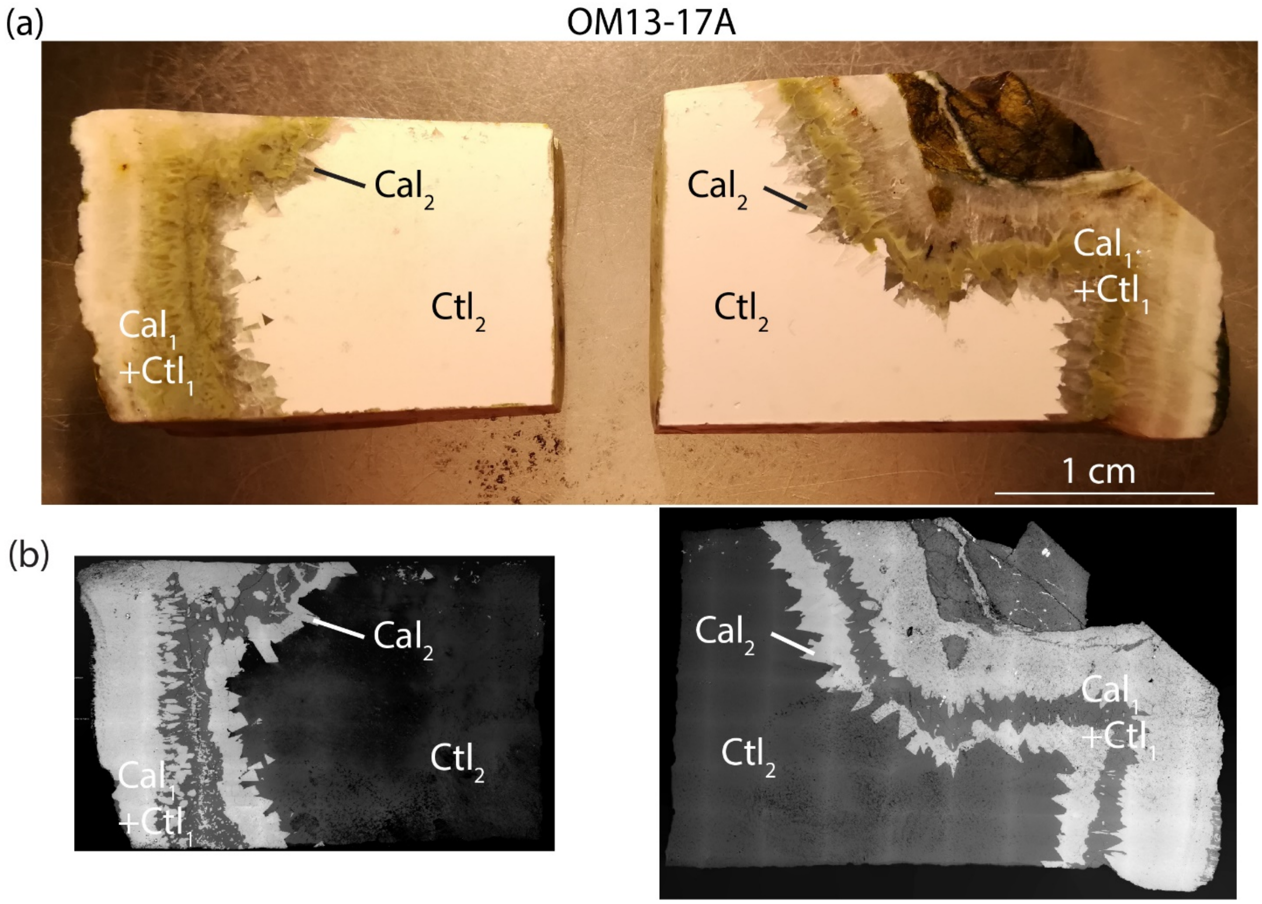

Fig. S7. (a) Reflected light and (b) SEM-BSE images of sample OM13-17A (Wadi Fins, Oman). Two rock billets were made to target this large vein. The vein is symmetric with a calcite + chrysotile assemblage on the outer edges (Cal$_1$+Ctl$_1$), a second calcite generation not coexisting with serpentine (Cal$_2$) and a second chrysotile generation not coexisting with carbonate in the center (Ctl$_2$). Cal–calcite, Ctl–chrysotile.

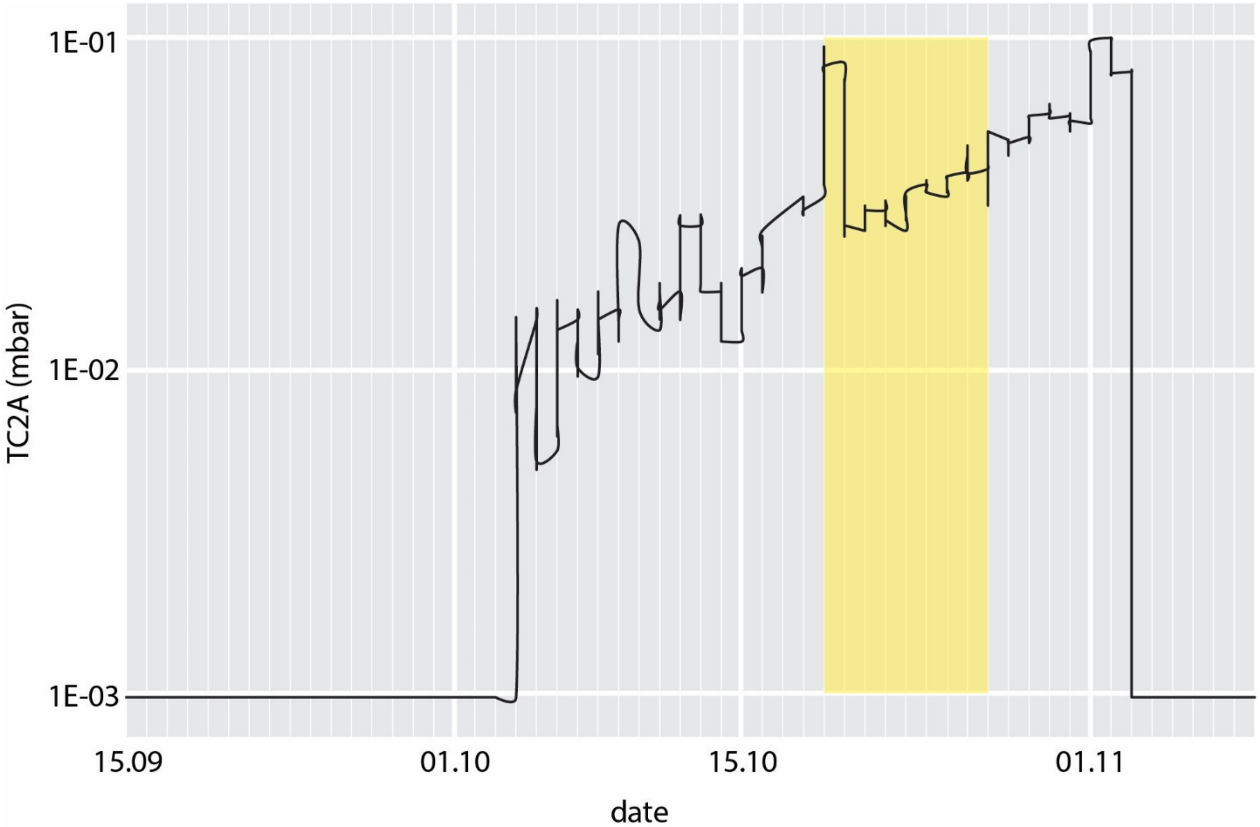

Fig. S8. Graph showing increase of the pre-amplifier pressure (TC2A) during the analytical session, from 19 to 27 of October 2020 (highlighted in yellow). Optimum pressure for stable analytical conditions is in the order of 1E-03 mbar.

SIMS session	Mount I.D.	File	Analysis I.D.
S1 (19-23 October 2020)			
	OM09-12		
	sample analysis		
		20201019@8	OM09-12-UWSrp-1-gr1
		20201019@8	OM09-12-UWSrp-1-gr1
		20201019@9	OM09-12-UWSrp-1-gr1
		20201019@9	OM09-12-UWSrp-1-gr1
		20201019@9	OM09-12-Srp-1
		20201019@9	OM09-12-Srp-2
		20201019@9	OM09-12-Srp-3
		20201019@9	OM09-12-Srp-4
		20201019@9	OM09-12-Srp-5
		20201019@9	OM09-12-Srp-6
		20201019@9	OM09-12-Srp-7
		20201019@9	OM09-12-Srp-8
		20201019@1	OM09-12-Srp-9
		20201019@1	OM09-12-Srp-10
		20201019@1	OM09-12-Srp-11
		20201019@1	OM09-12-Srp-12
		20201019@1	OM09-12-Srp-13
		20201019@1	OM09-12-Srp-14
		20201019@1	OM09-12-Srp-15
		20201019@1	OM09-12-Srp-16
		20201019@1	OM09-12-Srp-17
		20201019@1	OM09-12-Srp-18
		20201019@1	OM09-12-Srp-19
		20201019@1	OM09-12-Srp-20
			average and 2SD (Atg)
		20201019@1	OM09-12-UWSrp-1-gr1
		20201019@1	OM09-12-UWSrp-1-gr1
		20201019@1	OM09-12-UWSrp-1-gr1
		20201019@1	OM09-12-UWSrp-1-gr1
			average and 2SD
			bracket average and 2SD
			2SE
		20201019@1	OM09-12-UWQ-1

20201019@1	OM09-12-UWQ-1
20201019@1	OM09-12-UWQ-1
20201019@1	OM09-12-UWQ-1
20201019@1	OM09-12-Qtz-1
20201019@1	OM09-12-Qtz-2
20201019@1	OM09-12-Qtz-3
20201019@1	OM09-12-Qtz-4
20201019@1	OM09-12-Qtz-5
20201019@1	OM09-12-Qtz-6
20201019@1	OM09-12-Qtz-7
20201019@1	OM09-12-Qtz-8
20201019@1	OM09-12-Qtz-9
20201019@1	OM09-12-Qtz-10
20201019@1	OM09-12-Qtz-11
20201019@1	OM09-12-Qtz-12
20201019@1	OM09-12-Qtz-13
20201019@1	OM09-12-Qtz-14
20201019@1	OM09-12-Qtz-15
20201019@1	OM09-12-Qtz-16
20201019@1	OM09-12-Qtz-17
20201019@1	OM09-12-Qtz-18
20201019@1	OM09-12-Qtz-19
20201019@1	OM09-12-Qtz-20
	average and 2SD (Qtz)
20201019@1	OM09-12-UWQ-1
20201019@1	OM09-12-UWQ-1
20201019@1	OM09-12-UWQ-1
20201019@1	OM09-12-UWQ-1
	average and 2SD
	bracket average and 2SD
	2SE

OM13-1

sample analysis

20201019@1	OM13-1-UWSrp-1-gr1
20201019@1	OM13-1-UWSrp-1-gr1
20201019@1	OM13-1-UWSrp-1-gr1
20201019@1	OM13-1-UWSrp-1-gr1
20201019@1	OM13-1-UWSrp-1-gr1
20201019@1	OM13-1-Srp-1

20201019@1	OM13-1-Srp-2
20201019@1	OM13-1-Srp-3
20201019@1	OM13-1-Srp-4
20201019@1	OM13-1-Srp-5
20201019@1	OM13-1-Srp-6
20201019@1	OM13-1-Srp-7
20201019@1	OM13-1-Srp-8
20201019@1	OM13-1-Srp-9
20201019@1	OM13-1-Srp-10
20201019@1	OM13-1-Srp-11
20201019@1	OM13-1-Srp-12
20201019@1	OM13-1-Srp-13
20201019@1	OM13-1-Srp-14
20201019@1	OM13-1-Srp-15
20201019@1	OM13-1-UWSrp-1-gr1
20201019@1	OM13-1-UWSrp-1-gr1
20201019@1	OM13-1-UWSrp-1-gr1
20201019@1	OM13-1-UWSrp-1-gr1
20201019@1	OM13-1-UWSrp-1-gr1
20201019@1	OM13-1-UWSrp-1-gr1
	average and 2SD
	bracket average and 2SD
	2SE
20201019@1	OM13-1-Srp-16
20201019@1	OM13-1-Srp-17
20201019@1	OM13-1-Srp-18
20201019@1	OM13-1-Srp-19
20201019@1	OM13-1-Srp-20
20201019@1	OM13-1-Srp-21
20201019@1	OM13-1-Srp-22
20201019@1	OM13-1-Srp-23
20201019@1	OM13-1-Srp-24
20201019@1	OM13-1-Srp-25
20201019@1	OM13-1-Srp-26
20201019@1	OM13-1-Srp-27
20201019@1	OM13-1-Srp-28
20201019@1	OM13-1-Srp-29
20201019@1	OM13-1-Srp-30
	average and 2SD (Ctl I)
	average and 2SD (Ctl III)
	average and 2SD (Fe-Lz)

20201019@1	OM13-1-UWSrp-1-gr1
20201019@1	OM13-1-UWSrp-1-gr1
20201019@1	OM13-1-UWSrp-1-gr1
20201019@1	OM13-1-UWSrp-1-gr1
20201019@1	OM13-1-UWSrp-1-gr1
20201019@1	OM13-1-UWSrp-1-gr1
	average and 2SD
	bracket average and 2SD
	2SE

OM13-17A

sample analysis

20201019@1	OM13-17A-UWSrp-1-gr1
20201019@2	OM13-17A-UWSrp-1-gr1
20201019@2	OM13-17A-UWSrp-1-gr1
20201019@2	OM13-17A-UWSrp-1-gr1
20201019@2	OM13-17A-Srp-1
20201019@2	OM13-17A-Srp-2
20201019@2	OM13-17A-Srp-3
20201019@2	OM13-17A-Srp-4
20201019@2	OM13-17A-Srp-5
20201019@2	OM13-17A-Srp-6
20201019@2	OM13-17A-Srp-7
20201019@2	OM13-17A-Srp-8
20201019@2	OM13-17A-Srp-9
20201019@2	OM13-17A-Srp-10
20201019@2	OM13-17A-Srp-11
20201019@2	OM13-17A-Srp-12
20201019@2	OM13-17A-Srp-13
20201019@2	OM13-17A-Srp-14
20201019@2	OM13-17A-Srp-15
20201019@2	OM13-17A-Srp-16
20201019@2	OM13-17A-Srp-17
20201019@2	OM13-17A-Srp-18
20201019@2	OM13-17A-Srp-19
20201019@2	OM13-17A-Srp-20
20201019@2	OM13-17A-UWSrp-1-gr1
20201019@2	OM13-17A-UWSrp-1-gr1
20201019@2	OM13-17A-UWSrp-1-gr1
20201019@2	OM13-17A-UWSrp-1-gr1

	average and 2SD
	bracket average and 2SD
	2SE
20201019@2	OM13-17A-Srp-21
20201019@2	OM13-17A-Srp-22
20201019@2	OM13-17A-Srp-23
20201019@2	OM13-17A-Srp-24
20201019@2	OM13-17A-Srp-25
20201019@2	OM13-17A-Srp-26
20201019@2	OM13-17A-Srp-27
20201019@2	OM13-17A-Srp-28
20201019@2	OM13-17A-Srp-29
20201019@2	OM13-17A-Srp-30
20201019@2	OM13-17A-Srp-31
20201019@2	OM13-17A-Srp-32
20201019@2	OM13-17A-Srp-33
20201019@2	OM13-17A-Srp-34
20201019@2	OM13-17A-Srp-35
	average and 2SD (Ctl±Lz I)
20201019@2	OM13-17A-UWSrp-1-gr1
20201019@2	OM13-17A-UWSrp-1-gr1
20201019@2	OM13-17A-UWSrp-1-gr1
20201019@2	OM13-17A-UWSrp-1-gr1
	average and 2SD
	bracket average and 2SD
	2SE

S2 (24-27 October 2020)

OM13-11

sample analysis

20201019@1	OM13-11-UWSrp-1-gr2
20201019@1	OM13-11-UWSrp-1-gr2
20201019@1	OM13-11-UWSrp-1-gr2
20201019@1	OM13-11-UWSrp-1-gr2
20201019@1	OM13-11-Srp-1
20201019@1	OM13-11-Srp-2
20201019@1	OM13-11-Srp-3
20201019@1	OM13-11-Srp-4
20201019@1	OM13-11-Srp-5
20201019@1	OM13-11-Srp-6

20201019@1	OM13-11-Srp-7
20201019@1	OM13-11-Srp-8
20201019@1	OM13-11-Srp-9
20201019@1	OM13-11-Srp-10
20201019@1	OM13-11-UWSrp-1-gr2
20201019@1	OM13-11-UWSrp-1-gr2
20201019@1	OM13-11-UWSrp-1-gr2
20201019@1	OM13-11-UWSrp-1-gr2
	average and 2SD
	bracket average and 2SD
	2SE
20201019@1	OM13-11-Srp-11
20201019@1	OM13-11-Srp-12
20201019@1	OM13-11-Srp-13
20201019@1	OM13-11-Srp-14
20201019@1	OM13-11-Srp-15
20201019@1	OM13-11-Srp-16
20201019@1	OM13-11-Srp-17
20201019@1	OM13-11-Srp-18
20201019@1	OM13-11-Srp-19
20201019@1	OM13-11-Srp-20
20201019@1	OM13-11-UWSrp-1-gr2
20201019@1	OM13-11-UWSrp-1-gr2
20201019@1	OM13-11-UWSrp-1-gr2
20201019@1	OM13-11-UWSrp-1-gr2
	average and 2SD
	bracket average and 2SD
	2SE
20201019@1	OM13-11-Srp-21
20201019@1	OM13-11-Srp-22
20201019@1	OM13-11-Srp-23
20201019@1	OM13-11-Srp-24
20201019@1	OM13-11-Srp-25
20201019@1	OM13-11-Srp-26
20201019@1	OM13-11-Srp-27
20201019@1	OM13-11-Srp-28
20201019@1	OM13-11-Srp-29
20201019@1	OM13-11-Srp-30
20201019@1	OM13-11-Srp-31

20201019@1	OM13-11-Srp-32
20201019@1	OM13-11-Srp-33
20201019@1	OM13-11-Srp-34
20201019@1	OM13-11-Srp-35
	average and 2SD (Lz±Ctl I)

20201019@1	OM13-11-UWSrp-1-gr2
20201019@1	OM13-11-UWSrp-1-gr2
20201019@1	OM13-11-UWSrp-1-gr2
20201019@1	OM13-11-UWSrp-1-gr2
	average and 2SD
	bracket average and 2SD
	2SE

OM13-13

sample analysis

20201019@1	OM13-13-UWSrp-1-gr1
20201019@1	OM13-13-UWSrp-1-gr1
20201019@1	OM13-13-UWSrp-1-gr1
20201019@1	OM13-13-UWSrp-1-gr1
20201019@1	OM13-13-UWSrp-1-gr1
20201019@1	OM13-13-UWSrp-1-gr1

20201019@1	OM13-13-Srp-1
20201019@1	OM13-13-Srp-2
20201019@1	OM13-13-Srp-3
20201019@1	OM13-13-Srp-4
20201019@1	OM13-13-Srp-5
20201019@1	OM13-13-Srp-6
20201019@1	OM13-13-Srp-7
20201019@1	OM13-13-Srp-8
20201019@1	OM13-13-Srp-9
20201019@1	OM13-13-Srp-10
20201019@1	OM13-13-Srp-11
20201019@1	OM13-13-Srp-12
20201019@1	OM13-13-Srp-13
20201019@1	OM13-13-Srp-14
20201019@1	OM13-13-Srp-15
20201019@1	OM13-13-Srp-16
20201019@1	OM13-13-Srp-17
20201019@1	OM13-13-Srp-18
20201019@1	OM13-13-Srp-19
20201019@1	OM13-13-Srp-20

average and 2SD (Lz±Ctl I)
average and 2SD (Ctl II)

20201019@1 OM13-13-UWSrp-1-gr1
20201019@1 OM13-13-UWSrp-1-gr1
20201019@1 OM13-13-UWSrp-1-gr1
20201019@1 OM13-13-UWSrp-1-gr1

average and 2SD
bracket average and 2SD
2SE

OM13-14A

sample analysis

20201019@1 OM13-14A-UWSrp-1-gr2
20201019@1 OM13-14A-UWSrp-1-gr2
20201019@1 OM13-14A-UWSrp-1-gr2
20201019@1 OM13-14A-UWSrp-1-gr2

20201019@1 OM13-14A-Srp-1
20201019@1 OM13-14A-Srp-2
20201019@1 OM13-14A-Srp-3
20201019@1 OM13-14A-Srp-4
20201019@1 OM13-14A-Srp-5
20201019@1 OM13-14A-Srp-6
20201019@1 OM13-14A-Srp-7
20201019@1 OM13-14A-Srp-8
20201019@1 OM13-14A-Srp-9
20201019@1 OM13-14A-Srp-10
20201019@1 OM13-14A-Srp-11
20201019@1 OM13-14A-Srp-12
20201019@1 OM13-14A-Srp-13
20201019@1 OM13-14A-Srp-14
20201019@1 OM13-14A-Srp-15
20201019@1 OM13-14A-Srp-16
20201019@1 OM13-14A-Srp-17
20201019@1 OM13-14A-Srp-18
20201019@1 OM13-14A-Srp-19
20201019@1 OM13-14A-Srp-20

average and 2SD (Lz±Ctl I)
average and 2SD (Lz±Ctl II)

20201019@1 OM13-14A-UWSrp-1-gr2
20201019@1 OM13-14A-UWSrp-1-gr2

20201019@1	OM13-14A-UWSrp-1-gr2
20201019@1	OM13-14A-UWSrp-1-gr2
	average and 2SD
	bracket average and 2SD
	2SE

OM10-02

sample analysis

20201019@1	OM10-02-UWSrp-1-gr1
20201019@1	OM10-02-UWSrp-1-gr1
20201019@1	OM10-02-UWSrp-1-gr1
20201019@1	OM10-02-UWSrp-1-gr1
20201019@1	OM10-02-Srp-1
20201019@1	OM10-02-Srp-2
20201019@1	OM10-02-Srp-3
20201019@1	OM10-02-Srp-4
20201019@1	OM10-02-Srp-5
20201019@1	OM10-02-Srp-6
20201019@1	OM10-02-Srp-7
20201019@1	OM10-02-Srp-8
20201019@1	OM10-02-Srp-9
20201019@1	OM10-02-Srp-10
20201019@1	OM10-02-UWSrp-1-gr1
20201019@1	OM10-02-UWSrp-1-gr1
20201019@1	OM10-02-UWSrp-1-gr1
20201019@1	OM10-02-UWSrp-1-gr1
	average and 2SD
	bracket average and 2SD
	2SE
20201019@1	OM10-02-Srp-11
20201019@1	OM10-02-Srp-12
20201019@1	OM10-02-Srp-13
20201019@1	OM10-02-Srp-14
20201019@1	OM10-02-Srp-15
20201019@1	OM10-02-Srp-16
20201019@1	OM10-02-Srp-17
20201019@1	OM10-02-Srp-18
20201019@1	OM10-02-Srp-19
20201019@1	OM10-02-Srp-20
	average and 2SD (Ctl)

20201019@1	OM10-02-UWSrp-1-gr1
20201019@1	OM10-02-UWSrp-1-gr1
20201019@1	OM10-02-UWSrp-1-gr1
20201019@1	OM10-02-UWSrp-1-gr1
	average and 2SD
	bracket average and 2SD
	2SE
	bias* UWSrp-1 vs. UWC-3
	bias* UWC-3 vs. UWSrp-1
20201019@1	OM10-02-UWC-3-gr1
20201019@1	OM10-02-UWC-3-gr1
20201019@1	OM10-02-UWC-3-gr1
20201019@1	OM10-02-UWC-3-gr1
20201019@1	OM10-02-Tlc-1 (Srp-5b)
20201019@1	OM10-02-Tlc-2
20201019@1	OM10-02-Tlc-3
20201019@1	OM10-02-Tlc-4
20201019@1	OM10-02-Tlc-5
20201019@1	OM10-02-Tlc-6
20201019@1	OM10-02-Tlc-7
20201019@1	OM10-02-Tlc-8
20201019@1	OM10-02-Tlc-9
20201019@1	OM10-02-Tlc-10
20201019@1	OM10-02-UWC-3-gr1
20201019@1	OM10-02-UWC-3-gr1
20201019@1	OM10-02-UWC-3-gr1
20201019@1	OM10-02-UWC-3-gr1
	average and 2SD
	bracket average and 2SD
	2SE
20201019@1	OM10-02-Tlc-11
20201019@1	OM10-02-Tlc-12
20201019@1	OM10-02-Tlc-13
20201019@1	OM10-02-Tlc-14
20201019@1	OM10-02-Tlc-15
20201019@1	OM10-02-Tlc-16
20201019@1	OM10-02-Tlc-17
20201019@1	OM10-02-Tlc-18

20201019@1	OM10-02-Tlc-19
20201019@1	OM10-02-Tlc-20
	average and 2SD (Tlc)
20201019@1	OM10-02-UWC-3-gr1
20201019@1	OM10-02-UWC-3-gr1
20201019@1	OM10-02-UWC-3-gr1
20201019@1	OM10-02-UWC-3-gr1
	average and 2SD
	bracket average and 2SD
	2SE

Parameters for calculation of bias*(x) due to Mg/Fe (see Table S3 for details)

bias*(x) (‰) = ax^2 + b

Session S1:

x =	Mg# (mole %)
a =	0.096764
b =	-9.3793
2 RMSE (‰) =	0.41

Bias between lizardite and antigorite

bias*(x) (‰) =	-0.81
2σ (‰) =	0.48

Session S2:

x =	Mg# (mole %)
a =	0.116913
b =	-11.2253
2 RMSE (‰) =	0.31

Bias between lizardite and antigorite

bias*(x) (‰) =	-1.54
2σ (‰) =	0.44

Bias* Talc vs. UWC-3 = 10.30

Standard errors (2SE) of laser fluorination values for reference materials considered during calculation of 2σ

UWSrp-1 =	0.04	(see Scicchitano et al. 2020 GGR, Table 3)
L3431 =	0.10	(see Scicchitano et al. 2020 GGR, Table 3)
C22908 =	0.02	(see Scicchitano et al. 2020 GGR, Table 3)
UWG-2 =	0.01	(see Scicchitano et al. 2020 GGR, Table 3)
NBS-28 =	0.09	(see Scicchitano et al. 2020 GGR, Table 3)
UWC-3 =	0.02	(see Scicchitano et al. 2020 GGR, Table 3)
UWT1 (Talc) =	0.04	
UWQ-1 =	0.02	(see Kelly et al. 2007 Geoch. Cosmoch. Act

$\delta^{18}O$ ‰ (RAW)	2SE (int.)	Mg# (mole %)	Bias (‰)	$\delta^{18}O$ ‰ (V-SMOW)	2s (ext.)	2σ ‰
13.11	0.17					
13.41	0.15					
13.05	0.12					
13.38	0.10					
14.44	0.20	95.64	4.87	**9.52**	0.47	**0.50**
14.37	0.14	95.64	4.87	**9.45**	0.47	**0.48**
14.50	0.15	95.64	4.87	**9.58**	0.47	**0.48**
13.84	0.15	95.64	4.87	**8.93**	0.47	**0.48**
15.34	0.16	95.64	4.87	**10.42**	0.47	**0.48**
13.97	0.17	95.64	4.87	**9.06**	0.47	**0.48**
14.43	0.16	95.64	4.87	**9.52**	0.47	**0.48**
14.98	0.13	95.64	4.87	**10.06**	0.47	**0.47**
13.99	0.17	95.64	4.87	**9.08**	0.47	**0.48**
15.49	0.22					
16.79	0.12					
13.93	0.12	95.64	4.87	**9.01**	0.47	**0.47**
13.99	0.17	95.64	4.87	**9.08**	0.47	**0.48**
14.00	0.15	95.64	4.87	**9.09**	0.47	**0.48**
14.09	0.13	95.64	4.87	**9.18**	0.47	**0.47**
14.47	0.12	95.64	4.87	**9.56**	0.47	**0.47**
14.32	0.12	95.64	4.87	**9.41**	0.47	**0.47**
14.42	0.19	95.64	4.87	**9.51**	0.47	**0.49**
14.04	0.15	95.64	4.87	**9.13**	0.47	**0.48**
14.09	0.17	95.64	4.87	**9.17**	0.47	**0.48**
				9.4	**0.77**	
13.53	0.14					
13.62	0.17					
13.49	0.11					
13.73	0.20					
13.59	0.21					
13.41	**0.47**		**4.99**	**8.38**		
	0.17					
5.57	0.11					

5.41	0.19				
5.69	0.13				
5.52	0.18				
17.84	0.17		**24.7**	0.46	**0.26**
17.90	0.20		**24.8**	0.46	**0.28**
18.40	0.13		**25.3**	0.46	**0.23**
17.66	0.22		**24.6**	0.46	**0.29**
17.45	0.17		**24.4**	0.46	**0.25**
17.25	0.17		**24.2**	0.46	**0.26**
17.39	0.17		**24.3**	0.46	**0.25**
17.49	0.15		**24.4**	0.46	**0.24**
17.24	0.15		**24.1**	0.46	**0.24**
17.02	0.18		**23.9**	0.46	**0.26**
17.61	0.17		**24.5**	0.46	**0.25**
17.81	0.18		**24.7**	0.46	**0.26**
18.29	0.21		**25.2**	0.46	**0.28**
17.47	0.19		**24.4**	0.46	**0.27**
17.64	0.16		**24.5**	0.46	**0.25**
17.11	0.19		**24.0**	0.46	**0.27**
17.69	0.14		**24.6**	0.46	**0.24**
17.82	0.17		**24.7**	0.46	**0.25**
17.61	0.21		**24.5**	0.46	**0.28**
17.44	0.19		**24.3**	0.46	**0.27**
			24.5	**0.70**	
5.22	0.17				
5.33	0.18				
5.41	0.15				
5.95	0.20				
5.48	0.66				
5.51	**0.46**	**-6.74**	**12.33**		
	0.16				
13.81	0.32				
13.89	0.17				
13.05	0.10				
13.80	0.45				
13.83	0.23				
14.27	0.35				

16.24	0.30	96.91	5.52	**10.67**	0.33	**0.53**
15.85	0.30	96.91	5.52	**10.28**	0.33	**0.53**
16.36	0.36	96.91	5.52	**10.79**	0.33	**0.57**
14.10	0.40	96.91	5.52	**8.53**	0.33	**0.60**
16.70	0.34	96.91	5.52	**11.12**	0.33	**0.56**
14.63	0.35					
16.54	0.21					
16.44	0.35					
16.04	0.32	96.91	5.52	**10.46**	0.33	**0.54**
17.41	0.45	96.91	5.52	**11.83**	0.33	**0.63**
15.89	0.20	96.91	5.52	**10.32**	0.33	**0.48**
16.41	0.33	96.91	5.52	**10.83**	0.33	**0.55**
17.02	0.30	96.91	5.52	**11.44**	0.33	**0.53**
16.77	0.19	96.91	5.52	**11.19**	0.33	**0.48**
14.04	0.15					
12.35	0.54					
13.98	0.18					
13.35	0.62					
12.17	0.86					
14.26	0.16					
14.09	0.30					
13.94	**0.33**		**5.52**	**8.38**		
	0.13					
16.62	0.29	96.91	5.75	**10.82**	0.29	**0.53**
15.79	0.26	96.91	5.75	**9.99**	0.29	**0.51**
16.89	0.25	97.33	5.79	**11.04**	0.29	**0.50**
16.81	0.27	97.33	5.79	**10.96**	0.29	**0.51**
17.31	0.33	97.33	5.79	**11.46**	0.29	**0.55**
18.27	0.18	92.24	4.47	**13.74**	0.29	**0.68**
17.71	0.26	92.30	4.48	**13.17**	0.29	**0.71**
17.23	0.11	93.01	4.55	**12.62**	0.29	**0.67**
17.29	0.24	97.33	5.79	**11.44**	0.29	**0.50**
17.06	0.48	97.33	5.79	**11.21**	0.29	**0.65**
18.68	0.19	97.33	5.79	**12.82**	0.29	**0.48**
17.90	0.13	93.06	4.55	**13.28**	0.29	**0.67**
17.47	0.32	97.33	5.79	**11.62**	0.29	**0.54**
17.20	0.26	97.33	5.79	**11.35**	0.29	**0.51**
17.55	0.23	92.28	4.48	**13.02**	0.29	**0.70**
				10.6	**1.61**	
				11.5	**1.16**	
				13.2	**0.81**	

14.33	0.13					
16.09	0.73					
14.15	0.13					
14.36	0.20					
10.58	0.35					
14.12	0.16					
14.24	0.24					
14.18	**0.29**		**5.75**	**8.38**		
	0.11					

13.95	0.13					
14.17	0.14					
14.11	0.19					
14.02	0.19					
16.22	0.21	96.23	5.46	**10.70**	0.30	**0.48**
15.99	0.24	96.23	5.46	**10.47**	0.30	**0.50**
16.25	0.25	96.23	5.46	**10.72**	0.30	**0.50**
16.02	0.17	96.23	5.46	**10.50**	0.30	**0.47**
15.85	0.24	96.23	5.46	**10.33**	0.30	**0.49**
16.01	0.26	96.23	5.46	**10.49**	0.30	**0.50**
16.12	0.27	96.23	5.46	**10.60**	0.30	**0.51**
16.46	0.15	96.23	5.46	**10.93**	0.30	**0.46**
17.17	0.26	96.23	5.46	**11.64**	0.30	**0.51**
16.08	0.18	96.23	5.46	**10.56**	0.30	**0.47**
15.74	0.20	96.23	5.46	**10.22**	0.30	**0.48**
16.05	0.26	96.23	5.46	**10.53**	0.30	**0.50**
-2.04	0.35					
-0.15	0.43					
0.84	0.31					
15.73	0.21	94.87	5.33	**10.35**	0.30	**0.48**
15.37	0.15	94.87	5.33	**9.98**	0.30	**0.46**
15.87	0.16	94.87	5.33	**10.49**	0.30	**0.46**
15.41	0.21	94.87	5.33	**10.03**	0.30	**0.48**
15.34	0.24	94.87	5.33	**9.96**	0.30	**0.50**
13.96	0.13					
13.81	0.12					
13.71	0.16					
13.92	0.19					

13.85	0.23					
13.96	**0.30**		**5.53**	**8.38**		
	0.11					
16.22	0.20	94.87	5.27	**10.89**	0.25	**0.48**
15.79	0.16	94.87	5.27	**10.46**	0.25	**0.46**
15.69	0.21	94.87	5.27	**10.36**	0.25	**0.48**
-4.73	0.84					
-4.76	0.57					
-1.03	0.36					
0.55	0.56					
-0.48	0.61					
-0.74	0.47					
-0.14	0.61					
15.56	0.25	96.23	5.40	**10.10**	0.25	**0.50**
15.09	0.25	96.23	5.40	**9.64**	0.25	**0.50**
16.55	0.33	96.23	5.40	**11.08**	0.25	**0.55**
15.96	0.19	96.23	5.40	**10.50**	0.25	**0.47**
16.77	0.27	96.23	5.40	**11.31**	0.25	**0.51**
				10.5	**0.87**	
13.83	0.17					
13.84	0.12					
14.07	0.19					
14.05	0.15					
13.95	0.26					
13.90	**0.25**		**5.47**	**8.38**		
	0.09					
12.87	0.16					
13.05	0.15					
13.02	0.23					
13.40	0.22					
17.48	0.19					
18.16	0.17	97.46	3.32	**14.79**	0.40	**0.60**
17.62	0.18	97.46	3.32	**14.25**	0.40	**0.60**
16.84	0.18	95.86	3.13	**13.67**	0.40	**0.60**
17.34	0.19	95.86	3.13	**14.17**	0.40	**0.61**
17.89	0.19	97.77	3.35	**14.48**	0.40	**0.60**

17.55	0.21	97.77	3.35	**14.15**	0.40	**0.61**
17.39	0.18	97.57	3.33	**14.01**	0.40	**0.60**
16.78	0.20	96.00	3.15	**13.59**	0.40	**0.61**
16.26	0.16	97.57	3.33	**12.89**	0.40	**0.59**
12.96	0.14					
13.43	0.18					
13.16	0.15					
13.06	0.20					
13.15	0.40					
13.12	**0.40**		**4.70**	**8.38**		
	0.14					
17.24	0.21	97.57	3.27	**13.92**	0.59	**0.63**
16.75	0.20	97.57	3.27	**13.44**	0.59	**0.63**
16.63	0.20	97.57	3.27	**13.32**	0.59	**0.63**
17.58	0.23	97.57	3.27	**14.26**	0.59	**0.64**
16.94	0.22	97.57	3.27	**13.63**	0.59	**0.63**
17.06	0.17	97.57	3.27	**13.75**	0.59	**0.62**
14.60	0.18					
16.68	0.22	97.57	3.27	**13.37**	0.59	**0.63**
15.73	0.21					
17.21	0.21					
12.69	0.13					
12.60	0.17					
13.29	0.18					
13.27	0.11					
12.96	0.74					
13.06	**0.59**		**4.64**	**8.38**		
	0.21					
17.18	0.18	97.84	3.32	**13.81**	0.62	**0.63**
17.26	0.21	97.84	3.32	**13.89**	0.62	**0.64**
18.23	0.22	97.84	3.32	**14.86**	0.62	**0.64**
18.61	0.15	97.84	3.32	**15.24**	0.62	**0.62**
15.40	0.22	95.98	3.10	**12.26**	0.62	**0.64**
15.56	0.24	95.98	3.10	**12.42**	0.62	**0.65**
16.24	0.30	95.98	3.10	**13.10**	0.62	**0.67**
16.34	0.39					
16.42	0.36					
17.09	0.32					
16.84	0.22	97.39	3.27	**13.53**	0.62	**0.64**

18.40	0.15	97.39	3.27	**15.09**	0.62	**0.62**
17.46	0.18	97.39	3.27	**14.15**	0.62	**0.63**
16.04	0.30					
15.31	0.23					
				13.8	**1.47**	
14.29	0.21					
13.08	0.11					
13.23	0.14					
13.38	0.18					
13.23	0.29					
13.08	**0.62**		**4.66**	**8.38**		
	0.23					
12.97	0.16					
12.87	0.17					
15.15	0.23					
13.80	0.19					
12.77	0.18					
13.04	0.15					
15.31	0.29	93.9	2.80	**12.48**	0.29	**0.63**
15.87	0.16	93.9	2.80	**13.04**	0.29	**0.59**
14.70	0.25	93.9	2.80	**11.87**	0.29	**0.62**
15.23	0.14	93.9	2.80	**12.40**	0.29	**0.58**
15.81	0.24	93.9	2.80	**12.98**	0.29	**0.61**
15.04	0.15	93.9	2.80	**12.21**	0.29	**0.59**
15.83	0.25	93.9	2.80	**13.00**	0.29	**0.62**
15.30	0.19	93.9	2.80	**12.47**	0.29	**0.60**
15.39	0.17	93.9	2.80	**12.56**	0.29	**0.59**
15.50	0.13	93.9	2.80	**12.67**	0.29	**0.58**
15.68	0.17	93.9	2.80	**12.85**	0.29	**0.59**
16.35	0.21	95.5	4.53	**11.77**	0.29	**0.40**
16.12	0.12	95.5	4.53	**11.53**	0.29	**0.37**
17.09	0.19	96.1	4.60	**12.43**	0.29	**0.39**
15.74	0.15	96.1	4.61	**11.08**	0.29	**0.38**
15.63	0.20	93.9	2.80	**12.80**	0.29	**0.60**
15.78	0.27	93.9	2.80	**12.95**	0.29	**0.63**
15.57	0.22	93.9	2.80	**12.74**	0.29	**0.61**
15.57	0.30	93.9	2.80	**12.74**	0.29	**0.64**
16.20	0.47					

				12.6	**0.67**	
				11.9	**1.38**	
13.19	0.15					
13.02	0.18					
13.21	0.18					
13.03	0.16					
13.11	0.20					
13.01	**0.29**		**4.59**	**8.38**		
	0.10					
13.01	0.20					
13.05	0.17					
13.02	0.13					
13.09	0.12					
14.56	0.25	94.03	2.98	**11.55**	0.42	**0.45**
15.24	0.26	94.03	2.98	**12.22**	0.42	**0.46**
15.10	0.31	94.03	2.98	**12.09**	0.42	**0.49**
14.85	0.25	94.03	2.98	**11.83**	0.42	**0.45**
15.07	0.27	94.03	2.98	**12.05**	0.42	**0.46**
14.86	0.22	94.03	2.98	**11.84**	0.42	**0.44**
15.32	0.35	94.03	2.98	**12.30**	0.42	**0.52**
15.40	0.33	94.03	2.98	**12.38**	0.42	**0.50**
11.63	0.33					
14.88	0.24					
15.97	0.16					
15.31	0.27	94.03	2.98	**12.30**	0.42	**0.46**
18.10	0.19	98.10	3.46	**14.59**	0.42	**0.42**
15.88	0.21					
17.47	0.22	97.14	3.35	**14.08**	0.42	**0.43**
17.49	0.25	96.31	3.25	**14.20**	0.42	**0.45**
15.60	0.31					
16.13	0.20					
15.86	0.28	94.03	2.98	**12.84**	0.42	**0.47**
14.68	0.22	94.03	2.98	**11.66**	0.42	**0.44**
				12.1	**0.74**	
				14.3	**0.54**	
13.32	0.19					
13.25	0.15					

13.63	0.18					
13.10	0.14					
13.32	0.45					
13.18	**0.42**		**4.76**	**8.38**		
	0.15					
12.77	0.15					
12.94	0.15					
13.11	0.14					
13.15	0.15					
14.68	0.22	97.44	4.91	**9.72**	0.55	**0.44**
13.78	0.19	97.44	4.91	**8.82**	0.55	**0.43**
13.64	0.19	97.44	4.91	**8.69**	0.55	**0.43**
14.42	0.19	97.44	4.91	**9.46**	0.55	**0.43**
12.73	0.18		-0.16	**12.89**	0.55	**0.28**
14.15	0.21	97.44	4.91	**9.20**	0.55	**0.44**
13.55	0.15					
8.27	0.54					
14.33	0.15	97.44	4.91	**9.37**	0.55	**0.41**
14.00	0.22	97.44	4.91	**9.04**	0.55	**0.44**
13.40	0.21					
13.56	0.16					
12.96	0.16					
13.43	0.12					
13.34	0.52					
13.17	**0.55**		**4.75**	**8.38**		
	0.19					
13.86	0.14	97.44	5.02	**8.80**	0.42	**0.39**
13.77	0.18	97.44	5.02	**8.71**	0.42	**0.41**
12.35	0.17					
13.76	0.16	97.44	5.02	**8.70**	0.42	**0.40**
13.17	0.25					
14.21	0.17	97.44	5.02	**9.15**	0.42	**0.40**
13.65	0.17	97.44	5.02	**8.59**	0.42	**0.40**
13.01	0.14					
13.39	0.18					
14.43	0.18	97.44	5.02	**9.37**	0.42	**0.40**
				9.0	**0.71**	

13.23	0.18					
13.37	0.11					
13.02	0.15					
13.17	0.16					
13.20	0.29					
13.27	**0.42**		**4.85**	**8.38**		
	0.15					
			15.31			
			-15.02			
2.22	0.48					
1.94	0.46					
2.01	0.47					
2.18	0.48					
13.53	0.13					
13.34	0.17					
11.25	0.21					
12.80	0.24					
12.73	0.23					
13.77	0.20	97.44	5.08	**8.65**	0.30	**0.43**
13.49	0.19					
13.69	0.19	97.44	5.08	**8.57**	0.30	**0.42**
14.24	0.23	97.44	5.08	**9.12**	0.30	**0.44**
15.05	0.19					
2.29	0.44					
1.88	0.46					
2.15	0.48					
2.22	0.49					
2.13	0.36					
2.11	**0.30**		**-10.25**	**12.49**		
	0.10					
11.84	0.34		-0.12	**11.96**	0.31	**0.38**
12.45	0.20		-0.12	**12.57**	0.31	**0.25**
12.65	0.17		-0.12	**12.77**	0.31	**0.23**
12.99	0.19		-0.12	**13.11**	0.31	**0.24**
12.38	0.21					
13.30	0.23		-0.12	**13.42**	0.31	**0.28**
12.94	0.14		-0.12	**13.06**	0.31	**0.21**
13.08	0.17		-0.12	**13.20**	0.31	**0.23**

12.83	0.15		-0.12	**12.95**	0.31	**0.21**
12.75	0.17		-0.12	**12.87**	0.31	**0.23**
				12.9	**0.80**	
1.92	0.45					
2.08	0.45					
1.97	0.45					
1.90	0.43					
1.97	0.16					
2.05	**0.31**		**-10.31**	**12.49**		
	0.11					

a)

^{16}O (Gcps)	^{18}O (Mcps)	IP (nA)	Yield (Gcps/nA)	Relative yield	2s relative yield
2.34	4.76	1.94	1.21		
2.42	4.93	1.99	1.22		
2.45	4.97	2.01	1.22		
2.44	4.96	2.01	1.22		
2.39	4.86	2.00	1.19	0.98	0.01
2.40	4.88	2.00	1.20	0.99	0.01
2.40	4.87	1.99	1.20	0.99	0.01
2.43	4.94	1.98	1.22	1.01	0.01
2.38	4.84	1.98	1.20	0.99	0.01
2.38	4.84	1.97	1.21	1.00	0.01
2.43	4.94	1.97	1.23	1.01	0.01
2.41	4.90	1.97	1.22	1.01	0.01
2.45	4.99	1.96	1.25	1.03	0.01
2.62	5.33	1.96	1.33	1.10	0.01
2.72	5.56	2.02	1.35	1.11	0.01
2.54	5.16	2.03	1.25	1.03	0.01
2.51	5.11	2.03	1.24	1.02	0.01
2.45	4.98	2.02	1.21	1.00	0.01
2.44	4.97	2.02	1.21	1.00	0.01
2.45	4.98	2.01	1.22	1.00	0.01
2.44	4.95	2.00	1.22	1.00	0.01
2.45	4.98	2.00	1.22	1.01	0.01
2.45	4.98	2.00	1.23	1.01	0.01
2.43	4.94	1.99	1.22	1.00	0.01
2.42	4.91	1.98	1.22		
2.40	4.88	1.98	1.21		
2.38	4.85	1.97	1.21		
2.37	4.82	1.96	1.21		
			1.21		
2.68	5.40	1.95	1.37		

2.78	5.60	2.01	1.38		
2.76	5.56	2.03	1.36		
2.73	5.50	2.03	1.34		

2.69	5.50	2.03	1.33	0.98	0.04
2.73	5.58	2.02	1.35	0.99	0.04
2.70	5.51	2.02	1.34	0.98	0.04
2.69	5.50	2.01	1.34	0.98	0.04
2.71	5.53	2.01	1.35	0.99	0.04
2.71	5.53	2.01	1.35	0.99	0.04
2.71	5.54	2.00	1.35	1.00	0.04
2.68	5.46	2.00	1.34	0.98	0.04
2.70	5.50	2.00	1.35	0.99	0.04
2.70	5.51	1.99	1.36	1.00	0.04
2.70	5.52	1.98	1.36	1.00	0.04
2.68	5.47	1.98	1.35	0.99	0.04
2.63	5.37	1.98	1.33	0.98	0.04
2.67	5.44	1.97	1.35	1.00	0.04
2.64	5.38	1.96	1.34	0.99	0.04
2.65	5.40	1.96	1.35	0.99	0.04
2.73	5.57	2.03	1.35	0.99	0.04
2.65	5.41	2.04	1.30	0.95	0.04
2.78	5.67	2.05	1.36	1.00	0.04
2.77	5.66	2.05	1.35	0.99	0.04

2.81	5.66	2.05	1.37		
2.83	5.70	2.05	1.38		
2.77	5.58	2.05	1.35		
2.71	5.48	2.04	1.33		
			1.36		

2.16	4.39	1.76	1.23		
2.34	4.75	1.88	1.25		
2.52	5.13	2.06	1.23		
2.56	5.21	2.13	1.20		
2.68	5.46	2.15	1.25		

2.69	5.47	2.17	1.24	1.01	0.04

2.76	5.62	2.18	1.27	1.03	0.04
2.80	5.70	2.17	1.29	1.05	0.04
2.75	5.59	2.18	1.26	1.03	0.04
2.62	5.33	2.17	1.21	0.98	0.04
2.70	5.50	2.17	1.24	1.01	0.04
2.66	5.41	2.16	1.23	1.00	0.04
2.66	5.43	2.15	1.24	1.01	0.04
2.69	5.47	2.15	1.25	1.02	0.04
2.73	5.56	2.14	1.27	1.04	0.04
2.53	5.16	2.13	1.19	0.97	0.04
2.64	5.38	2.11	1.25	1.02	0.04
2.64	5.37	2.11	1.25	1.02	0.04
2.64	5.38	2.10	1.26	1.03	0.04
2.57	5.25	2.09	1.23	1.01	0.04
2.48	5.04	2.07	1.20		
2.41	4.89	2.06	1.17		
2.51	5.10	2.05	1.22		
2.44	4.97	2.04	1.20		
2.31	4.69	2.04	1.13		
2.50	5.08	2.02	1.24		
			1.23		
2.48	5.05	2.01	1.23	1.01	0.04
2.51	5.11	1.99	1.26	1.04	0.04
2.42	4.94	1.99	1.22	1.00	0.04
2.44	4.98	1.98	1.24	1.01	0.04
2.45	4.99	1.97	1.24	1.02	0.04
2.36	4.83	1.96	1.21	0.99	0.04
2.42	4.93	2.01	1.20	0.99	0.04
2.50	5.09	2.00	1.25	1.03	0.04
2.49	5.07	2.01	1.24	1.02	0.04
2.45	5.00	2.00	1.22	1.01	0.04
2.45	5.01	2.00	1.23	1.01	0.04
2.44	4.97	1.99	1.22	1.00	0.04
2.47	5.04	1.98	1.25	1.03	0.04
2.47	5.03	1.97	1.25	1.03	0.04
2.41	4.92	1.96	1.23	1.01	0.04

2.37	4.81	1.95	1.21		
2.37	4.83	2.05	1.16		
2.64	5.38	2.18	1.21		
2.62	5.32	2.20	1.19		
2.39	4.84	2.19	1.09		
2.74	5.57	2.19	1.25		
			1.22		
2.53	5.14	2.05	1.24		
2.48	5.05	2.04	1.22		
2.48	5.03	2.04	1.22		
2.47	5.02	2.03	1.22		
2.49	5.08	2.02	1.24	1.02	0.02
2.49	5.08	2.01	1.24	1.02	0.02
2.50	5.10	2.01	1.25	1.03	0.02
2.51	5.11	2.00	1.25	1.03	0.02
2.50	5.09	1.98	1.26	1.04	0.02
2.46	5.01	1.97	1.24	1.02	0.02
2.42	4.92	1.97	1.23	1.01	0.02
2.42	4.94	1.96	1.23	1.01	0.02
2.44	4.98	1.96	1.25	1.03	0.02
2.50	5.10	2.02	1.24	1.02	0.02
2.51	5.12	2.03	1.23	1.02	0.02
2.53	5.15	2.04	1.24	1.02	0.02
1.76	3.52	2.04	0.86	0.71	0.02
1.85	3.71	2.04	0.91	0.75	0.02
1.85	3.72	2.03	0.91	0.75	0.02
2.52	5.14	2.02	1.25	1.03	0.02
2.52	5.13	2.02	1.24	1.02	0.02
2.45	4.99	2.02	1.21	1.00	0.02
2.51	5.12	2.02	1.24	1.02	0.02
2.55	5.18	2.02	1.26	1.04	0.02
2.44	4.95	2.01	1.21		
2.42	4.91	2.01	1.20		
2.43	4.95	2.01	1.21		
2.41	4.91	2.00	1.20		

1.22

2.43	4.94	1.99	1.22	1.02	0.02
2.42	4.93	1.98	1.22	1.02	0.02
2.50	5.08	1.98	1.26	1.05	0.02
1.59	3.18	1.98	0.80	0.67	0.02
1.58	3.16	1.98	0.80	0.67	0.02
1.73	3.47	1.98	0.88	0.73	0.02
1.53	3.08	1.98	0.78	0.65	0.02
1.72	3.44	1.97	0.87	0.73	0.02
1.72	3.44	1.96	0.87	0.73	0.02
1.73	3.46	1.96	0.88	0.73	0.02
2.48	5.06	2.02	1.23	1.03	0.02
2.54	5.18	2.04	1.25	1.04	0.02
2.51	5.11	2.04	1.23	1.02	0.02
2.50	5.09	2.05	1.22	1.02	0.02
2.52	5.14	2.05	1.23	1.03	0.02

2.44	4.95	2.05	1.19
2.44	4.96	2.04	1.19
2.43	4.95	2.04	1.19
2.42	4.92	2.04	1.19

1.20

2.46	4.99	2.00	1.23
2.46	4.99	2.00	1.23
2.44	4.95	2.00	1.22
2.42	4.93	2.00	1.21

2.43	4.96	2.00	1.22	1.00	0.01
2.37	4.83	1.99	1.19	0.97	0.01
2.36	4.83	1.99	1.19	0.98	0.01
2.41	4.92	1.98	1.22	1.00	0.01
2.41	4.92	1.98	1.21	1.00	0.01
2.39	4.87	1.98	1.20	0.99	0.01

2.42	4.93	1.98	1.22	1.00	0.01
2.37	4.83	1.98	1.20	0.98	0.01
2.39	4.88	1.98	1.21	0.99	0.01
2.46	5.02	1.98	1.25	1.02	0.01
2.42	4.91	1.98	1.22		
2.40	4.87	1.97	1.21		
2.40	4.88	1.97	1.22		
2.39	4.86	1.97	1.21		
			1.22		
2.42	4.94	1.97	1.23	1.01	0.01
2.43	4.96	1.97	1.24	1.02	0.01
2.44	4.97	1.97	1.24	1.02	0.01
2.41	4.91	1.96	1.23	1.01	0.01
2.43	4.95	1.97	1.23	1.01	0.01
2.43	4.96	1.97	1.24	1.02	0.01
2.42	4.91	1.96	1.23	1.01	0.01
2.40	4.89	1.95	1.23	1.01	0.01
2.43	4.95	2.00	1.21	1.00	0.01
2.46	5.01	2.02	1.22	1.00	0.01
2.49	5.05	2.04	1.22		
2.53	5.13	2.07	1.22		
2.53	5.13	2.08	1.22		
2.54	5.15	2.08	1.22		
			1.22		
2.57	5.24	2.09	1.23	1.01	0.01
2.57	5.23	2.09	1.23	1.01	0.01
2.54	5.20	2.09	1.21	1.00	0.01
2.55	5.21	2.10	1.22	1.00	0.01
2.66	5.42	2.09	1.27	1.04	0.01
2.63	5.35	2.09	1.25	1.03	0.01
2.62	5.34	2.09	1.25	1.03	0.01
2.89	5.89	2.09	1.38	1.14	0.01
3.17	6.47	2.08	1.52	1.25	0.01
2.84	5.80	2.08	1.37	1.12	0.01
2.54	5.18	2.07	1.23	1.01	0.01

2.51	5.12	2.07	1.21	0.99	0.01
2.56	5.23	2.07	1.24	1.02	0.01
2.55	5.20	2.07	1.23	1.01	0.01
2.98	6.07	2.07	1.44	1.19	0.01

2.45	4.99	2.06	1.19
2.50	5.09	2.06	1.22
2.51	5.09	2.06	1.22
2.49	5.06	2.06	1.21
			1.22

2.50	5.08	2.06	1.21
2.45	4.98	2.02	1.21
2.30	4.69	2.00	1.15
2.38	4.84	1.99	1.20
2.42	4.91	1.97	1.22
2.37	4.82	1.96	1.21

2.43	4.94	1.94	1.25	1.02	0.02
2.52	5.14	1.99	1.27	1.03	0.02
2.51	5.10	2.01	1.25	1.02	0.02
2.46	5.01	2.00	1.23	1.00	0.02
2.53	5.14	2.00	1.26	1.03	0.02
2.44	4.96	1.99	1.23	1.00	0.02
2.48	5.05	1.99	1.25	1.02	0.02
2.44	4.96	1.99	1.23	1.00	0.02
2.48	5.05	1.98	1.26	1.03	0.02
2.45	5.00	1.97	1.24	1.02	0.02
2.50	5.08	1.97	1.27	1.04	0.02
2.41	4.92	1.95	1.24	1.01	0.02
2.50	5.09	2.01	1.24	1.01	0.02
2.51	5.11	2.03	1.23	1.01	0.02
2.55	5.19	2.03	1.25	1.02	0.02
2.52	5.14	2.03	1.24	1.01	0.02
2.57	5.24	2.03	1.27	1.04	0.02
2.55	5.19	2.02	1.26	1.03	0.02
2.55	5.18	2.02	1.26	1.03	0.02
3.71	7.57	2.01	1.84	1.51	0.02

2.48	5.03	2.01	1.23
2.47	5.03	2.00	1.23
2.46	5.00	2.00	1.23
2.48	5.03	2.00	1.24
			1.22

2.43	4.94	1.98	1.23
2.41	4.89	1.97	1.22
2.40	4.88	1.97	1.22
2.41	4.90	1.97	1.23

2.49	5.06	1.96	1.27	1.04	0.01
2.43	4.95	1.96	1.24	1.01	0.01
2.57	5.23	2.02	1.27	1.04	0.01
2.60	5.28	2.03	1.28	1.04	0.01
2.57	5.22	2.03	1.26	1.03	0.01
2.56	5.21	2.04	1.26	1.03	0.01
2.65	5.39	2.04	1.30	1.06	0.01
2.55	5.20	2.04	1.25	1.02	0.01
2.84	5.76	2.03	1.40	1.14	0.01
2.56	5.22	2.03	1.27	1.03	0.01
2.52	5.13	2.02	1.24	1.02	0.01
2.53	5.14	2.02	1.25	1.02	0.01
2.48	5.06	2.02	1.23	1.00	0.01
2.54	5.17	2.02	1.26	1.03	0.01
2.45	5.00	2.01	1.22	0.99	0.01
2.47	5.04	2.01	1.23	1.00	0.01
2.51	5.11	2.00	1.25	1.02	0.01
2.45	5.00	2.00	1.23	1.00	0.01
2.47	5.03	1.99	1.24	1.01	0.01
2.48	5.05	1.99	1.25	1.02	0.01

2.43	4.93	1.98	1.22
2.43	4.95	1.98	1.23

2.41	4.91	1.98	1.22		
2.42	4.91	1.97	1.23		
			1.22		
2.50	5.08	1.99	1.26		
2.50	5.07	1.99	1.26		
2.48	5.05	1.99	1.25		
2.48	5.03	1.98	1.25		
2.46	5.01	1.99	1.24	0.99	0.02
2.46	5.00	1.99	1.24	0.99	0.02
2.46	5.00	1.98	1.24	0.99	0.02
2.42	4.93	1.98	1.22	0.98	0.02
2.49	5.05	1.98	1.26	1.01	0.02
2.45	4.99	1.97	1.25	1.00	0.02
2.44	4.97	1.97	1.24	0.99	0.02
3.60	7.29	1.97	1.83	1.46	0.02
2.44	4.97	1.97	1.24	0.99	0.02
2.43	4.95	1.97	1.24	0.99	0.02
2.45	4.99	1.97	1.25		
2.43	4.94	1.96	1.24		
2.45	4.98	1.96	1.25		
2.43	4.93	1.96	1.24		
			1.25		
2.52	5.13	2.07	1.22	0.98	0.02
2.67	5.43	2.17	1.23	0.99	0.02
2.68	5.44	2.23	1.20	0.96	0.02
2.79	5.66	2.25	1.24	0.99	0.02
2.79	5.67	2.27	1.23	0.99	0.02
2.77	5.62	2.28	1.22	0.98	0.02
2.81	5.70	2.28	1.23	0.99	0.02
2.80	5.69	2.29	1.22	0.98	0.02
2.81	5.70	2.29	1.22	0.98	0.02
2.85	5.79	2.29	1.24	1.00	0.02

2.87	5.84	2.30	1.25
2.84	5.78	2.30	1.24
2.86	5.81	2.30	1.24
2.89	5.87	2.30	1.26
			1.25
4.45	8.95	2.29	1.94
4.47	8.99	2.29	1.95
4.37	8.78	2.29	1.91
4.33	8.69	2.29	1.89
2.88	5.85	2.29	1.26
2.85	5.79	2.28	1.25
2.96	6.00	2.28	1.30
2.90	5.89	2.28	1.27
2.89	5.86	2.28	1.27
2.80	5.69	2.28	1.23
2.84	5.77	2.27	1.25
2.75	5.58	2.27	1.21
2.74	5.57	2.28	1.20
2.71	5.52	2.27	1.19
4.33	8.71	2.27	1.91
4.27	8.58	2.26	1.89
4.30	8.65	2.26	1.91
4.26	8.55	2.25	1.89
2.69	5.46	2.26	1.19
2.79	5.67	2.26	1.24
2.83	5.76	2.26	1.26
2.80	5.68	2.25	1.24
2.84	5.77	2.25	1.26
2.85	5.79	2.25	1.27
2.75	5.58	2.25	1.22
2.80	5.68	2.25	1.24

2.82	5.74	2.25	1.26
2.79	5.66	2.25	1.24
4.33	8.69	2.24	1.93
4.33	8.70	2.24	1.93
4.30	8.63	2.24	1.92
4.25	8.54	2.23	1.91

$^{16}OH/^{16}O$	^{16}OH (cps)	Date	Time	X	Y	DTFA-X
3.53E-02	8.27E+07	10/19/20	8:37:00 PM	1297	2051	-2
3.54E-02	8.58E+07	10/19/20	8:42:00 PM	1341	2154	-3
3.55E-02	8.69E+07	10/19/20	8:45:00 PM	1151	2003	-1
3.54E-02	8.66E+07	10/19/20	8:48:00 PM	1096	1982	-1
3.49E-02	8.33E+07	10/19/20	8:51:00 PM	2100	-1544	-1
3.43E-02	8.22E+07	10/19/20	8:54:00 PM	1998	-1554	0
3.44E-02	8.23E+07	10/19/20	8:57:00 PM	2732	-1638	-1
3.51E-02	8.52E+07	10/19/20	9:00:00 PM	2811	-1834	0
3.44E-02	8.18E+07	10/19/20	9:03:00 PM	2907	-1866	-4
3.50E-02	8.32E+07	10/19/20	9:06:00 PM	3016	-1812	-1
3.40E-02	8.25E+07	10/19/20	9:08:00 PM	3141	-1691	-4
3.27E-02	7.87E+07	10/19/20	9:11:00 PM	4394	-1993	-9
3.37E-02	8.27E+07	10/19/20	9:14:00 PM	4374	-1897	-8
2.03E-02	5.31E+07	10/19/20	9:17:00 PM	4168	-1941	-7
1.01E-02	2.75E+07	10/19/20	9:22:00 PM	4281	-2084	-8
3.49E-02	8.84E+07	10/19/20	9:25:00 PM	5128	-2111	-7
3.45E-02	8.67E+07	10/19/20	9:28:00 PM	5562	-2111	-8
3.51E-02	8.60E+07	10/19/20	9:31:00 PM	5781	-2153	-7
3.48E-02	8.50E+07	10/19/20	9:34:00 PM	5908	-2190	-7
3.50E-02	8.58E+07	10/19/20	9:37:00 PM	6029	-2284	-7
3.50E-02	8.52E+07	10/19/20	9:40:00 PM	5977	-2339	-6
3.52E-02	8.60E+07	10/19/20	9:43:00 PM	5998	-2371	-6
3.52E-02	8.64E+07	10/19/20	9:46:00 PM	6297	-2312	-7
3.52E-02	8.53E+07	10/19/20	9:49:00 PM	6229	-2644	-5
3.54E-02	8.56E+07	10/19/20	9:52:00 PM	1131	1900	-3
3.54E-02	8.49E+07	10/19/20	9:55:00 PM	1431	1847	-4
3.54E-02	8.45E+07	10/19/20	9:58:00 PM	1414	1879	-3
3.54E-02	8.40E+07	10/19/20	##########	1426	1971	-3
3.54E-02						
8.80E-04	2.36E+06	10/19/20	##########	1508	1340	-7

8.23E-04	2.29E+06	10/19/20	##########	1528	1340	-7
8.85E-04	2.44E+06	10/19/20	##########	1528	1320	-7
9.80E-04	2.67E+06	10/19/20	##########	1508	1320	-7
2.01E-03	5.43E+06	10/19/20	##########	1983	-1481	-3
2.10E-03	5.73E+06	10/19/20	##########	3105	-1716	-4
1.78E-03	4.80E+06	10/19/20	##########	3058	-1702	-6
2.80E-03	7.55E+06	10/19/20	##########	3131	-1797	-5
2.54E-03	6.89E+06	10/19/20	##########	3028	-1925	-5
2.97E-03	8.06E+06	10/19/20	##########	4063	-1945	-8
2.81E-03	7.63E+06	10/19/20	##########	4180	-2110	-9
2.55E-03	6.84E+06	10/19/20	##########	4114	-2036	-9
1.91E-03	5.16E+06	10/19/20	##########	4468	-1963	-11
1.95E-03	5.27E+06	10/19/20	##########	4192	-2263	-10
2.12E-03	5.74E+06	10/19/20	##########	6268	-2398	-8
1.76E-03	4.71E+06	10/19/20	##########	5941	-2600	-10
2.05E-03	5.39E+06	10/19/20	##########	6120	-2745	-8
1.63E-03	4.35E+06	10/19/20	##########	5651	-2608	-9
1.52E-03	4.00E+06	10/19/20	##########	5642	-2706	-8
1.55E-03	4.10E+06	10/19/20	##########	5708	-2448	-9
1.68E-03	4.59E+06	10/19/20	##########	5610	-2465	-9
3.43E-03	9.10E+06	10/19/20	##########	3083	-2068	-4
2.22E-03	6.15E+06	10/19/20	##########	3875	-2062	-8
2.71E-03	7.52E+06	10/19/20	##########	3872	-1969	-8

8.21E-04	2.30E+06	10/19/20	##########	1296	1096	-6
7.90E-04	2.24E+06	10/19/20	##########	1316	1096	-8
8.54E-04	2.36E+06	10/19/20	##########	1316	1076	-7
9.48E-04	2.57E+06	10/19/20	##########	1296	1076	-7

8.73E-04

3.62E-02	7.81E+07	10/20/20	8:06:00 AM	-136	318	-4
3.63E-02	8.48E+07	10/20/20	8:11:00 AM	-129	289	-9
3.61E-02	9.12E+07	10/20/20	8:16:00 AM	-356	359	8
3.59E-02	9.20E+07	10/20/20	8:19:00 AM	-409	295	-5
3.66E-02	9.84E+07	10/20/20	8:22:00 AM	-592	203	-9
2.82E-02	7.58E+07	10/20/20	8:27:00 AM	-2510	4324	-22

3.11E-02	8.57E+07	10/20/20	8:30:00 AM	-2446	4426	-9
2.78E-02	7.77E+07	10/20/20	8:34:00 AM	-2510	4507	-25
2.42E-02	6.65E+07	10/20/20	8:37:00 AM	-2360	4569	-9
2.52E-02	6.60E+07	10/20/20	8:41:00 AM	-2288	4499	-19
2.31E-02	6.24E+07	10/20/20	8:44:00 AM	-2232	4470	-9
2.31E-02	6.14E+07	10/20/20	8:48:00 AM	-1985	4552	-19
2.34E-02	6.23E+07	10/20/20	8:53:00 AM	-1968	4640	-9
2.73E-02	7.32E+07	10/20/20	8:56:00 AM	-1557	4840	-9
2.67E-02	7.29E+07	10/20/20	9:00:00 AM	-1376	4992	-9
2.50E-02	6.32E+07	10/20/20	9:06:00 AM	-866	5272	-17
2.59E-02	6.83E+07	10/20/20	9:10:00 AM	-865	5387	-25
2.64E-02	6.95E+07	10/20/20	9:13:00 AM	-802	5339	-10
2.87E-02	7.58E+07	10/20/20	9:17:00 AM	-528	5533	-10
2.47E-02	6.36E+07	10/20/20	9:20:00 AM	-21	5899	-9
3.57E-02	8.85E+07	10/20/20	9:25:00 AM	-88	256	1
3.57E-02	8.62E+07	10/20/20	9:28:00 AM	46	172	-1
3.60E-02	9.02E+07	10/20/20	9:31:00 AM	125	195	-1
3.60E-02	8.80E+07	10/20/20	9:34:00 AM	111	340	0
3.67E-02	8.48E+07	10/20/20	9:37:00 AM	-161	553	1
3.64E-02	9.09E+07	10/20/20	9:40:00 AM	-136	456	-16

3.62E-02

2.67E-02	6.62E+07	10/20/20	9:45:00 AM	-382	5864	4
3.53E-02	8.85E+07	10/20/20	9:49:00 AM	479	4914	-11
3.05E-02	7.39E+07	10/20/20	9:54:00 AM	3679	-2578	11
2.95E-02	7.20E+07	10/20/20	9:57:00 AM	3772	-2632	10
3.18E-02	7.78E+07	10/20/20	##########	3509	-2740	10
4.35E-02	1.03E+08	10/20/20	##########	3572	-2775	7
4.21E-02	1.02E+08	10/20/20	##########	3709	-2713	9
4.32E-02	1.08E+08	10/20/20	##########	5133	-2574	-12
4.03E-02	1.00E+08	10/20/20	##########	4829	-2906	10
3.32E-02	8.15E+07	10/20/20	##########	-3897	3629	-6
3.13E-02	7.68E+07	10/20/20	##########	-3609	3758	-9
4.33E-02	1.05E+08	10/20/20	##########	-3514	3689	-9
3.89E-02	9.61E+07	10/20/20	##########	-4854	2995	-4
3.57E-02	8.82E+07	10/20/20	##########	-5157	2870	-4
4.23E-02	1.02E+08	10/20/20	##########	-4724	3041	-8

3.59E-02	8.50E+07	10/20/20	##########	64	526	1
3.45E-02	8.19E+07	10/20/20	##########	156	473	-6
3.63E-02	9.60E+07	10/20/20	##########	-20	445	1
3.61E-02	9.44E+07	10/20/20	##########	-219	410	1
3.65E-02	8.71E+07	10/20/20	##########	-161	491	-8
3.65E-02	1.00E+08	10/20/20	##########	-294	482	-18

3.45E-02	8.72E+07	10/20/20	##########	-1354	674	-7
3.43E-02	8.53E+07	10/20/20	##########	-1302	659	-8
3.44E-02	8.51E+07	10/20/20	##########	-1257	645	-8
3.43E-02	8.46E+07	10/20/20	##########	-1176	620	-8
3.38E-02	8.44E+07	10/20/20	1:00:00 PM	-655	-1704	-5
3.12E-02	7.79E+07	10/20/20	1:03:00 PM	-958	-1835	-6
3.29E-02	8.24E+07	10/20/20	1:07:00 PM	-801	-2047	-8
3.29E-02	8.24E+07	10/20/20	1:10:00 PM	-699	-2304	-7
3.26E-02	8.15E+07	10/20/20	1:15:00 PM	-746	-2964	-8
3.53E-02	8.68E+07	10/20/20	1:18:00 PM	-609	-3110	-8
3.26E-02	7.87E+07	10/20/20	1:23:00 PM	-752	-3361	-10
3.44E-02	8.34E+07	10/20/20	1:26:00 PM	-532	-3466	-8
3.27E-02	7.98E+07	10/20/20	1:30:00 PM	-740	-3821	-11
3.47E-02	8.69E+07	10/20/20	1:35:00 PM	-704	-4035	-9
3.52E-02	8.84E+07	10/20/20	1:38:00 PM	-2635	-2387	-10
3.39E-02	8.56E+07	10/20/20	1:41:00 PM	-2581	-1758	-8
3.41E-02	6.00E+07	10/20/20	1:45:00 PM	1885	-1979	-13
3.35E-02	6.18E+07	10/20/20	1:48:00 PM	2213	-1938	-13
3.32E-02	6.14E+07	10/20/20	1:51:00 PM	2405	-2048	-12
3.63E-02	9.16E+07	10/20/20	1:56:00 PM	2873	-1002	-10
3.67E-02	9.24E+07	10/20/20	2:00:00 PM	-1131	3264	-7
3.88E-02	9.51E+07	10/20/20	2:03:00 PM	-128	4115	2
3.62E-02	9.10E+07	10/20/20	2:06:00 PM	-1678	4128	-7
3.17E-02	8.08E+07	10/20/20	2:09:00 PM	-1810	3948	-8
3.43E-02	8.36E+07	10/20/20	2:14:00 PM	-1170	561	-9
3.41E-02	8.26E+07	10/20/20	2:17:00 PM	-1245	553	-8
3.43E-02	8.34E+07	10/20/20	2:20:00 PM	-1467	704	-7
3.44E-02	8.31E+07	10/20/20	2:23:00 PM	-1441	623	-8

3.43E-02

3.41E-02	8.27E+07	10/20/20	2:51:00 PM	-417	5139	13
3.80E-02	9.19E+07	10/20/20	2:54:00 PM	-1088	4997	8
3.33E-02	8.31E+07	10/20/20	2:57:00 PM	-1599	4737	1
3.45E-02	5.50E+07	10/20/20	3:00:00 PM	3230	2042	-4
3.45E-02	5.46E+07	10/20/20	3:03:00 PM	3198	2309	-3
3.39E-02	5.87E+07	10/20/20	3:06:00 PM	3249	2862	-2
3.37E-02	5.17E+07	10/20/20	3:09:00 PM	-1846	2392	-3
3.37E-02	5.79E+07	10/20/20	3:12:00 PM	-2037	2507	3
3.39E-02	5.81E+07	10/20/20	3:15:00 PM	-1914	2149	6
3.35E-02	5.78E+07	10/20/20	3:18:00 PM	-2348	2111	4
3.12E-02	7.74E+07	10/20/20	3:23:00 PM	-840	-4005	-3
2.88E-02	7.31E+07	10/20/20	3:26:00 PM	-862	-3751	-4
3.27E-02	8.19E+07	10/20/20	3:29:00 PM	-516	-3275	-8
3.52E-02	8.79E+07	10/20/20	3:31:00 PM	-605	-2752	1
3.42E-02	8.61E+07	10/20/20	3:34:00 PM	-560	-2440	0

3.43E-02	8.35E+07	10/20/20	3:37:00 PM	-1354	548	0
3.43E-02	8.36E+07	10/20/20	3:40:00 PM	-1378	491	0
3.42E-02	8.33E+07	10/20/20	3:43:00 PM	-1325	469	-1
3.43E-02	8.31E+07	10/20/20	3:46:00 PM	-1275	490	-1

3.43E-02

3.48E-02	8.54E+07	10/24/20	8:58:00 PM	1284	-543	-10
3.45E-02	8.49E+07	10/24/20	9:01:00 PM	1181	-551	-10
3.48E-02	8.47E+07	10/24/20	9:04:00 PM	1092	-585	-11
3.45E-02	8.37E+07	10/24/20	9:07:00 PM	1055	-612	-12
2.98E-02	7.23E+07	10/24/20	9:10:00 PM	-1425	2645	-8
3.16E-02	7.47E+07	10/24/20	9:13:00 PM	-1196	2579	-6
3.14E-02	7.43E+07	10/24/20	9:16:00 PM	-1087	2645	-6
3.22E-02	7.78E+07	10/24/20	9:18:00 PM	-1174	2405	-7
3.23E-02	7.78E+07	10/24/20	9:21:00 PM	-982	2440	-7
3.17E-02	7.57E+07	10/24/20	9:24:00 PM	-810	2758	-3

3.07E-02	7.42E+07	10/24/20	9:27:00 PM	-891	2789	-8
3.22E-02	7.62E+07	10/24/20	9:30:00 PM	-479	2828	-3
3.31E-02	7.93E+07	10/24/20	9:33:00 PM	-419	2654	-7
3.55E-02	8.75E+07	10/24/20	9:36:00 PM	1153	4483	-7

3.47E-02	8.39E+07	10/24/20	9:39:00 PM	1095	-685	-11
3.46E-02	8.29E+07	10/24/20	9:42:00 PM	1199	-688	-11
3.45E-02	8.28E+07	10/24/20	9:45:00 PM	1369	-775	-10
3.45E-02	8.25E+07	10/24/20	9:48:00 PM	1408	-757	-8

3.46E-02

3.78E-02	9.15E+07	10/24/20	9:51:00 PM	1261	4407	-7
3.69E-02	8.97E+07	10/24/20	9:54:00 PM	1180	4320	-6
3.67E-02	8.94E+07	10/24/20	9:57:00 PM	1208	4154	-7
3.74E-02	8.99E+07	10/24/20	##########	1327	4022	-8
3.57E-02	8.66E+07	10/24/20	##########	1189	5709	-8
3.80E-02	9.25E+07	10/24/20	##########	1186	5620	-7
3.87E-02	9.34E+07	10/24/20	##########	1283	5618	-8
3.63E-02	8.70E+07	10/24/20	##########	1261	5369	-6
3.24E-02	7.89E+07	10/24/20	##########	478	-2019	-7
3.98E-02	9.77E+07	10/24/20	##########	563	-2141	-5

3.50E-02	8.70E+07	10/24/20	##########	1420	-692	-10
3.49E-02	8.82E+07	10/24/20	##########	1424	-649	-9
3.46E-02	8.74E+07	10/24/20	##########	1510	-635	-10
3.46E-02	8.77E+07	10/24/20	##########	1540	-536	-10

3.47E-02

3.65E-02	9.39E+07	10/24/20	##########	702	-1899	-5
3.41E-02	8.74E+07	10/24/20	##########	666	-1981	-5
3.57E-02	9.08E+07	10/24/20	##########	741	-2017	-6
4.19E-02	1.07E+08	10/24/20	##########	705	-2075	-7
3.21E-02	8.53E+07	10/24/20	##########	784	-2036	-8
3.24E-02	8.52E+07	10/24/20	##########	771	-2068	-8
3.16E-02	8.27E+07	10/24/20	##########	877	-1864	-8
2.21E-02	6.39E+07	10/24/20	##########	819	-2011	-9
1.78E-02	5.65E+07	10/24/20	##########	796	-2069	-7
2.15E-02	6.12E+07	10/24/20	##########	784	-2099	-5
3.61E-02	9.18E+07	10/24/20	##########	902	-3137	-9

3.69E-02	9.25E+07	10/24/20	##########	998	-3182	-8
3.74E-02	9.60E+07	10/24/20	##########	997	-3271	-8
3.06E-02	7.80E+07	10/24/20	##########	1080	-3199	-9
2.79E-02	8.33E+07	10/24/20	##########	1041	-3127	-7

3.42E-02	8.38E+07	10/24/20	##########	1575	-536	-10
3.47E-02	8.69E+07	10/24/20	##########	1523	-424	-11
3.47E-02	8.70E+07	10/24/20	##########	1407	-410	-11
3.47E-02	8.62E+07	10/24/20	##########	1395	-455	-10

3.47E-02

3.48E-02	8.71E+07	10/25/20	8:08:00 AM	-350	2846	-12
3.48E-02	8.54E+07	10/25/20	8:11:00 AM	-350	2826	-13
3.39E-02	7.80E+07	10/25/20	8:14:00 AM	-350	2806	-15
3.44E-02	8.19E+07	10/25/20	8:17:00 AM	-331	2887	-15
3.49E-02	8.44E+07	10/25/20	8:20:00 AM	-429	2817	-14
3.50E-02	8.29E+07	10/25/20	8:23:00 AM	-359	2760	-15

3.38E-02	8.21E+07	10/25/20	8:28:00 AM	934	4107	-11
3.49E-02	8.79E+07	10/25/20	8:33:00 AM	1023	4275	-10
3.60E-02	9.04E+07	10/25/20	8:36:00 AM	1160	3876	-5
3.92E-02	9.66E+07	10/25/20	8:40:00 AM	620	3866	-12
3.67E-02	9.27E+07	10/25/20	8:43:00 AM	589	4085	-12
3.96E-02	9.65E+07	10/25/20	8:48:00 AM	-717	4035	-10
3.97E-02	9.84E+07	10/25/20	8:51:00 AM	-781	3932	-10
3.99E-02	9.72E+07	10/25/20	8:54:00 AM	-747	4384	-12
3.88E-02	9.64E+07	10/25/20	8:59:00 AM	-1004	4833	-13
3.93E-02	9.66E+07	10/25/20	9:02:00 AM	-1219	5720	-15
3.57E-02	8.91E+07	10/25/20	9:06:00 AM	-1940	5591	-17
3.91E-02	9.43E+07	10/25/20	9:12:00 AM	-2920	3927	-12
3.89E-02	9.72E+07	10/25/20	9:17:00 AM	-2684	4133	-11
3.95E-02	9.92E+07	10/25/20	9:21:00 AM	3711	3992	-13
3.98E-02	1.01E+08	10/25/20	9:24:00 AM	3533	3959	-12
3.79E-02	9.57E+07	10/25/20	9:28:00 AM	3649	3903	-12
3.70E-02	9.51E+07	10/25/20	9:31:00 AM	-475	-2476	-12
3.80E-02	9.67E+07	10/25/20	9:35:00 AM	-1162	-3018	-11
3.82E-02	9.73E+07	10/25/20	9:38:00 AM	2791	-2008	-8
1.61E-03	5.97E+06	10/25/20	9:41:00 AM	3651	-2872	-9

3.48E-02	8.63E+07	10/25/20	9:45:00 AM	-397	2733	-16
3.48E-02	8.61E+07	10/25/20	9:48:00 AM	-371	2693	-16
3.47E-02	8.53E+07	10/25/20	9:51:00 AM	-328	2647	-15
3.48E-02	8.62E+07	10/25/20	9:54:00 AM	-205	2557	-16

3.48E-02

3.51E-02	8.53E+07	10/25/20	##########	2872	-770	-5
3.49E-02	8.39E+07	10/25/20	##########	2949	-630	-4
3.50E-02	8.40E+07	10/25/20	##########	3055	-709	-3
3.50E-02	8.44E+07	10/25/20	##########	3062	-884	-4

4.10E-02	1.02E+08	10/25/20	##########	-1822	6014	-8
3.52E-02	8.56E+07	10/25/20	##########	-1758	5795	-8
3.09E-02	7.93E+07	10/25/20	##########	-1642	5775	-9
2.92E-02	7.57E+07	10/25/20	##########	-2542	4476	-11
4.07E-02	1.04E+08	10/25/20	##########	-204	5132	-5
3.87E-02	9.91E+07	10/25/20	##########	-1286	4848	-6
3.27E-02	8.66E+07	10/25/20	##########	-1452	4726	-6
3.18E-02	8.12E+07	10/25/20	##########	1437	5763	5
5.45E-02	1.55E+08	10/25/20	##########	1997	5611	5
3.54E-02	9.07E+07	10/25/20	##########	2112	5570	5
4.15E-02	1.05E+08	10/25/20	##########	2018	5840	3
3.27E-02	8.26E+07	10/25/20	##########	1729	5404	7
3.95E-02	9.80E+07	10/25/20	##########	4538	6221	6
2.75E-02	6.98E+07	10/25/20	##########	4133	6813	5
3.38E-02	8.28E+07	10/25/20	##########	4040	4387	5
3.65E-02	9.02E+07	10/25/20	##########	4610	3606	3
3.39E-02	8.51E+07	10/25/20	##########	2161	5211	6
4.02E-02	9.87E+07	10/25/20	##########	2153	4650	6
3.03E-02	7.46E+07	10/25/20	##########	1841	2893	7
3.97E-02	9.85E+07	10/25/20	##########	273	2869	3

3.51E-02	8.51E+07	10/25/20	##########	2976	-660	-6
3.51E-02	8.54E+07	10/25/20	##########	3069	-660	-7

3.48E-02	8.40E+07	10/25/20	##########	3080	-610	-6
3.49E-02	8.44E+07	10/25/20	##########	3132	-668	-5

3.50E-02

3.54E-02	8.87E+07	10/26/20	##########	-163	1131	-19
3.52E-02	8.79E+07	10/26/20	##########	-286	1110	-21
3.51E-02	8.71E+07	10/26/20	##########	-317	1110	-21
3.50E-02	8.67E+07	10/26/20	##########	-340	1192	-22
3.69E-02	9.08E+07	10/26/20	##########	1035	7228	-16
3.81E-02	9.38E+07	10/26/20	##########	986	7215	-16
3.78E-02	9.28E+07	10/26/20	##########	925	7198	-17
3.78E-02	9.14E+07	10/26/20	##########	835	7192	-18
1.77E-02	4.40E+07	10/26/20	##########	748	7178	-19
3.78E-02	9.27E+07	10/26/20	##########	-113	3150	-23
3.94E-02	9.62E+07	10/26/20	##########	-228	3089	-24
7.86E-03	2.83E+07	10/26/20	##########	4358	4829	-16
3.87E-02	9.47E+07	10/26/20	##########	4559	4470	-19
3.91E-02	9.51E+07	10/26/20	##########	5415	3571	-12
3.50E-02	8.59E+07	10/26/20	##########	-321	1256	-24
3.49E-02	8.47E+07	10/26/20	##########	-242	1236	-21
3.52E-02	8.64E+07	10/26/20	##########	-207	1225	-21
3.51E-02	8.52E+07	10/26/20	##########	-1	1029	-20

3.51E-02

3.80E-02	9.60E+07	10/26/20	##########	7718	-2082	-4
3.79E-02	1.01E+08	10/26/20	##########	7715	-2048	-4
3.73E-02	9.98E+07	10/26/20	##########	7711	-2028	-3
3.90E-02	1.08E+08	10/26/20	##########	4140	-1942	-8
3.40E-02	9.51E+07	10/26/20	##########	4228	-2080	-9
3.90E-02	1.08E+08	10/26/20	##########	4284	-2183	-10
3.82E-02	1.07E+08	10/26/20	##########	4183	-1803	-9
3.69E-02	1.03E+08	10/26/20	##########	3603	-2132	-9
3.96E-02	1.11E+08	10/26/20	##########	3604	-2093	-12
3.85E-02	1.10E+08	10/26/20	##########	3606	-1889	-11

3.54E-02	1.02E+08	10/26/20	##########	-149	957	-22
3.51E-02	9.99E+07	10/26/20	##########	-212	1087	-21
3.52E-02	1.01E+08	10/27/20	##########	-251	982	-20
3.53E-02	1.02E+08	10/27/20	##########	-375	1002	-24

3.52E-02

1.94E-03	8.62E+06	10/27/20	##########	1892	246	-21
1.92E-03	8.57E+06	10/27/20	##########	1912	246	-23
1.93E-03	8.43E+06	10/27/20	##########	1912	226	-19
1.94E-03	8.37E+06	10/27/20	##########	1892	226	-22

3.83E-02	1.10E+08	10/27/20	##########	634	7159	-18
3.84E-02	1.09E+08	10/27/20	##########	624	7121	-22
3.98E-02	1.18E+08	10/27/20	##########	618	7095	-20
2.28E-02	6.61E+07	10/27/20	##########	65	3211	-22
2.91E-02	8.40E+07	10/27/20	##########	19	3190	-20
3.90E-02	1.09E+08	10/27/20	##########	4477	4698	-15
1.63E-02	4.63E+07	10/27/20	##########	5443	3588	-18
3.84E-02	1.05E+08	10/27/20	##########	7730	-2164	-3
3.81E-02	1.04E+08	10/27/20	##########	7712	-2174	-4
3.09E-02	8.37E+07	10/27/20	##########	7735	-2233	-5

1.95E-03	8.46E+06	10/27/20	##########	1881	193	-25
1.97E-03	8.41E+06	10/27/20	##########	1901	193	-22
1.92E-03	8.28E+06	10/27/20	##########	1901	173	-24
2.00E-03	8.51E+06	10/27/20	##########	1881	173	-24

1.77E-02	4.76E+07	10/27/20	1:02:00 AM	7739	-2275	-1
2.13E-02	5.96E+07	10/27/20	1:05:00 AM	7751	-2326	-3
2.87E-02	8.14E+07	10/27/20	1:08:00 AM	4102	-1971	-9
1.76E-02	4.91E+07	10/27/20	1:11:00 AM	4174	-2002	-10
1.72E-02	4.88E+07	10/27/20	1:14:00 AM	4106	-2166	-10
1.45E-02	4.12E+07	10/27/20	1:16:00 AM	4197	-2272	-10
1.69E-02	4.64E+07	10/27/20	1:19:00 AM	4278	-2133	-4
1.68E-02	4.70E+07	10/27/20	1:22:00 AM	3715	-2267	-11

1.94E-02	5.49E+07	10/27/20	1:25:00 AM	3725	-2299	-9
1.67E-02	4.66E+07	10/27/20	1:28:00 AM	3741	-2344	-11
1.93E-03	8.35E+06	10/27/20	1:31:00 AM	1759	176	-23
1.92E-03	8.33E+06	10/27/20	1:34:00 AM	1789	172	-24
1.94E-03	8.35E+06	10/27/20	1:37:00 AM	1979	132	-21
1.96E-03	8.35E+06	10/27/20	1:40:00 AM	2039	163	-22

DTFA-Y	Mass	L2p-bkg	H1-bkg	Sample Name	Chamber Pressure	Comment
9	899155	850190	87932	Al-mesh/#1	9.80E-08	
9	899155	850190	87932	Al-mesh/#1	9.80E-08	
4	899155	850190	87932	Al-mesh/#1	9.70E-08	
4	899155	850190	87932	Al-mesh/#1	9.90E-08	
-12	899155	850190	87932	Al-mesh/#1	9.80E-08	Atg±Ctl
-12	899155	850190	87932	Al-mesh/#1	9.80E-08	Atg±Ctl
-9	899155	850190	87932	Al-mesh/#1	9.80E-08	Atg±Ctl
-8	899155	850190	87932	Al-mesh/#1	9.80E-08	Atg±Ctl
-6	899155	850190	87932	Al-mesh/#1	9.80E-08	Atg±Ctl
-7	899155	850190	87932	Al-mesh/#1	9.80E-08	Atg±Ctl
-8	899155	850190	87932	Al-mesh/#1	9.80E-08	Atg±Ctl
-1	899155	850190	87932	Al-mesh/#1	9.90E-08	Atg±Ctl
-1	899155	850190	87932	Al-mesh/#1	9.80E-08	Atg±Ctl
-2	899155	850190	87932	Al-mesh/#1	9.80E-08	touch quartz
-1	899155	850190	87932	Al-mesh/#1	9.80E-08	touch quartz
2	899155	850190	87932	Al-mesh/#1	9.80E-08	Atg±Ctl
4	899155	850190	87932	Al-mesh/#1	9.80E-08	Atg±Ctl
5	899155	850190	87932	Al-mesh/#1	9.80E-08	Atg±Ctl
6	899155	850190	87932	Al-mesh/#1	9.80E-08	Atg±Ctl
6	899155	850190	87932	Al-mesh/#1	9.70E-08	Atg±Ctl
6	899155	850190	87932	Al-mesh/#1	9.60E-08	Atg±Ctl
6	899155	850190	87932	Al-mesh/#1	9.60E-08	Atg±Ctl
7	899155	850190	87932	Al-mesh/#1	9.80E-08	Atg±Ctl
8	899155	850190	87932	Al-mesh/#1	9.70E-08	Atg±Ctl
4	899155	850190	87932	Al-mesh/#1	9.70E-08	
5	899155	850190	87932	Al-mesh/#1	9.60E-08	
5	899155	850190	87932	Al-mesh/#1	9.60E-08	
6	899155	850190	87932	Al-mesh/#1	9.60E-08	
3	899155	850190	87932	Al-mesh/#1	9.60E-08	

4	899155	850190	87932	Al-mesh/#1	9.50E-08	
3	899155	850190	87932	Al-mesh/#1	9.60E-08	
2	899155	850190	87932	Al-mesh/#1	9.50E-08	
-10	899155	850190	87932	Al-mesh/#1	9.50E-08	
-6	899155	850190	87932	Al-mesh/#1	9.50E-08	
-7	899155	850190	87932	Al-mesh/#1	9.50E-08	
-6	899155	850190	87932	Al-mesh/#1	9.40E-08	
-7	899155	850190	87932	Al-mesh/#1	9.50E-08	
-2	899155	850190	87932	Al-mesh/#1	9.50E-08	
-1	899155	850190	87932	Al-mesh/#1	9.50E-08	
-2	899155	850190	87932	Al-mesh/#1	9.50E-08	
0	899155	850190	87932	Al-mesh/#1	9.50E-08	
-1	899155	850190	87932	Al-mesh/#1	9.50E-08	
7	899155	850190	87932	Al-mesh/#1	9.50E-08	
6	899155	850190	87932	Al-mesh/#1	9.50E-08	
8	899155	850190	87932	Al-mesh/#1	9.40E-08	
6	899155	850190	87932	Al-mesh/#1	9.40E-08	
6	899155	850190	87932	Al-mesh/#1	9.50E-08	
6	899155	850190	87932	Al-mesh/#1	9.50E-08	
6	899155	850190	87932	Al-mesh/#1	9.30E-08	
-3	899155	850190	87932	Al-mesh/#1	9.40E-08	
0	899155	850190	87932	Al-mesh/#1	9.30E-08	
-1	899155	850190	87932	Al-mesh/#1	9.30E-08	
4	899155	850190	87932	Al-mesh/#1	9.20E-08	
3	899155	850190	87932	Al-mesh/#1	9.30E-08	
2	899155	850190	87932	Al-mesh/#1	9.20E-08	
2	899155	850190	87932	Al-mesh/#1	9.20E-08	
3	899159	934318	87817	Al-mesh/#1	1.10E-07	
1	899159	934318	87817	Al-mesh/#1	1.10E-07	
4	899159	934318	87817	Al-mesh/#1	1.10E-07	
3	899159	934318	87817	Al-mesh/#1	1.10E-07	
1	899159	934318	87817	Al-mesh/#1	1.20E-07	
-7	899159	934318	87817	Al-mesh/#1	1.20E-07	on fracture

-5	899159	934318	87817	Al-mesh/#1	1.20E-07	Ctl I
-9	899159	934318	87817	Al-mesh/#1	1.20E-07	Ctl I
-7	899159	934318	87817	Al-mesh/#1	1.20E-07	Ctl I
-10	899159	934318	87817	Al-mesh/#1	1.20E-07	Ctl I
-6	899159	934318	87817	Al-mesh/#1	1.20E-07	Ctl I
-8	899159	934318	87817	Al-mesh/#1	1.20E-07	touch calcite
-7	899159	934318	87817	Al-mesh/#1	1.20E-07	on fracture
-6	899159	934318	87817	Al-mesh/#1	1.20E-07	on fracture
-6	899159	934318	87817	Al-mesh/#1	1.20E-07	Ctl I
-5	899159	934318	87817	Al-mesh/#1	1.20E-07	Ctl I
-8	899159	934318	87817	Al-mesh/#1	1.20E-07	Ctl I
-6	899159	934318	87817	Al-mesh/#1	1.10E-07	Ctl I
-6	899159	934318	87817	Al-mesh/#1	1.10E-07	Ctl I
-4	899159	934318	87817	Al-mesh/#1	1.10E-07	Ctl I
5	899159	934318	87817	Al-mesh/#1	1.10E-07	
4	899159	934318	87817	Al-mesh/#1	1.10E-07	
4	899159	934318	87817	Al-mesh/#1	1.10E-07	
-2	899159	934318	87817	Al-mesh/#1	1.10E-07	
4	899159	934318	87817	Al-mesh/#1	1.10E-07	
1	899159	934318	87817	Al-mesh/#1	1.10E-07	
-8	899159	934318	87817	Al-mesh/#1	1.10E-07	Ctl I
-7	899159	934318	87817	Al-mesh/#1	1.10E-07	Ctl I
2	899159	934318	87817	Al-mesh/#1	1.10E-07	Ctl III
3	899159	934318	87817	Al-mesh/#1	1.10E-07	Ctl III
3	899159	934318	87817	Al-mesh/#1	1.10E-07	Ctl III
2	899159	934318	87817	Al-mesh/#1	1.10E-07	Fe-rich lizard
2	899159	934318	87817	Al-mesh/#1	1.10E-07	Fe-rich lizard
5	899159	934318	87817	Al-mesh/#1	1.10E-07	Fe-rich lizard
9	899159	934318	87817	Al-mesh/#1	1.10E-07	Ctl III
-10	899159	934318	87817	Al-mesh/#1	1.10E-07	Ctl III
-9	899159	934318	87817	Al-mesh/#1	1.10E-07	Ctl III
-7	899159	934318	87817	Al-mesh/#1	1.10E-07	Fe-rich lizard
-8	899159	934318	87817	Al-mesh/#1	1.10E-07	Ctl III
-7	899159	934318	87817	Al-mesh/#1	1.10E-07	Ctl III
-8	899159	934318	87817	Al-mesh/#1	1.10E-07	Fe-rich lizard

5	899159	934318	87817	Al-mesh/#1	1.10E-07	
4	899159	934318	87817	Al-mesh/#1	1.10E-07	
3	899159	934318	87817	Al-mesh/#1	1.10E-07	
4	899159	934318	87817	Al-mesh/#1	1.10E-07	
2	899159	934318	87817	Al-mesh/#1	1.10E-07	
2	899159	934318	87817	Al-mesh/#1	1.10E-07	

9	899159	934318	87817	Al-mesh/#1	4.20E-08	
10	899159	934318	87817	Al-mesh/#1	4.20E-08	
10	899159	934318	87817	Al-mesh/#1	4.20E-08	
9	899159	934318	87817	Al-mesh/#1	4.20E-08	
2	899159	934318	87817	Al-mesh/#1	4.20E-08	Ctl±Lz I
6	899159	934318	87817	Al-mesh/#1	4.10E-08	Ctl±Lz I
7	899159	934318	87817	Al-mesh/#1	4.10E-08	Ctl±Lz I
8	899159	934318	87817	Al-mesh/#1	4.20E-08	Ctl±Lz I
12	899159	934318	87817	Al-mesh/#1	4.10E-08	Ctl±Lz I
14	899159	934318	87817	Al-mesh/#1	4.10E-08	Ctl±Lz I
15	899159	934318	87817	Al-mesh/#1	4.10E-08	Ctl±Lz I
15	899159	934318	87817	Al-mesh/#1	4.10E-08	Ctl±Lz I
19	899159	934318	87817	Al-mesh/#1	4.10E-08	Ctl±Lz I
18	899159	934318	87817	Al-mesh/#1	4.10E-08	Ctl±Lz I
15	899159	934318	87817	Al-mesh/#1	4.10E-08	Ctl±Lz I
8	899159	934318	87817	Al-mesh/#1	4.00E-08	Ctl±Lz I
7	899159	934318	87817	Al-mesh/#1	4.10E-08	Ctl II (low yi
7	899159	934318	87817	Al-mesh/#1	4.10E-08	Ctl II (low yi
8	899159	934318	87817	Al-mesh/#1	4.10E-08	Ctl II (low yi
7	899159	934318	87817	Al-mesh/#1	4.00E-08	Ctl±Lz I
10	899159	934318	87817	Al-mesh/#1	4.00E-08	Ctl±Lz I
1	899159	934318	87817	Al-mesh/#1	4.10E-08	Ctl±Lz I
8	899159	934318	87817	Al-mesh/#1	4.10E-08	Ctl±Lz I
9	899159	934318	87817	Al-mesh/#1	4.00E-08	Ctl±Lz I
10	899159	934318	87817	Al-mesh/#1	4.00E-08	
10	899159	934318	87817	Al-mesh/#1	4.00E-08	
10	899159	934318	87817	Al-mesh/#1	4.00E-08	
10	899159	934318	87817	Al-mesh/#1	3.90E-08	

3	899159	934318	87817	Al-mesh/#1	4.00E-08	Ctl±Lz I
4	899159	934318	87817	Al-mesh/#1	3.90E-08	Ctl±Lz I
5	899159	934318	87817	Al-mesh/#1	3.90E-08	Ctl±Lz I
11	899159	934318	87817	Al-mesh/#1	4.00E-08	Ctl II (low yi
12	899159	934318	87817	Al-mesh/#1	4.00E-08	Ctl II (low yi
8	899159	934318	87817	Al-mesh/#1	4.00E-08	Ctl II (low yi
7	899159	934318	87817	Al-mesh/#1	3.90E-08	Ctl II (low yi
5	899159	934318	87817	Al-mesh/#1	3.90E-08	Ctl II (low yi
7	899159	934318	87817	Al-mesh/#1	3.90E-08	Ctl II (low yi
5	899159	934318	87817	Al-mesh/#1	3.90E-08	Ctl II (low yi
18	899159	934318	87817	Al-mesh/#1	3.90E-08	Ctl±Lz I
17	899159	934318	87817	Al-mesh/#1	3.90E-08	Ctl±Lz I
13	899159	934318	87817	Al-mesh/#1	3.80E-08	Ctl±Lz I
11	899159	934318	87817	Al-mesh/#1	3.90E-08	Ctl±Lz I
8	899159	934318	87817	Al-mesh/#1	3.80E-08	Ctl±Lz I

8	899159	934318	87817	Al-mesh/#1	3.80E-08
8	899159	934318	87817	Al-mesh/#1	3.80E-08
9	899159	934318	87817	Al-mesh/#1	3.80E-08
8	899159	934318	87817	Al-mesh/#1	3.80E-08

-2	899152	860662	87430	Al-mesh/#1	4.20E-08
-2	899152	860662	87430	Al-mesh/#1	4.10E-08
-3	899152	860662	87430	Al-mesh/#1	4.10E-08
-3	899152	860662	87430	Al-mesh/#1	4.10E-08

3	899152	860662	87430	Al-mesh/#1	4.10E-08	on fracture
3	899152	860662	87430	Al-mesh/#1	4.10E-08	Lz±Ctl I
3	899152	860662	87430	Al-mesh/#1	4.10E-08	Lz±Ctl I
4	899152	860662	87430	Al-mesh/#1	4.00E-08	Lz±Ctl I
3	899152	860662	87430	Al-mesh/#1	4.10E-08	Lz±Ctl I
0	899152	860662	87430	Al-mesh/#1	4.10E-08	Lz±Ctl I

1	899152	860662	87430	Al-mesh/#1	4.10E-08	Lz±Ctl I
2	899152	860662	87430	Al-mesh/#1	4.00E-08	Lz±Ctl I
4	899152	860662	87430	Al-mesh/#1	4.00E-08	Lz±Ctl I
-2	899152	860662	87430	Al-mesh/#1	4.20E-08	Lz±Ctl I
-3	899152	860662	87430	Al-mesh/#1	4.10E-08	
-2	899152	860662	87430	Al-mesh/#1	4.10E-08	
-2	899152	860662	87430	Al-mesh/#1	4.20E-08	
-2	899152	860662	87430	Al-mesh/#1	4.10E-08	
-1	899152	860662	87430	Al-mesh/#1	4.10E-08	Lz±Ctl I
-1	899152	860662	87430	Al-mesh/#1	4.10E-08	Lz±Ctl I
-1	899152	860662	87430	Al-mesh/#1	4.10E-08	Lz±Ctl I
-1	899152	860662	87430	Al-mesh/#1	4.10E-08	Lz±Ctl I
-2	899152	860662	87430	Al-mesh/#1	4.10E-08	Lz±Ctl I
-2	899152	860662	87430	Al-mesh/#1	4.10E-08	Lz±Ctl I
-2	899152	860662	87430	Al-mesh/#1	4.10E-08	on fracture
-2	899152	860662	87430	Al-mesh/#1	4.00E-08	Lz±Ctl I
-2	899152	860662	87430	Al-mesh/#1	4.10E-08	on fracture
-1	899152	860662	87430	Al-mesh/#1	4.10E-08	on fracture
-2	899152	860662	87430	Al-mesh/#1	4.10E-08	
-2	899152	860662	87430	Al-mesh/#1	4.10E-08	
-2	899152	860662	87430	Al-mesh/#1	4.10E-08	
-2	899152	860662	87430	Al-mesh/#1	4.10E-08	
-2	899152	860662	87430	Al-mesh/#1	4.10E-08	Lz±Ctl I
-2	899152	860662	87430	Al-mesh/#1	4.00E-08	Lz±Ctl I
-1	899152	860662	87430	Al-mesh/#1	4.10E-08	Lz±Ctl I
-2	899152	860662	87430	Al-mesh/#1	4.00E-08	Lz±Ctl I
-1	899152	860662	87430	Al-mesh/#1	4.10E-08	Lz±Ctl I
-1	899152	860662	87430	Al-mesh/#1	4.00E-08	Lz±Ctl I
-2	899152	860662	87430	Al-mesh/#1	4.10E-08	Lz±Ctl I
0	899152	860662	87430	Al-mesh/#1	4.00E-08	touch calcite
-1	899152	860662	87430	Al-mesh/#1	4.10E-08	touch calcite
-1	899152	860662	87430	Al-mesh/#1	4.00E-08	touch calcite
1	899152	860662	87430	Al-mesh/#1	4.00E-08	Lz±Ctl I

2	899152	860662	87430	Al-mesh/#1	4.00E-08	Lz±Ctl I
2	899152	860662	87430	Al-mesh/#1	4.00E-08	Lz±Ctl I
3	899152	860662	87430	Al-mesh/#1	4.10E-08	touch calcite
3	899152	860662	87430	Al-mesh/#1	4.00E-08	touch calcite

-2	899152	860662	87430	Al-mesh/#1	4.00E-08
-2	899152	860662	87430	Al-mesh/#1	4.00E-08
-2	899152	860662	87430	Al-mesh/#1	4.00E-08
-2	899152	860662	87430	Al-mesh/#1	4.00E-08

9	899162	858110	87650	Al-mesh/#1	4.20E-08	
8	899162	858110	87650	Al-mesh/#1	4.20E-08	
7	899162	858110	87650	Al-mesh/#1	4.20E-08	
8	899162	858110	87650	Al-mesh/#1	4.10E-08	
5	899162	858110	87650	Al-mesh/#1	4.20E-08	
5	899162	858110	87650	Al-mesh/#1	4.20E-08	
6	899162	858110	87650	Al-mesh/#1	4.20E-08	Lz±Ctl I
7	899162	858110	87650	Al-mesh/#1	4.20E-08	Lz±Ctl I
8	899162	858110	87650	Al-mesh/#1	4.20E-08	Lz±Ctl I
6	899162	858110	87650	Al-mesh/#1	4.20E-08	Lz±Ctl I
6	899162	858110	87650	Al-mesh/#1	4.30E-08	Lz±Ctl I
6	899162	858110	87650	Al-mesh/#1	4.30E-08	Lz±Ctl I
6	899162	858110	87650	Al-mesh/#1	4.20E-08	Lz±Ctl I
2	899162	858110	87650	Al-mesh/#1	4.20E-08	Lz±Ctl I
1	899162	858110	87650	Al-mesh/#1	4.20E-08	Lz±Ctl I
-1	899162	858110	87650	Al-mesh/#1	4.30E-08	Lz±Ctl I
0	899162	858110	87650	Al-mesh/#1	4.30E-08	Lz±Ctl I
0	899162	858110	87650	Al-mesh/#1	4.20E-08	Ctl II
-1	899162	858110	87650	Al-mesh/#1	4.20E-08	Ctl II
2	899162	858110	87650	Al-mesh/#1	4.30E-08	Ctl II
1	899162	858110	87650	Al-mesh/#1	4.30E-08	Ctl II
2	899162	858110	87650	Al-mesh/#1	4.30E-08	Lz±Ctl II
3	899162	858110	87650	Al-mesh/#1	4.30E-08	Lz±Ctl I
3	899162	858110	87650	Al-mesh/#1	4.20E-08	Lz±Ctl I
2	899162	858110	87650	Al-mesh/#1	4.30E-08	Lz±Ctl I
3	899162	858110	87650	Al-mesh/#1	4.20E-08	high yield, ot

3	899162	858110	87650	Al-mesh/#1	4.20E-08	
3	899162	858110	87650	Al-mesh/#1	4.20E-08	
2	899162	858110	87650	Al-mesh/#1	4.20E-08	
3	899162	858110	87650	Al-mesh/#1	4.20E-08	

-4	899162	858110	87650	Al-mesh/#1	5.00E-08	
-3	899162	858110	87650	Al-mesh/#1	5.00E-08	
-2	899162	858110	87650	Al-mesh/#1	5.00E-08	
-3	899162	858110	87650	Al-mesh/#1	5.00E-08	
-11	899162	858110	87650	Al-mesh/#1	5.10E-08	Lz±Ctl I
-9	899162	858110	87650	Al-mesh/#1	5.10E-08	Lz±Ctl I
-10	899162	858110	87650	Al-mesh/#1	5.10E-08	Lz±Ctl I
-9	899162	858110	87650	Al-mesh/#1	5.10E-08	Lz±Ctl I
-9	899162	858110	87650	Al-mesh/#1	5.10E-08	Lz±Ctl I
-7	899162	858110	87650	Al-mesh/#1	5.20E-08	Lz±Ctl I
-7	899162	858110	87650	Al-mesh/#1	5.10E-08	Lz±Ctl I
-14	899162	858110	87650	Al-mesh/#1	5.20E-08	Lz±Ctl I
-12	899162	858110	87650	Al-mesh/#1	5.20E-08	touch calcite
-13	899162	858110	87650	Al-mesh/#1	5.20E-08	mix with Fe-1
-14	899162	858110	87650	Al-mesh/#1	5.20E-08	on fracture
-12	899162	858110	87650	Al-mesh/#1	5.10E-08	Lz±Ctl I
-18	899162	858110	87650	Al-mesh/#1	5.20E-08	Lz±Ctl II
-16	899162	858110	87650	Al-mesh/#1	5.20E-08	mix
-9	899162	858110	87650	Al-mesh/#1	5.20E-08	Lz±Ctl II
-8	899162	858110	87650	Al-mesh/#1	5.20E-08	Lz±Ctl II
-11	899162	858110	87650	Al-mesh/#1	5.20E-08	pit not found
-7	899162	858110	87650	Al-mesh/#1	5.20E-08	mix with Fe-1
1	899162	858110	87650	Al-mesh/#1	5.20E-08	Lz±Ctl I
1	899162	858110	87650	Al-mesh/#1	5.20E-08	Lz±Ctl I

-5	899162	858110	87650	Al-mesh/#1	5.20E-08
-4	899162	858110	87650	Al-mesh/#1	5.10E-08

-3	899162	858110	87650	Al-mesh/#1	5.20E-08	
-3	899162	858110	87650	Al-mesh/#1	5.20E-08	
-5	899159	900966	87421	Al-mesh/#1	4.60E-08	
-6	899159	900966	87421	Al-mesh/#1	4.50E-08	
-6	899159	900966	87421	Al-mesh/#1	4.60E-08	
-5	899159	900966	87421	Al-mesh/#1	4.60E-08	
-12	899159	900966	87421	Al-mesh/#1	4.60E-08	Ctl
-12	899159	900966	87421	Al-mesh/#1	4.60E-08	Ctl
-12	899159	900966	87421	Al-mesh/#1	4.60E-08	Ctl
-11	899159	900966	87421	Al-mesh/#1	4.60E-08	Ctl
-11	899159	900966	87421	Al-mesh/#1	4.60E-08	Talc (Tlc 1b)
-7	899159	900966	87421	Al-mesh/#1	4.60E-08	Ctl
-7	899159	900966	87421	Al-mesh/#1	4.50E-08	touch oxide v
-21	899159	900966	87421	Al-mesh/#1	4.60E-08	different phas
-19	899159	900966	87421	Al-mesh/#1	4.60E-08	Ctl
-18	899159	900966	87421	Al-mesh/#1	4.60E-08	Ctl
-5	899159	900966	87421	Al-mesh/#1	4.60E-08	
-5	899159	900966	87421	Al-mesh/#1	4.50E-08	
-5	899159	900966	87421	Al-mesh/#1	4.60E-08	
-5	899159	900966	87421	Al-mesh/#1	4.50E-08	
3	899159	900966	87421	Al-mesh/#1	4.60E-08	Ctl
4	899159	900966	87421	Al-mesh/#1	4.60E-08	Ctl
4	899159	900966	87421	Al-mesh/#1	4.60E-08	on fracture
-5	899159	900966	87421	Al-mesh/#1	4.60E-08	Ctl
-4	899159	900966	87421	Al-mesh/#1	4.60E-08	touch talc
-4	899159	900966	87421	Al-mesh/#1	4.60E-08	Ctl
-5	899159	900966	87421	Al-mesh/#1	4.60E-08	Ctl
-4	899159	900966	87421	Al-mesh/#1	4.50E-08	touch talc
-4	899159	900966	87421	Al-mesh/#1	4.60E-08	touch talc
-6	899159	900966	87421	Al-mesh/#1	4.60E-08	Ctl

-5	899159	900966	87421	Al-mesh/#1	4.50E-08	
-5	899159	900966	87421	Al-mesh/#1	4.60E-08	
-5	899159	900966	87421	Al-mesh/#1	4.50E-08	
-6	899159	900966	87421	Al-mesh/#1	4.50E-08	
-8	899159	900966	87421	Al-mesh/#1	4.60E-08	
-8	899159	900966	87421	Al-mesh/#1	4.50E-08	
-8	899159	900966	87421	Al-mesh/#1	4.50E-08	
-9	899159	900966	87421	Al-mesh/#1	4.50E-08	
-10	899159	900966	87421	Al-mesh/#1	4.50E-08	Serpentine (S
-11	899159	900966	87421	Al-mesh/#1	4.50E-08	mix Tlc+Srp
-10	899159	900966	87421	Al-mesh/#1	4.50E-08	mix Tlc+Srp
-7	899159	900966	87421	Al-mesh/#1	4.50E-08	mix Tlc+Srp
-7	899159	900966	87421	Al-mesh/#1	4.50E-08	mix Tlc+Srp
-20	899159	900966	87421	Al-mesh/#1	4.50E-08	Serpentine (S
-19	899159	900966	87421	Al-mesh/#1	4.50E-08	on fracture
4	899159	900966	87421	Al-mesh/#1	4.60E-08	Serpentine (S
4	899159	900966	87421	Al-mesh/#1	4.50E-08	Serpentine (S
4	899159	900966	87421	Al-mesh/#1	4.50E-08	mix Tlc+Srp
-9	899159	900966	87421	Al-mesh/#1	4.50E-08	
-9	899159	900966	87421	Al-mesh/#1	4.50E-08	
-10	899159	900966	87421	Al-mesh/#1	4.50E-08	
-9	899159	900966	87421	Al-mesh/#1	4.50E-08	
5	899159	900966	87421	Al-mesh/#1	4.50E-08	
5	899159	900966	87421	Al-mesh/#1	4.50E-08	
-6	899159	900966	87421	Al-mesh/#1	4.60E-08	
-5	899159	900966	87421	Al-mesh/#1	4.60E-08	
-5	899159	900966	87421	Al-mesh/#1	4.60E-08	on fracture
-3	899159	900966	87421	Al-mesh/#1	4.60E-08	
-3	899159	900966	87421	Al-mesh/#1	4.60E-08	
-3	899159	900966	87421	Al-mesh/#1	4.60E-08	

-3	899159	900966	87421	Al-mesh/#1	4.60E-08
-3	899159	900966	87421	Al-mesh/#1	4.60E-08

-9	899159	900966	87421	Al-mesh/#1	4.50E-08
-9	899159	900966	87421	Al-mesh/#1	4.60E-08
-9	899159	900966	87421	Al-mesh/#1	4.60E-08
-8	899159	900966	87421	Al-mesh/#1	4.50E-08

ite rim
ite rim
ite rim

ite rim

ite rim

eld, very porous)
eld, very porous)
eld, very porous)

eld, very porous)
eld, very porous)
eld, very porous)
eld, very porous)
eld, very porous)
eld, very porous)
eld, very porous)

her phase

rich serpentine

rich serpentine

rp-5b) - on fracture

rp-9b)

rp-9b)
rp-10b)

SUMMARY OF EPMA ANALYSES IN SILICATES

Number of oxygen	14	14	14
Sample	OM09-12	OM09-12	OM09-12
SIMS pit	Srp-1	Srp-2	Srp-4
SIMS session	S1	S1	S1
Mineral	Atg	Atg	Atg
Texture	intergrown with quartz	intergrown with quartz	intergrown with quartz
wt.%			
SiO_2	44.72	44.66	44.12
TiO_2	<0,04	<0,04	<0,04
Al_2O_3	0.27	0.60	0.69
Cr_2O_3	<0,05	<0,05	<0,05
FeO(total)	3.47	3.36	3.76
MnO	0.05	<0,05	<0,05
MgO	41.00	40.83	40.41
CaO	<0,02	<0,02	<0,02
Na_2O	<0,03	<0,03	<0,03
NiO	0.15	0.15	0.18
H_2O	10.05	10.07	11.54
Total	**99.70**	**99.68**	**100.69**
apfu			
Si	4.063	4.054	4.037
Ti	0.000	0.000	0.000
Al	0.029	0.064	0.074
Cr	0.000	0.000	0.000
Fe^{2+}	0.264	0.255	0.287
Mn	0.004	0.000	0.000
Mg	5.554	5.526	5.512
Ca	0.000	0.000	0.000
Na	0.000	0.000	0.000
Ni	0.011	0.011	0.013
Sum of Cations	**9.923**	**9.911**	**9.923**
Mg# (mole %)*	**95.5**	**95.6**	**95.0**
n OH	8	8	8
Sum oxygen units	2.56	2.57	2.55

14	14	14	14
OM09-12	OM09-12	OM09-12	OM09-12
Srp-5	Srp-6	Srp-7	Srp-9
S1	S1	S1	S1
Atg	Atg	Atg	Atg
intergrown with quartz	intergrown with quartz	intergrown with quartz	intergrown with quartz
43.97	46.30	44.84	48.77
<0,04	<0,04	<0,04	<0,04
0.68	0.35	0.31	0.68
<0,05	<0,05	<0,05	<0,05
3.16	3.41	2.46	3.51
<0,05	<0,05	0.05	<0,05
40.63	39.82	40.80	37.09
0.02	0.03	<0,02	<0,02
<0,03	<0,03	<0,03	<0,03
0.18	0.11	0.14	0.17
12.85	8.43	7.99	6.67
101.49	**98.44**	**96.59**	**96.88**
4.034	4.168	4.096	4.345
0.000	0.000	0.000	0.000
0.073	0.037	0.034	0.071
0.000	0.000	0.000	0.000
0.243	0.257	0.188	0.261
0.000	0.000	0.004	0.000
5.558	5.343	5.555	4.927
0.002	0.002	0.000	0.000
0.000	0.000	0.000	0.000
0.013	0.008	0.010	0.012
9.923	**9.815**	**9.886**	**9.616**
95.8	**95.4**	**96.7**	**95.0**
8	8	8	8
2.54	2.59	2.55	2.62

14	14	14	14
OM09-12	OM09-12	OM09-12	OM13-1
Srp-14	Srp-16	Srp-20	Srp-2
S1	S1	S1	S1
Atg	Atg	Atg	Ctl
intergrown with quartz	intergrown with quartz	intergrown with quartz	intergrown with calcite
44.52	43.45	44.44	45.00
<0,04	<0,04	<0,04	<0,04
0.13	0.85	0.68	0.11
<0,05	<0,05	<0,05	<0,05
3.08	3.46	3.19	1.97
0.07	<0,05	<0,05	<0,05
41.14	40.86	41.73	39.88
<0,02	<0,02	<0,02	0.31
<0,03	<0,03	<0,03	<0,03
0.10	0.14	0.11	0.14
7.64	11.17	12.20	8.13
96.67	**99.93**	**102.34**	**95.53**
4.066	3.993	4.012	4.151
0.000	0.000	0.000	0.000
0.014	0.092	0.072	0.011
0.000	0.000	0.000	0.000
0.235	0.266	0.241	0.152
0.005	0.000	0.000	0.000
5.600	5.599	5.616	5.484
0.000	0.000	0.000	0.031
0.000	0.000	0.000	0.000
0.007	0.010	0.008	0.010
9.927	**9.960**	**9.949**	**9.839**
96.0	**95.5**	**95.9**	**97.3**
8	8	8	8
2.55	2.54	2.58	2.53

14	14	14	14
OM13-1	OM13-1	OM13-1	OM13-1
Srp-3	Srp-4	Srp-5	Srp-6
S1	S1	S1	S1
Ctl	Ctl	Ctl	Ctl
intergrown with calcite	intergrown with calcite	intergrown with calcite	intergrown with calcite
44.01	43.26	42.83	42.95
<0,04	<0,04	<0,04	<0,04
0.08	0.10	0.12	0.11
<0,05	<0,05	<0,05	<0,05
1.97	2.47	1.97	1.91
0.05	<0,05	0.07	<0,05
38.28	38.98	37.60	37.41
0.46	0.43	0.38	0.80
<0,03	<0,03	<0,03	<0,03
0.19	<0,07	0.07	0.16
6.47	8.06	7.50	6.28
91.50	**93.30**	**90.54**	**89.62**
4.176	4.109	4.161	4.162
0.000	0.000	0.000	0.000
0.008	0.011	0.014	0.012
0.000	0.000	0.000	0.000
0.157	0.196	0.160	0.155
0.004	0.000	0.006	0.000
5.415	5.519	5.446	5.405
0.047	0.043	0.040	0.083
0.000	0.000	0.000	0.000
0.014	0.000	0.005	0.013
9.821	**9.880**	**9.832**	**9.829**
97.2	**96.6**	**97.1**	**97.2**
8	8	8	8
2.46	2.45	2.40	2.40

14	14	14	14
OM13-1	OM13-1	OM13-1	OM13-1
Srp-8	Srp-9	Srp-10	Srp-11
S1	S1	S1	S1
Ctl	Ctl	Ctl	Ctl
intergrown with calcite	intergrown with calcite	intergrown with calcite	intergrown with calcite
43.75	45.00	44.93	44.79
<0,04	<0,04	<0,04	<0,04
0.11	0.08	0.09	0.12
<0,05	<0,05	<0,05	<0,05
2.07	2.29	2.51	1.95
<0,05	<0,05	<0,05	<0,05
38.02	38.49	38.94	39.06
0.38	0.45	0.35	0.38
<0,03	<0,03	<0,03	<0,03
0.21	0.17	0.15	0.16
5.40	6.87	5.42	6.06
89.94	**93.36**	**92.39**	**92.52**
4.175	4.197	4.175	4.175
0.000	0.000	0.000	0.000
0.012	0.009	0.010	0.013
0.000	0.000	0.000	0.000
0.165	0.179	0.195	0.152
0.000	0.000	0.000	0.000
5.410	5.352	5.393	5.427
0.039	0.045	0.035	0.038
0.000	0.000	0.000	0.000
0.016	0.013	0.011	0.012
9.817	**9.794**	**9.818**	**9.817**
97.0	**96.8**	**96.5**	**97.3**
8	8	8	8
2.44	2.50	2.51	2.50

14	14	14	14
OM13-1	OM13-1	OM13-1	OM13-1
Srp-12	Srp-13	Srp-14	Srp-15
S1	S1	S1	S1
Ctl	Ctl	Ctl	Ctl
intergrown with calcite	intergrown with calcite	intergrown with calcite	intergrown with calcite
43.21	44.59	44.51	43.86
<0,04	<0,04	<0,04	<0,04
0.06	0.11	0.10	0.06
<0,05	<0,05	<0,05	<0,05
2.05	2.45	2.27	2.22
<0,05	<0,05	<0,05	<0,05
38.66	38.13	38.01	38.50
0.33	0.34	0.46	0.38
<0,03	<0,03	<0,03	<0,03
0.18	0.13	0.20	0.18
6.62	5.24	6.62	6.45
91.11	**90.98**	**92.17**	**91.66**
4.132	4.197	4.198	4.159
0.000	0.000	0.000	0.000
0.007	0.012	0.011	0.007
0.000	0.000	0.000	0.000
0.164	0.193	0.179	0.176
0.000	0.000	0.000	0.000
5.512	5.350	5.344	5.442
0.034	0.034	0.046	0.039
0.000	0.000	0.000	0.000
0.014	0.010	0.015	0.014
9.863	**9.795**	**9.793**	**9.838**
97.1	**96.5**	**96.8**	**96.9**
8	8	8	8
2.44	2.48	2.47	2.46

14	14	14	14
OM13-1	OM13-1	OM13-1	OM13-1
Srp-16	Srp-17	Srp-18	Srp-21
S1	S1	S1	S1
Ctl	Ctl	Ctl	Fe-rich Lz
intergrown with calcite	intergrown with calcite	intergrown with calcite	-
43.18	43.99	45.95	42.04
<0,04	<0,04	<0,04	<0,04
0.07	0.07	0.03	<0,02
<0,05	<0,05	<0,05	<0,05
2.30	2.21	2.09	5.82
0.05	<0,05	<0,05	0.15
36.85	38.10	39.59	38.83
0.40	0.43	0.10	0.18
<0,03	<0,03	<0,03	<0,03
0.21	0.14	0.13	<0,07
6.04	5.35	7.19	14.91
89.09	**90.31**	**95.08**	**101.94**
4.199	4.180	4.206	3.998
0.000	0.000	0.000	0.000
0.008	0.008	0.003	0.000
0.000	0.000	0.000	0.000
0.187	0.176	0.160	0.463
0.004	0.000	0.000	0.012
5.342	5.397	5.402	5.505
0.041	0.044	0.009	0.019
0.000	0.000	0.000	0.000
0.016	0.011	0.010	0.000
9.798	**9.816**	**9.791**	**9.997**
96.6	**96.8**	**97.1**	**92.2**
8	8	8	8
2.40	2.45	2.55	2.45

14	14	14	14
OM13-1	OM13-1	OM13-1	OM13-1
Srp-22	Srp-23	Srp-24	Srp-25
S1	S1	S1	S1
Fe-rich Lz	Fe-rich Lz	Ctl	Ctl
-	-	intergrown with calcite	intergrown with calcite
41.89	42.06	43.70	45.88
<0,04	<0,04	<0,04	<0,04
<0,02	0.03	0.02	0.02
<0,05	<0,05	<0,05	<0,05
5.93	5.18	1.75	2.29
0.07	0.08	<0,05	<0,05
39.85	38.69	41.51	40.59
0.14	0.27	0.09	0.11
<0,03	0.06	<0,03	0.04
<0,07	<0,07	<0,07	0.09
14.01	11.45	10.34	6.75
101.89	**97.83**	**97.40**	**95.78**
3.953	4.017	4.054	4.159
0.000	0.000	0.000	0.000
0.000	0.004	0.002	0.002
0.000	0.000	0.000	0.000
0.468	0.414	0.136	0.173
0.006	0.006	0.000	0.000
5.606	5.508	5.740	5.485
0.014	0.028	0.009	0.011
0.000	0.011	0.000	0.007
0.000	0.000	0.000	0.007
10.047	**9.987**	**9.941**	**9.843**
92.3	**93.0**	**97.7**	**96.9**
8	8	8	8
2.47	2.44	2.51	2.57

14	14	14	14
OM13-1	OM13-1	OM13-1	OM13-1
Srp-26	Srp-27	Srp-28	Srp-30
S1	S1	S1	S1
Ctl	Fe-rich Lz	Ctl	Fe-rich Lz
intergrown with calcite	-	intergrown with calcite	-
45.20	41.63	44.59	41.73
<0,04	<0,04	<0,04	<0,04
0.03	<0,02	<0,02	<0,02
<0,05	<0,05	<0,05	<0,05
1.95	5.22	1.86	5.79
<0,05	0.09	<0,05	0.07
40.33	39.24	41.50	38.77
0.06	0.30	0.07	0.21
<0,03	<0,03	0.06	<0,03
<0,07	<0,07	0.08	<0,07
7.87	12.61	8.54	12.10
95.43	**99.10**	**96.69**	**98.67**
4.154	3.977	4.085	4.086
0.000	0.000	0.000	0.000
0.003	0.000	0.000	0.000
0.000	0.000	0.000	0.000
0.150	0.417	0.143	0.474
0.000	0.007	0.000	0.006
5.526	5.589	5.668	5.660
0.006	0.031	0.006	0.022
0.000	0.000	0.010	0.000
0.000	0.000	0.006	0.000
9.839	**10.021**	**9.918**	**10.247**
97.4	**93.1**	**97.5**	**92.3**
8	8	8	8
2.54	2.44	2.54	2.38

14	14	14	14
OM13-17A	OM13-17A	OM13-17A	OM13-17A
Srp-1	Srp-3	Srp-5	Srp-6
S1	S1	S1	S1
Ctl±Lz	Ctl±Lz	Ctl±Lz	Ctl±Lz
intergrown with calcite	intergrown with calcite	intergrown with calcite	intergrown with calcite
43.76	44.73	44.41	44.51
<0,04	<0,04	<0,04	<0,04
0.08	0.08	0.06	0.13
<0,05	<0,05	<0,05	<0,05
2.76	2.59	2.70	2.87
<0,05	<0,05	<0,05	<0,05
41.45	41.52	41.67	41.72
0.13	0.09	0.02	0.02
<0,03	0.03	<0,03	0.03
<0,07	<0,07	<0,07	<0,07
7.54	5.32	6.29	5.91
95.73	**94.35**	**95.16**	**95.20**
4.033	4.072	4.054	4.049
0.000	0.000	0.000	0.000
0.009	0.008	0.006	0.014
0.000	0.000	0.000	0.000
0.213	0.197	0.206	0.218
0.000	0.000	0.000	0.000
5.695	5.635	5.671	5.658
0.013	0.009	0.002	0.002
0.000	0.005	0.000	0.004
0.000	0.000	0.000	0.000
9.962	**9.926**	**9.940**	**9.946**
96.4	**96.6**	**96.5**	**96.3**
8	8	8	8
2.53	2.56	2.55	2.56

14	14	14	14
OM13-17A	OM13-17A	OM13-17A	OM13-17A
Srp-9	Srp-10	Srp-11	Srp-16
S1	S1	S1	S1
Ctl±Lz	Ctl±Lz	Ctl±Lz	Ctl±Lz
intergrown with calcite	intergrown with calcite	intergrown with calcite	intergrown with calcite
44.70	44.07	44.76	43.86
<0,04	<0,04	<0,04	<0,04
0.06	0.15	0.08	0.11
<0,05	<0,05	<0,05	<0,05
2.40	3.13	2.72	3.69
<0,05	<0,05	<0,05	<0,05
41.86	41.71	42.21	40.91
0.04	0.03	0.03	0.06
0.07	<0,03	<0,03	0.05
<0,07	<0,07	<0,07	<0,07
7.34	7.95	6.62	7.77
96.47	**97.05**	**96.42**	**96.45**
4.063	4.025	4.045	4.036
0.000	0.000	0.000	0.000
0.007	0.016	0.008	0.012
0.000	0.000	0.000	0.000
0.182	0.239	0.205	0.284
0.000	0.000	0.000	0.000
5.671	5.680	5.686	5.612
0.004	0.003	0.003	0.006
0.012	0.000	0.000	0.010
0.000	0.000	0.000	0.000
9.938	**9.964**	**9.948**	**9.959**
96.9	**96.0**	**96.5**	**95.2**
8	8	8	8
2.56	2.55	2.58	2.53

14	14	14	14
OM13-17A	OM13-17A	OM13-17A	OM13-17A
Srp-17	Srp-18	Srp-19	Srp-20
S1	S1	S1	S1
Ctl±Lz	Ctl±Lz	Ctl±Lz	Ctl±Lz
intergrown with calcite	intergrown with calcite	intergrown with calcite	intergrown with calcite
44.90	43.21	44.13	45.01
<0,04	<0,04	<0,04	<0,04
0.14	0.17	0.10	0.09
<0,05	<0,05	<0,05	<0,05
3.21	4.30	3.62	3.06
<0,05	<0,05	<0,05	<0,05
41.91	40.90	41.66	41.62
0.04	0.03	0.03	0.06
0.05	0.07	<0,03	<0,03
<0,07	<0,07	<0,07	<0,07
6.51	9.15	8.15	7.12
96.75	**97.83**	**97.69**	**96.97**
4.047	3.995	4.022	4.068
0.000	0.000	0.000	0.000
0.015	0.019	0.011	0.010
0.000	0.000	0.000	0.000
0.242	0.332	0.276	0.231
0.000	0.000	0.000	0.000
5.632	5.638	5.660	5.608
0.004	0.003	0.003	0.006
0.008	0.013	0.000	0.000
0.000	0.000	0.000	0.000
9.948	**10.000**	**9.971**	**9.923**
95.9	**94.4**	**95.4**	**96.0**
8	8	8	8
2.59	2.52	2.56	2.58

14	14	14	14
OM13-17A	OM13-17A	OM13-11	OM13-11
Srp-21	Srp-22	Srp-1	Srp-3
S1	S1	S2	S2
Ctl±Lz	Ctl±Lz	Lz±Ctl	Lz±Ctl
intergrown with calcite	intergrown with calcite	intergrown with calcite	intergrown with calcite
43.81	44.10	46.12	46.40
<0,04	<0,04	<0,04	<0,04
0.12	0.12	<0,02	0.02
<0,05	<0,05	<0,05	<0,05
4.01	3.92	2.52	1.88
<0,05	<0,05	<0,05	<0,05
40.58	41.24	39.95	40.56
0.04	0.03	0.14	0.08
<0,03	0.08	0.04	0.11
<0,07	<0,07	<0,07	0.09
7.50	8.56	8.95	8.48
96.06	**98.04**	**97.70**	**97.62**
4.042	4.026	4.190	4.187
0.000	0.000	0.000	0.000
0.013	0.013	0.000	0.002
0.000	0.000	0.000	0.000
0.309	0.299	0.191	0.142
0.000	0.000	0.000	0.000
5.582	5.613	5.410	5.456
0.004	0.003	0.013	0.008
0.000	0.013	0.006	0.020
0.000	0.000	0.000	0.006
9.950	**9.968**	**9.810**	**9.820**
94.8	**94.9**	**96.6**	**97.5**
8	8	8	8
2.53	2.55	2.57	2.58

14	14	14	14
OM13-11	OM13-11	OM13-11	OM13-11
Srp-5	Srp-6	Srp-8	Srp-9
S2	S2	S2	S2
Lz±Ctl	Lz±Ctl	Lz±Ctl	Lz±Ctl
intergrown with calcite	intergrown with calcite	intergrown with calcite	intergrown with calcite
45.24	46.92	46.47	46.21
<0,04	<0,04	<0,04	<0,04
0.02	0.03	0.02	<0,02
<0,05	<0,05	<0,05	<0,05
3.03	1.65	1.81	3.00
<0,05	<0,05	<0,05	0.07
39.37	40.61	40.75	40.35
0.13	0.13	0.12	0.12
0.04	0.03	<0,03	<0,03
<0,07	<0,07	<0,07	<0,07
8.91	8.61	8.35	6.24
96.76	**97.97**	**97.51**	**95.99**
4.167	4.210	4.187	4.166
0.000	0.000	0.000	0.000
0.003	0.003	0.002	0.000
0.000	0.000	0.000	0.000
0.234	0.124	0.136	0.226
0.000	0.000	0.000	0.005
5.405	5.431	5.473	5.422
0.013	0.012	0.011	0.011
0.007	0.005	0.000	0.000
0.000	0.000	0.000	0.000
9.829	**9.785**	**9.810**	**9.831**
95.9	**97.8**	**97.6**	**96.0**
8	8	8	8
2.53	2.60	2.59	2.58

14	14	14	14
OM13-11	OM13-11	OM13-11	OM13-11
Srp-10	Srp-11	Srp-13	Srp-14
S2	S2	S2	S2
Lz±Ctl	Lz±Ctl	Lz±Ctl	Lz±Ctl
intergrown with calcite	intergrown with calcite	intergrown with calcite	intergrown with calcite
45.21	44.86	45.18	45.12
<0,04	<0,04	<0,04	<0,04
<0,02	0.02	<0,02	0.03
<0,05	<0,05	<0,05	<0,05
1.73	1.99	1.89	1.78
<0,05	<0,05	<0,05	<0,05
40.59	40.56	40.37	40.53
0.05	0.09	0.06	0.07
<0,03	<0,03	<0,03	<0,03
<0,07	<0,07	<0,07	<0,07
10.07	10.88	10.47	11.26
97.65	**98.39**	**97.96**	**98.79**
4.149	4.132	4.154	4.147
0.000	0.000	0.000	0.000
0.000	0.002	0.000	0.004
0.000	0.000	0.000	0.000
0.133	0.153	0.145	0.137
0.000	0.000	0.000	0.000
5.554	5.570	5.533	5.553
0.005	0.009	0.006	0.007
0.000	0.000	0.000	0.000
0.000	0.000	0.000	0.000
9.841	**9.866**	**9.838**	**9.847**
97.7	**97.3**	**97.4**	**97.6**
8	8	8	8
2.54	2.53	2.53	2.54

14	14	14	14
OM13-11	OM13-11	OM13-11	OM13-11
Srp-15	Srp-18	Srp-21	Srp-23
S2	S2	S2	S2
Lz±Ctl	Lz±Ctl	Lz±Ctl	Lz±Ctl
intergrown with calcite	intergrown with calcite	intergrown with calcite	intergrown with calcite
45.20	44.97	46.24	45.55
<0,04	<0,04	<0,04	<0,04
0.02	0.02	<0,02	0.02
<0,05	<0,05	0.05	<0,05
1.69	1.73	1.57	1.65
<0,05	<0,05	<0,05	0.05
40.83	40.67	40.77	41.29
0.08	0.08	0.09	0.05
0.04	<0,03	<0,03	<0,03
<0,07	<0,07	<0,07	<0,07
11.26	10.34	9.14	9.51
99.12	**97.81**	**97.87**	**98.12**
4.141	4.137	4.182	4.136
0.000	0.000	0.000	0.000
0.002	0.002	0.000	0.003
0.000	0.000	0.003	0.000
0.129	0.133	0.119	0.126
0.000	0.000	0.000	0.003
5.576	5.577	5.498	5.590
0.008	0.008	0.008	0.005
0.008	0.000	0.000	0.000
0.000	0.000	0.000	0.000
9.863	**9.856**	**9.810**	**9.863**
97.7	**97.7**	**97.9**	**97.8**
8	8	8	8
2.54	2.53	2.58	2.57

14	14	14	14
OM13-11	OM13-11	OM13-13	OM13-13
Srp-25	Srp-32	Srp-1	Srp-2
S2	S2	S2	S2
Lz±Ctl	Lz±Ctl	Lz±Ctl	Lz±Ctl
intergrown with calcite	intergrown with calcite	intergrown with calcite	intergrown with calcite
45.25	44.86	43.51	44.11
<0,04	<0,04	<0,04	<0,04
<0,02	0.03	0.10	0.07
<0,05	<0,05	<0,05	<0,05
2.85	1.95	4.14	4.34
0.05	<0,05	<0,05	<0,05
38.17	40.66	40.87	40.45
0.25	0.08	0.06	0.09
<0,03	<0,03	<0,03	<0,03
<0,07	0.07	<0,07	<0,07
8.53	10.25	9.06	7.23
95.10	**97.90**	**97.74**	**96.28**
4.220	4.128	4.017	4.051
0.000	0.000	0.000	0.000
0.000	0.003	0.011	0.007
0.000	0.000	0.000	0.000
0.222	0.150	0.319	0.333
0.004	0.000	0.000	0.000
5.307	5.577	5.624	5.540
0.025	0.008	0.006	0.009
0.000	0.000	0.000	0.000
0.000	0.005	0.000	0.000
9.777	**9.871**	**9.977**	**9.940**
96.0	**97.4**	**94.6**	**94.3**
8	8	8	8
2.50	2.53	2.52	2.54

14	14	14	14
OM13-13	OM13-13	OM13-13	OM13-13
Srp-3	Srp-4	Srp-6	Srp-8
S2	S2	S2	S2
Lz±Ctl	Lz±Ctl	Lz±Ctl	Lz±Ctl
intergrown with calcite	intergrown with calcite	intergrown with calcite	intergrown with calcite
44.50	43.85	42.82	43.03
<0,04	<0,04	<0,04	<0,04
0.07	0.07	0.09	0.05
<0,05	<0,05	<0,05	<0,05
4.17	4.24	5.37	5.28
<0,05	<0,05	<0,05	0.07
40.27	40.19	39.86	39.19
0.10	0.06	0.06	0.08
<0,03	<0,03	0.03	<0,03
<0,07	<0,07	<0,07	<0,07
8.59	10.23	10.45	10.30
97.70	**98.65**	**98.69**	**98.00**
4.078	4.055	4.001	4.039
0.000	0.000	0.000	0.000
0.008	0.007	0.010	0.006
0.000	0.000	0.000	0.000
0.320	0.328	0.420	0.415
0.000	0.000	0.000	0.006
5.502	5.541	5.552	5.483
0.010	0.006	0.006	0.008
0.000	0.000	0.006	0.000
0.000	0.000	0.000	0.000
9.917	**9.938**	**9.995**	**9.956**
94.5	**94.4**	**93.0**	**93.0**
8	8	8	8
2.54	2.52	2.49	2.48

14	14	14	14
OM13-13	OM13-13	OM13-13	OM13-13
Srp-10	Srp-11	Srp-13	Srp-14
S2	S2	S2	S2
Lz±Ctl	Lz±Ctl	Ctl	Ctl
intergrown with calcite	intergrown with calcite	-	-
44.08	43.36	43.56	43.51
<0,04	<0,04	<0,04	<0,04
0.07	0.15	0.07	0.07
<0,05	<0,05	<0,05	<0,05
4.43	5.41	3.43	3.03
<0,05	0.05	<0,05	<0,05
40.10	39.79	40.87	41.55
0.10	0.09	0.06	0.04
<0,03	<0,03	<0,03	<0,03
<0,07	0.07	<0,07	<0,07
10.25	9.81	9.90	10.73
99.04	**98.73**	**97.90**	**98.93**
4.063	4.020	4.035	4.015
0.000	0.000	0.000	0.000
0.008	0.016	0.008	0.008
0.000	0.000	0.000	0.000
0.342	0.419	0.266	0.234
0.000	0.004	0.000	0.000
5.511	5.499	5.644	5.717
0.010	0.009	0.006	0.004
0.000	0.000	0.000	0.000
0.000	0.005	0.000	0.000
9.933	**9.973**	**9.959**	**9.978**
94.2	**92.9**	**95.5**	**96.1**
8	8	8	8
2.53	2.51	2.52	2.52

14	14	14	14
OM13-13	OM13-13	OM13-13	OM13-13
Srp-15	Srp-16	Srp-17	Srp-19
S2	S2	S2	S2
Ctl	Lz±Ctl	Lz±Ctl	Lz±Ctl
-	-	intergrown with calcite	intergrown with calcite
43.87	43.47	44.20	43.17
<0,04	<0,04	<0,04	<0,04
0.07	0.19	0.07	0.05
<0,05	<0,05	<0,05	<0,05
2.99	4.58	4.28	4.63
<0,05	<0,05	0.10	<0,05
41.67	39.61	39.80	39.77
0.03	0.07	0.07	0.06
<0,03	<0,03	<0,03	0.06
<0,07	<0,07	<0,07	<0,07
9.58	9.47	10.07	11.19
98.21	**97.38**	**98.58**	**98.93**
4.025	4.049	4.081	4.036
0.000	0.000	0.000	0.000
0.008	0.021	0.007	0.006
0.000	0.000	0.000	0.000
0.230	0.356	0.330	0.362
0.000	0.000	0.007	0.000
5.700	5.501	5.478	5.543
0.003	0.007	0.007	0.006
0.000	0.000	0.000	0.010
0.000	0.000	0.000	0.000
9.966	**9.935**	**9.912**	**9.963**
96.1	**93.9**	**94.3**	**93.9**
8	8	8	8
2.54	2.50	2.52	2.49

14	14	14	14
OM13-14A	OM13-14A	OM13-14A	OM13-14A
Srp-1	Srp-2	Srp-3	Srp-4
S2	S2	S2	S2
Lz±Ctl	Lz±Ctl	Lz±Ctl	Lz±Ctl
intergrown with calcite	intergrown with calcite	intergrown with calcite	intergrown w
42.72	45.07	45.98	45.98
<0,04	<0,04	<0,04	<0,04
0.02	<0,02	<0,02	0.03
<0,05	<0,05	<0,05	<0,05
4.92	4.29	4.32	3.79
<0,05	<0,05	<0,05	<0,05
39.03	40.43	38.05	37.80
0.05	0.06	0.12	0.17
<0,03	0.03	<0,03	0.04
<0,07	<0,07	<0,07	<0,07
11.29	8.41	6.85	6.25
98.03	**98.28**	**95.31**	**94.06**
4.046	4.095	4.222	4.241
0.000	0.000	0.000	0.000
0.002	0.000	0.000	0.003
0.000	0.000	0.000	0.000
0.389	0.326	0.332	0.292
0.000	0.000	0.000	0.000
5.512	5.476	5.209	5.198
0.005	0.006	0.011	0.017
0.000	0.005	0.000	0.008
0.000	0.000	0.000	0.000
9.954	**9.907**	**9.775**	**9.758**
93.4	**94.4**	**94.0**	**94.7**
8	8	8	8
2.46	2.56	2.54	2.53

14	14	14	14
OM13-14A	OM13-14A	OM13-14A	OM13-14A
Srp-5	Srp-6	Srp-7	Srp-8
S2	S2	S2	S2
Lz±Ctl	Lz±Ctl	Lz±Ctl	Lz±Ctl
intergrown with calcite	intergrown with calcite	intergrown with calcite	intergrown with calcite
43.24	45.85	42.55	45.45
<0,04	<0,04	<0,04	<0,04
<0,02	0.02	0.02	<0,02
<0,05	<0,05	<0,05	<0,05
4.01	4.36	4.92	4.54
<0,05	<0,05	<0,05	<0,05
38.89	38.73	40.30	37.90
0.07	0.13	0.02	0.07
<0,03	0.05	<0,03	<0,03
<0,07	<0,07	<0,07	<0,07
12.17	7.70	11.33	7.57
98.38	**96.84**	**99.16**	**95.53**
4.093	4.186	3.988	4.206
0.000	0.000	0.000	0.000
0.000	0.002	0.003	0.000
0.000	0.000	0.000	0.000
0.317	0.333	0.386	0.351
0.000	0.000	0.000	0.000
5.488	5.272	5.631	5.228
0.007	0.013	0.002	0.007
0.000	0.008	0.000	0.000
0.000	0.000	0.000	0.000
9.905	**9.814**	**10.009**	**9.793**
94.5	**94.1**	**93.6**	**93.7**
8	8	8	8
2.46	2.55	2.49	2.52

14	14	14	14
OM13-14A	OM13-14A	OM13-14A	OM13-14A
Srp-11	Srp-12	Srp-13	Srp-14
S2	S2	S2	S2
Lz±Ctl	Ctl	Ctl	Ctl
intergrown with calcite	intergrown with calcite	intergrown with calcite	intergrown with calcite
43.26	45.52	45.05	43.25
<0,04	<0,04	<0,04	<0,04
0.03	<0,02	<0,02	<0,02
<0,05	<0,05	<0,05	<0,05
4.55	4.15	1.41	2.70
<0,05	0.05	<0,05	<0,05
36.35	38.12	40.82	38.64
0.20	0.09	0.06	0.08
<0,03	0.09	<0,03	<0,03
<0,07	<0,07	0.07	<0,07
6.70	7.88	9.66	7.88
91.10	**95.89**	**97.07**	**92.54**
4.182	4.204	4.142	4.133
0.000	0.000	0.000	0.000
0.004	0.000	0.000	0.000
0.000	0.000	0.000	0.000
0.368	0.321	0.109	0.216
0.000	0.004	0.000	0.000
5.239	5.248	5.595	5.504
0.021	0.009	0.006	0.008
0.000	0.017	0.000	0.000
0.000	0.000	0.005	0.000
9.814	**9.802**	**9.857**	**9.861**
93.4	**94.2**	**98.1**	**96.2**
8	8	8	8
2.41	2.52	2.53	2.44

14	14	14	14
OM13-14A	OM13-14A	OM13-14A	OM13-14A
Srp-15	Srp-16	Srp-19	Srp-20
S2	S2	S2	S2
Ctl	Lz±Ctl	Lz±Ctl	Lz±Ctl
intergrown with calcite	intergrown with calcite	intergrown with calcite	intergrown with calcite
46.15	44.55	46.50	43.61
<0,04	<0,04	<0,04	<0,04
<0,02	0.06	<0,02	0.03
<0,05	<0,05	<0,05	<0,05
2.11	2.77	4.57	4.21
<0,05	0.24	<0,05	<0,05
40.11	40.66	38.03	41.38
0.07	0.05	0.07	0.03
0.07	<0,03	0.03	0.05
<0,07	<0,07	<0,07	<0,07
10.06	10.50	6.57	11.14
98.56	**98.85**	**95.77**	**100.45**
4.193	4.090	4.236	4.001
0.000	0.000	0.000	0.000
0.000	0.007	0.000	0.003
0.000	0.000	0.000	0.000
0.160	0.213	0.349	0.323
0.000	0.019	0.000	0.000
5.433	5.566	5.165	5.661
0.007	0.005	0.006	0.003
0.012	0.000	0.006	0.009
0.000	0.000	0.000	0.000
9.805	**9.900**	**9.763**	**10.000**
97.1	**96.3**	**93.7**	**94.6**
8	8	8	8
2.56	2.54	2.56	2.54

14	14	14	14
OM10-02	OM10-02	OM10-02	OM10-02
Srp-1	Srp-3	Srp-4	Srp-5b
S2	S2	S2	S2
Ctl	Ctl	Ctl	Ctl
intergrown with talc	intergrown with talc	intergrown with talc	intergrown with talc
43.65	43.86	43.78	43.27
<0,04	<0,04	<0,04	<0,04
0.07	0.07	0.06	0.14
<0,05	<0,05	<0,05	<0,05
1.87	2.01	1.70	2.25
<0,05	<0,05	<0,05	<0,05
42.36	42.16	42.98	41.92
<0,02	<0,02	<0,02	<0,02
<0,03	<0,03	<0,03	<0,03
0.29	0.28	0.24	0.28
9.40	7.84	8.89	9.78
97.64	**96.22**	**97.65**	**97.64**
4.009	4.024	3.996	4.000
0.000	0.000	0.000	0.000
0.008	0.007	0.006	0.016
0.000	0.000	0.000	0.000
0.144	0.154	0.130	0.174
0.000	0.000	0.000	0.000
5.801	5.765	5.848	5.779
0.000	0.000	0.000	0.000
0.000	0.000	0.000	0.000
0.021	0.021	0.018	0.021
9.983	**9.971**	**9.999**	**9.989**
97.6	**97.4**	**97.8**	**97.1**
8	8	8	8
2.54	2.54	2.55	2.52

14	14	14	14
OM10-02	OM10-02	OM10-02	OM10-02
Srp-6	Srp-8	Srp-9b	Srp-10
S2	S2	S2	S2
Ctl	Ctl	Ctl	Ctl
intergrown with talc	intergrown with talc	intergrown with talc	intergrown with talc
43.84	43.23	43.68	43.76
<0,04	<0,04	<0,04	<0,04
0.14	0.02	0.04	0.09
<0,05	<0,05	<0,05	<0,05
1.95	2.00	1.97	2.31
0.06	<0,05	0.05	<0,05
41.89	42.45	42.62	42.24
<0,02	0.02	<0,02	0.02
<0,03	<0,03	<0,03	<0,03
0.28	0.18	0.24	0.29
8.48	9.91	9.81	9.69
96.64	**97.81**	**98.41**	**98.41**
4.031	3.992	4.000	4.008
0.000	0.000	0.000	0.000
0.015	0.003	0.005	0.010
0.000	0.000	0.000	0.000
0.150	0.155	0.151	0.177
0.005	0.000	0.004	0.000
5.741	5.842	5.818	5.768
0.000	0.002	0.000	0.002
0.000	0.000	0.000	0.000
0.021	0.013	0.017	0.022
9.961	**10.006**	**9.995**	**9.987**
97.5	**97.4**	**97.5**	**97.0**
8	8	8	8
2.53	2.52	2.54	2.54

14	14	14	14
OM10-02	OM10-02	OM10-02	OM10-02
Srp-11	Srp-14	Srp-14b	Srp-16
S2	S2	S2	S2
Ctl	Ctl	Ctl	Ctl
intergrown with talc	intergrown with talc	intergrown with talc	intergrown with talc
43.43	44.32	43.77	43.72
<0,04	<0,04	<0,04	<0,04
0.12	0.07	0.11	0.09
<0,05	<0,05	<0,05	<0,05
1.92	2.08	1.86	2.07
<0,05	<0,05	<0,05	0.05
42.55	42.39	42.92	42.93
<0,02	<0,02	<0,02	<0,02
0.03	0.06	<0,03	<0,03
0.27	0.20	0.24	0.25
8.66	9.66	9.62	9.52
96.99	**98.79**	**98.53**	**98.62**
3.990	4.030	3.991	3.985
0.000	0.000	0.000	0.000
0.013	0.008	0.012	0.010
0.000	0.000	0.000	0.000
0.148	0.158	0.142	0.158
0.000	0.000	0.000	0.004
5.827	5.747	5.833	5.834
0.000	0.000	0.000	0.000
0.005	0.010	0.000	0.000
0.020	0.015	0.018	0.018
10.004	**9.969**	**9.996**	**10.010**
97.5	**97.3**	**97.6**	**97.4**
8	8	8	8
2.54	2.56	2.56	2.56

14	14	11	11
OM10-02	OM10-02	OM10-02	OM10-02
Srp-17	Srp-20	Tlc-1b	Tlc-7
S2	S2	S2	S2
Ctl	Ctl	Tlc	Tlc
intergrown with talc	intergrown with talc	intergrown with chrysotile	intergrown with chrysotile
43.76	44.20	54.09	55.00
<0,04	<0,04	<0,04	<0,04
0.09	0.07	0.06	0.11
<0,05	<0,05	<0,05	<0,05
1.89	1.90	3.62	3.71
0.05	<0,05	<0,05	<0,05
42.58	42.79	34.35	33.88
<0,02	<0,02	<0,02	<0,02
0.03	<0,03	0.03	0.11
0.16	0.20	0.61	0.49
9.39	8.23	3.21	4.60
97.96	**97.39**	**95.98**	**97.91**
4.006	4.017	3.649	3.681
0.000	0.000	0.000	0.000
0.010	0.007	0.005	0.009
0.000	0.000	0.000	0.000
0.145	0.145	0.205	0.208
0.003	0.000	0.000	0.000
5.811	5.797	3.455	3.381
0.000	0.000	0.000	0.000
0.005	0.000	0.004	0.014
0.011	0.014	0.033	0.027
9.992	**9.980**	**7.351**	**7.320**
97.6	**97.6**	**94.4**	**94.2**
8	8		
2.55	2.56	2.71	2.74

11	11	11
OM10-02	OM10-02	OM10-02
Tlc-11	Tlc-12	Tlc-13
S2	S2	S2
Tlc	Tlc	Tlc
intergrown with chrysotile	intergrown with chrysotile	intergrown with chrysotile
55.77	56.33	57.37
<0,04	<0,04	<0,04
0.10	0.08	0.11
<0,05	<0,05	<0,05
3.69	3.20	3.37
<0,05	<0,05	<0,05
33.72	34.35	33.34
<0,02	<0,02	<0,02
0.03	0.07	0.04
0.38	0.39	0.30
3.04	2.94	1.95
96.73	**97.36**	**96.48**
3.709	3.709	3.763
0.000	0.000	0.000
0.008	0.006	0.009
0.000	0.000	0.000
0.205	0.176	0.185
0.000	0.000	0.000
3.343	3.371	3.259
0.000	0.000	0.000
0.004	0.009	0.006
0.020	0.021	0.016
7.289	**7.292**	**7.236**
94.2	**95.0**	**94.6**
2.75	2.78	2.79

11	11	11
OM10-02	OM10-02	OM10-02
Tlc-16	Tlc-17	Tlc-18
S2	S2	S2
Tlc	Tlc	Tlc
intergrown with chrysotile	intergrown with chrysotile	intergrown with chrysotile
58.95	56.46	50.29
<0,04	<0,04	<0,04
0.10	0.10	0.04
<0,05	<0,05	<0,05
3.11	3.80	2.28
<0,05	<0,05	<0,05
32.38	33.49	37.98
<0,02	<0,02	<0,02
0.05	0.05	0.04
0.31	0.27	0.21
1.15	3.38	5.60
96.05	**97.54**	**96.45**
3.831	3.731	3.470
0.000	0.000	0.000
0.008	0.008	0.004
0.000	0.000	0.000
0.169	0.210	0.132
0.000	0.000	0.000
3.137	3.299	3.908
0.000	0.000	0.000
0.006	0.007	0.006
0.016	0.014	0.012
7.168	**7.269**	**7.531**
94.9	**94.0**	**96.7**
2.82	2.77	2.65

11
OM10-02
Tlc-20
S2
Tlc
intergrown with chrysotile
57.03
<0,04
0.12
<0,05
2.99
<0,05
32.84
0.03
0.10
0.25
2.01
95.36
3.778
0.000
0.009
0.000
0.165
0.000
3.242
0.002
0.012
0.013
7.222
95.1
2.76

REPRESENTATIVE RAMAN SPECTRA FOR SERPENTINE

Sample OM09-12

Antigorite

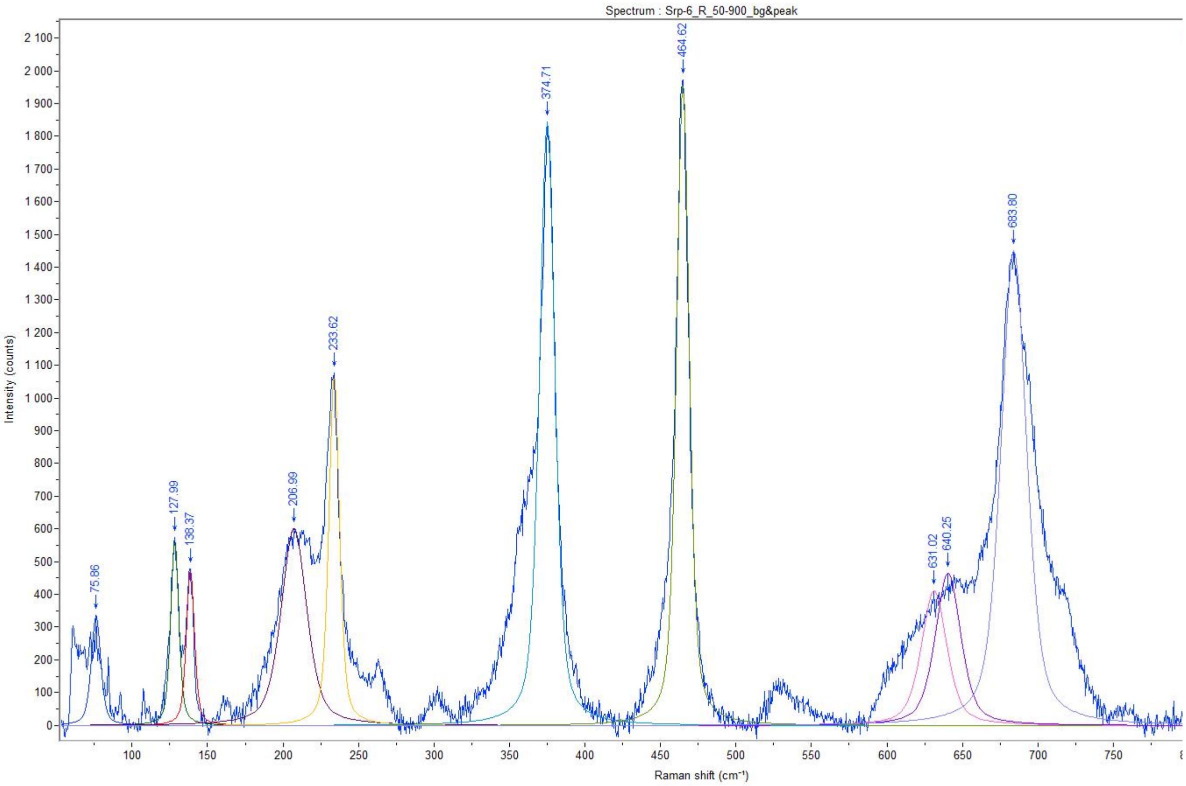

Sample OM10-02

Chrysotile

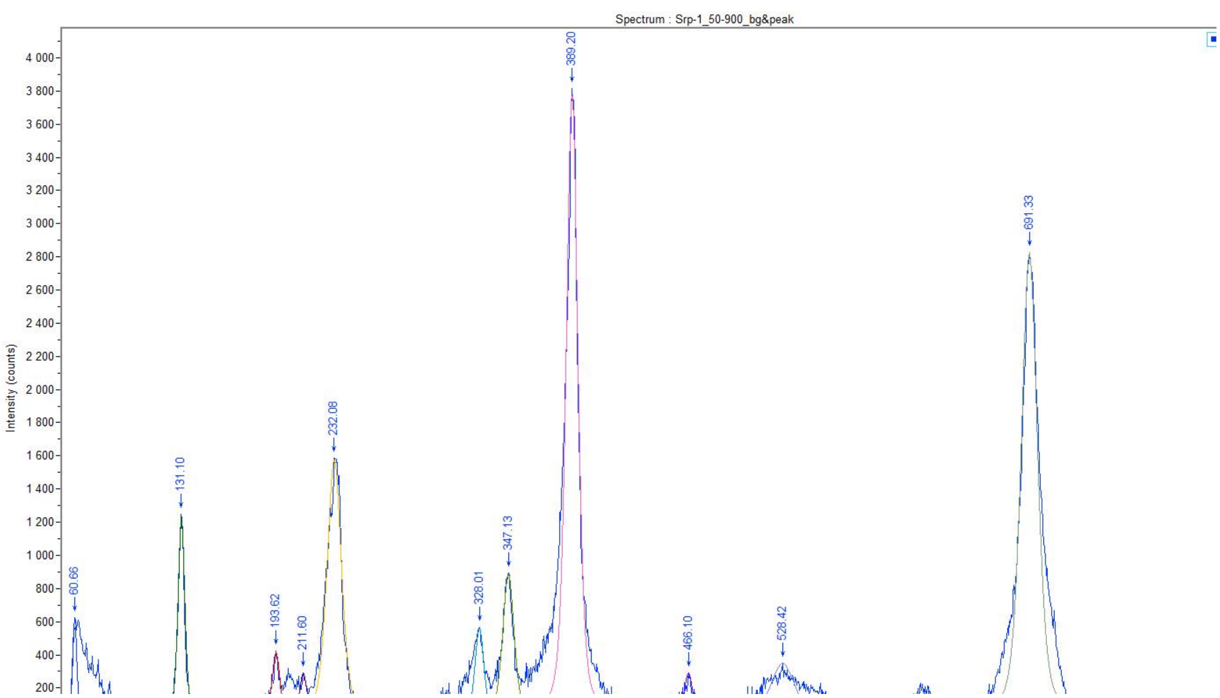

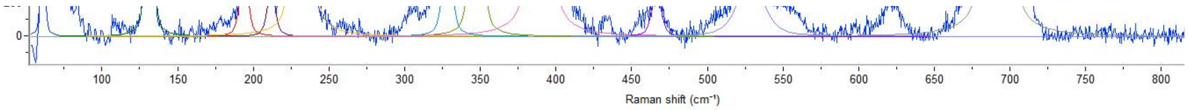

Sample OM13-1

Chrysotile + Fe-rich lizardite rim

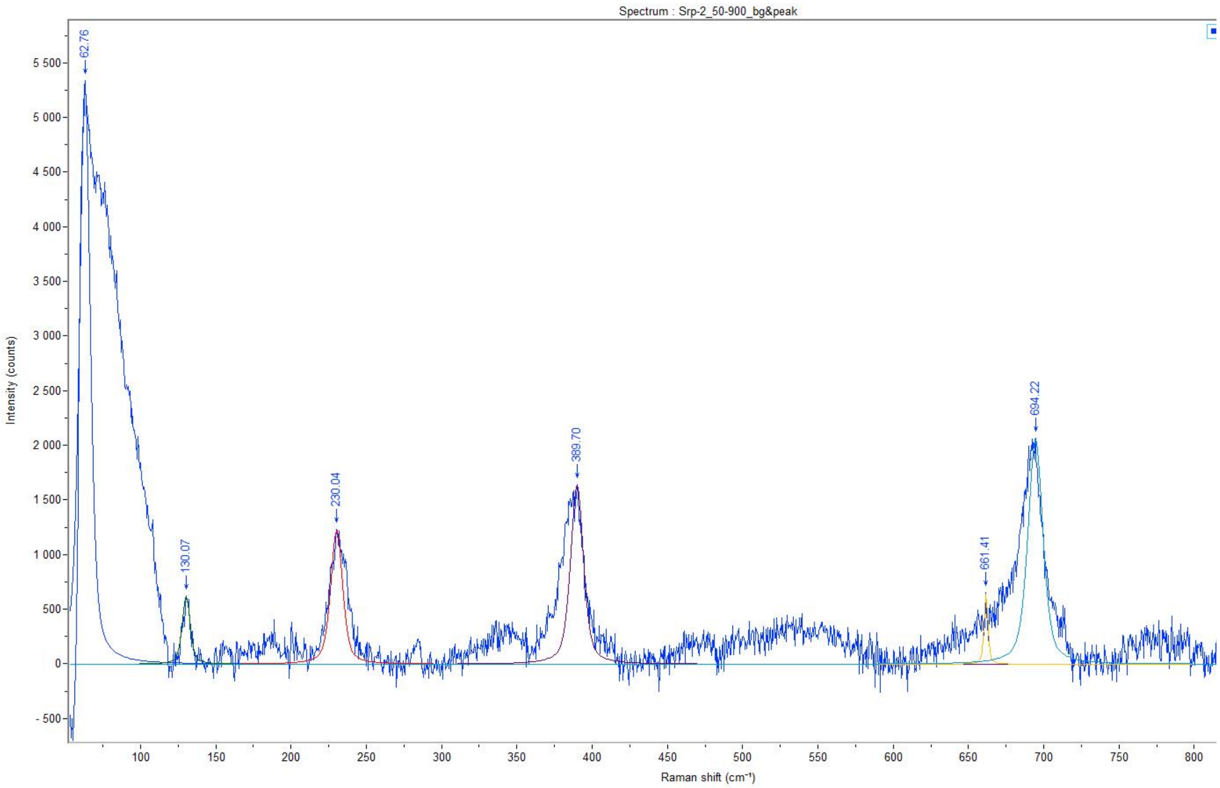

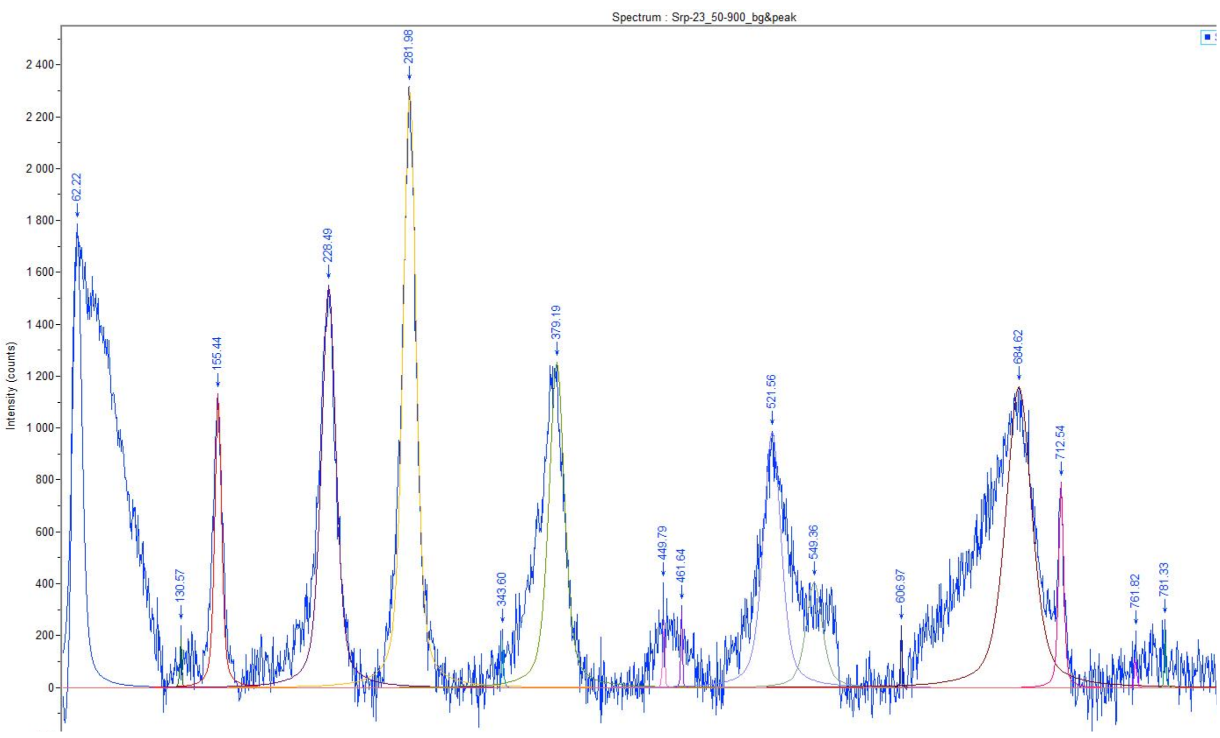

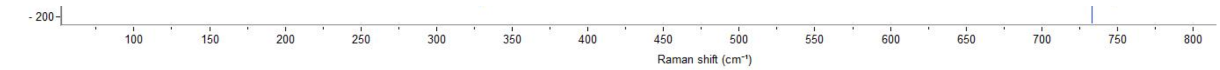

Sample OM13-13

Lizardite±chysotile, Chrysotile

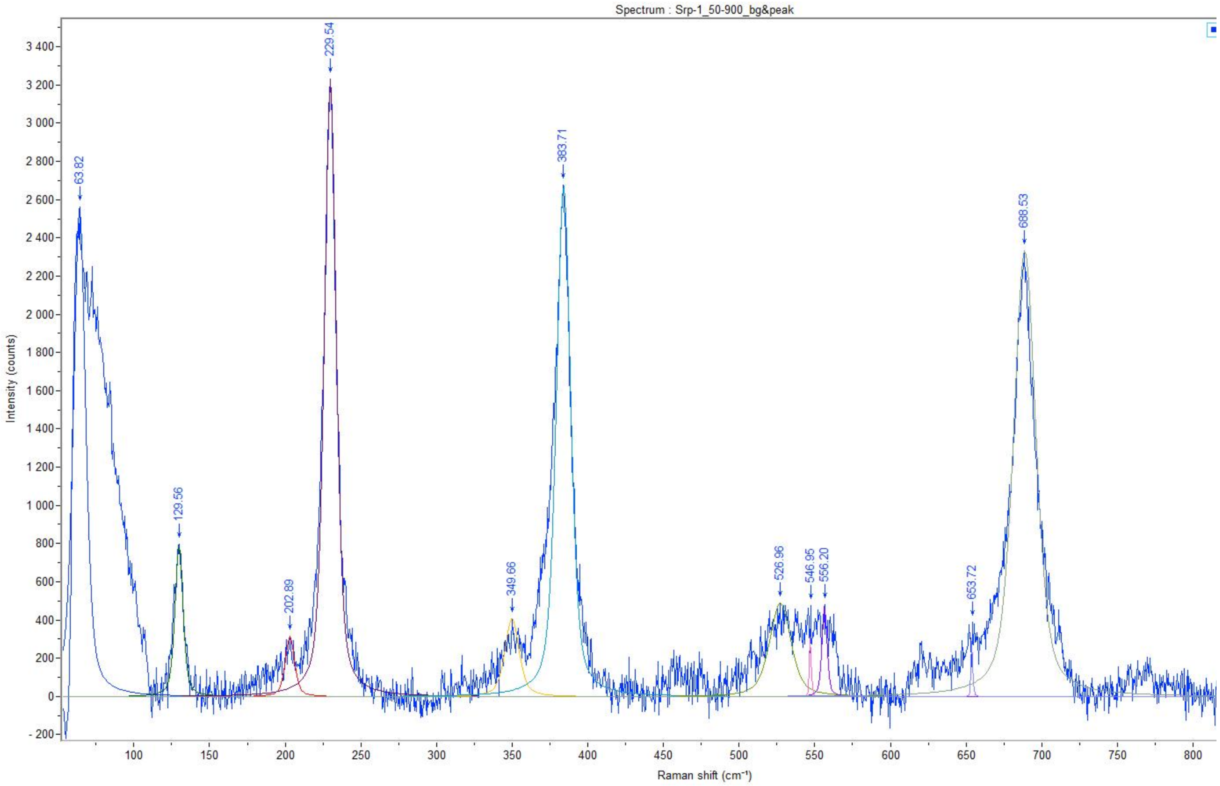

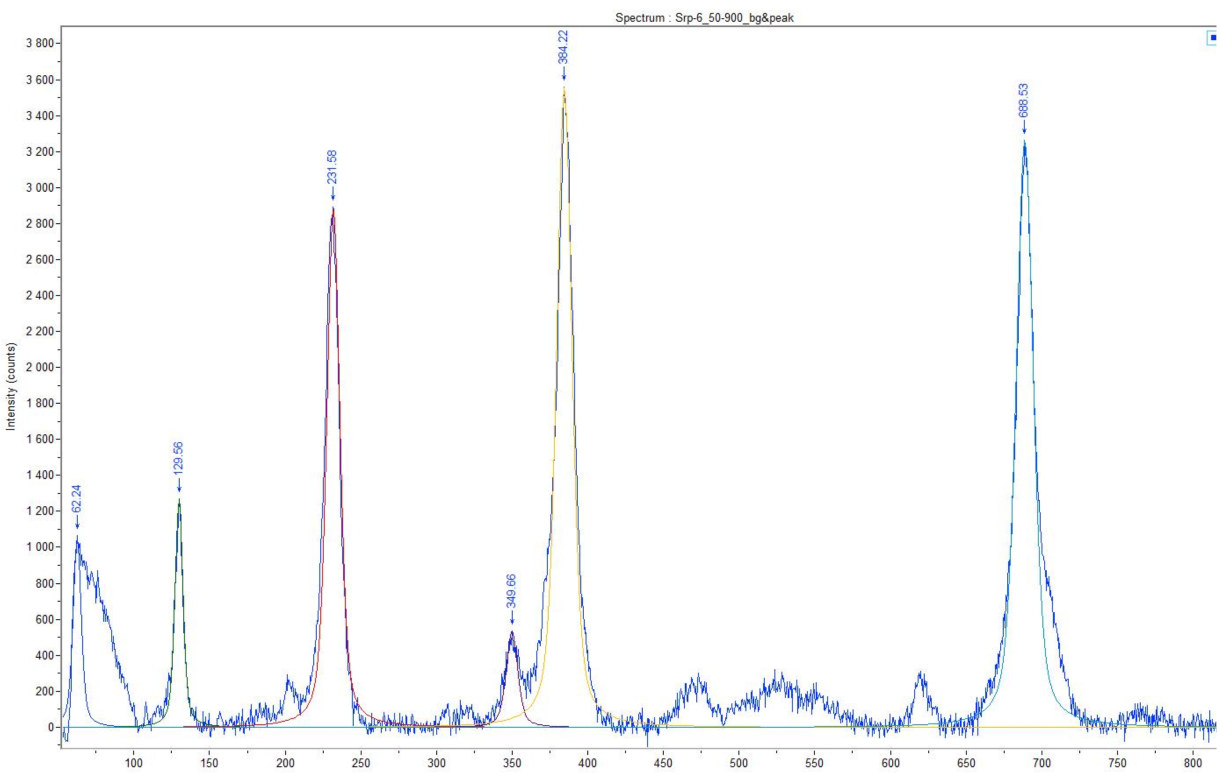

Raman shift (cm⁻¹)

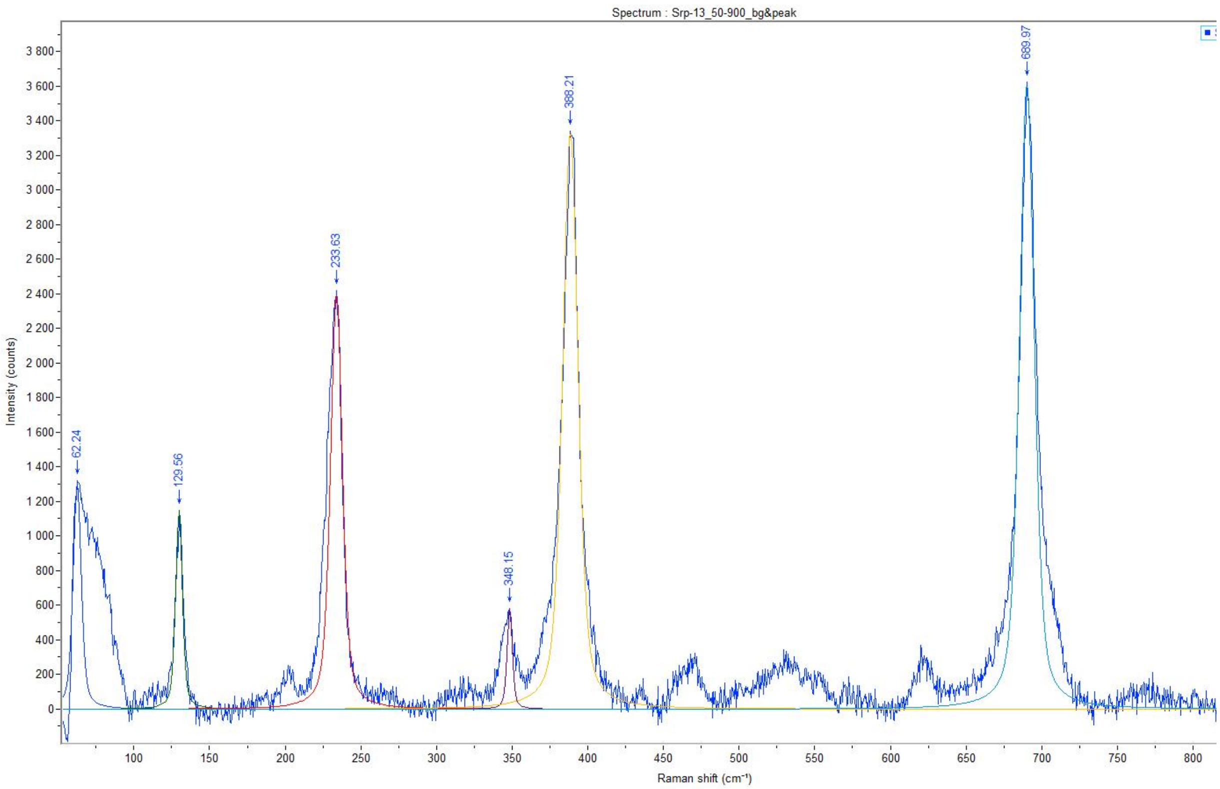

Sample OM13-14A

Lizardite±chysotile

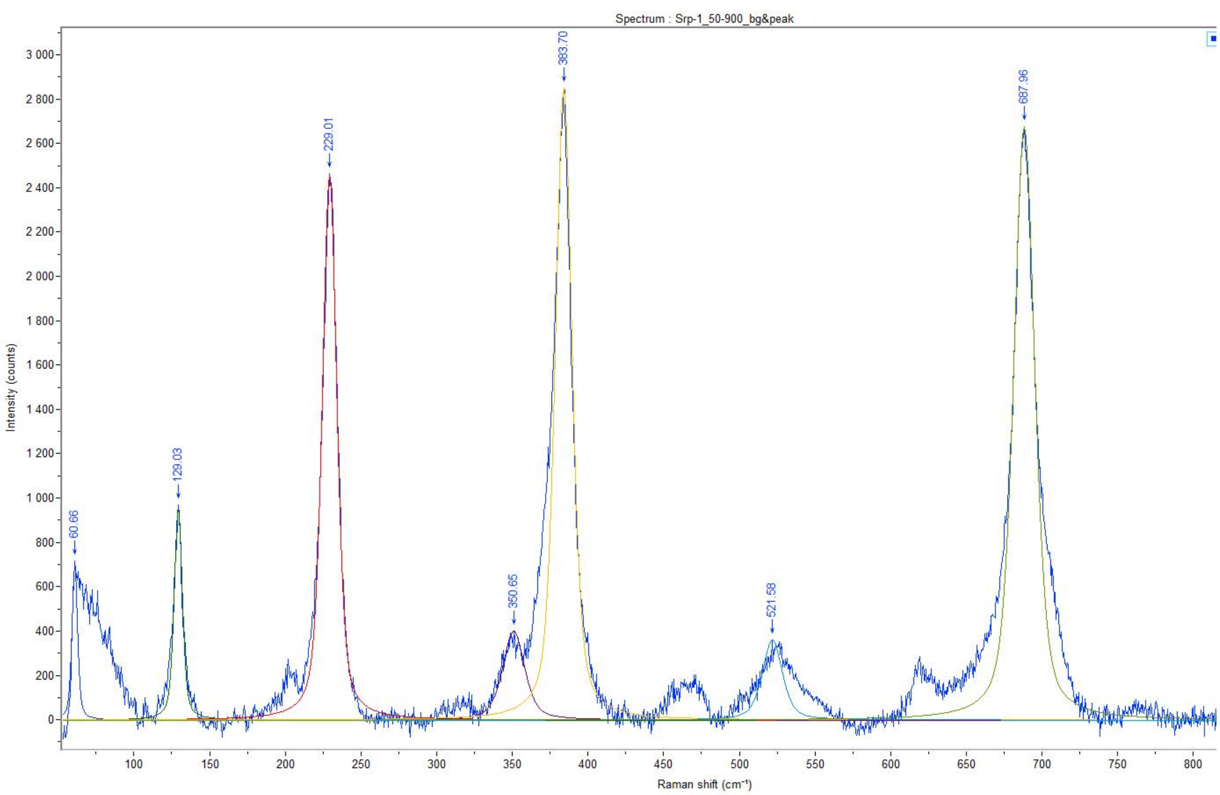

Sample OM13-17A

Chysotile±lizardite, Chrysotile

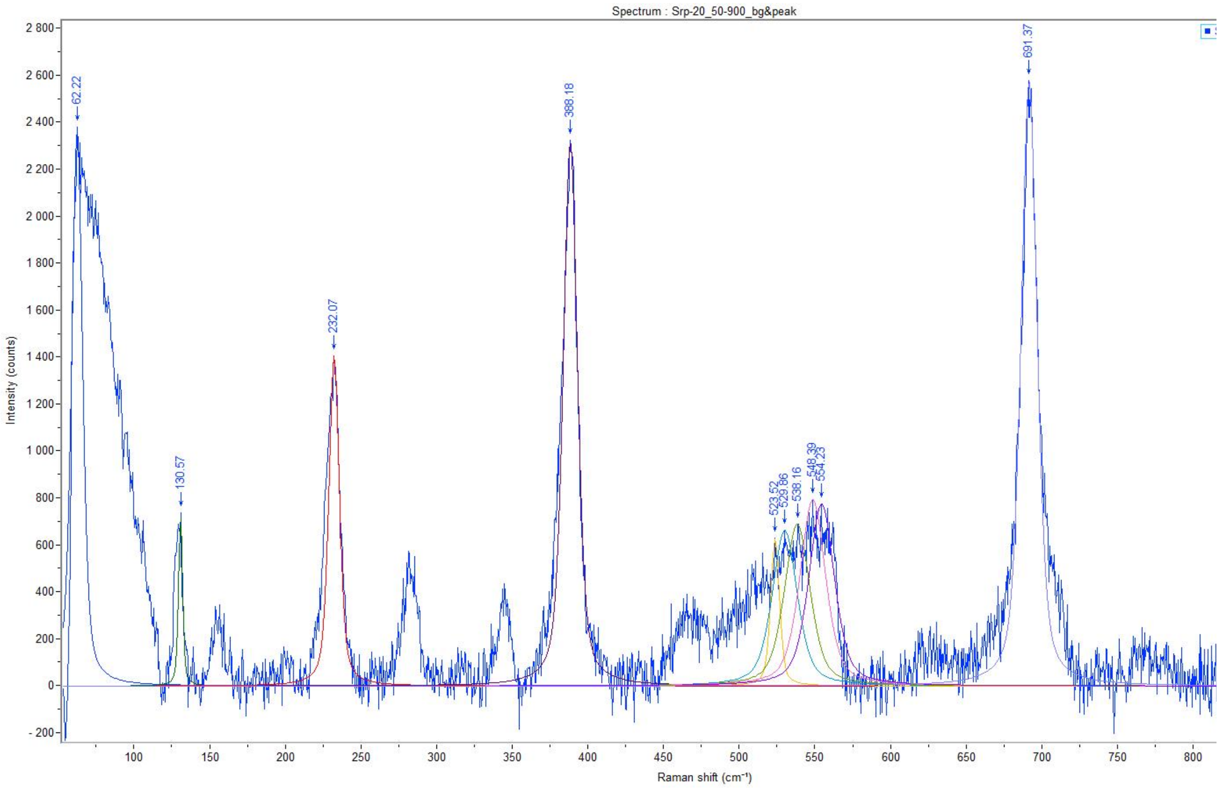

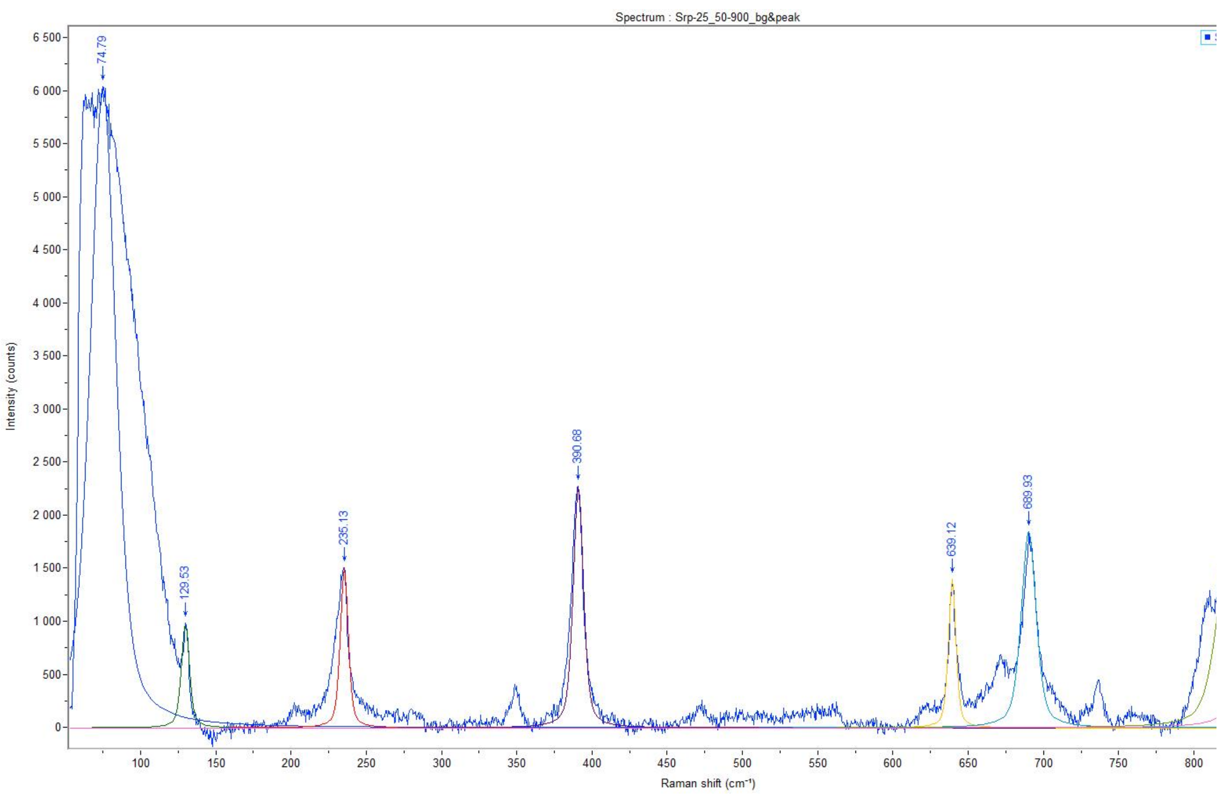

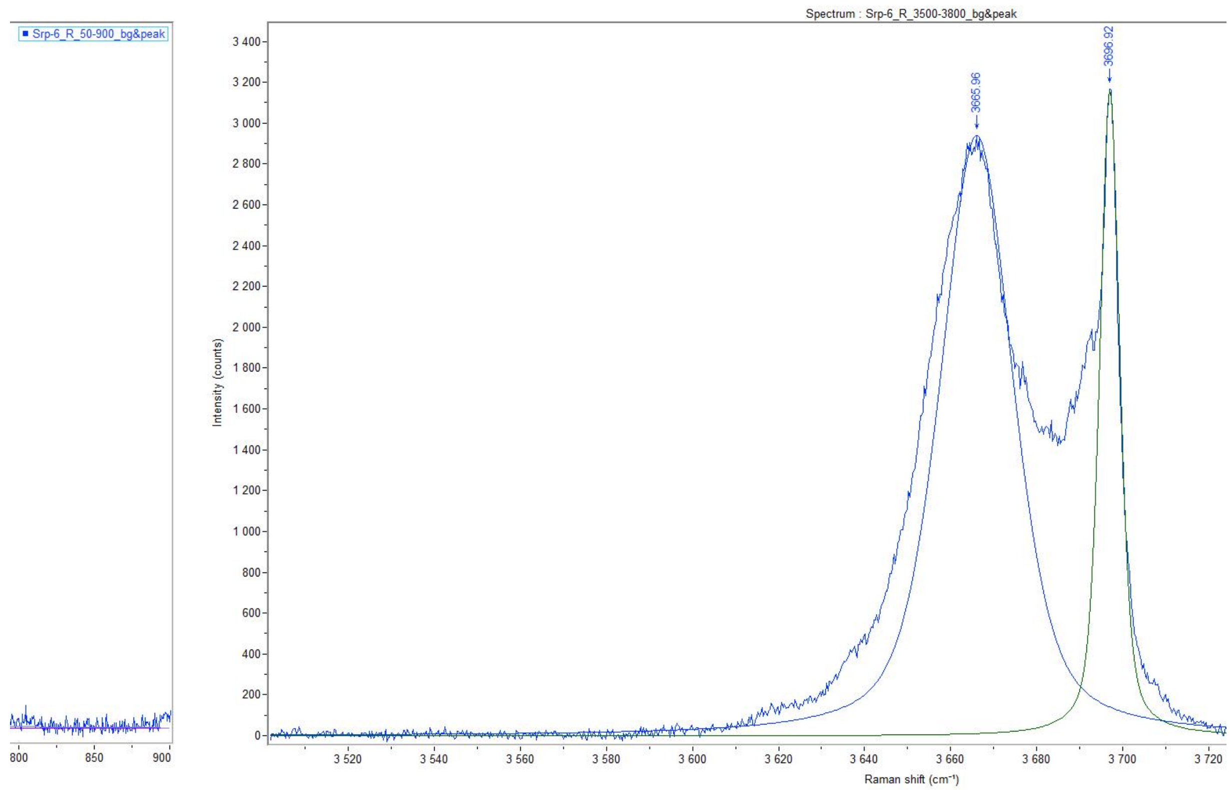
Srp-6_R_50-900_bg&peak
800
850
900
Spectrum : Srp-6_R_3500-3800_bg&peak
Intensity (counts)
3 400
3 200
3 000
2 800
2 600
2 400
2 200
2 000
1 800
1 600
1 400
1 200
1 000
800
600
400
200
0
3 520
3 540
3 560
3 580
3 600
3 620
3 640
3 660
3 680
3 700
3 720
Raman shift (cm⁻¹)
3665.96
3696.92


Srp-1_50-900_bg&peak
Spectrum : Srp-1_3500-3800_bg&peak
Intensity (counts)
7 000
6 500
6 000
5 500
5 000
4 500
4 000
3 500
3 000
2 500
2 000
1 500
1 000
500
3697.19
3648.22
3653.42

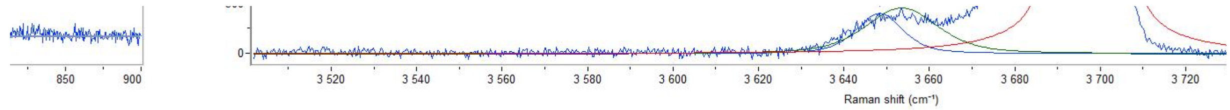

850
900
3 520
3 540
3 560
3 580
3 600
3 620
3 640
3 660
3 680
3 700
3 720
Raman shift (cm⁻¹)

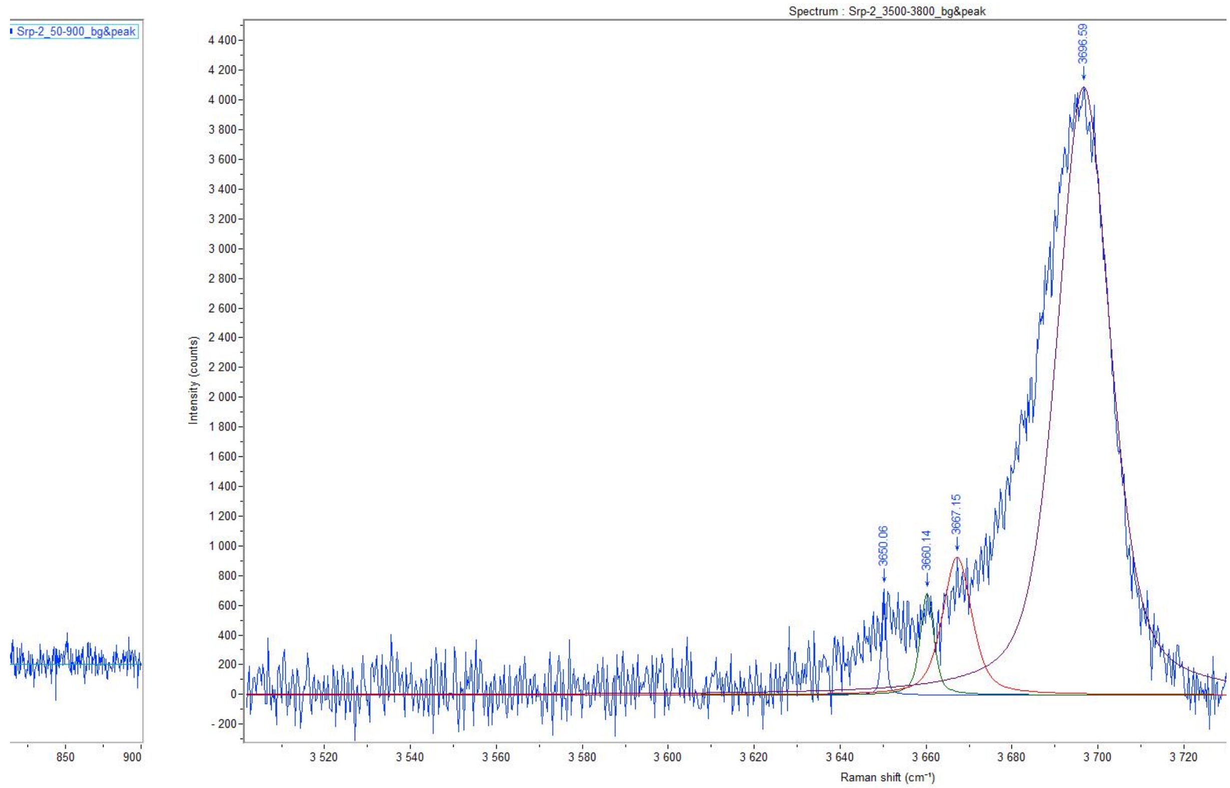

Srp-2_50-900_bg&peak
Spectrum : Srp-2_3500-3800_bg&peak
Intensity (counts)
3696.59
3667.15
3660.14
3650.06
850
900
Raman shift (cm⁻¹)

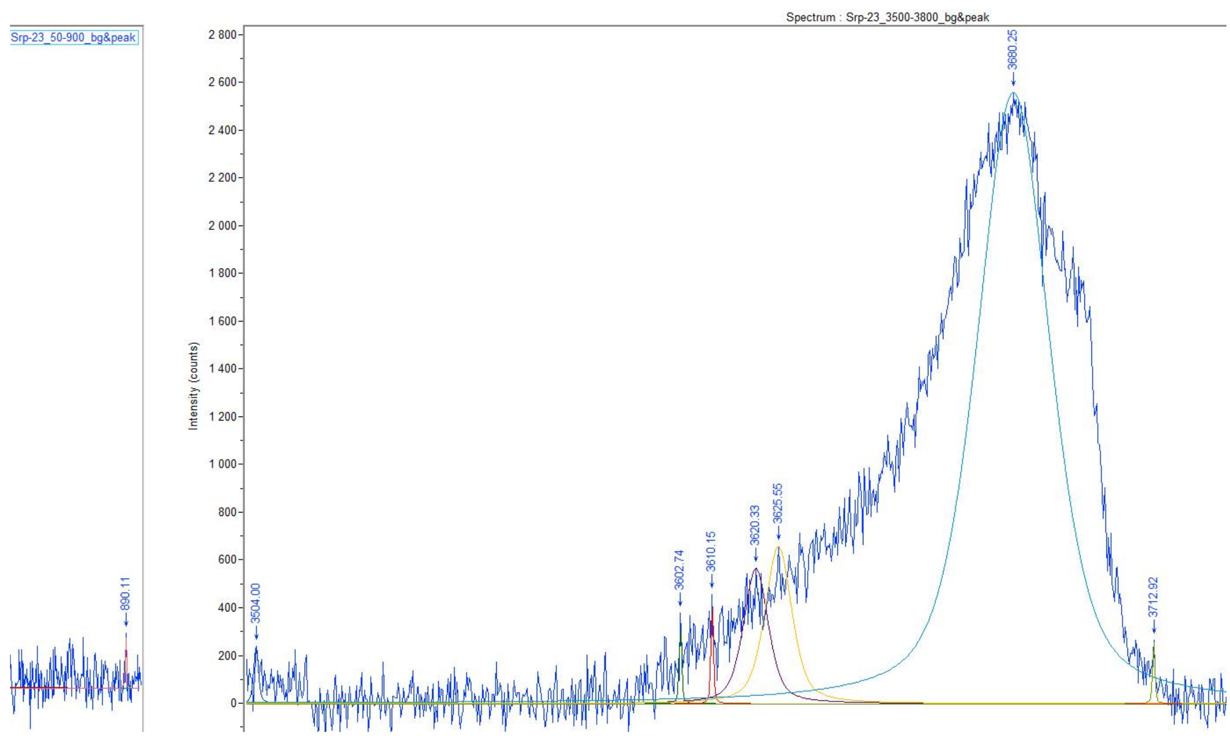

Srp-23_50-900_bg&peak
Spectrum : Srp-23_3500-3800_bg&peak
Intensity (counts)
890.11
3504.00
3602.74
3610.15
3620.33
3625.55
3680.25
3712.92

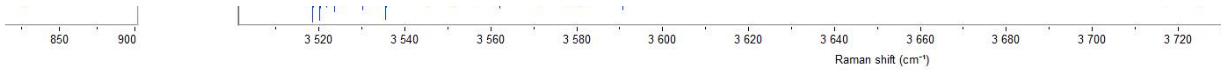

850
900
3 520
3 540
3 560
3 580
3 600
3 620
3 640
3 660
3 680
3 700
3 720
Raman shift (cm⁻¹)

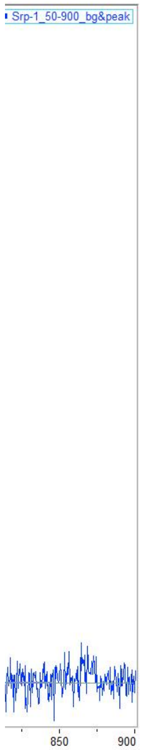

Srp-1_50-900_bg&peak
850
900

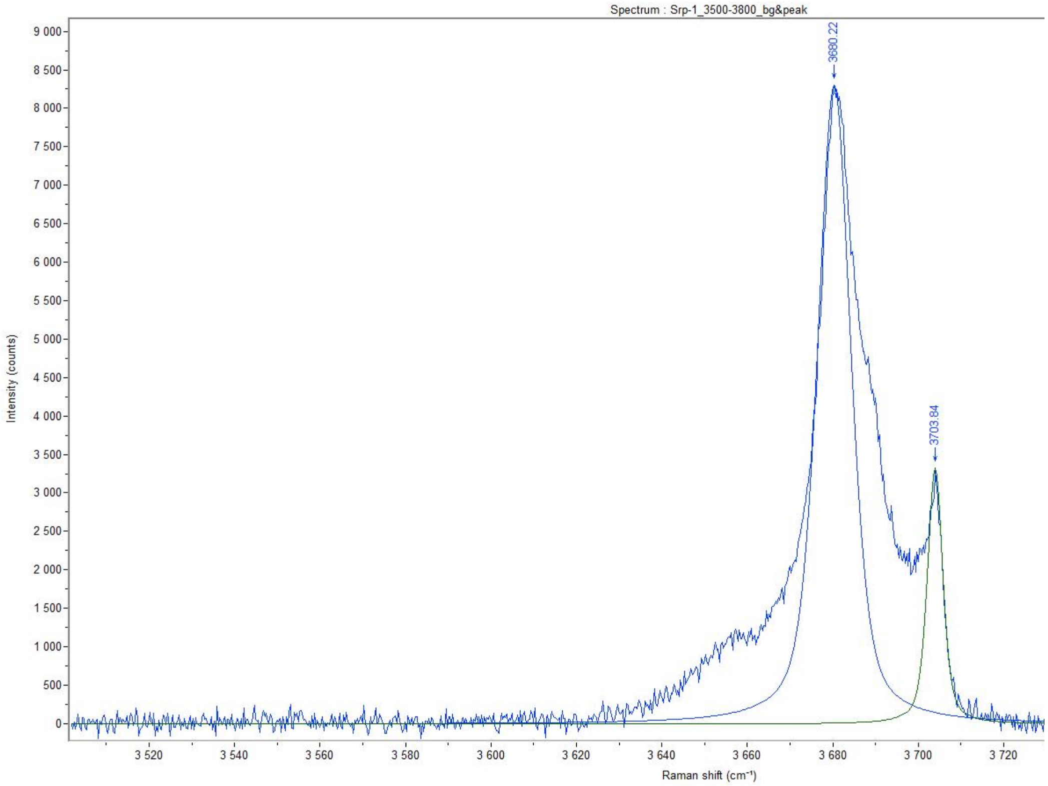

Spectrum : Srp-1_3500-3800_bg&peak
Intensity (counts)
Raman shift (cm⁻¹)
3680.22
3703.84

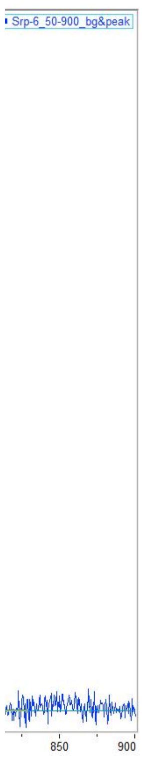

Srp-6_50-900_bg&peak
850
900

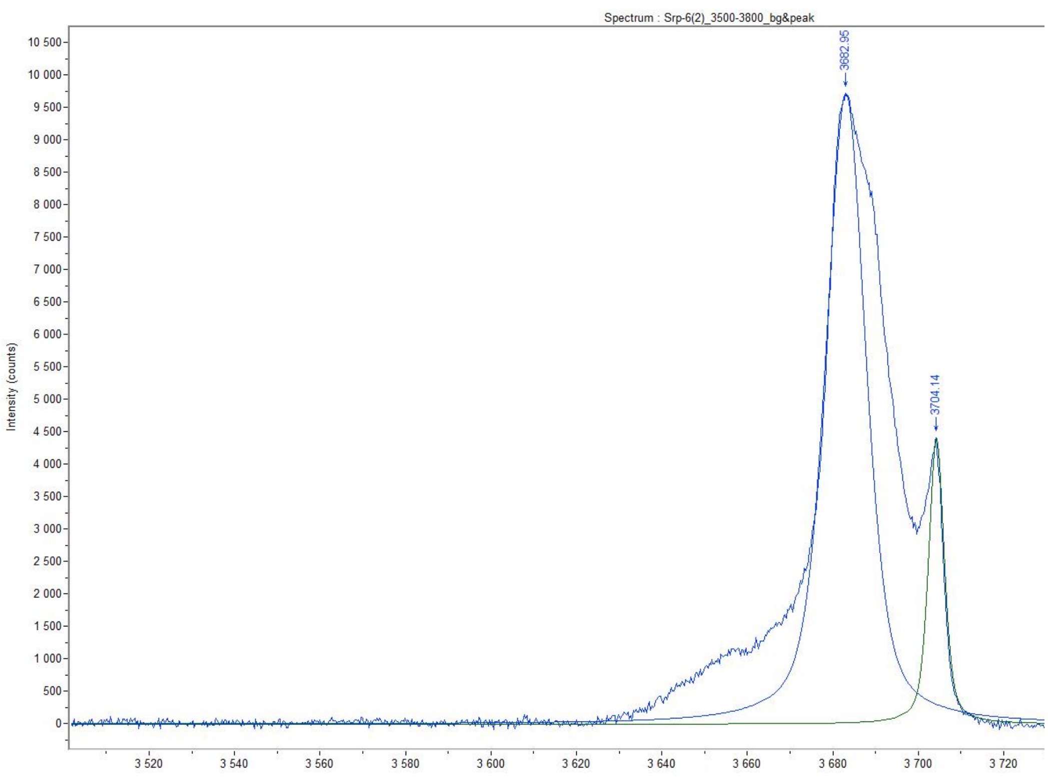

Spectrum : Srp-6(2)_3500-3800_bg&peak
Intensity (counts)
3682.95
3704.14

Raman shift (cm⁻¹)

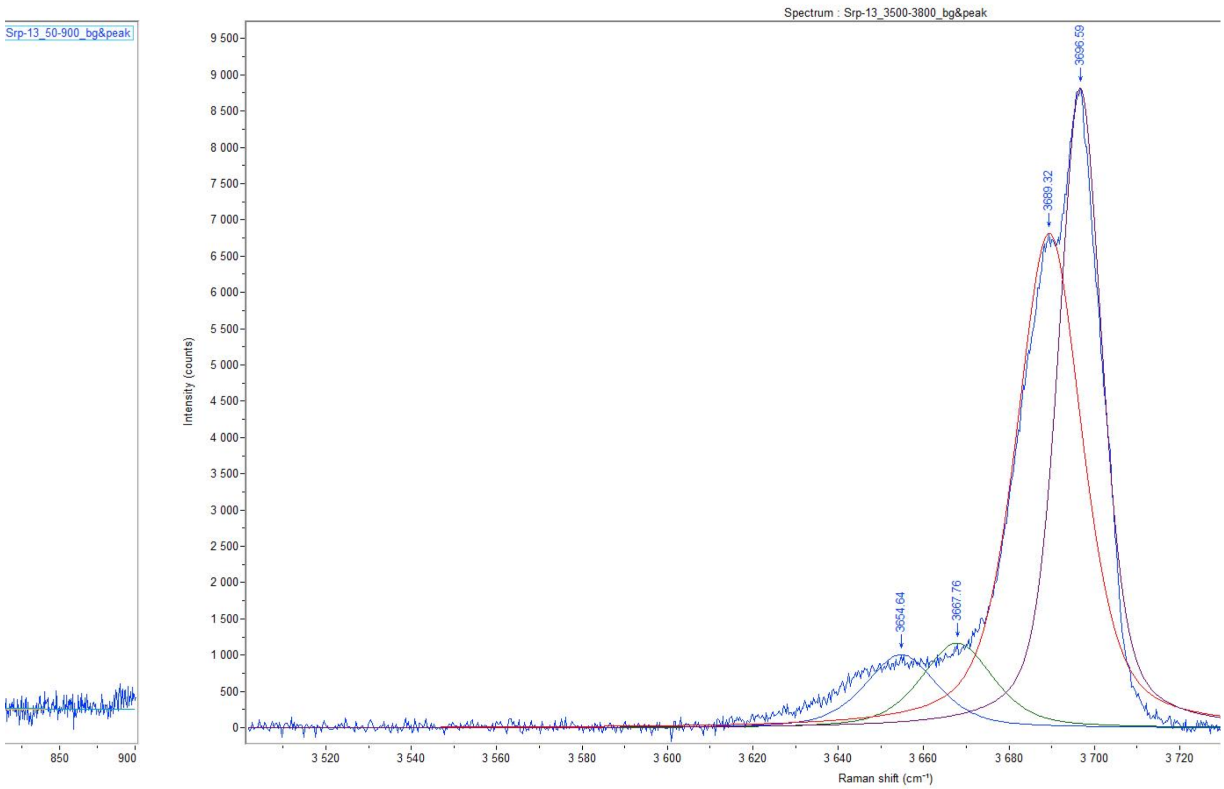

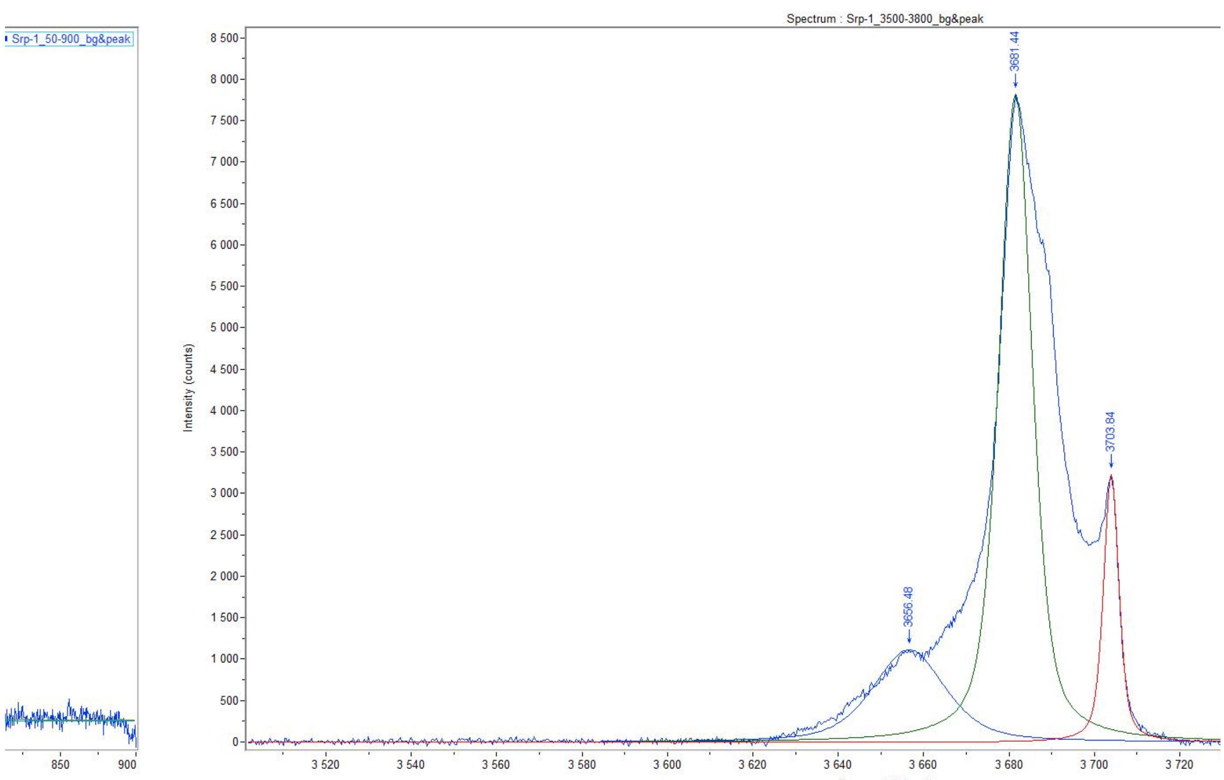

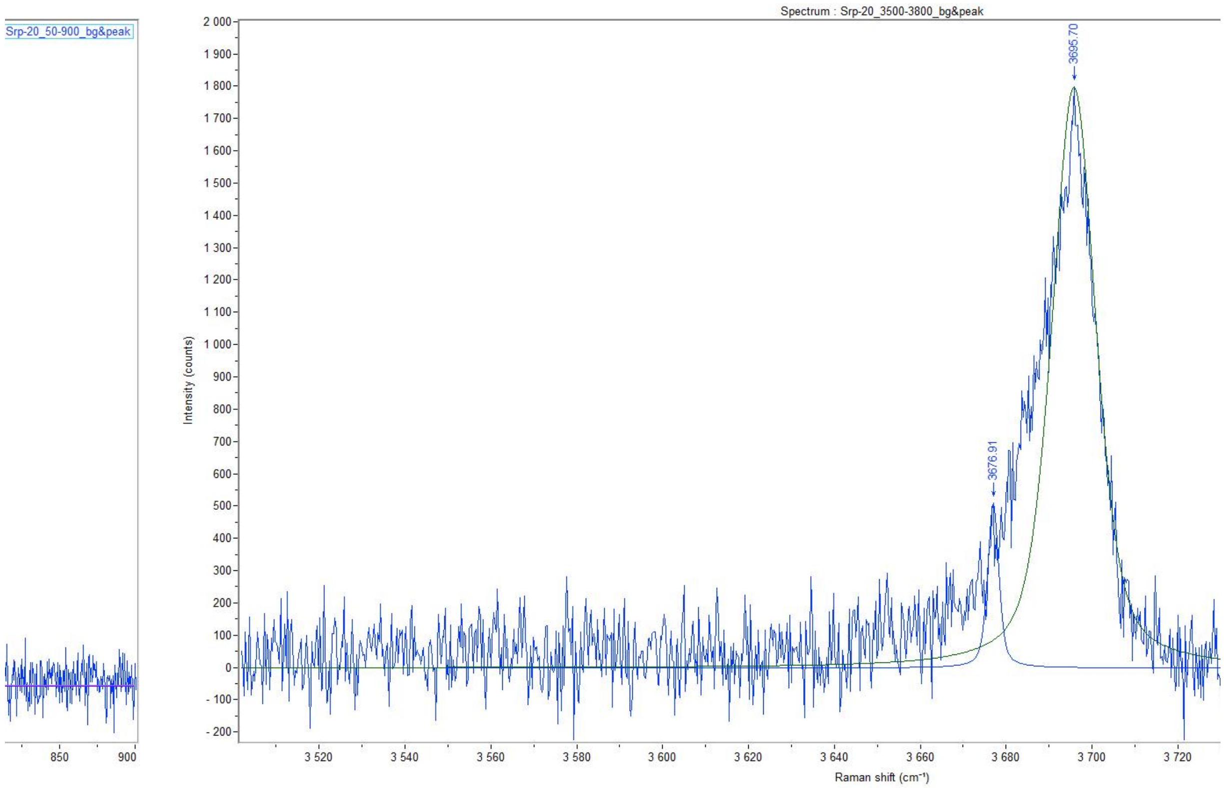
Srp-20_50-900_bg&peak
850
900
Spectrum : Srp-20_3500-3800_bg&peak
3695.70
3676.91
Intensity (counts)
Raman shift (cm⁻¹)
2 000
1 900
1 800
1 700
1 600
1 500
1 400
1 300
1 200
1 100
1 000
900
800
700
600
500
400
300
200
100
0
- 100
- 200
3 520
3 540
3 560
3 580
3 600
3 620
3 640
3 660
3 680
3 700
3 720

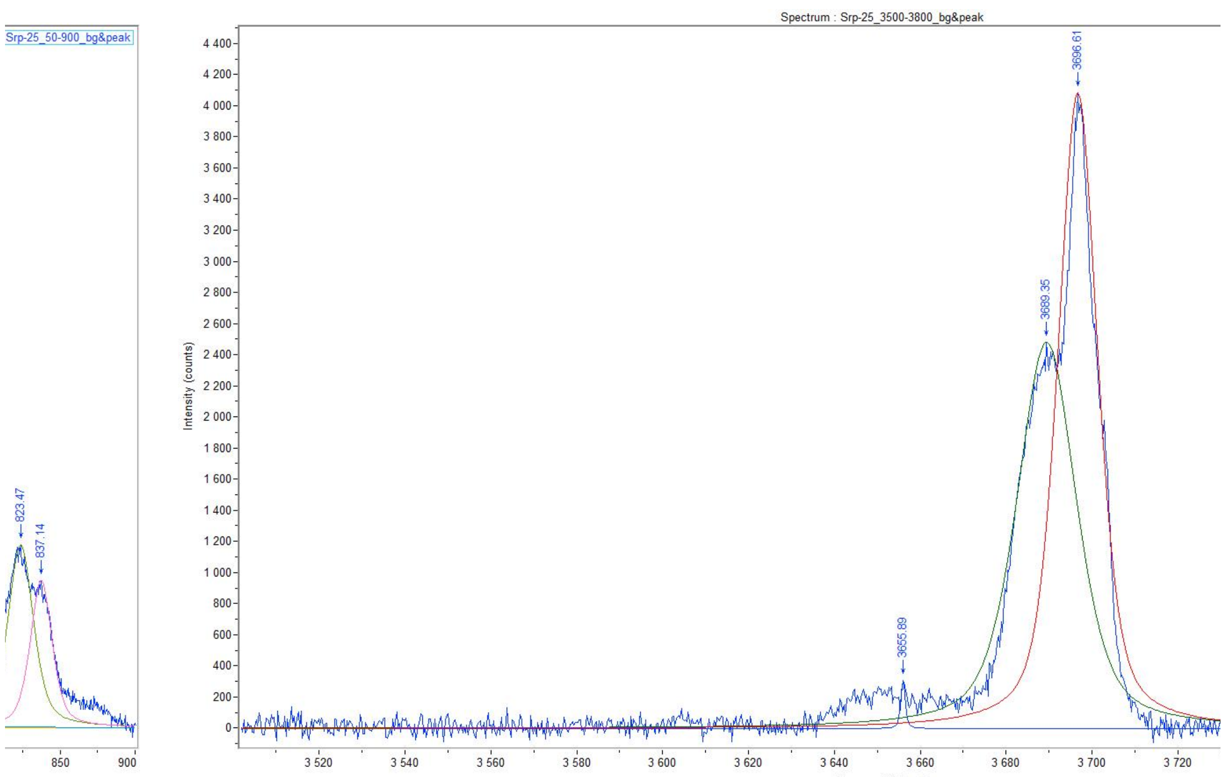
Srp-25_50-900_bg&peak
823.47
837.14
850
900
Spectrum : Srp-25_3500-3800_bg&peak
3696.61
3689.35
3655.89
Intensity (counts)
Raman shift (cm⁻¹)
4 400
4 200
4 000
3 800
3 600
3 400
3 200
3 000
2 800
2 600
2 400
2 200
2 000
1 800
1 600
1 400
1 200
1 000
800
600
400
200
0
3 520
3 540
3 560
3 580
3 600
3 620
3 640
3 660
3 680
3 700
3 720

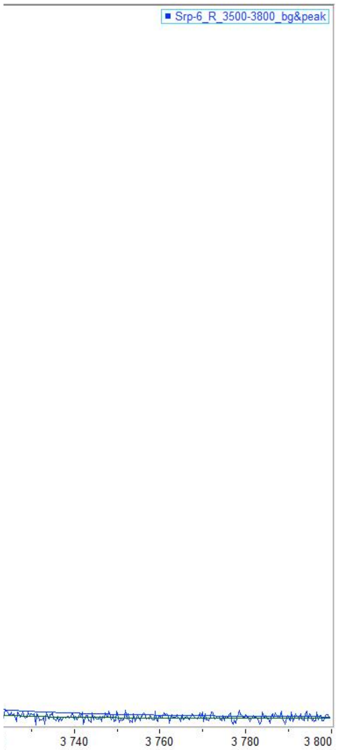

Srp-6_R_3500-3800_bg&peak
3 740
3 760
3 780
3 800

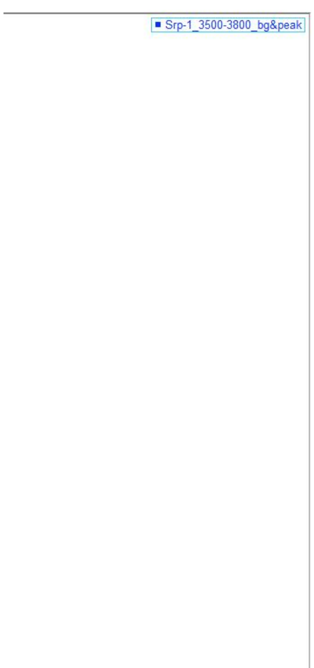

Srp-1_3500-3800_bg&peak

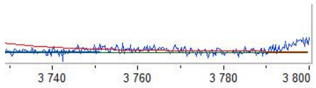
3 740
3 760
3 780
3 800

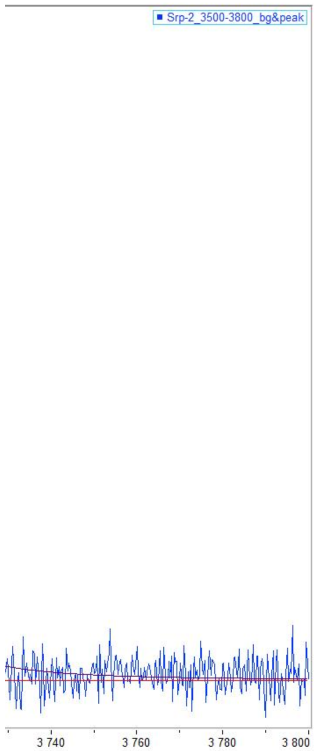
Srp-2_3500-3800_bg&peak
3 740
3 760
3 780
3 800

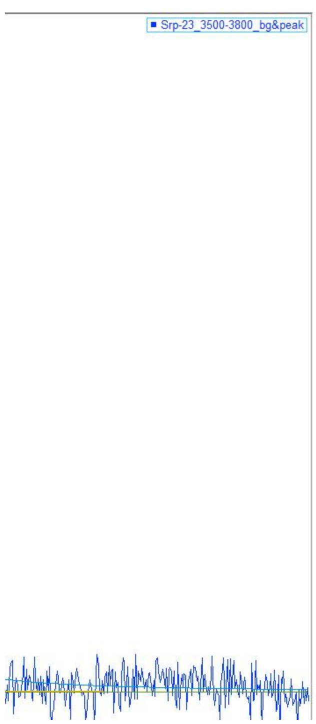
Srp-23_3500-3800_bg&peak

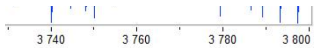
3 740
3 760
3 780
3 800

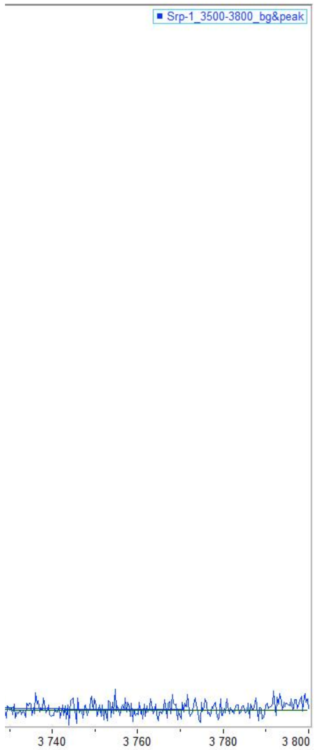
Srp-1_3500-3800_bg&peak
3 740
3 760
3 780
3 800

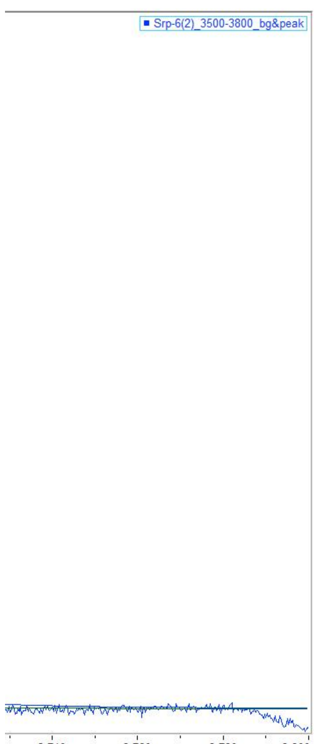
Srp-6(2)_3500-3800_bg&peak
3 740
3 760
3 780
3 800

SIMS session	Mount I.D.	File	Analysis I.D.	$\delta^{18}O$ ‰ (RAW)
S1 (19 October 2020)				
	OM13-17A			
	sample analysis			
		20201019@4	OM13-17A-UWC-3-gr2	4.93
		20201019@4	OM13-17A-UWC-3-gr2	4.97
		20201019@4	OM13-17A-UWC-3-gr2	4.93
		20201019@4	OM13-17A-UWC-3-gr2	4.69
		20201019@4	OM13-17A-Cal-1	19.69
		20201019@4	OM13-17A-Cal-2	18.45
		20201019@4	OM13-17A-Cal-3	19.43
		20201019@4	OM13-17A-Cal-4	19.49
		20201019@4	OM13-17A-Cal-5	19.82
		20201019@4	OM13-17A-Cal-6	19.73
		20201019@4	OM13-17A-Cal-7	19.79
		20201019@4	OM13-17A-Cal-8	19.57
		20201019@4	OM13-17A-Cal-9	19.67
		20201019@4	OM13-17A-Cal-10	18.72
		20201019@4	OM13-17A-Cal-11	18.88
		20201019@4	OM13-17A-Cal-12	19.26
		20201019@4	OM13-17A-Cal-13	20.00
		20201019@4	OM13-17A-Cal-14	19.71
		20201019@4	OM13-17A-Cal-15	20.19
		20201019@4	OM13-17A-Cal-16	19.60
		20201019@4	OM13-17A-Cal-17	21.11
		20201019@4	OM13-17A-Cal-18	18.02
		20201019@4	OM13-17A-Cal-19	16.78
		20201019@4	OM13-17A-Cal-20	16.36
		20201019@4	OM13-17A-UWC-3-gr2	5.12
		20201019@4	OM13-17A-UWC-3-gr2	5.01
		20201019@4	OM13-17A-UWC-3-gr2	5.48
		20201019@4	OM13-17A-UWC-3-gr2	4.81
			average and 2SD	5.10
			bracket average and 2SD	**4.99**
			2SE	
		20201019@4	OM13-17A-Cal-1b	20.14

20201019@4	OM13-17A-Cal-4b	20.43
20201019@4	OM13-17A-Cal-21	20.12
20201019@4	OM13-17A-Cal-22	15.73
20201019@4	OM13-17A-Cal-23	16.23
20201019@4	OM13-17A-Cal-24	17.11
20201019@4	OM13-17A-Cal-25	17.50
20201019@4	OM13-17A-Cal-26	17.42
20201019@4	OM13-17A-Cal-27	15.20
20201019@4	OM13-17A-Cal-28	18.92
20201019@4	OM13-17A-Cal-29	18.57
20201019@4	OM13-17A-Cal-30	20.65
20201019@4	OM13-17A-Cal-31	20.14
20201019@4	OM13-17A-Cal-32	20.03
20201019@4	OM13-17A-Cal-33	20.42
20201019@4	OM13-17A-Cal-34	16.59
20201019@4	OM13-17A-Cal-35	16.66
20201019@4	OM13-17A-Cal-36	16.43
20201019@4	OM13-17A-Cal-37	16.50
20201019@4	OM13-17A-Cal-38	16.04
20201019@4	OM13-17A-Cal-39	16.56
20201019@4	OM13-17A-Cal-40	16.13
20201019@4	OM13-17A-Cal-41	18.56
20201019@4	OM13-17A-Cal-42	19.61
20201019@4	OM13-17A-Cal-43	20.33
20201019@4	OM13-17A-Cal-44	20.38
	average and 2SD (Cal I)	
	average and 2SD (Cal II)	

20201019@4	OM13-17A-UWC-3-gr2	4.82
20201019@4	OM13-17A-UWC-3-gr2	4.93
20201019@4	OM13-17A-UWC-3-gr2	4.84
20201019@4	OM13-17A-UWC-3-gr2	5.29
	average and 2SD	4.97
	bracket average and 2SD	**5.04**
	2SE	

<u>OM13-1</u>

sample analysis

20201019@1	OM-13-1-UWC-3-gr1	3.32
20201019@1	OM-13-1-UWC-3-gr1	3.54
20201019@1	OM-13-1-UWC-3-gr1	3.37
20201019@1	OM-13-1-UWC-3-gr1	3.56

20201019@1	OM-13-1-Cal-1	20.32
20201019@1	OM-13-1-Cal-2	21.34
20201019@1	OM-13-1-Cal-3	16.77
20201019@1	OM-13-1-Cal-4	11.05
20201019@1	OM-13-1-Cal-5	18.37
20201019@1	OM-13-1-Cal-6	20.84
20201019@1	OM-13-1-Cal-7	20.65
20201019@1	OM-13-1-Cal-8	16.54
20201019@1	OM-13-1-Cal-9	13.17
20201019@1	OM-13-1-Cal-10	11.56
20201019@1	OM-13-1-Cal-11	11.13
20201019@1	OM-13-1-Cal-12	12.27
20201019@1	OM-13-1-Cal-13	18.62
20201019@1	OM-13-1-Cal-14	10.26
20201019@1	OM-13-1-Cal-15	19.54
20201019@1	OM-13-1-UWC-3-gr1	3.52
20201019@1	OM-13-1-UWC-3-gr1	3.78
20201019@1	OM-13-1-UWC-3-gr1	3.87
20201019@1	OM-13-1-UWC-3-gr1	3.47
	average and 2SD	3.66
	bracket average and 2SD	**3.55**
	2SE	
20201019@1	OM-13-1-Cal-16	16.21
20201019@1	OM-13-1-Cal-17	12.45
20201019@1	OM-13-1-Cal-18	12.46
20201019@1	OM-13-1-Cal-19	11.29
20201019@1	OM-13-1-Cal-20	17.45
20201019@1	OM-13-1-Cal-21	13.12
20201019@1	OM-13-1-Cal-22	11.61
20201019@1	OM-13-1-Cal-23	18.27
20201019@1	OM-13-1-Cal-24	18.87
20201019@1	OM-13-1-Cal-25	18.96
20201019@1	OM-13-1-Cal-26	18.91
20201019@1	OM-13-1-Cal-27	16.87
20201019@1	OM-13-1-Cal-28	12.73
20201019@1	OM-13-1-Cal-29	11.34
20201019@1	OM-13-1-Cal-30	13.96
20201019@1	OM-13-1-Cal-31	18.57
20201019@1	OM-13-1-Cal-32	17.84
	average and 2SD (Cal I)	
	average and 2SD (Cal III)	

20201019@1	OM-13-1-UWC-3-gr1	3.59
20201019@1	OM-13-1-UWC-3-gr1	3.93
20201019@1	OM-13-1-UWC-3-gr1	3.38
20201019@1	OM-13-1-UWC-3-gr1	4.02
	average and 2SD	3.73
	bracket average and 2SD	**3.70**
	2SE	

OM13-11

sample analysis

20201019@1	OM-13-11-UWC-3-gr1	4.02
20201019@1	OM-13-11-UWC-3-gr1	3.58
20201019@1	OM-13-11-UWC-3-gr1	3.76
20201019@1	OM-13-11-UWC-3-gr1	4.10
20201019@1	OM-13-11-Cal-1	18.99
20201019@1	OM-13-11-Cal-2	19.86
20201019@1	OM-13-11-Cal-3	18.82
20201019@1	OM-13-11-Cal-4	18.52
20201019@1	OM-13-11-Cal-5	18.96
20201019@1	OM-13-11-Cal-6	19.33
20201019@1	OM-13-11-Cal-7	13.31
20201019@1	OM-13-11-Cal-8	12.34
20201019@1	OM-13-11-Cal-9	19.43
20201019@1	OM-13-11-Cal-10	18.73
20201019@1	OM-13-11-Cal-11	18.79
20201019@1	OM-13-11-Cal-12	19.37
20201019@1	OM-13-11-Cal-13	19.19
20201019@1	OM-13-11-Cal-14	19.75
20201019@1	OM-13-11-Cal-15	19.49
20201019@1	OM-13-11-Cal-16	19.48
20201019@1	OM-13-11-Cal-17	11.87
20201019@1	OM-13-11-Cal-18	10.72
20201019@1	OM-13-11-Cal-19	19.13
20201019@1	OM-13-11-Cal-20	9.43
20201019@1	OM-13-11-Cal-21	9.52
20201019@1	OM-13-11-UWC-3-gr1	5.04
20201019@1	OM-13-11-UWC-3-gr1	4.21
20201019@1	OM-13-11-UWC-3-gr1	4.14
20201019@1	OM-13-11-UWC-3-gr1	3.92
20201019@1	OM-13-11-UWC-3-gr1	4.02

	average and 2SD	4.07
	bracket average and 2SD	**3.97**
	2SE	

20201019@1	OM-13-11-Cal-22	18.85
20201019@1	OM-13-11-Cal-23	18.72
20201019@1	OM-13-11-Cal-24	18.66
20201019@1	OM-13-11-Cal-25	18.85
20201019@1	OM-13-11-Cal-26	19.31
20201019@1	OM-13-11-Cal-27	19.18
20201019@1	OM-13-11-Cal-28	19.86
20201019@1	OM-13-11-Cal-29	18.27
20201019@1	OM-13-11-Cal-30	19.46
20201019@1	OM-13-11-Cal-31	19.13
20201019@1	OM-13-11-Cal-32	19.31
20201019@1	OM-13-11-Cal-33	18.57
20201019@1	OM-13-11-Cal-34	18.64
20201019@1	OM-13-11-Cal-35	19.67
20201019@1	OM-13-11-Cal-36	19.58
20201019@1	OM-13-11-Cal-37	19.19
20201019@1	OM-13-11-Cal-39	18.36
20201019@1	OM-13-11-Cal-38	19.40
20201019@1	OM-13-11-Cal-40	19.45
20201019@1	OM-13-11-Cal-41	18.76
20201019@1	OM-13-11-Cal-42	19.15
20201019@1	OM-13-11-Cal-43	18.76
	average and 2SD (Cal I)	
	average and 2SD (Cal vein)	
	average and 2SD (Cal II)	

20201019@1	OM-13-11-UWC-3-gr1	4.36
20201019@1	OM-13-11-UWC-3-gr1	4.39
20201019@1	OM-13-11-UWC-3-gr1	4.09
20201019@1	OM-13-11-UWC-3-gr1	4.53
	average and 2SD	4.34
	bracket average and 2SD	**4.21**
	2SE	

<u>OM13-13</u>

sample analysis

20201019@1	OM-13-13-UWC-3-gr1	3.46
20201019@1	OM-13-13-UWC-3-gr1	3.67
20201019@1	OM-13-13-UWC-3-gr1	3.67

20201019@1	OM-13-13-UWC-3-gr1	3.29
20201019@1	OM-13-13-Cal-1	17.40
20201019@1	OM-13-13-Cal-2	17.18
20201019@1	OM-13-13-Cal-3	16.97
20201019@1	OM-13-13-Cal-4	17.01
20201019@1	OM-13-13-Cal-5	8.65
20201019@1	OM-13-13-Cal-6	14.92
20201019@1	OM-13-13-Cal-7	10.90
20201019@1	OM-13-13-Cal-8	10.22
20201019@1	OM-13-13-Cal-9	17.11
20201019@1	OM-13-13-Cal-10	17.43
20201019@1	OM-13-13-Cal-11	13.28
20201019@1	OM-13-13-Cal-12	10.24
20201019@1	OM-13-13-Cal-13	17.63
20201019@1	OM-13-13-Cal-14	18.66
20201019@1	OM-13-13-Cal-15	17.92
20201019@1	OM-13-13-Cal-16	15.45
20201019@1	OM-13-13-Cal-17	15.80
20201019@1	OM-13-13-Cal-18	16.26
20201019@1	OM-13-13-Cal-19	18.03
20201019@1	OM-13-13-Cal-20	17.21
20201019@1	OM-13-13-UWC-3-gr1	3.75
20201019@1	OM-13-13-UWC-3-gr1	3.90
20201019@1	OM-13-13-UWC-3-gr1	3.62
20201019@1	OM-13-13-UWC-3-gr1	3.73
	average and 2SD	3.75
	bracket average and 2SD	**3.64**
	2SE	
20201019@1	OM-13-13-Cal-21	17.15
20201019@1	OM-13-13-Cal-22	17.22
20201019@1	OM-13-13-Cal-23	17.40
20201019@1	OM-13-13-Cal-24	18.37
20201019@1	OM-13-13-Cal-25	17.01
20201019@1	OM-13-13-Cal-26	10.49
20201019@1	OM-13-13-Cal-27	15.80
20201019@1	OM-13-13-Cal-28	17.31
20201019@1	OM-13-13-Cal-29	15.28
20201019@1	OM-13-13-Cal-30	17.38
20201019@1	OM-13-13-Cal-31	17.61
20201019@1	OM-13-13-Cal-32	17.73

20201019@1	OM-13-13-Cal-33	17.11
20201019@1	OM-13-13-Cal-34	15.76
20201019@1	OM-13-13-Cal-35	18.45
20201019@1	OM-13-13-Cal-36	16.45
20201019@1	OM-13-13-Cal-37	11.79
20201019@1	OM-13-13-Cal-38	16.31
20201019@1	OM-13-13-Cal-39	19.64
20201019@1	OM-13-13-Cal-40	16.65
	average and 2SD (Cal I)	
	average and 2SD (Cal II)	

20201019@1	OM-13-13-UWC-3-gr1	3.87
20201019@1	OM-13-13-UWC-3-gr1	3.96
20201019@1	OM-13-13-UWC-3-gr1	4.02
20201019@1	OM-13-13-UWC-3-gr1	3.95
	average and 2SD	3.95
	bracket average and 2SD	**3.85**
	2SE	

OM13-14A

sample analysis

20201019@1	OM-13-14A-UWC-3-gr2	3.92
20201019@1	OM-13-14A-UWC-3-gr2	4.01
20201019@1	OM-13-14A-UWC-3-gr2	2.48
20201019@1	OM-13-14A-UWC-3-gr2	3.99
20201019@1	OM-13-14A-UWC-3-gr2	3.43

20201019@1	OM-13-14A-Cal-1	19.44
20201019@1	OM-13-14A-Cal-2	18.59
20201019@1	OM-13-14A-Cal-3	17.61
20201019@1	OM-13-14A-Cal-4	16.96
20201019@1	OM-13-14A-Cal-5	17.07
20201019@1	OM-13-14A-Cal-6	18.97
20201019@1	OM-13-14A-Cal-7	21.30
20201019@1	OM-13-14A-Cal-8	19.91
20201019@1	OM-13-14A-Cal-9	18.61
20201019@1	OM-13-14A-Cal-10	18.80
20201019@1	OM-13-14A-Cal-11	11.72
20201019@1	OM-13-14A-Cal-12	18.63
20201019@1	OM-13-14A-Cal-13	18.13
20201019@1	OM-13-14A-Cal-14	19.90
20201019@1	OM-13-14A-Cal-15	18.57
20201019@1	OM-13-14A-Cal-16	18.14

20201019@1	OM-13-14A-Cal-17	18.05
20201019@1	OM-13-14A-Cal-18	18.41
20201019@1	OM-13-14A-Cal-19	19.29
20201019@1	OM-13-14A-Cal-20	18.08
	average and 2SD (Cal I)	
	average and 2SD (Cal II)	
20201019@1	OM-13-14A-UWC-3-gr2	3.67
20201019@1	OM-13-14A-UWC-3-gr2	4.15
20201019@1	OM-13-14A-UWC-3-gr2	4.04
20201019@1	OM-13-14A-UWC-3-gr2	3.69
	average and 2SD	3.88
	bracket average and 2SD	**3.86**
	2SE	

2SE (int.)	Bias (‰)	$\delta^{18}O$ ‰ (V-SMOW)	2s (ext.)	^{16}O (Gcps)	^{18}O (Mcps)	IP (nA)
0.53				1.85	3.73	0.99
0.54				1.85	3.73	0.99
0.64				1.85	3.72	0.99
0.60				1.85	3.73	0.99
0.66		**27.30**	**0.47**	1.68	3.44	0.99
0.58		**26.05**	**0.47**	1.70	3.47	0.99
0.47		**27.04**	**0.47**	1.68	3.43	0.99
0.59		**27.10**	**0.47**	1.74	3.56	0.98
0.55		**27.43**	**0.47**	1.72	3.51	0.98
0.65		**27.34**	**0.47**	1.73	3.53	0.98
0.55				1.75	3.57	0.98
0.59		**27.17**	**0.47**	1.73	3.53	0.98
0.57		**27.28**	**0.47**	1.69	3.45	0.98
0.53		**26.32**	**0.47**	1.72	3.51	0.98
0.65		**26.48**	**0.47**	1.74	3.55	0.98
0.67		**26.86**	**0.47**	1.69	3.46	0.98
0.55		**27.61**	**0.47**	1.65	3.37	0.98
0.64		**27.31**	**0.47**	1.71	3.50	0.98
0.67		**27.80**	**0.47**	1.72	3.51	0.98
0.51		**27.21**	**0.47**	1.81	3.71	0.98
0.59		**28.73**	**0.47**	1.76	3.60	0.98
0.60		**25.61**	**0.47**	1.82	3.71	0.98
0.54		**24.37**	**0.47**	1.79	3.64	0.98
0.52		**23.94**	**0.47**	1.79	3.64	0.98
0.61				1.81	3.65	0.98
0.56				1.81	3.64	0.98
0.56				1.81	3.66	0.97
0.60				1.80	3.64	0.97
0.56						
0.47		**-7.41**	**12.49**			
0.17						
0.47		**27.70**	**0.49**	1.63	3.34	0.97

0.54	**27.99**	**0.49**	1.69	3.46	0.97
0.55	**27.69**	**0.49**	1.69	3.45	0.97
0.58	**23.26**	**0.49**	1.77	3.60	0.97
0.64	**23.77**	**0.49**	1.75	3.56	0.96
0.57	**24.66**	**0.49**	1.78	3.63	0.96
0.59	**25.04**	**0.49**	1.78	3.62	0.96
0.60	**24.97**	**0.49**	1.76	3.58	0.96
0.55	**22.73**	**0.49**	1.74	3.54	0.96
0.62	**26.48**	**0.49**	1.76	3.59	0.96
0.65	**26.12**	**0.49**	1.76	3.58	0.96
0.57	**28.22**	**0.49**	1.75	3.57	0.96
0.51	**27.71**	**0.49**	1.76	3.59	0.96
0.66	**27.59**	**0.49**	1.64	3.35	0.96
0.50	**27.99**	**0.49**	1.62	3.32	0.96
0.55	**24.13**	**0.49**	1.73	3.53	0.96
0.50	**24.20**	**0.49**	1.77	3.60	0.96
0.60	**23.97**	**0.49**	1.74	3.55	0.96
0.57	**24.04**	**0.49**	1.75	3.57	0.96
0.56	**23.58**	**0.49**	1.73	3.52	0.96
0.57	**24.10**	**0.49**	1.71	3.49	0.96
0.57	**23.66**	**0.49**	1.75	3.57	0.96
0.63	**26.11**	**0.49**	1.74	3.55	0.96
0.64	**27.17**	**0.49**	1.74	3.57	0.96
0.62	**27.89**	**0.49**	1.75	3.57	0.96
0.59	**27.95**	**0.49**	1.77	3.63	0.96
	27.30	**1.34**			
	24.13	**1.42**			
0.55			1.78	3.59	0.96
0.49			1.78	3.58	0.95
0.68			1.77	3.56	0.95
0.49			1.78	3.59	0.95
0.44					
0.49	**-7.36**	**12.49**			
0.17					
0.58			1.96	3.94	1.04
0.53			1.96	3.94	1.04
0.52			1.96	3.94	1.04
0.56			1.95	3.93	1.04

0.62	**29.41**	**0.38**	1.93	3.94	1.03
0.53	**30.43**	**0.38**	1.92	3.93	1.03
0.68	**25.83**	**0.38**	1.99	4.05	1.03
0.53	**20.05**	**0.38**	1.95	3.95	1.03
0.85	**27.44**	**0.38**	1.90	3.88	1.03
0.55	**29.93**	**0.38**	1.93	3.94	1.03
0.52	**29.74**	**0.38**	1.92	3.94	1.02
0.87	**25.59**	**0.38**	1.90	3.88	1.02
0.60	**22.19**	**0.38**	1.88	3.82	1.02
0.60	**20.57**	**0.38**	1.86	3.78	1.02
0.60	**20.14**	**0.38**	1.88	3.82	1.02
0.46	**21.29**	**0.38**	1.85	3.76	1.02
0.49	**27.68**	**0.38**	1.88	3.83	1.02
0.52	**19.26**	**0.38**	1.87	3.79	1.02
0.52	**28.61**	**0.38**	1.88	3.85	1.01
0.61			1.92	3.85	1.01
0.64			1.91	3.85	1.01
0.54			1.90	3.83	1.01
0.59			1.91	3.84	1.01
0.39					
0.38	**-8.83**	**12.49**			
0.13					
0.35	**25.11**	**0.47**	1.84	3.76	1.01
0.82	**21.32**	**0.47**	1.83	3.71	1.01
0.31	**21.33**	**0.47**	1.83	3.71	1.01
0.62	**20.15**	**0.47**	1.85	3.75	1.01
0.55	**26.36**	**0.47**	1.85	3.77	1.00
0.49	**22.00**	**0.47**	1.84	3.74	1.00
0.43	**20.48**	**0.47**	1.82	3.69	1.00
0.60	**27.19**	**0.47**	1.72	3.51	1.00
0.64	**27.80**	**0.47**	1.76	3.59	1.00
0.67	**27.88**	**0.47**	1.78	3.63	1.00
0.65	**27.84**	**0.47**	1.77	3.62	1.00
0.65	**25.78**	**0.47**	1.76	3.59	1.00
0.31			1.85	3.75	0.99
0.62	**20.20**	**0.47**	1.84	3.74	0.99
1.41			1.75	3.55	0.99
0.59	**27.49**	**0.47**	1.80	3.67	0.99
0.62	**26.75**	**0.47**	1.85	3.77	0.99
	24.31	**7.77**			
	26.37	**5.18**			

0.55			1.87	3.76	0.99
0.56			1.86	3.75	0.99
0.57			1.85	3.72	0.99
0.56			1.86	3.75	0.99
0.60					
0.47	**-8.69**	**12.49**			
0.17					
0.50			1.88	3.79	0.99
0.47			1.87	3.76	0.99
0.53			1.87	3.76	0.98
0.55			1.87	3.77	0.98
0.57	**27.64**	**0.42**	1.81	3.70	0.98
0.47	**28.52**	**0.42**	1.81	3.71	0.98
0.49	**27.47**	**0.42**	1.81	3.70	0.98
0.60	**27.16**	**0.42**	1.81	3.71	0.98
0.67	**27.61**	**0.42**	1.77	3.61	0.98
0.56	**27.99**	**0.42**	1.81	3.69	0.98
0.55	**21.91**	**0.42**	1.77	3.61	0.98
0.68	**20.93**	**0.42**	1.79	3.64	0.98
0.56	**28.08**	**0.42**	1.79	3.67	0.97
0.58	**27.38**	**0.42**	1.81	3.71	0.97
0.58	**27.44**	**0.42**	1.81	3.70	0.97
0.56	**28.02**	**0.42**	1.80	3.67	0.97
0.55	**27.84**	**0.42**	1.79	3.65	0.97
0.48	**28.40**	**0.42**	1.80	3.69	0.97
0.62	**28.14**	**0.42**	1.82	3.72	0.97
0.62	**28.13**	**0.42**	1.81	3.70	0.97
0.63	**20.46**	**0.42**	1.77	3.58	0.97
0.56	**19.29**	**0.42**	1.78	3.60	0.97
0.63	**27.78**	**0.42**	1.79	3.65	0.97
0.62	**17.99**	**0.42**	1.63	3.31	0.97
0.65	**18.09**	**0.42**	1.77	3.58	0.97
0.64			1.82	3.66	0.97
0.54			1.81	3.65	0.96
0.56			1.80	3.63	0.96
0.51			1.82	3.66	0.96
0.58			1.80	3.63	0.96

0.26					
0.42	**-8.42**	**12.49**			
0.15					
0.58	**27.25**	**0.41**	1.82	3.73	0.96
0.55	**27.12**	**0.41**	1.80	3.68	0.96
0.49	**27.06**	**0.41**	1.77	3.62	0.96
0.55	**27.26**	**0.41**	1.76	3.59	0.96
0.53	**27.71**	**0.41**	1.75	3.57	0.95
0.70	**27.58**	**0.41**	1.79	3.65	0.95
0.59	**28.27**	**0.41**	1.77	3.63	0.95
0.60	**26.66**	**0.41**	1.77	3.62	0.95
0.70	**27.87**	**0.41**	1.76	3.60	0.95
0.58	**27.54**	**0.41**	1.73	3.54	0.95
0.54	**27.72**	**0.41**	1.78	3.63	0.95
0.60	**26.97**	**0.41**	1.77	3.62	0.95
0.58	**27.04**	**0.41**	1.84	3.76	0.98
0.55	**28.08**	**0.41**	1.82	3.72	0.98
0.48	**27.99**	**0.41**	1.77	3.61	0.98
0.63	**27.59**	**0.41**	1.80	3.68	0.98
0.56	**26.76**	**0.41**	1.84	3.75	0.99
0.56	**27.81**	**0.41**	1.82	3.72	0.99
0.60	**27.86**	**0.41**	1.84	3.75	0.99
0.61	**27.16**	**0.41**	1.83	3.75	0.99
0.56	**27.56**	**0.41**	1.78	3.65	0.99
0.49	**27.17**	**0.41**	1.79	3.65	0.99
	27.61	**0.91**			
	20.65	**2.17**			
	18.04	**0.14**			
0.55			1.83	3.68	0.99
0.61			1.85	3.74	0.99
0.55			1.86	3.75	0.98
0.61			1.85	3.72	0.98
0.37					
0.41	**-8.18**	**12.49**			
0.15					
0.57			1.82	3.66	0.98
0.60			1.84	3.69	0.98
0.60			1.98	3.99	1.03

0.56			2.09	4.21	1.09
0.64	**26.37**	**0.37**	1.97	4.01	1.10
0.61	**26.15**	**0.37**	1.97	4.01	1.09
0.58	**25.94**	**0.37**	1.92	3.92	1.08
0.61	**25.99**	**0.37**	1.94	3.95	1.07
0.49	**17.54**	**0.37**	1.97	3.98	1.07
0.61	**23.87**	**0.37**	1.97	4.01	1.06
0.67	**19.82**	**0.37**	1.95	3.96	1.06
0.59			2.14	4.33	1.06
0.56	**26.09**	**0.37**	1.91	3.89	1.06
0.66	**26.41**	**0.37**	1.92	3.92	1.05
0.35	**22.22**	**0.37**	1.92	3.90	1.06
0.68	**19.15**	**0.37**	1.92	3.89	1.05
0.54	**26.61**	**0.37**	1.92	3.91	1.05
0.58	**27.65**	**0.37**	1.95	3.97	1.05
0.59	**26.90**	**0.37**	1.97	4.02	1.05
0.60	**24.41**	**0.37**	1.94	3.94	1.05
0.48	**24.77**	**0.37**	1.92	3.91	1.04
0.73	**25.22**	**0.37**	1.92	3.92	1.04
0.57	**27.01**	**0.37**	1.92	3.91	1.04
0.64	**26.18**	**0.37**	1.91	3.89	1.04
0.54			1.93	3.88	1.04
0.61			1.93	3.89	1.04
0.50			1.95	3.92	1.03
0.52			1.97	3.96	1.03
0.23					
0.37	**-8.74**	**12.49**			
0.13					
0.54	**25.90**	**0.27**	1.92	3.92	1.03
0.62	**25.98**	**0.27**	1.89	3.86	1.03
0.66	**26.16**	**0.27**	1.86	3.79	1.03
0.65	**27.14**	**0.27**	1.93	3.93	1.03
0.65	**25.77**	**0.27**	1.89	3.85	1.03
0.66	**19.19**	**0.27**	1.90	3.86	1.03
0.65	**24.54**	**0.27**	1.91	3.88	1.03
0.62	**26.07**	**0.27**	1.85	3.77	1.02
0.60	**24.02**	**0.27**	1.87	3.81	1.02
0.56	**26.14**	**0.27**	1.87	3.81	1.02
0.58	**26.37**	**0.27**	1.84	3.76	1.02
0.60	**26.49**	**0.27**	1.84	3.76	1.01

0.64	**25.87**	**0.27**	1.87	3.81	1.01
0.47	**24.51**	**0.27**	1.87	3.80	1.01
0.65	**27.22**	**0.27**	1.87	3.81	1.01
0.65	**25.20**	**0.27**	1.85	3.78	1.01
0.65	**20.50**	**0.27**	1.87	3.79	1.01
0.65	**25.06**	**0.27**	1.86	3.79	1.01
0.65	**28.41**	**0.27**	1.83	3.75	1.01
0.65	**25.40**	**0.27**	1.82	3.72	1.01
	26.06	**1.95**			
	21.40	**5.60**			
0.59			1.87	3.77	1.01
0.53			1.89	3.81	1.01
0.53			1.90	3.83	1.00
0.51			1.91	3.85	1.00
0.12					
0.27	**-8.53**	**12.49**			
0.10					
0.55			1.88	3.79	0.99
0.62			1.86	3.74	0.99
0.56			1.86	3.74	0.99
0.51			1.85	3.72	0.98
0.62			1.83	3.69	0.98
0.65	**28.20**	**0.48**	1.79	3.66	0.98
0.63	**27.34**	**0.48**	1.80	3.68	0.97
0.55	**26.36**	**0.48**	1.74	3.56	0.97
0.66	**25.70**	**0.48**	1.77	3.61	0.98
0.67	**25.81**	**0.48**	1.77	3.61	0.98
0.68	**27.73**	**0.48**	1.80	3.67	0.98
0.57	**30.08**	**0.48**	1.81	3.71	0.98
0.53	**28.68**	**0.48**	1.82	3.73	0.98
0.60	**27.36**	**0.48**	1.83	3.74	0.98
0.46	**27.55**	**0.48**	1.81	3.69	0.98
0.60	**20.42**	**0.48**	1.74	3.53	0.98
0.57	**27.39**	**0.48**	1.77	3.62	0.97
0.61	**26.89**	**0.48**	1.83	3.74	0.97
0.68	**28.66**	**0.48**	1.72	3.51	0.98
0.52	**27.32**	**0.48**	1.79	3.66	0.97
0.60	**26.89**	**0.48**	1.78	3.63	0.97

0.67	**26.80**	**0.48**	1.72	3.51	0.97
0.57	**27.17**	**0.48**	1.77	3.61	0.97
0.62	**28.05**	**0.48**	1.78	3.65	0.97
0.54	**26.83**	**0.48**	1.79	3.66	0.97
	27.33	**2.25**			
	27.72	**1.27**			
0.61			1.83	3.68	0.97
0.63			1.81	3.65	0.97
0.60			1.83	3.69	0.97
0.57			1.82	3.66	0.97
0.49					
0.48	**-8.52**	**12.49**			
0.17					

Yield (Gcps/nA)	Relative yield	2s relative yield	$^{16}OH/^{16}O$	^{16}OH (cps)	$^{16}OH/^{16}O$ background corrected
1.86			1.52E-03	2.82E+06	
1.86			1.56E-03	2.89E+06	
1.86			1.57E-03	2.90E+06	
1.86			1.56E-03	2.89E+06	
1.70	0.92	0.01	2.27E-03	3.81E+06	6.99E-04
1.72	0.93	0.01	1.56E-03	2.65E+06	-1.12E-05
1.70	0.92	0.01	1.75E-03	2.93E+06	1.82E-04
1.77	0.95	0.01	1.73E-03	3.01E+06	1.62E-04
1.75	0.94	0.01	2.13E-03	3.65E+06	5.61E-04
1.76	0.94	0.01	2.12E-03	3.67E+06	5.56E-04
1.78	0.96	0.01	2.07E-03	3.61E+06	5.00E-04
1.76	0.95	0.01	2.17E-03	3.75E+06	6.04E-04
1.72	0.92	0.01	7.24E-03	1.22E+07	5.67E-03
1.75	0.94	0.01	2.13E-03	3.66E+06	5.59E-04
1.77	0.95	0.01	4.45E-03	7.73E+06	2.88E-03
1.72	0.93	0.01	1.95E-03	3.30E+06	3.80E-04
1.68	0.90	0.01	2.09E-03	3.44E+06	5.22E-04
1.74	0.93	0.01	1.93E-03	3.30E+06	3.61E-04
1.75	0.94	0.01	2.13E-03	3.65E+06	5.61E-04
1.85	1.00	0.01	1.65E-03	3.00E+06	8.61E-05
1.80	0.97	0.01	2.03E-03	3.58E+06	4.66E-04
1.86	1.00	0.01	1.63E-03	2.96E+06	6.00E-05
1.82	0.98	0.01	1.57E-03	2.81E+06	5.93E-06
1.82	0.98	0.01	1.61E-03	2.88E+06	4.63E-05
1.85			1.59E-03	2.89E+06	
1.85			1.61E-03	2.90E+06	
1.86			1.56E-03	2.83E+06	
1.85			1.56E-03	2.81E+06	
1.86			**1.57E-03**		
1.68	0.90	0.02	2.24E-03	3.67E+06	6.74E-04

1.74	0.94	0.02	2.19E-03	3.71E+06	6.21E-04
1.74	0.93	0.02	2.00E-03	3.38E+06	4.34E-04
1.83	0.98	0.02	1.56E-03	2.76E+06	-6.03E-06
1.81	0.97	0.02	1.56E-03	2.73E+06	-4.43E-06
1.84	0.99	0.02	1.57E-03	2.79E+06	-1.05E-06
1.84	0.99	0.02	1.60E-03	2.85E+06	3.49E-05
1.82	0.98	0.02	1.59E-03	2.79E+06	1.94E-05
1.80	0.97	0.02	2.22E-03	3.86E+06	6.49E-04
1.82	0.98	0.02	2.55E-03	4.47E+06	9.78E-04
1.82	0.98	0.02	2.32E-03	4.08E+06	7.54E-04
1.81	0.97	0.02	1.94E-03	3.38E+06	3.67E-04
1.83	0.98	0.02	1.69E-03	2.97E+06	1.25E-04
1.70	0.91	0.02	2.32E-03	3.81E+06	7.54E-04
1.69	0.91	0.02	2.03E-03	3.29E+06	4.57E-04
1.80	0.96	0.02	1.66E-03	2.87E+06	9.15E-05
1.84	0.99	0.02	1.69E-03	2.98E+06	1.17E-04
1.81	0.97	0.02	1.55E-03	2.70E+06	-1.70E-05
1.83	0.98	0.02	1.57E-03	2.76E+06	4.23E-06
1.80	0.97	0.02	1.72E-03	2.97E+06	1.49E-04
1.79	0.96	0.02	1.48E-03	2.54E+06	-8.60E-05
1.82	0.98	0.02	1.46E-03	2.56E+06	-1.05E-04
1.81	0.97	0.02	2.35E-03	4.09E+06	7.83E-04
1.82	0.98	0.02	2.23E-03	3.89E+06	6.57E-04
1.82	0.98	0.02	1.82E-03	3.18E+06	2.53E-04
1.85	0.99	0.02	1.75E-03	3.10E+06	1.81E-04

1.87			1.55E-03	2.76E+06
1.87			1.56E-03	2.77E+06
1.86			1.59E-03	2.81E+06
1.87			1.54E-03	2.75E+06
1.86			**1.57E-03**	

1.88			6.27E-03	1.23E+07
1.88			6.31E-03	1.24E+07
1.88			6.34E-03	1.24E+07
1.89			6.38E-03	1.24E+07

1.86	0.99	0.01	6.56E-03	1.26E+07	2.59E-04
1.86	0.99	0.01	6.32E-03	1.21E+07	1.52E-05
1.93	1.02	0.01	8.28E-03	1.65E+07	1.98E-03
1.89	1.00	0.01	6.74E-03	1.31E+07	4.36E-04
1.85	0.98	0.01	1.02E-02	1.94E+07	3.94E-03
1.88	1.00	0.01	6.11E-03	1.18E+07	-1.90E-04
1.88	1.00	0.01	6.40E-03	1.23E+07	9.76E-05
1.86	0.99	0.01	7.83E-03	1.49E+07	1.53E-03
1.84	0.98	0.01	7.67E-03	1.44E+07	1.37E-03
1.83	0.97	0.01	6.11E-03	1.14E+07	-1.87E-04
1.85	0.98	0.01	5.95E-03	1.12E+07	-3.51E-04
1.82	0.97	0.01	6.35E-03	1.18E+07	4.72E-05
1.84	0.98	0.01	6.18E-03	1.16E+07	-1.24E-04
1.84	0.98	0.01	5.76E-03	1.08E+07	-5.41E-04
1.86	0.98	0.01	5.88E-03	1.11E+07	-4.25E-04
1.89			6.30E-03	1.21E+07	
1.89			6.27E-03	1.20E+07	
1.88			6.31E-03	1.20E+07	
1.89			6.25E-03	1.19E+07	
1.88			**6.30E-03**		
1.83	0.97	0.01	6.13E-03	1.13E+07	-7.86E-05
1.81	0.96	0.01	5.76E-03	1.05E+07	-4.50E-04
1.81	0.96	0.01	5.72E-03	1.05E+07	-4.95E-04
1.84	0.98	0.01	5.94E-03	1.10E+07	-2.74E-04
1.84	0.98	0.01	5.91E-03	1.09E+07	-3.07E-04
1.84	0.98	0.01	5.50E-03	1.01E+07	-7.11E-04
1.82	0.96	0.01	5.54E-03	1.01E+07	-6.75E-04
1.72	0.91	0.01	6.65E-03	1.15E+07	4.41E-04
1.76	0.93	0.01	6.64E-03	1.17E+07	4.24E-04
1.78	0.94	0.01	6.45E-03	1.15E+07	2.35E-04
1.78	0.95	0.01	5.66E-03	1.00E+07	-5.56E-04
1.77	0.94	0.01	6.60E-03	1.16E+07	3.91E-04
1.86	0.99	0.01	6.52E-03	1.20E+07	3.03E-04
1.85	0.98	0.01	6.46E-03	1.19E+07	2.42E-04
1.76	0.93	0.01	5.69E-02	9.93E+07	5.07E-02
1.81	0.96	0.01	7.78E-03	1.40E+07	1.56E-03
1.86	0.99	0.01	6.61E-03	1.22E+07	4.01E-04

1.88			6.18E-03	1.15E+07	
1.88			6.10E-03	1.14E+07	
1.87			6.12E-03	1.13E+07	
1.88			6.19E-03	1.15E+07	
1.88			**6.21E-03**		
1.91			3.47E-03	6.52E+06	
1.89			3.46E-03	6.46E+06	
1.90			3.47E-03	6.48E+06	
1.90			3.49E-03	6.52E+06	
1.85	0.98	0.03	3.80E-03	6.88E+06	3.79E-04
1.86	0.98	0.03	4.13E-03	7.50E+06	7.11E-04
1.85	0.98	0.03	4.13E-03	7.46E+06	7.02E-04
1.86	0.98	0.03	3.80E-03	6.90E+06	3.81E-04
1.81	0.96	0.03	4.46E-03	7.88E+06	1.04E-03
1.85	0.98	0.03	4.16E-03	7.52E+06	7.39E-04
1.82	0.96	0.03	3.49E-03	6.19E+06	6.64E-05
1.83	0.97	0.03	3.57E-03	6.40E+06	1.44E-04
1.84	0.97	0.03	4.06E-03	7.29E+06	6.41E-04
1.87	0.99	0.03	3.87E-03	7.02E+06	4.46E-04
1.87	0.99	0.03	3.78E-03	6.86E+06	3.60E-04
1.85	0.98	0.03	3.91E-03	7.01E+06	4.82E-04
1.85	0.98	0.03	3.60E-03	6.44E+06	1.77E-04
1.87	0.99	0.03	3.79E-03	6.84E+06	3.67E-04
1.88	0.99	0.03	3.76E-03	6.83E+06	3.34E-04
1.87	0.99	0.03	4.02E-03	7.27E+06	5.95E-04
1.82	0.96	0.03	3.50E-03	6.19E+06	8.08E-05
1.83	0.97	0.03	3.44E-03	6.12E+06	2.03E-05
1.85	0.98	0.03	3.79E-03	6.78E+06	3.71E-04
1.69	0.90	0.03	4.34E-03	7.09E+06	9.20E-04
1.83	0.97	0.03	4.08E-03	7.21E+06	6.52E-04
1.88			3.50E-03	6.36E+06	
1.88			3.38E-03	6.13E+06	
1.87			3.37E-03	6.08E+06	
1.89			3.36E-03	6.12E+06	
1.87			3.39E-03	6.10E+06	

1.89			**3.42E-03**		
1.90	1.01	0.03	4.20E-03	7.66E+06	9.31E-04
1.88	1.00	0.03	3.87E-03	6.98E+06	6.05E-04
1.85	0.99	0.03	3.90E-03	6.92E+06	6.37E-04
1.84	0.98	0.03	3.90E-03	6.86E+06	6.38E-04
1.83	0.98	0.03	3.85E-03	6.72E+06	5.83E-04
1.87	1.00	0.03	3.58E-03	6.39E+06	3.14E-04
1.86	0.99	0.03	3.82E-03	6.77E+06	5.51E-04
1.86	0.99	0.03	3.56E-03	6.31E+06	2.90E-04
1.85	0.99	0.03	3.51E-03	6.18E+06	2.43E-04
1.82	0.97	0.03	3.63E-03	6.29E+06	3.63E-04
1.87	1.00	0.03	4.09E-03	7.26E+06	8.21E-04
1.86	0.99	0.03	3.85E-03	6.82E+06	5.86E-04
1.89	1.01	0.03	3.60E-03	6.63E+06	3.39E-04
1.86	0.99	0.03	3.81E-03	6.93E+06	5.41E-04
1.79	0.96	0.03	3.87E-03	6.83E+06	6.07E-04
1.83	0.98	0.03	3.71E-03	6.68E+06	4.40E-04
1.86	0.99	0.03	3.61E-03	6.64E+06	3.50E-04
1.84	0.98	0.03	3.73E-03	6.79E+06	4.69E-04
1.86	0.99	0.03	3.65E-03	6.71E+06	3.89E-04
1.86	0.99	0.03	3.87E-03	7.10E+06	6.04E-04
1.81	0.96	0.03	3.92E-03	7.00E+06	6.59E-04
1.81	0.96	0.03	3.53E-03	6.31E+06	2.68E-04

1.85			3.21E-03	5.85E+06
1.88			3.12E-03	5.79E+06
1.89			3.14E-03	5.86E+06
1.88			3.15E-03	5.81E+06
1.88			**3.26E-03**	
1.85			4.61E-03	8.38E+06
1.88			4.56E-03	8.37E+06
1.93			4.35E-03	8.63E+06

1.91			4.27E-03	8.93E+06	
1.79	0.95	0.06	4.37E-03	8.60E+06	1.42E-05
1.81	0.96	0.06	4.38E-03	8.62E+06	2.13E-05
1.79	0.95	0.06	1.33E-02	2.57E+07	8.98E-03
1.81	0.96	0.06	4.45E-03	8.62E+06	9.32E-05
1.84	0.98	0.06	4.30E-03	8.46E+06	-5.43E-05
1.85	0.98	0.06	4.29E-03	8.44E+06	-7.41E-05
1.84	0.98	0.06	4.39E-03	8.56E+06	2.68E-05
2.02	1.07	0.06	5.83E-03	1.25E+07	1.47E-03
1.81	0.96	0.06	4.39E-03	8.37E+06	2.60E-05
1.82	0.97	0.06	4.47E-03	8.58E+06	1.06E-04
1.82	0.96	0.06	4.39E-03	8.43E+06	3.54E-05
1.82	0.96	0.06	4.51E-03	8.65E+06	1.52E-04
1.82	0.97	0.06	4.45E-03	8.54E+06	9.49E-05
1.85	0.98	0.06	4.87E-03	9.48E+06	5.15E-04
1.88	1.00	0.06	4.69E-03	9.24E+06	3.30E-04
1.85	0.98	0.06	4.46E-03	8.64E+06	1.04E-04
1.84	0.98	0.06	4.66E-03	8.94E+06	2.97E-04
1.84	0.98	0.06	5.46E-03	1.05E+07	1.11E-03
1.84	0.97	0.06	4.87E-03	9.34E+06	5.15E-04
1.84	0.97	0.06	4.28E-03	8.17E+06	-8.02E-05
1.86			4.28E-03	8.25E+06	
1.87			4.27E-03	8.26E+06	
1.89			4.26E-03	8.29E+06	
1.91			4.28E-03	8.42E+06	
1.89			**4.36E-03**		
1.86	0.99	0.04	4.67E-03	8.99E+06	4.53E-04
1.83	0.97	0.04	8.48E-03	1.61E+07	4.26E-03
1.80	0.96	0.04	4.76E-03	8.83E+06	5.38E-04
1.87	0.99	0.04	4.93E-03	9.50E+06	7.11E-04
1.84	0.98	0.04	5.55E-03	1.05E+07	1.33E-03
1.85	0.98	0.04	3.98E-03	7.58E+06	-2.41E-04
1.85	0.99	0.04	4.15E-03	7.92E+06	-6.65E-05
1.81	0.96	0.04	4.85E-03	8.96E+06	6.30E-04
1.84	0.98	0.04	4.15E-03	7.78E+06	-6.53E-05
1.84	0.98	0.04	4.48E-03	8.37E+06	2.62E-04
1.81	0.96	0.04	4.24E-03	7.82E+06	2.06E-05
1.82	0.97	0.04	4.24E-03	7.81E+06	2.01E-05

1.85	0.98	0.04	4.36E-03	8.16E+06	1.45E-04
1.85	0.98	0.04	4.36E-03	8.13E+06	1.38E-04
1.85	0.98	0.04	4.25E-03	7.93E+06	2.91E-05
1.83	0.97	0.04	4.12E-03	7.65E+06	-9.60E-05
1.84	0.98	0.04	4.01E-03	7.49E+06	-2.14E-04
1.84	0.98	0.04	4.06E-03	7.56E+06	-1.61E-04
1.82	0.97	0.04	4.30E-03	7.87E+06	7.71E-05
1.81	0.96	0.04	7.23E-03	1.32E+07	3.01E-03

1.86			4.16E-03	7.79E+06	
1.88			4.17E-03	7.88E+06	
1.89			4.16E-03	7.90E+06	
1.91			4.17E-03	7.98E+06	
1.88			**4.22E-03**		

1.91			6.24E-03	1.17E+07	
1.89			6.43E-03	1.20E+07	
1.89			6.64E-03	1.23E+07	
1.88			6.26E-03	1.16E+07	
1.87			6.41E-03	1.17E+07	
1.84	0.97	0.02	6.22E-03	1.11E+07	-6.56E-05
1.85	0.98	0.02	5.82E-03	1.05E+07	-4.59E-04
1.79	0.95	0.02	6.15E-03	1.07E+07	-1.33E-04
1.81	0.96	0.02	5.86E-03	1.04E+07	-4.22E-04
1.81	0.96	0.02	6.12E-03	1.08E+07	-1.62E-04
1.84	0.98	0.02	6.36E-03	1.14E+07	7.52E-05
1.86	0.99	0.02	6.36E-03	1.15E+07	7.75E-05
1.87	0.99	0.02	5.86E-03	1.07E+07	-4.25E-04
1.88	1.00	0.02	5.83E-03	1.07E+07	-4.56E-04
1.85	0.98	0.02	5.53E-03	9.99E+06	-7.53E-04
1.78	0.95	0.02	5.59E-03	9.73E+06	-6.93E-04
1.82	0.96	0.02	6.35E-03	1.12E+07	6.61E-05
1.88	1.00	0.02	5.92E-03	1.08E+07	-3.59E-04
1.76	0.93	0.02	7.35E-03	1.26E+07	1.07E-03
1.84	0.97	0.02	6.04E-03	1.08E+07	-2.40E-04
1.83	0.97	0.02	6.08E-03	1.08E+07	-2.04E-04

1.77	0.94	0.02	6.48E-03	1.11E+07	1.94E-04
1.83	0.97	0.02	6.42E-03	1.13E+07	1.42E-04
1.84	0.97	0.02	6.59E-03	1.18E+07	3.09E-04
1.84	0.98	0.02	6.19E-03	1.11E+07	-9.35E-05

1.89	6.18E-03	1.13E+07
1.88	6.15E-03	1.11E+07
1.89	6.45E-03	1.18E+07
1.88	6.13E-03	1.12E+07
1.89	**6.28E-03**	

2s $^{16}OH/^{16}O$	Date	Time	X	Y	DTFA-X	DTFA-Y
	10/21/20	9:19:00 AM	669	-448	-6	7
	10/21/20	9:21:00 AM	689	-448	-6	7
	10/21/20	9:24:00 AM	689	-468	-6	6
	10/21/20	9:27:00 AM	669	-468	-6	6
5.07E-05	10/21/20	9:41:00 AM	-725	-1882	-4	5
5.07E-05	10/21/20	9:44:00 AM	-864	-1771	-2	6
5.07E-05	10/21/20	9:47:00 AM	-1016	-1933	-3	6
5.07E-05	10/21/20	9:50:00 AM	-951	-2147	-4	6
5.07E-05	10/21/20	9:53:00 AM	-569	-2107	-3	8
5.07E-05	10/21/20	9:56:00 AM	-795	-2395	-4	8
5.07E-05	10/21/20	9:59:00 AM	-868	-2966	-4	11
5.07E-05	10/21/20	##########	-645	-3046	-4	14
5.07E-05	10/21/20	##########	-836	-3222	-6	15
5.07E-05	10/21/20	##########	-754	-3496	-4	15
5.07E-05	10/21/20	##########	-792	-3672	-5	16
5.07E-05	10/21/20	##########	-691	-3743	-7	14
5.07E-05	10/21/20	##########	-647	-3844	-6	19
5.07E-05	10/21/20	##########	-952	-3845	-4	17
5.07E-05	10/21/20	##########	-1078	-4012	-7	20
5.07E-05	10/21/20	##########	-2762	-2709	-10	19
5.07E-05	10/21/20	##########	-2429	-1640	-6	11
5.07E-05	10/21/20	##########	1185	-1890	-7	7
5.07E-05	10/21/20	##########	961	-1773	-3	7
5.07E-05	10/21/20	##########	692	-1641	-4	5
	10/21/20	##########	652	-401	-6	8
	10/21/20	##########	654	-496	-6	7
	10/21/20	##########	845	-513	-7	7
	10/21/20	##########	964	-390	-6	8
4.82E-05	10/21/20	##########	-743	-1854	-3	4

4.82E-05	10/21/20	##########	-990	-2105	-3	7
4.82E-05	10/21/20	##########	-1123	-2136	-5	9
4.82E-05	10/21/20	##########	946	-1927	-6	7
4.82E-05	10/21/20	##########	905	-1985	-6	7
4.82E-05	10/21/20	##########	2778	2307	-7	11
4.82E-05	10/21/20	##########	2690	2435	-6	11
4.82E-05	10/21/20	##########	2628	3076	-5	10
4.82E-05	10/21/20	##########	2829	2728	-4	10
4.82E-05	10/21/20	##########	-2016	3841	-6	9
4.82E-05	10/21/20	##########	-1473	3157	-4	11
4.82E-05	10/21/20	##########	-1397	3009	-4	11
4.82E-05	10/21/20	##########	3161	-494	-9	6
4.82E-05	10/21/20	##########	3624	-1041	-3	13
4.82E-05	10/21/20	##########	3867	-567	-4	9
4.82E-05	10/21/20	##########	4505	-1179	-3	16
4.82E-05	10/21/20	##########	309	-1623	-4	3
4.82E-05	10/21/20	##########	515	-2378	-5	8
4.82E-05	10/21/20	##########	416	-2226	-5	8
4.82E-05	10/21/20	##########	355	-2500	-4	8
4.82E-05	10/21/20	##########	882	-3261	-9	12
4.82E-05	10/21/20	##########	909	-3751	-11	15
4.82E-05	10/21/20	##########	-2251	3928	-8	6
4.82E-05	10/21/20	##########	3063	-182	-12	5
4.82E-05	10/21/20	##########	2961	292	-11	5
4.82E-05	10/21/20	1:00:00 PM	-2893	-3167	-15	17
	10/21/20	1:04:00 PM	1038	-59	-8	8
	10/21/20	1:07:00 PM	1009	-106	-8	8
	10/21/20	1:10:00 PM	985	-119	-8	7
	10/21/20	1:13:00 PM	1036	63	-9	8
	10/23/20	8:46:00 AM	1596	-476	-10	11
	10/23/20	8:49:00 AM	1596	-496	-11	11
	10/23/20	8:52:00 AM	1596	-516	-11	10
	10/23/20	8:55:00 AM	1596	-536	-11	10

8.21E-05	10/23/20	9:00:00 AM	-1895	4362	-5	1
8.21E-05	10/23/20	9:03:00 AM	-1799	4505	-5	-1
8.21E-05	10/23/20	9:06:00 AM	-2058	4318	-5	-1
8.21E-05	10/23/20	9:10:00 AM	-2133	4128	-6	1
8.21E-05	10/23/20	9:14:00 AM	-1765	4338	-15	-1
8.21E-05	10/23/20	9:19:00 AM	-1342	4670	-14	-1
8.21E-05	10/23/20	9:22:00 AM	-1441	4628	-14	-1
8.21E-05	10/23/20	9:26:00 AM	-1366	4521	-13	-2
8.21E-05	10/23/20	9:30:00 AM	-1244	4462	-14	-1
8.21E-05	10/23/20	9:34:00 AM	-1038	4691	-3	-1
8.21E-05	10/23/20	9:37:00 AM	-973	4764	-3	-1
8.21E-05	10/23/20	9:41:00 AM	-915	4755	-3	0
8.21E-05	10/23/20	9:44:00 AM	-955	4864	-4	-1
8.21E-05	10/23/20	9:47:00 AM	-758	4834	-3	-2
8.21E-05	10/23/20	9:50:00 AM	-720	4955	-4	-1
	10/23/20	9:54:00 AM	1620	-473	-13	7
	10/23/20	9:57:00 AM	1620	-493	-13	7
	10/23/20	##########	1620	-513	-13	6
	10/23/20	##########	1620	-533	-12	6
1.56E-04	10/23/20	##########	-348	5127	-3	-3
1.56E-04	10/23/20	##########	-216	5196	-1	-1
1.56E-04	10/23/20	##########	-125	5206	-2	0
1.56E-04	10/23/20	##########	66	5265	-12	-2
1.56E-04	10/23/20	##########	362	5651	-1	-2
1.56E-04	10/23/20	##########	335	5725	-7	-2
1.56E-04	10/23/20	##########	1092	4734	1	1
1.56E-04	10/23/20	##########	3564	-3339	-7	12
1.56E-04	10/23/20	##########	3314	-3431	-7	7
1.56E-04	10/23/20	##########	3264	-3362	-10	12
1.56E-04	10/23/20	##########	4401	-3775	-5	18
1.56E-04	10/23/20	##########	4386	-3514	-6	16
1.56E-04	10/23/20	##########	-3608	4003	-8	-5
1.56E-04	10/23/20	##########	-3280	4154	-20	-6
1.56E-04	10/23/20	##########	-2990	3738	-6	0
1.56E-04	10/23/20	##########	-4756	2989	-12	-3
1.56E-04	10/23/20	##########	-4508	2887	-13	-1

	10/23/20	##########	1584	-555	-21	7
	10/23/20	##########	1604	-555	-21	6
	10/23/20	##########	1600	-577	-12	8
	10/23/20	##########	1578	-592	-20	7

	10/23/20	##########	-1246	-798	-19	-1
	10/23/20	##########	-1226	-798	-9	-1
	10/23/20	##########	-1206	-798	-18	-2
	10/23/20	##########	-1186	-798	-18	-3

1.06E-04	10/23/20	##########	-1105	2642	-15	1
1.06E-04	10/23/20	##########	-1049	2752	-17	-2
1.06E-04	10/23/20	##########	-971	2989	-8	-1
1.06E-04	10/23/20	##########	-1320	2944	-8	-1
1.06E-04	10/23/20	##########	-1420	3260	-8	-1
1.06E-04	10/23/20	##########	-1257	3240	-8	-1
1.06E-04	10/23/20	##########	-1101	2411	-5	1
1.06E-04	10/23/20	##########	-982	2448	-15	-1
1.06E-04	10/23/20	##########	-984	2285	-8	3
1.06E-04	10/23/20	##########	-1124	2154	-8	4
1.06E-04	10/23/20	##########	-1217	2049	-8	4
1.06E-04	10/23/20	##########	-1262	2201	-8	4
1.06E-04	10/23/20	##########	-484	2884	-13	0
1.06E-04	10/23/20	##########	-297	2950	-16	-2
1.06E-04	10/23/20	##########	-215	3177	-15	-2
1.06E-04	10/23/20	##########	-264	3720	-16	-3
1.06E-04	10/23/20	##########	-450	2661	-14	-1
1.06E-04	10/23/20	##########	-204	2686	-5	-1
1.06E-04	10/23/20	##########	-29	2513	-7	2
1.06E-04	10/23/20	##########	82	2324	-7	3
1.06E-04	10/23/20	##########	44	2268	-6	4

	10/23/20	##########	-1255	-821	-20	-4
	10/23/20	1:00:00 PM	-1235	-821	-17	-3
	10/23/20	1:03:00 PM	-1215	-821	-9	-2
	10/23/20	1:06:00 PM	-1195	-821	-9	-2
	10/23/20	1:09:00 PM	-1196	-841	-8	-1

2.40E-04	10/23/20	1:27:00 PM	1070	4282	-17	-3
2.40E-04	10/23/20	1:30:00 PM	962	4351	-17	-2
2.40E-04	10/23/20	1:33:00 PM	931	4160	-7	1
2.40E-04	10/23/20	1:36:00 PM	1531	4266	-4	0
2.40E-04	10/23/20	1:39:00 PM	1543	4062	-7	-1
2.40E-04	10/23/20	1:42:00 PM	1095	5248	-17	-3
2.40E-04	10/23/20	1:45:00 PM	808	5183	-14	-2
2.40E-04	10/23/20	1:48:00 PM	980	5570	-17	-2
2.40E-04	10/23/20	1:51:00 PM	1534	5598	-13	-2
2.40E-04	10/23/20	1:54:00 PM	1494	5379	-7	-2
2.40E-04	10/23/20	1:57:00 PM	276	-2293	-18	0
2.40E-04	10/23/20	2:00:00 PM	228	-1985	-18	-1
2.40E-04	10/23/20	2:05:00 PM	327	-1869	-18	-2
2.40E-04	10/23/20	2:08:00 PM	1104	-1834	-16	-2
2.40E-04	10/23/20	2:11:00 PM	910	-2038	-6	1
2.40E-04	10/23/20	2:14:00 PM	874	-2114	-16	-1
2.40E-04	10/23/20	2:16:00 PM	896	-2511	-14	0
2.40E-04	10/23/20	2:19:00 PM	802	-2246	-15	0
2.40E-04	10/23/20	2:22:00 PM	1077	-3142	-16	1
2.40E-04	10/23/20	2:25:00 PM	905	-3117	-15	3
2.40E-04	10/23/20	2:28:00 PM	737	-3216	-8	3
2.40E-04	10/23/20	2:31:00 PM	762	-3292	-8	3
	10/23/20	2:35:00 PM	-1236	-842	-11	-3
	10/23/20	2:38:00 PM	-1216	-842	-20	-5
	10/23/20	2:41:00 PM	-1216	-862	-20	-4
	10/23/20	2:44:00 PM	-1236	-862	-20	-4
	10/23/20	3:11:00 PM	-1201	1277	-12	-6
	10/23/20	3:14:00 PM	-1181	1277	-13	-6
	10/23/20	3:16:00 PM	-1161	1277	-13	-6

	10/23/20	3:19:00 PM	-1141	1277	-13	-6
2.85E-04	10/23/20	3:23:00 PM	877	4003	-11	2
2.85E-04	10/23/20	3:27:00 PM	813	4217	-12	2
2.85E-04	10/23/20	3:30:00 PM	1286	4367	-10	1
2.85E-04	10/23/20	3:33:00 PM	1345	4741	-9	-1
2.85E-04	10/23/20	3:36:00 PM	309	4147	-14	0
2.85E-04	10/23/20	3:40:00 PM	464	4614	-13	0
2.85E-04	10/23/20	3:43:00 PM	218	3828	-13	2
2.85E-04	10/23/20	3:46:00 PM	168	3888	-13	2
2.85E-04	10/23/20	3:50:00 PM	1330	3886	-11	2
2.85E-04	10/23/20	3:53:00 PM	1498	3932	-11	1
2.85E-04	10/23/20	3:57:00 PM	-618	3871	-13	2
2.85E-04	10/23/20	4:00:00 PM	-457	3991	-12	1
2.85E-04	10/23/20	4:03:00 PM	-927	4168	-13	2
2.85E-04	10/23/20	4:06:00 PM	-1654	4064	-14	-1
2.85E-04	10/23/20	4:09:00 PM	-1755	4340	-14	-1
2.85E-04	10/23/20	4:13:00 PM	-2011	4603	-15	-4
2.85E-04	10/23/20	4:16:00 PM	-2018	4280	-14	-2
2.85E-04	10/23/20	4:20:00 PM	-1405	4425	-14	-1
2.85E-04	10/23/20	4:23:00 PM	-1251	4683	-14	-3
2.85E-04	10/23/20	4:27:00 PM	-1602	5276	-16	-3
	10/23/20	4:31:00 PM	-1184	1259	-14	-8
	10/23/20	4:34:00 PM	-1164	1259	-14	-8
	10/23/20	4:37:00 PM	-1144	1259	-13	-8
	10/23/20	4:40:00 PM	-1124	1259	-14	-8
1.15E-04	10/23/20	4:43:00 PM	-1752	5472	-16	-5
1.15E-04	10/23/20	4:47:00 PM	-1829	5607	-16	-4
1.15E-04	10/23/20	4:50:00 PM	-2032	5549	-16	-5
1.15E-04	10/23/20	4:54:00 PM	-2687	6031	-20	-7
1.15E-04	10/23/20	4:57:00 PM	-1332	6268	-16	-4
1.15E-04	10/23/20	5:00:00 PM	-651	6144	-14	-3
1.15E-04	10/23/20	5:04:00 PM	93	5356	-14	-3
1.15E-04	10/23/20	5:07:00 PM	738	5495	-13	-2
1.15E-04	10/23/20	5:11:00 PM	2819	4894	-11	-5
1.15E-04	10/23/20	5:14:00 PM	2905	4548	-12	-3
1.15E-04	10/23/20	5:18:00 PM	-799	-2397	-14	-1
1.15E-04	10/23/20	5:21:00 PM	-1300	-2705	-14	-1

1.15E-04	10/23/20	5:24:00 PM	-1389	-2396	-15	-1
1.15E-04	10/23/20	5:27:00 PM	-2133	-2761	-16	0
1.15E-04	10/23/20	5:31:00 PM	-2433	-3359	-17	2
1.15E-04	10/23/20	5:34:00 PM	-525	-3025	-13	1
1.15E-04	10/23/20	5:37:00 PM	40	-2820	-13	1
1.15E-04	10/23/20	5:41:00 PM	2723	-1364	-12	-3
1.15E-04	10/23/20	5:44:00 PM	3257	-2667	-10	0
1.15E-04	10/23/20	5:47:00 PM	4069	-3432	-10	-2
	10/23/20	5:51:00 PM	-1165	1237	-13	-7
	10/23/20	5:54:00 PM	-1145	1237	-13	-8
	10/23/20	5:57:00 PM	-1125	1237	-13	-6
	10/23/20	6:00:00 PM	-1105	1237	-12	-7
	10/23/20	6:24:00 PM	732	-375	-19	-8
	10/23/20	6:27:00 PM	752	-375	-16	-7
	10/23/20	6:30:00 PM	752	-395	-11	-8
	10/23/20	6:33:00 PM	732	-395	-13	-8
	10/23/20	6:36:00 PM	728	-417	-14	-8
2.63E-04	10/23/20	6:59:00 PM	-1746	5474	-12	-9
2.63E-04	10/23/20	7:02:00 PM	-241	6465	-22	-16
2.63E-04	10/23/20	7:05:00 PM	227	5241	-19	-11
2.63E-04	10/23/20	7:08:00 PM	11	4867	-17	-9
2.63E-04	10/23/20	7:11:00 PM	402	4620	-16	-9
2.63E-04	10/23/20	7:14:00 PM	-1556	4701	-25	-9
2.63E-04	10/23/20	7:17:00 PM	-2937	3933	-26	-12
2.63E-04	10/23/20	7:20:00 PM	1632	6323	-18	-19
2.63E-04	10/23/20	7:23:00 PM	4384	6522	-16	-19
2.63E-04	10/23/20	7:26:00 PM	4445	6639	-10	-19
2.63E-04	10/23/20	7:29:00 PM	1942	5613	-9	-16
2.63E-04	10/23/20	7:32:00 PM	2033	4549	-8	-11
2.63E-04	10/23/20	7:35:00 PM	2363	4695	-7	-11
2.63E-04	10/23/20	7:38:00 PM	4951	3178	-12	-8
2.63E-04	10/23/20	7:41:00 PM	5149	4091	-9	-12
2.63E-04	10/23/20	7:44:00 PM	2597	3284	-6	-3

2.63E-04	10/23/20	7:47:00 PM	1435	3168	-9	-2
2.63E-04	10/23/20	7:50:00 PM	-361	2766	-19	1
2.63E-04	10/23/20	7:53:00 PM	-2183	2461	-13	-7
2.63E-04	10/23/20	7:56:00 PM	-2072	2957	-8	-6

10/23/20	7:59:00 PM	776	-459	-19	-7
10/23/20	8:02:00 PM	834	-460	-20	-7
10/23/20	8:05:00 PM	827	-500	-20	-7
10/23/20	8:07:00 PM	787	-520	-16	-7

Mass	L2p-bkg	H1-bkg	Sample Name	Chamber Pressure	Comment
899141	833470	87562	Al-mesh/#1	2.90E-08	
899141	833470	87562	Al-mesh/#1	3.00E-08	
899141	833470	87562	Al-mesh/#1	2.90E-08	
899141	833470	87562	Al-mesh/#1	3.00E-08	
899141	833470	87562	Al-mesh/#1	3.00E-08	Cal I
899141	833470	87562	Al-mesh/#1	3.00E-08	Cal I
899141	833470	87562	Al-mesh/#1	3.00E-08	Cal I
899141	833470	87562	Al-mesh/#1	3.00E-08	Cal I
899141	833470	87562	Al-mesh/#1	3.00E-08	Cal I
899141	833470	87562	Al-mesh/#1	3.10E-08	Cal I
899141	833470	87562	Al-mesh/#1	3.00E-08	on crack
899141	833470	87562	Al-mesh/#1	3.00E-08	Cal I
899141	833470	87562	Al-mesh/#1	3.00E-08	Cal I
899141	833470	87562	Al-mesh/#1	3.00E-08	Cal I
899141	833470	87562	Al-mesh/#1	3.10E-08	Cal I
899141	833470	87562	Al-mesh/#1	3.10E-08	Cal I
899141	833470	87562	Al-mesh/#1	3.00E-08	Cal I
899141	833470	87562	Al-mesh/#1	3.00E-08	Cal I
899141	833470	87562	Al-mesh/#1	3.00E-08	Cal I
899141	833470	87562	Al-mesh/#1	3.10E-08	Cal I
899141	833470	87562	Al-mesh/#1	3.00E-08	Cal I
899141	833470	87562	Al-mesh/#1	3.00E-08	Cal II
899141	833470	87562	Al-mesh/#1	3.00E-08	Cal II
899141	833470	87562	Al-mesh/#1	3.10E-08	Cal II
899141	833470	87562	Al-mesh/#1	3.00E-08	
899141	833470	87562	Al-mesh/#1	3.00E-08	
899141	833470	87562	Al-mesh/#1	3.00E-08	
899141	833470	87562	Al-mesh/#1	3.00E-08	
899141	833470	87562	Al-mesh/#1	3.00E-08	Cal I

899141	833470	87562	Al-mesh/#1	3.00E-08	Cal I
899141	833470	87562	Al-mesh/#1	3.00E-08	Cal I
899141	833470	87562	Al-mesh/#1	3.00E-08	Cal II
899141	833470	87562	Al-mesh/#1	3.00E-08	Cal II
899141	833470	87562	Al-mesh/#1	3.00E-08	Cal II
899141	833470	87562	Al-mesh/#1	3.00E-08	Cal II
899141	833470	87562	Al-mesh/#1	3.00E-08	Cal II
899141	833470	87562	Al-mesh/#1	3.00E-08	Cal II
899141	833470	87562	Al-mesh/#1	3.00E-08	Cal I
899141	833470	87562	Al-mesh/#1	3.00E-08	Cal I
899141	833470	87562	Al-mesh/#1	3.00E-08	Cal I
899141	833470	87562	Al-mesh/#1	3.00E-08	Cal I
899141	833470	87562	Al-mesh/#1	3.00E-08	Cal I
899141	833470	87562	Al-mesh/#1	3.00E-08	Cal I
899141	833470	87562	Al-mesh/#1	3.00E-08	Cal II
899141	833470	87562	Al-mesh/#1	3.10E-08	Cal II
899141	833470	87562	Al-mesh/#1	3.00E-08	Cal II
899141	833470	87562	Al-mesh/#1	3.00E-08	Cal II
899141	833470	87562	Al-mesh/#1	3.00E-08	Cal II
899141	833470	87562	Al-mesh/#1	3.00E-08	Cal II
899141	833470	87562	Al-mesh/#1	3.00E-08	Cal II
899141	833470	87562	Al-mesh/#1	3.00E-08	Cal I
899141	833470	87562	Al-mesh/#1	3.00E-08	Cal I
899141	833470	87562	Al-mesh/#1	3.00E-08	Cal I
899141	833470	87562	Al-mesh/#1	3.00E-08	Cal I

899141	833470	87562	Al-mesh/#1	3.00E-08
899141	833470	87562	Al-mesh/#1	3.00E-08
899141	833470	87562	Al-mesh/#1	3.00E-08
899141	833470	87562	Al-mesh/#1	3.00E-08

899149	858990	87685	Al-mesh/#1	8.50E-08
899149	858990	87685	Al-mesh/#1	8.70E-08
899149	858990	87685	Al-mesh/#1	8.70E-08
899149	858990	87685	Al-mesh/#1	8.70E-08

899149	858990	87685	Al-mesh/#1	8.90E-08	Cal I
899149	858990	87685	Al-mesh/#1	8.90E-08	Cal I
899149	858990	87685	Al-mesh/#1	8.80E-08	Cal I
899149	858990	87685	Al-mesh/#1	8.70E-08	Cal I
899149	858990	87685	Al-mesh/#1	8.80E-08	Cal I
899149	858990	87685	Al-mesh/#1	8.90E-08	Cal I
899149	858990	87685	Al-mesh/#1	8.90E-08	Cal I
899149	858990	87685	Al-mesh/#1	9.00E-08	Cal I
899149	858990	87685	Al-mesh/#1	8.90E-08	Cal I
899149	858990	87685	Al-mesh/#1	8.90E-08	Cal I
899149	858990	87685	Al-mesh/#1	8.90E-08	Cal I
899149	858990	87685	Al-mesh/#1	8.90E-08	Cal I
899149	858990	87685	Al-mesh/#1	8.90E-08	Cal I
899149	858990	87685	Al-mesh/#1	8.90E-08	Cal I
899149	858990	87685	Al-mesh/#1	8.90E-08	Cal I
899149	858990	87685	Al-mesh/#1	8.90E-08	
899149	858990	87685	Al-mesh/#1	8.90E-08	
899149	858990	87685	Al-mesh/#1	8.90E-08	
899149	858990	87685	Al-mesh/#1	8.90E-08	

899149	858990	87685	Al-mesh/#1	8.90E-08	Cal I
899149	858990	87685	Al-mesh/#1	8.90E-08	Cal I
899149	858990	87685	Al-mesh/#1	8.90E-08	Cal I
899149	858990	87685	Al-mesh/#1	8.80E-08	Cal I
899149	858990	87685	Al-mesh/#1	8.70E-08	Cal I
899149	858990	87685	Al-mesh/#1	8.70E-08	Cal I
899149	858990	87685	Al-mesh/#1	8.80E-08	Cal I
899149	858990	87685	Al-mesh/#1	8.70E-08	Cal III
899149	858990	87685	Al-mesh/#1	8.70E-08	Cal III
899149	858990	87685	Al-mesh/#1	8.70E-08	Cal III
899149	858990	87685	Al-mesh/#1	8.70E-08	Cal III
899149	858990	87685	Al-mesh/#1	8.70E-08	Cal III
899149	858990	87685	Al-mesh/#1	8.70E-08	on fracture
899149	858990	87685	Al-mesh/#1	8.60E-08	Cal III
899149	858990	87685	Al-mesh/#1	8.60E-08	large SE
899149	858990	87685	Al-mesh/#1	8.50E-08	Cal III
899149	858990	87685	Al-mesh/#1	8.50E-08	Cal III

899149	858990	87685	Al-mesh/#1	8.50E-08	
899149	858990	87685	Al-mesh/#1	8.50E-08	
899149	858990	87685	Al-mesh/#1	8.50E-08	
899149	858990	87685	Al-mesh/#1	8.50E-08	
899149	858990	87685	Al-mesh/#1	7.90E-08	
899149	858990	87685	Al-mesh/#1	7.80E-08	
899149	858990	87685	Al-mesh/#1	7.70E-08	
899149	858990	87685	Al-mesh/#1	7.80E-08	
899149	858990	87685	Al-mesh/#1	7.80E-08	Cal I
899149	858990	87685	Al-mesh/#1	7.80E-08	Cal I
899149	858990	87685	Al-mesh/#1	7.90E-08	Cal I
899149	858990	87685	Al-mesh/#1	7.80E-08	Cal I
899149	858990	87685	Al-mesh/#1	7.80E-08	Cal I
899149	858990	87685	Al-mesh/#1	7.80E-08	Cal I
899149	858990	87685	Al-mesh/#1	7.80E-08	Cal vein
899149	858990	87685	Al-mesh/#1	7.80E-08	Cal vein
899149	858990	87685	Al-mesh/#1	7.70E-08	Cal I
899149	858990	87685	Al-mesh/#1	7.70E-08	Cal I
899149	858990	87685	Al-mesh/#1	7.70E-08	Cal I
899149	858990	87685	Al-mesh/#1	7.70E-08	Cal I
899149	858990	87685	Al-mesh/#1	7.70E-08	Cal I
899149	858990	87685	Al-mesh/#1	7.70E-08	Cal I
899149	858990	87685	Al-mesh/#1	7.70E-08	Cal I
899149	858990	87685	Al-mesh/#1	7.60E-08	Cal I
899149	858990	87685	Al-mesh/#1	7.60E-08	Cal vein
899149	858990	87685	Al-mesh/#1	7.70E-08	Cal vein
899149	858990	87685	Al-mesh/#1	7.60E-08	Cal I
899149	858990	87685	Al-mesh/#1	7.70E-08	Cal II
899149	858990	87685	Al-mesh/#1	7.60E-08	Cal II
899149	858990	87685	Al-mesh/#1	7.60E-08	
899149	858990	87685	Al-mesh/#1	7.50E-08	
899149	858990	87685	Al-mesh/#1	7.50E-08	
899149	858990	87685	Al-mesh/#1	7.40E-08	
899149	858990	87685	Al-mesh/#1	7.40E-08	

899149	858990	87685	Al-mesh/#1	7.50E-08	Cal I
899149	858990	87685	Al-mesh/#1	7.40E-08	Cal I
899149	858990	87685	Al-mesh/#1	7.50E-08	Cal I
899149	858990	87685	Al-mesh/#1	7.40E-08	Cal I
899149	858990	87685	Al-mesh/#1	7.40E-08	Cal I
899149	858990	87685	Al-mesh/#1	7.40E-08	Cal I
899149	858990	87685	Al-mesh/#1	7.40E-08	Cal I
899149	858990	87685	Al-mesh/#1	7.40E-08	Cal I
899149	858990	87685	Al-mesh/#1	7.40E-08	Cal I
899149	858990	87685	Al-mesh/#1	7.40E-08	Cal I
899149	858990	87685	Al-mesh/#1	7.30E-08	Cal I
899149	858990	87685	Al-mesh/#1	7.30E-08	Cal I
899149	858990	87685	Al-mesh/#1	7.40E-08	Cal I
899149	858990	87685	Al-mesh/#1	7.20E-08	Cal I
899149	858990	87685	Al-mesh/#1	7.20E-08	Cal I
899149	858990	87685	Al-mesh/#1	7.20E-08	Cal I
899149	858990	87685	Al-mesh/#1	7.20E-08	Cal I
899149	858990	87685	Al-mesh/#1	7.20E-08	Cal I
899149	858990	87685	Al-mesh/#1	7.20E-08	Cal I
899149	858990	87685	Al-mesh/#1	7.20E-08	Cal I
899149	858990	87685	Al-mesh/#1	7.20E-08	Cal I
899149	858990	87685	Al-mesh/#1	7.20E-08	Cal I

899149	858990	87685	Al-mesh/#1	7.10E-08
899149	858990	87685	Al-mesh/#1	7.20E-08
899149	858990	87685	Al-mesh/#1	7.10E-08
899149	858990	87685	Al-mesh/#1	7.10E-08

899149	858990	87685	Al-mesh/#1	9.30E-08
899149	858990	87685	Al-mesh/#1	9.50E-08
899149	858990	87685	Al-mesh/#1	9.30E-08

899149	858990	87685	Al-mesh/#1	9.30E-08	
899149	858990	87685	Al-mesh/#1	9.30E-08	Cal I
899149	858990	87685	Al-mesh/#1	9.30E-08	Cal I
899149	858990	87685	Al-mesh/#1	9.30E-08	Cal I
899149	858990	87685	Al-mesh/#1	9.40E-08	Cal I
899149	858990	87685	Al-mesh/#1	9.30E-08	Cal II
899149	858990	87685	Al-mesh/#1	9.30E-08	Cal II
899149	858990	87685	Al-mesh/#1	9.30E-08	Cal II
899149	858990	87685	Al-mesh/#1	9.30E-08	dolomite
899149	858990	87685	Al-mesh/#1	9.30E-08	Cal I
899149	858990	87685	Al-mesh/#1	9.20E-08	Cal I
899149	858990	87685	Al-mesh/#1	9.30E-08	Cal II
899149	858990	87685	Al-mesh/#1	9.30E-08	Cal II
899149	858990	87685	Al-mesh/#1	9.20E-08	Cal I
899149	858990	87685	Al-mesh/#1	9.40E-08	Cal I
899149	858990	87685	Al-mesh/#1	9.20E-08	Cal I
899149	858990	87685	Al-mesh/#1	9.30E-08	Cal I
899149	858990	87685	Al-mesh/#1	9.20E-08	Cal I
899149	858990	87685	Al-mesh/#1	9.30E-08	Cal I
899149	858990	87685	Al-mesh/#1	9.30E-08	Cal I
899149	858990	87685	Al-mesh/#1	9.20E-08	Cal I
899149	858990	87685	Al-mesh/#1	9.30E-08	
899149	858990	87685	Al-mesh/#1	9.20E-08	
899149	858990	87685	Al-mesh/#1	9.30E-08	
899149	858990	87685	Al-mesh/#1	9.10E-08	
899149	858990	87685	Al-mesh/#1	9.20E-08	Cal I
899149	858990	87685	Al-mesh/#1	9.00E-08	Cal I
899149	858990	87685	Al-mesh/#1	9.00E-08	Cal I
899149	858990	87685	Al-mesh/#1	9.00E-08	Cal I
899149	858990	87685	Al-mesh/#1	8.90E-08	Cal I
899149	858990	87685	Al-mesh/#1	9.10E-08	Cal II
899149	858990	87685	Al-mesh/#1	8.90E-08	Cal I
899149	858990	87685	Al-mesh/#1	8.90E-08	Cal I
899149	858990	87685	Al-mesh/#1	9.00E-08	Cal I
899149	858990	87685	Al-mesh/#1	8.90E-08	Cal I
899149	858990	87685	Al-mesh/#1	8.90E-08	Cal I
899149	858990	87685	Al-mesh/#1	8.90E-08	Cal I

899149	858990	87685	Al-mesh/#1	8.80E-08	Cal I
899149	858990	87685	Al-mesh/#1	8.90E-08	Cal I
899149	858990	87685	Al-mesh/#1	8.80E-08	Cal I
899149	858990	87685	Al-mesh/#1	8.80E-08	Cal II
899149	858990	87685	Al-mesh/#1	8.70E-08	Cal II
899149	858990	87685	Al-mesh/#1	8.80E-08	Cal II
899149	858990	87685	Al-mesh/#1	8.70E-08	Cal I
899149	858990	87685	Al-mesh/#1	8.80E-08	Cal I

899149	858990	87685	Al-mesh/#1	8.70E-08
899149	858990	87685	Al-mesh/#1	8.70E-08
899149	858990	87685	Al-mesh/#1	8.70E-08
899149	858990	87685	Al-mesh/#1	8.70E-08

899149	858990	87685	Al-mesh/#1	9.00E-08
899149	858990	87685	Al-mesh/#1	9.10E-08
899149	858990	87685	Al-mesh/#1	9.20E-08
899149	858990	87685	Al-mesh/#1	9.20E-08
899149	858990	87685	Al-mesh/#1	9.00E-08

899149	858990	87685	Al-mesh/#1	9.20E-08	Cal I
899149	858990	87685	Al-mesh/#1	9.20E-08	Cal I
899149	858990	87685	Al-mesh/#1	9.20E-08	Cal I
899149	858990	87685	Al-mesh/#1	9.20E-08	Cal I
899149	858990	87685	Al-mesh/#1	9.20E-08	Cal I
899149	858990	87685	Al-mesh/#1	9.20E-08	Cal I
899149	858990	87685	Al-mesh/#1	9.20E-08	Cal I
899149	858990	87685	Al-mesh/#1	9.20E-08	Cal I
899149	858990	87685	Al-mesh/#1	9.10E-08	Cal II
899149	858990	87685	Al-mesh/#1	9.00E-08	Cal II
899149	858990	87685	Al-mesh/#1	9.10E-08	outlier
899149	858990	87685	Al-mesh/#1	8.90E-08	Cal I
899149	858990	87685	Al-mesh/#1	9.20E-08	Cal I
899149	858990	87685	Al-mesh/#1	9.00E-08	Cal II
899149	858990	87685	Al-mesh/#1	9.20E-08	Cal II
899149	858990	87685	Al-mesh/#1	9.10E-08	Cal I

899149	858990	87685	Al-mesh/#1	9.00E-08	Cal I
899149	858990	87685	Al-mesh/#1	9.00E-08	Cal I
899149	858990	87685	Al-mesh/#1	9.00E-08	Cal I
899149	858990	87685	Al-mesh/#1	9.00E-08	Cal I

899149	858990	87685	Al-mesh/#1	9.10E-08
899149	858990	87685	Al-mesh/#1	8.90E-08
899149	858990	87685	Al-mesh/#1	8.90E-08
899149	858990	87685	Al-mesh/#1	8.90E-08

SUMMARY OF EPMA ANALYSES IN CARBONATES

Number of oxygen	3	3
Sample	OM13-17A	OM13-17A
SIMS pit	Cal-1	Cal-3
Mineral	Cal	Cal
Texture	intergrown with serpentine	intergrown with serpentine
wt.%		
FeO(total)	0.05	0.17
MnO	0.17	0.17
MgO	1.59	1.30
CaO	55.51	55.21
SrO	0.05	0.06
CO_2	43.79	43.84
Total	**101.15**	**100.76**
apfu		
Fe^{2+}	0.001	0.002
Mn	0.002	0.002
Mg	0.039	0.032
Ca	0.982	0.980
Sr	0.000	0.001
C	0.987	0.991
Sum of Cations	**2.012**	**2.009**
Mg# (mole %)*	**98.23**	**93.01**
Sum oxygen units	3.02	3.01

3	3	3
OM13-17A	OM13-17A	OM13-17A
Cal-7	Cal-12	Cal-15
Cal	Cal	Cal
intergrown with serpentine	intergrown with serpentine	intergrown with serpentine
0.40	<0,05	<0,05
0.09	0.15	0.18
4.45	1.07	1.42
50.29	56.19	54.82
0.08	0.09	0.06
44.63	43.68	43.96
99.94	**101.17**	**100.43**
0.005	0.000	0.000
0.001	0.002	0.003
0.109	0.026	0.035
0.884	0.996	0.973
0.001	0.001	0.001
1.000	0.987	0.994
2.000	**2.013**	**2.005**
95.21	**100.00**	**100.00**
3.04	3.02	3.01

3	3	3
OM13-17A	OM13-17A	OM13-17A
Cal-17	Cal-18	Cal-20
Cal	Cal	Cal
intergrown with serpentine	intergrown with serpentine	intergrown with serpentine
<0,05	<0,05	<0,05
0.09	0.68	0.49
1.17	1.07	0.76
55.46	54.09	55.39
0.04	<0,04	<0,04
43.88	44.06	43.83
100.64	**99.90**	**100.47**
0.000	0.000	0.000
0.001	0.010	0.007
0.029	0.027	0.019
0.984	0.964	0.986
0.000	0.000	0.000
0.992	1.000	0.994
2.007	**2.000**	**2.006**
100.00	**100.00**	**100.00**
3.01	3.00	3.01

3	3	3
OM13-17A	OM13-17A	OM13-17A
Cal-23	Cal-24	Cal-26
Cal	Cal	Cal
intergrown with serpentine	intergrown with serpentine	intergrown with serpentine
<0,05	<0,05	<0,05
0.44	0.51	0.37
0.49	0.72	0.75
54.31	56.16	55.48
<0,04	0.06	<0,04
44.12	43.62	43.83
99.35	**101.08**	**100.42**
0.000	0.000	0.000
0.006	0.007	0.005
0.012	0.018	0.019
0.971	0.998	0.987
0.000	0.001	0.000
1.005	0.988	0.994
1.994	**2.012**	**2.005**
100.00	**100.00**	**100.00**
2.99	3.01	3.01

3	3	3
OM13-17A	OM13-17A	OM13-17A
Cal-27	Cal-28	Cal-29
Cal	Cal	Cal
intergrown with serpentine	intergrown with serpentine	intergrown with serpentine
<0,05	<0,05	<0,05
0.43	<0,05	0.06
0.62	1.25	1.29
56.20	54.93	55.50
<0,04	0.07	<0,04
43.67	44.01	43.88
100.93	**100.26**	**100.74**
0.000	0.000	0.000
0.006	0.000	0.001
0.015	0.031	0.032
0.999	0.976	0.984
0.000	0.001	0.000
0.989	0.996	0.991
2.010	**2.003**	**2.008**
100.00	**100.00**	**100.00**
3.01	3.01	3.02

3	3	3
OM13-17A	OM13-17A	OM13-17A
Cal-30	Cal-31	Cal-32
Cal	Cal	Cal
intergrown with serpentine	intergrown with serpentine	intergrown with serpentine
<0,05	<0,05	0.05
0.08	<0,05	0.15
1.15	1.23	1.39
55.82	56.16	54.61
0.08	<0,04	0.09
43.79	43.76	44.00
100.92	**101.15**	**100.28**
0.000	0.000	0.001
0.001	0.000	0.002
0.028	0.030	0.034
0.990	0.994	0.970
0.001	0.000	0.001
0.990	0.987	0.996
2.010	**2.012**	**2.004**
100.00	**100.00**	**98.03**
3.02	3.02	3.01

3	3	3
OM13-17A	OM13-17A	OM13-17A
Cal-33	Cal-36	Cal-37
Cal	Cal	Cal
intergrown with serpentine	intergrown with serpentine	intergrown with serpentine
0.07	<0,05	<0,05
0.13	0.61	0.55
1.23	0.75	0.92
55.51	54.76	55.07
0.08	0.05	0.05
43.82	43.92	43.87
100.83	**100.09**	**100.46**
0.001	0.000	0.000
0.002	0.009	0.008
0.030	0.019	0.023
0.985	0.976	0.980
0.001	0.001	0.000
0.991	0.998	0.995
2.009	**2.002**	**2.005**
96.95	**100.00**	**100.00**
3.02	3.00	3.01

3	3	3
OM13-17A	OM13-1	OM13-1
Cal-40	Cal-2	Cal-3
Cal	Cal	Cal
intergrown with serpentine	intergrown with serpentine	intergrown with serpentine
<0,05	<0,05	<0,05
0.36	0.48	0.54
0.46	0.95	0.99
56.28	55.54	55.57
0.05	<0,04	<0,04
43.67	43.77	43.75
100.83	**100.73**	**100.84**
0.000	0.000	0.000
0.005	0.007	0.008
0.011	0.023	0.024
1.002	0.987	0.987
0.000	0.000	0.000
0.991	0.991	0.990
2.009	**2.008**	**2.009**
100.00	**100.00**	**100.00**
3.01	3.01	3.01

3	3	3
OM13-1	OM13-1	OM13-1
Cal-4	Cal-5	Cal-6
Cal	Cal	Cal
intergrown with serpentine	intergrown with serpentine	intergrown with serpentine
<0,05	<0,05	0.10
0.32	0.40	0.25
0.89	0.76	2.27
56.09	54.79	53.91
0.04	<0,04	<0,04
43.69	43.99	44.07
101.03	**99.94**	**100.61**
0.000	0.000	0.001
0.005	0.006	0.003
0.022	0.019	0.056
0.996	0.977	0.953
0.000	0.000	0.000
0.988	0.999	0.993
2.011	**2.001**	**2.007**
100.00	**100.00**	**97.51**
3.01	3.00	3.03

3	3	3
OM13-1	OM13-1	OM13-1
Cal-8	Cal-11	Cal-11b
Cal	Cal	Cal
intergrown with serpentine	intergrown with serpentine	intergrown with serpentine
0.17	0.23	<0,05
0.42	0.24	0.44
0.77	3.14	0.71
54.95	51.71	55.04
0.07	<0,04	<0,04
43.88	44.45	43.92
100.24	**99.76**	**100.11**
0.002	0.003	0.000
0.006	0.003	0.006
0.019	0.077	0.018
0.979	0.914	0.981
0.001	0.000	0.000
0.996	1.001	0.997
2.004	**1.999**	**2.002**
89.12	**96.07**	**100.00**
3.00	3.03	3.00

3	3	3
OM13-1	OM13-1	OM13-1
Cal-14	Cal-15	Cal-16
Cal	Cal	Cal
intergrown with serpentine	intergrown with serpentine	intergrown with serpentine
<0,05	<0,05	<0,05
0.31	0.49	0.32
0.56	0.76	1.01
56.32	54.98	54.28
0.10	0.05	0.04
43.65	43.91	44.10
100.95	**100.19**	**99.75**
0.000	0.000	0.000
0.004	0.007	0.005
0.014	0.019	0.025
1.002	0.980	0.967
0.001	0.000	0.000
0.989	0.997	1.001
2.010	**2.003**	**1.999**
100.00	**100.00**	**100.00**
3.01	3.00	3.00

3	3	3
OM13-1	OM13-1	OM13-1
Cal-19	Cal-23	Cal-27
Cal	Cal	Cal
intergrown with serpentine	intergrown with serpentine	intergrown with serpentine
<0,05	0.05	<0,05
0.36	0.36	0.28
0.75	0.68	0.50
55.99	55.54	56.05
0.06	0.08	0.06
43.71	43.80	43.73
100.87	**100.51**	**100.63**
0.000	0.001	0.000
0.005	0.005	0.004
0.018	0.017	0.012
0.995	0.989	0.998
0.001	0.001	0.001
0.990	0.994	0.992
2.010	**2.006**	**2.007**
100.00	**95.69**	**100.00**
3.01	3.00	3.00

3	3	3
OM13-1	OM13-1	OM13-11
Cal-29	Cal-32	Cal-1
Cal	Cal	Cal
intergrown with serpentine	intergrown with serpentine	intergrown with serpentine
0.07	<0,05	<0,05
0.42	0.23	0.42
0.46	0.66	1.77
55.20	54.94	53.47
0.05	<0,04	0.10
43.88	44.01	44.15
100.09	**99.85**	**99.92**
0.001	0.000	0.000
0.006	0.003	0.006
0.012	0.016	0.044
0.985	0.980	0.950
0.001	0.000	0.001
0.998	1.000	0.999
2.002	**2.000**	**2.000**
92.49	**100.00**	**100.00**
3.00	3.00	3.01

3	3	3
OM13-11	OM13-11	OM13-11
Cal-3	Cal-6	Cal-8
Cal	Cal	Cal
intergrown with serpentine	intergrown with serpentine	intergrown with serpentine
<0,05	<0,05	0.05
0.34	0.25	0.58
1.68	2.01	0.67
54.61	54.57	55.75
0.09	0.09	0.04
43.94	43.94	43.70
100.66	**100.86**	**100.80**
0.000	0.000	0.001
0.005	0.003	0.008
0.041	0.050	0.017
0.968	0.965	0.992
0.001	0.001	0.000
0.992	0.990	0.991
2.008	**2.010**	**2.009**
100.00	**100.00**	**95.82**
3.02	3.02	3.01

3	3	3
OM13-11	OM13-11	OM13-11
Cal-9	Cal-10	Cal-15
Cal	Cal	Cal
intergrown with serpentine	intergrown with serpentine	intergrown with serpentine
0.05	<0,05	0.06
0.56	0.50	0.52
1.50	1.62	1.52
54.96	53.81	52.93
0.06	<0,04	0.04
43.80	44.08	44.28
100.93	**100.01**	**99.36**
0.001	0.000	0.001
0.008	0.007	0.007
0.037	0.040	0.038
0.975	0.956	0.943
0.001	0.000	0.000
0.990	0.998	1.005
2.010	**2.001**	**1.995**
98.32	**100.00**	**97.91**
3.02	3.01	3.00

3	3	3
OM13-11	OM13-11	OM13-11
Cal-17	Cal-18	Cal-19
Cal	Cal	Cal
intergrown with serpentine	intergrown with serpentine	intergrown with serpentine
0.12	<0,05	0.06
0.38	0.44	0.56
0.61	0.75	1.50
56.07	55.43	54.96
0.05	<0,04	0.06
43.67	43.83	43.80
100.90	**100.45**	**100.94**
0.002	0.000	0.001
0.005	0.006	0.008
0.015	0.019	0.037
0.997	0.987	0.975
0.000	0.000	0.001
0.990	0.994	0.990
2.010	**2.005**	**2.010**
89.77	**100.00**	**97.74**
3.01	3.01	3.02

3	3	3
OM13-11	OM13-11	OM13-11
Cal-20	Cal-21	Cal-23
Cal	Cal	Cal
intergrown with serpentine	intergrown with serpentine	intergrown with serpentine
<0,05	<0,05	0.05
0.35	0.35	0.54
0.71	0.71	1.57
55.45	55.23	54.08
0.07	<0,04	0.06
43.83	43.91	44.00
100.42	**100.21**	**100.30**
0.000	0.000	0.001
0.005	0.005	0.008
0.018	0.018	0.039
0.987	0.984	0.961
0.001	0.000	0.001
0.995	0.997	0.996
2.005	**2.003**	**2.004**
100.00	**100.00**	**98.26**
3.00	3.00	3.01

3	3	3
OM13-11	OM13-11	OM13-13
Cal-26	Cal-29	Cal-1
Cal	Cal	Cal
intergrown with serpentine	intergrown with serpentine	intergrown with serpentine
<0,05	<0,05	0.19
0.43	0.33	0.12
1.74	1.86	0.49
54.78	54.78	56.25
0.08	0.12	<0,04
43.86	43.87	43.72
100.90	**100.96**	**100.77**
0.000	0.000	0.003
0.006	0.005	0.002
0.043	0.046	0.012
0.970	0.970	1.001
0.001	0.001	0.000
0.990	0.989	0.991
2.010	**2.010**	**2.009**
100.00	**100.00**	**82.10**
3.02	3.02	3.01

3	3	3
OM13-13	OM13-13	OM13-13
Cal-2	Cal-4	Cal-5
Cal	Cal	Cal
intergrown with serpentine	intergrown with serpentine	intergrown with serpentine
<0,05	0.08	<0,05
0.06	0.23	0.41
0.43	0.51	0.38
55.90	55.77	56.22
<0,04	<0,04	<0,04
43.86	43.82	43.73
100.25	**100.41**	**100.74**
0.000	0.001	0.000
0.001	0.003	0.006
0.011	0.013	0.009
0.996	0.993	1.001
0.000	0.000	0.000
0.996	0.995	0.992
2.004	**2.005**	**2.008**
100.00	**91.85**	**100.00**
3.00	3.00	3.01

3	3	3
OM13-13	OM13-13	OM13-13
Cal-6	Cal-9	Cal-11
Cal	Cal	Cal
intergrown with serpentine	intergrown with serpentine	intergrown with serpentine
<0,05	0.06	<0,05
0.35	0.21	0.37
0.45	0.49	0.41
56.48	56.97	55.98
<0,04	<0,04	<0,04
43.64	43.56	43.74
100.92	**101.28**	**100.50**
0.000	0.001	0.000
0.005	0.003	0.005
0.011	0.012	0.010
1.005	1.012	0.997
0.000	0.000	0.000
0.989	0.986	0.993
2.010	**2.014**	**2.006**
100.00	**93.70**	**100.00**
3.01	3.01	3.00

3	3	3
OM13-13	OM13-13	OM13-13
Cal-12	Cal-13	Cal-14
Cal	Cal	Cal
intergrown with serpentine	intergrown with serpentine	intergrown with serpentine
<0,05	0.06	0.06
0.30	0.16	0.25
0.34	0.50	0.40
56.00	56.51	56.43
0.09	0.05	<0,04
43.74	43.66	43.67
100.47	**100.94**	**100.81**
0.000	0.001	0.001
0.004	0.002	0.003
0.008	0.012	0.010
0.998	1.005	1.004
0.001	0.000	0.000
0.994	0.990	0.990
2.006	**2.010**	**2.009**
100.00	**93.76**	**91.71**
3.00	3.01	3.01

3	3	3
OM13-13	OM13-13	OM13-13
Cal-19	Cal-20	Cal-22
Cal	Cal	Cal
intergrown with serpentine	intergrown with serpentine	intergrown with serpentine
0.37	<0,05	0.11
0.06	0.30	0.07
2.06	0.48	0.46
54.38	56.30	55.31
<0,04	0.07	<0,04
43.94	43.68	43.98
100.82	**100.84**	**99.93**
0.005	0.000	0.002
0.001	0.004	0.001
0.051	0.012	0.011
0.962	1.002	0.987
0.000	0.001	0.000
0.990	0.991	1.000
2.009	**2.009**	**2.000**
90.79	**100.00**	**88.03**
3.02	3.01	3.00

3	3	3
OM13-13	OM13-13	OM13-13
Cal-31	Cal-32	Cal-33
Cal	Cal	Cal
intergrown with serpentine	intergrown with serpentine	intergrown with serpentine
<0,05	<0,05	<0,05
0.13	0.10	0.16
0.66	0.54	0.51
56.22	56.25	56.07
0.09	<0,04	0.05
43.73	43.76	43.78
100.83	**100.66**	**100.56**
0.000	0.000	0.000
0.002	0.001	0.002
0.016	0.013	0.013
1.000	1.001	0.998
0.001	0.000	0.000
0.991	0.992	0.993
2.009	**2.008**	**2.007**
100.00	**100.00**	**100.00**
3.01	3.01	3.00

3	3	3
OM13-13	OM13-13	OM13-13
Cal-36	Cal-38	Cal-39
Cal	Cal	Cal
intergrown with serpentine	intergrown with serpentine	intergrown with serpentine
<0,05	<0,05	0.05
0.33	0.36	0.17
0.54	0.48	0.59
56.40	55.37	55.20
0.05	0.04	<0,04
43.66	43.89	43.97
100.97	**100.14**	**99.98**
0.000	0.000	0.001
0.005	0.005	0.002
0.013	0.012	0.015
1.003	0.988	0.984
0.000	0.000	0.000
0.989	0.997	0.999
2.011	**2.003**	**2.001**
100.00	**100.00**	**95.65**
3.01	3.00	3.00

3	3	3
OM13-13	OM13-14A	OM13-14A
Cal-40	Cal-1	Cal-3
Cal	Cal	Cal
intergrown with serpentine	intergrown with serpentine	intergrown with serpentine
0.32	0.08	<0,05
0.10	<0,05	0.20
1.65	0.91	1.07
52.79	55.54	54.63
0.06	0.04	<0,04
44.35	43.91	44.07
99.27	**100.48**	**99.98**
0.004	0.001	0.000
0.001	0.000	0.003
0.041	0.023	0.027
0.940	0.987	0.972
0.001	0.000	0.000
1.006	0.994	0.999
1.994	**2.006**	**2.001**
90.16	**95.49**	**100.00**
3.00	3.01	3.01

3	3	3
OM13-14A	OM13-14A	OM13-14A
Cal-4	Cal-6	Cal-8
Cal	Cal	Cal
intergrown with serpentine	intergrown with serpentine	intergrown with serpentine
0.05	<0,05	0.12
0.31	0.06	0.32
1.02	1.15	0.95
55.04	55.11	54.98
<0,04	<0,04	0.07
43.92	44.00	43.89
100.34	**100.32**	**100.34**
0.001	0.000	0.002
0.004	0.001	0.005
0.025	0.028	0.024
0.979	0.979	0.979
0.000	0.000	0.001
0.995	0.996	0.995
2.005	**2.004**	**2.005**
97.41	**100.00**	**93.30**
3.01	3.01	3.01

3	3	3
OM13-14A	OM13-14A	OM13-14A
Cal-10	Cal-11	Cal-12
Cal	Cal	Cal
intergrown with serpentine	intergrown with serpentine	intergrown with serpentine
<0,05	0.09	0.25
0.42	0.21	0.05
1.52	0.72	1.33
53.91	54.89	55.22
0.06	<0,04	<0,04
44.08	44.00	43.86
99.99	**99.90**	**100.72**
0.000	0.001	0.004
0.006	0.003	0.001
0.038	0.018	0.033
0.958	0.979	0.980
0.001	0.000	0.000
0.999	1.000	0.992
2.001	**2.000**	**2.008**
100.00	**93.51**	**90.32**
3.01	3.00	3.02

3	3	3
OM13-14A	OM13-14A	OM13-14A
Cal-13	Cal-16	Cal-17
Cal	Cal	Cal
intergrown with serpentine	intergrown with serpentine	intergrown with serpentine
0.20	<0,05	<0,05
0.45	0.34	0.22
1.48	1.31	0.96
54.00	54.51	55.80
0.05	0.09	<0,04
44.01	43.98	43.78
100.19	**100.24**	**100.76**
0.003	0.000	0.000
0.006	0.005	0.003
0.037	0.032	0.024
0.960	0.969	0.991
0.001	0.001	0.000
0.997	0.996	0.991
2.003	**2.003**	**2.009**
92.99	**100.00**	**100.00**
3.01	3.01	3.01

3
OM13-14A
Cal-18
Cal
intergrown with serpentine
0.06
0.09
1.00
56.62
<0,04
43.63
101.42
0.001
0.001
0.025
1.003
0.000
0.985
2.015
96.73
3.02

SIMS session	Mount I.D.	File	Analysis I.D.
S1 (19 October 2020)			
	WI-STD-97		
	Serpentine RMs		
		20201019@1	WI-STD-97-UWSrp-1-gr1
		20201019@2	WI-STD-88-UWSrp-1-gr1
		20201019@3	WI-STD-97-UWSrp-1-gr2
		20201019@4	WI-STD-97-UWSrp-1-gr4
		20201019@5	WI-STD-97-UWSrp-4-gr1
		20201019@6	WI-STD-97-UWSrp-4-gr3
		20201019@7	WI-STD-97-UWSrp-4-gr4
		20201019@8	WI-STD-97-UWSrp-4-gr5
			average and 2SD
			bias*(UWSrp-1)
			2SE
		20201019@9	WI-STD-97-UWSrp-5-gr1
		20201019@1	WI-STD-97-UWSrp-5-gr3
		20201019@1	WI-STD-97-UWSrp-5-gr4
		20201019@1	WI-STD-97-UWSrp-5-gr5
			average and 2SD
			bias*(UWSrp-1)
			2SE
		20201019@1	WI-STD-97-UWSrp-6-gr1
		20201019@1	WI-STD-97-UWSrp-6-gr2
		20201019@1	WI-STD-97-UWSrp-6-gr4
		20201019@1	WI-STD-97-UWSrp-6-gr5
			average and 2SD
			bias*(UWSrp-1)
			2SE
		20201019@1	WI-STD-97-UWSrp-7-gr1
		20201019@1	WI-STD-97-UWSrp-7-gr2
		20201019@1	WI-STD-97-UWSrp-7-gr3
		20201019@2	WI-STD-97-UWSrp-7-gr5
			average and 2SD
			bias*(UWSrp-1)

	2SE
20201019@2	WI-STD-97-L3431-gr1
20201019@2	WI-STD-97-L3431-gr1b (vein)
20201019@2	WI-STD-97-L3431-gr2
20201019@2	WI-STD-97-L3431-gr2b (vein)
20201019@2	WI-STD-97-L3431-gr8
20201019@2	WI-STD-97-L3431-gr8b (vein)
20201019@2	WI-STD-97-L3431-gr9
	average and 2SD
	bias*(UWSrp-1)
	2SE
20201019@2	WI-STD-97-UWSrp-1-gr1
20201019@2	WI-STD-97-UWSrp-1-gr2
20201019@3	WI-STD-97-UWSrp-1-gr4
20201019@3	WI-STD-97-UWSrp-1-gr8
	average and 2SD
	bracket average and 2SD
	2SE
20201019@3	WI-STD-97-UWSrp-8-gr1
20201019@3	WI-STD-97-UWSrp-8-gr2
20201019@3	WI-STD-97-UWSrp-8-gr3
20201019@3	WI-STD-97-UWSrp-8-gr5
	average and 2SD
	bias*(UWSrp-1)
	2SE
20201019@3	WI-STD-97-UWSrp-9-gr1
20201019@3	WI-STD-97-UWSrp-9-gr2
20201019@3	WI-STD-97-UWSrp-9-gr3
20201019@3	WI-STD-97-UWSrp-9-gr4
20201019@4	WI-STD-97-UWSrp-9-gr1
20201019@4	WI-STD-97-UWSrp-9-gr3
	average and 2SD
	bias*(UWSrp-1)
	2SE
20201019@4	WI-STD-97-C22908-gr1
20201019@4	WI-STD-97-C22908-gr1
20201019@4	WI-STD-97-C22908-gr1
20201019@4	WI-STD-97-C22908-gr1

	average and 2SD
	bias*(UWSrp-1)
	2SE
20201019@4	WI-STD-97-UWC-3-gr2
20201019@4	WI-STD-97-UWC-3-gr2
20201019@4	WI-STD-97-UWC-3-gr2
20201019@4	WI-STD-97-UWC-3-gr2
	average and 2SD
	bias*(UWSrp-1)
	2SE
	bias* (UWC-3)
20201019@5	WI-STD-97-UWQ-1-gr1
20201019@5	WI-STD-97-UWQ-1-gr1
20201019@5	WI-STD-97-UWQ-1-gr1
20201019@5	WI-STD-97-UWQ-1-gr1
	average and 2SD
	bias*(UWSrp-1)
	2SE
20201019@5	WI-STD-97-L3431-gr3b (vein)
20201019@5	WI-STD-97-L3431-gr7b (vein)
20201019@5	WI-STD-97-L3431-gr6b (vein)
20201019@5	WI-STD-97-L3431-gr10b (vein)
20201019@5	WI-STD-97-L3431-gr5b (vein)
20201019@5	WI-STD-97-L3431-gr9b (vein)
	total average and 2SD (vein)
20201019@6	WI-STD-97-UWSrp-1-gr1
20201019@6	WI-STD-97-UWSrp-1-gr2
20201019@6	WI-STD-97-UWSrp-1-gr4
20201019@6	WI-STD-97-UWSrp-1-gr8
	average and 2SD
	bracket average and 2SD
	2SE
	total average and 2SD
	total 2SE

S2 (24 October 2020)

UWSrp-GGR2020

Serpentine RMs

20201019@1	UWSrp-GGR2020-UWSrp-1-gr2

20201019@1	UWSrp-GGR2020-UWSrp-1-gr2
20201019@1	UWSrp-GGR2020-UWSrp-1-gr2
20201019@1	UWSrp-GGR2020-UWSrp-1-gr2
20201019@1	UWSrp-GGR2020-UWSrp-1-gr2
20201019@1	UWSrp-GGR2020-UWSrp-1-gr2
20201019@1	UWSrp-GGR2020-UWSrp-4-gr1
20201019@1	UWSrp-GGR2020-UWSrp-4-gr2
20201019@1	UWSrp-GGR2020-UWSrp-4-gr3
20201019@1	UWSrp-GGR2020-UWSrp-4-gr4
20201019@1	UWSrp-GGR2020-UWSrp-4-gr5
20201019@1	UWSrp-GGR2020-UWSrp-4-gr1
20201019@1	UWSrp-GGR2020-UWSrp-4-gr3
	average and 2SD
	bias*(UWSrp-1)
	2SE
20201019@1	UWSrp-GGR2020-UWSrp-5-gr1
20201019@1	UWSrp-GGR2020-UWSrp-5-gr2
20201019@1	UWSrp-GGR2020-UWSrp-5-gr3
20201019@1	UWSrp-GGR2020-UWSrp-5-gr4
20201019@1	UWSrp-GGR2020-UWSrp-5-gr5
	average and 2SD
	bias*(UWSrp-1)
	2SE
20201019@1	UWSrp-GGR2020-UWSrp-6-gr1
20201019@1	UWSrp-GGR2020-UWSrp-6-gr2
20201019@1	UWSrp-GGR2020-UWSrp-6-gr3
20201019@1	UWSrp-GGR2020-UWSrp-6-gr4
20201019@1	UWSrp-GGR2020-UWSrp-6-gr5
	average and 2SD
	bias*(UWSrp-1)
	2SE
20201019@1	UWSrp-GGR2020-UWSrp-7-gr1
20201019@1	UWSrp-GGR2020-UWSrp-7-gr2
20201019@1	UWSrp-GGR2020-UWSrp-7-gr3
20201019@1	UWSrp-GGR2020-UWSrp-7-gr5
	average and 2SD
	bias*(UWSrp-1)
	2SE

20201019@1	UWSrp-GGR2020-UWSrp-8-gr1
20201019@1	UWSrp-GGR2020-UWSrp-8-gr5
20201019@1	UWSrp-GGR2020-UWSrp-8-gr3
20201019@1	UWSrp-GGR2020-UWSrp-8-gr6
	average and 2SD
	bias*(UWSrp-1)
	2SE
20201019@1	UWSrp-GGR2020-UWSrp-1-gr2
20201019@1	UWSrp-GGR2020-UWSrp-1-gr2
20201019@1	UWSrp-GGR2020-UWSrp-1-gr2
20201019@1	UWSrp-GGR2020-UWSrp-1-gr2
	average and 2SD
	bracket average and 2SD
	2SE
20201019@1	UWSrp-GGR2020-UWSrp-9-gr1
20201019@1	UWSrp-GGR2020-UWSrp-9-gr1
20201019@1	UWSrp-GGR2020-UWSrp-9-gr2
20201019@1	UWSrp-GGR2020-UWSrp-9-gr3
20201019@1	UWSrp-GGR2020-UWSrp-9-gr4
20201019@1	UWSrp-GGR2020-UWSrp-9-gr5
	average and 2SD
	bias*(UWSrp-1)
	2SE
20201019@1	UWSrp-GGR2020-C22908-gr2
20201019@1	UWSrp-GGR2020-C22908-gr2
20201019@1	UWSrp-GGR2020-C22908-gr2
20201019@1	UWSrp-GGR2020-C22908-gr2
20201019@1	UWSrp-GGR2020-C22908-gr1
20201019@1	UWSrp-GGR2020-C22908-gr1
20201019@1	UWSrp-GGR2020-C22908-gr1
20201019@1	UWSrp-GGR2020-C22908-gr1
	average and 2SD
	bias*(UWSrp-1)
	2SE
20201019@1	UWSrp-GGR2020-L3431-gr2
20201019@1	UWSrp-GGR2020-L3431-gr1
20201019@1	UWSrp-GGR2020-L3431-gr11
20201019@1	UWSrp-GGR2020-L3431-gr10

20201019@1	UWSrp-GGR2020-L3431-gr9
20201019@1	UWSrp-GGR2020-L3431-gr9
20201019@1	UWSrp-GGR2020-L3431-gr8
20201019@1	UWSrp-GGR2020-L3431-gr2
20201019@1	UWSrp-GGR2020-L3431-gr2
20201019@1	UWSrp-GGR2020-L3431-gr10
20201019@1	UWSrp-GGR2020-L3431-gr10
20201019@1	UWSrp-GGR2020-L3431-gr9
20201019@1	UWSrp-GGR2020-L3431-gr9
20201019@1	UWSrp-GGR2020-L3431-gr9
20201019@1	UWSrp-GGR2020-L3431-gr9
20201019@1	UWSrp-GGR2020-L3431-gr9
	average and 2SD
	bias*(UWSrp-1)
	2SE

20201019@1	UWSrp-GGR2020-UWC-3-gr1
20201019@1	UWSrp-GGR2020-UWC-3-gr1
20201019@1	UWSrp-GGR2020-UWC-3-gr1
20201019@1	UWSrp-GGR2020-UWC-3-gr1
20201019@1	UWSrp-GGR2020-UWC-3-gr1
	average and 2SD
	bias*(UWSrp-1)
	2SE
	bias* (UWC-3)

20201019@1	UWSrp-GGR2020-UWSrp-1-gr2
20201019@1	UWSrp-GGR2020-UWSrp-1-gr2
20201019@1	UWSrp-GGR2020-UWSrp-1-gr2
20201019@1	UWSrp-GGR2020-UWSrp-1-gr2
	average and 2SD
	bracket average and 2SD
	2SE
	total average and 2SD
	total 2SE

S3 (27 October 2020)

<u>Srp STD 1b</u>

Serpentine RMs

20201019@1	Srp STD 1b-UWC-3-gr1
20201019@1	Srp STD 1b-UWC-3-gr1
20201019@1	Srp STD 1b-UWC-3-gr1
20201019@1	Srp STD 1b-UWC-3-gr1

	20201019@2	Srp STD 1b-L3431-gr1
	20201019@2	Srp STD 1b-L3431-gr2
	20201019@2	Srp STD 1b-L3431-gr3
	20201019@2	Srp STD 1b-L3431-gr4
		average and 2SD (parallel)
		bias*(UWC-3)
		bias*(UWSrp-1)
		2SE
	20201019@2	Srp STD 1b-UWC-3-gr1
	20201019@2	Srp STD 1b-UWC-3-gr1
	20201019@2	Srp STD 1b-UWC-3-gr1
	20201019@2	Srp STD 1b-UWC-3-gr1
	20201019@2	Srp STD 1b-UWC-3-gr1
		average and 2SD
		bracket average and 2SD
		2SE
Srp STD 1b		
Serpentine RMs		
	20201019@2	Srp STD 1b-UWC-3-gr1
	20201019@2	Srp STD 1b-UWC-3-gr1
	20201019@2	Srp STD 1b-UWC-3-gr1
	20201019@2	Srp STD 1b-UWC-3-gr1
	20201019@2	Srp STD 1b-UWSrp-5-gr1
	20201019@2	Srp STD 1b-UWSrp-5-gr2
	20201019@2	Srp STD 1b-UWSrp-5-gr3
	20201019@2	Srp STD 1b-UWSrp-5-gr4
		average and 2SD
		bias*(UWC-3)
		bias*(UWSrp-1)
		2SE
	20201019@2	Srp STD 1b-UWSrp-4-gr1
	20201019@2	Srp STD 1b-UWSrp-4-gr2
	20201019@2	Srp STD 1b-UWSrp-4-gr3
	20201019@2	Srp STD 1b-UWSrp-4-gr4
		average and 2SD
		bias*(UWC-3)
		bias*(UWSrp-1)
		2SE

20201019@2	Srp STD 1b-UWSrp-7-gr1
20201019@2	Srp STD 1b-UWSrp-7-gr2
20201019@2	Srp STD 1b-UWSrp-7-gr3
20201019@2	Srp STD 1b-UWSrp-7-gr4
	average and 2SD
	bias*(UWC-3)
	bias*(UWSrp-1)
	2SE
20201019@2	Srp STD 1b-UWC-3-gr1
20201019@2	Srp STD 1b-UWC-3-gr1
20201019@2	Srp STD 1b-UWC-3-gr1
20201019@2	Srp STD 1b-UWC-3-gr1
	average and 2SD
	bracket average and 2SD
	2SE
20201019@2	Srp STD 1b-UWSrp-6-gr1
20201019@2	Srp STD 1b-UWSrp-6-gr2
20201019@2	Srp STD 1b-UWSrp-6-gr3
20201019@2	Srp STD 1b-UWSrp-6-gr4
	average and 2SD
	bias*(UWC-3)
	bias*(UWSrp-1)
	2SE
20201019@2	Srp STD 1b-UWSrp-8-gr1
20201019@2	Srp STD 1b-UWSrp-8-gr2
20201019@2	Srp STD 1b-UWSrp-8-gr3
20201019@2	Srp STD 1b-UWSrp-8-gr4
	average and 2SD
	bias*(UWC-3)
	bias*(UWSrp-1)
	2SE
20201019@2	Srp STD 1b-Al06-44A-gr1
20201019@2	Srp STD 1b-Al06-44A-gr2
20201019@2	Srp STD 1b-Al06-44A-gr3
20201019@2	Srp STD 1b-Al06-44A-gr4
	average and 2SD
	bias*(UWC-3)
	bias*(UWSrp-1)

	2SE
20201019@2	Srp STD 1b-UWC-3-gr1
20201019@2	Srp STD 1b-UWC-3-gr1
20201019@2	Srp STD 1b-UWC-3-gr1
20201019@2	Srp STD 1b-UWC-3-gr1
	average and 2SD
	bracket average and 2SD
	2SE

$\delta^{18}O$ ‰ (RAW)	2SE (int.)	Mg# (mole %)	Bias (‰)	$\delta^{18}O$ ‰ (V-SMOW)	2s (ext.)	2σ ‰
13.34	0.17					
13.04	0.13					
13.23	0.13					
13.29	0.20					
11.70	0.15					
11.76	0.18					
11.80	0.14					
11.67	0.13					
11.73	**0.12**		**4.18**	**7.52**		
			-0.71			
	0.06					
12.97	0.16					
13.14	0.15					
13.20	0.12					
13.11	0.16					
13.10	**0.19**		**4.19**	**8.88**		
			-0.70			
	0.10					
10.65	0.16					
10.79	0.12					
10.83	0.12					
11.07	0.12					
10.84	**0.35**		**5.22**	**5.59**		
			0.32			
	0.17					
8.68	0.12					
9.13	0.13					
8.76	0.14					
8.92	0.16					
8.87	**0.39**		**5.16**	**3.69**		
			0.27			

	0.20		
9.46	0.16		
9.75	0.16		
9.65	0.15		
10.22	0.19		
9.32	0.14		
9.28	0.16		
9.76	0.18		
9.55	**0.39**	**4.21**	**5.32**
		-0.68	
	0.19		
13.34	0.11		
13.34	0.14		
13.36	0.10		
13.54	0.18		
13.40	0.19		
13.31	**0.28**	**4.89**	**8.38**
	0.10		
9.67	0.13		
9.59	0.15		
9.81	0.15		
9.59	0.13		
9.66	**0.21**	**3.19**	**6.45**
		-1.83	
	0.10		
6.99	0.14		
7.63	0.18		
7.09	0.14		
7.33	0.18		
7.44	0.14		
7.31	0.16		
7.30	**0.46**	**4.93**	**2.36**
		-0.10	
	0.19		
8.63	0.18		
8.66	0.22		
8.51	0.15		
8.99	0.21		

8.70	**0.42**	**4.02**	**4.66**
		-1.00	
	0.21		
2.82	0.54		
3.13	0.51		
3.21	0.53		
2.77	0.50		
2.98	**0.44**	**-9.39**	**12.49**
		-14.35	
	0.22		
		14.55	
5.26	0.22		
5.16	0.17		
5.17	0.16		
5.50	0.16		
5.27	**0.32**	**-6.97**	**12.33**
		-11.94	
	0.16		
9.37	0.12		
10.08	0.16		
9.70	0.10		
9.83	0.16		
9.68	0.24		
9.94	0.16		
9.76	**0.61**		
13.55	0.15		
13.42	0.15		
13.46	0.15		
13.56	0.18		
13.50	0.14		
13.45	**0.19**	**5.03**	**8.38**
	0.07		
13.38	**0.30**		
	0.09		
13.53	0.15		

14.20	0.34		
13.55	0.15		
13.32	0.15		
11.85	0.16		
13.31	0.13		
11.82	0.15		
12.85	0.13		
11.91	0.13		
12.16	0.33		
11.33	0.12		
12.04	0.32		
12.16	0.18		
11.80	**0.70**	**4.25**	**7.52**
		-0.67	
	0.35		
12.94	0.18		
12.74	0.40		
13.23	0.13		
13.41	0.16		
13.42	0.14		
13.25	**0.44**	**4.33**	**8.88**
		-0.59	
	0.22		
12.34	0.61		
11.20	0.12		
10.98	0.14		
10.80	0.18		
10.82	0.14		
10.95	**0.37**	**5.33**	**5.59**
		0.41	
	0.18		
8.88	0.14		
9.12	0.25		
8.78	0.21		
8.87	0.24		
8.91	**0.29**	**5.20**	**3.69**
		0.28	
	0.15		

8.84	0.13		
9.30	0.14		
9.21	0.18		
9.49	0.22		
9.21	**0.54**	**2.74**	**6.45**
		-2.17	
	0.27		
13.11	0.14		
13.17	0.17		
13.41	0.14		
13.34	0.28		
13.26	0.29		
13.34	**0.31**	**4.92**	**8.38**
	0.11		
-18.29	1.38		
6.96	0.15		
7.21	0.16		
7.47	0.21		
6.30	0.13		
7.47	0.21		
7.28	**0.49**	**4.91**	**2.36**
		0.18	
	0.25		
5.48	0.19		
5.52	0.16		
8.11	0.15		
7.51	0.15		
8.38	0.24		
8.73	0.20		
9.06	0.25		
8.96	0.15		
8.78	**0.61**	**4.10**	**4.66**
		-0.63	
	0.30		
8.84	0.20		
7.84	0.21		
5.86	0.19		
8.15	0.19		

8.62	0.20		
9.56	0.28		
7.67	0.20		
8.50	0.23		
10.51	0.22		
7.73	0.17		
7.87	0.22		
8.77	0.22		
8.75	0.19		
8.63	0.26		
8.95	0.21		
8.45	0.17		
8.79	**0.66**	**3.45**	**5.32**
		-1.28	
	0.22		
2.32	0.45		
2.24	0.51		
2.11	0.54		
4.55	0.68		
2.30	0.48		
2.24	**0.19**	**-10.12**	**12.49**
		-14.78	
	0.09		
		15.00	
13.08	0.16		
12.70	0.23		
13.26	0.20		
13.13	0.14		
13.04	0.48		
13.15	**0.43**	**4.73**	**8.38**
	0.15		
13.24	**0.46**		
	0.13		
2.06	0.47		
2.09	0.45		
1.77	0.45		
2.16	0.50		

8.73	0.25		
8.84	0.23		
9.08	0.20		
8.88	0.27		
8.88	**0.29**	**3.54**	**5.32**
		13.98	
		-1.01	
	0.14		
2.24	0.47		
2.01	0.47		
2.10	0.49		
2.68	0.48		
2.10	0.48		
2.11	0.19		
2.07	**0.28**	**-10.29**	**12.49**
	0.10		
2.46	0.43		
2.66	0.48		
2.27	0.45		
2.38	0.49		
13.16	0.17		
13.29	0.15		
12.87	0.18		
13.04	0.16		
13.09	**0.36**	**4.17**	**8.88**
		14.34	
		-0.65	
	0.18		
11.79	0.18		
11.88	0.21		
11.49	0.14		
11.52	0.24		
11.67	**0.39**	**4.12**	**7.52**
		14.29	
		-0.71	
	0.19		

8.95	0.18		
8.85	0.16		
8.89	0.17		
8.75	0.19		
8.86	**0.17**	**5.15**	**3.69**
		15.33	
		0.32	
	0.09		
2.08	0.54		
2.48	0.51		
2.44	0.44		
1.96	0.41		
2.24	0.51		
2.34	**0.46**	**-10.02**	**12.49**
	0.16		
10.83	0.17		
11.14	0.20		
11.00	0.15		
11.03	0.15		
11.00	**0.26**	**5.38**	**5.59**
		15.70	
		0.69	
	0.13		
9.70	0.13		
9.55	0.17		
9.64	0.14		
9.63	0.11		
9.63	**0.12**	**3.16**	**6.45**
		13.45	
		-1.53	
	0.06		
13.33	0.17		
13.36	0.12		
13.29	0.13		
13.08	0.16		
13.26	**0.26**	**5.20**	**8.02**
		15.52	
		0.51	

	0.13		
2.27	0.47		
2.04	0.44		
2.14	0.47		
2.22	0.44		
2.17	0.20		
2.20	**0.37**	**-10.16**	**12.49**
	0.13		

^{16}O (Gcps)	^{18}O (Mcps)	IP (nA)	Yield (Gcps/nA)	Relative yield	2s relative yield	$^{16}OH/^{16}O$
2.25	4.57	1.82	1.24			3.38E-02
2.39	4.85	1.91	1.25			3.40E-02
2.39	4.85	1.93	1.24			3.39E-02
2.38	4.84	1.93	1.23			3.36E-02
2.40	4.87	1.93	1.25	1.01	0.01	3.41E-02
2.42	4.91	1.92	1.26	1.02	0.01	3.41E-02
2.49	5.06	1.98	1.26	1.02	0.01	3.43E-02
2.47	5.01	1.99	1.24	1.00	0.01	3.41E-02
2.49	5.06	1.99	1.25	1.01	0.01	3.46E-02
2.51	5.11	1.99	1.26	1.02	0.01	3.36E-02
2.49	5.06	1.98	1.26	1.02	0.01	3.38E-02
2.47	5.03	1.97	1.26	1.02	0.01	3.38E-02
2.39	4.84	1.96	1.22	0.99	0.01	3.44E-02
2.48	5.03	2.01	1.24	1.00	0.01	3.45E-02
2.48	5.02	2.02	1.23	0.99	0.01	3.44E-02
2.48	5.02	2.02	1.22	0.99	0.01	3.43E-02
2.46	4.98	2.04	1.21	0.98	0.01	3.33E-02
2.41	4.87	2.03	1.18	0.96	0.01	3.32E-02
2.43	4.92	2.02	1.20	0.97	0.01	3.34E-02
2.43	4.91	2.01	1.21	0.98	0.01	3.33E-02

2.48	5.02	2.00	1.24	1.01	0.01	3.12E-02
2.47	5.00	1.98	1.25	1.01	0.01	3.68E-02
2.42	4.90	1.97	1.23	1.00	0.01	3.03E-02
2.45	4.96	1.96	1.25	1.01	0.01	3.50E-02
2.43	4.92	1.95	1.25	1.01	0.01	3.00E-02
2.48	5.02	1.99	1.24	1.01	0.01	3.33E-02
2.48	5.03	2.00	1.24	1.01	0.01	3.12E-02

2.45	4.98	1.98	1.24			3.40E-02
2.43	4.93	1.97	1.23			3.40E-02
2.43	4.93	1.97	1.23			3.36E-02
2.41	4.90	1.96	1.23			3.41E-02
			1.24			

2.62	5.30	1.96	1.34	1.09	0.01	3.55E-02
2.71	5.48	2.01	1.35	1.10	0.01	3.50E-02
2.70	5.47	2.02	1.34	1.09	0.01	3.52E-02
2.65	5.36	2.02	1.31	1.07	0.01	3.54E-02

2.45	4.94	2.01	1.22	0.99	0.01	3.37E-02
2.43	4.90	2.00	1.21	0.99	0.01	3.41E-02
2.43	4.90	1.99	1.22	0.99	0.01	3.45E-02
2.36	4.76	1.98	1.19	0.97	0.01	3.44E-02
2.38	4.81	1.97	1.21	0.98	0.01	3.38E-02
2.37	4.79	1.96	1.21	0.99	0.01	3.43E-02

2.47	5.00	2.02	1.22	0.99	0.01	4.36E-02
2.48	5.02	2.04	1.22	0.99	0.01	4.18E-02
2.48	5.01	2.04	1.21	0.99	0.01	4.32E-02
2.47	4.99	2.03	1.21	0.99	0.01	4.00E-02

3.85	7.74	2.00	1.92			1.15E-03
3.81	7.67	2.00	1.91			1.18E-03
3.79	7.62	1.99	1.91			1.22E-03
3.78	7.60	1.98	1.91			1.19E-03
						1.18E-03

2.74	5.53	1.97	1.39			5.57E-04
2.70	5.45	1.96	1.38			5.59E-04
2.82	5.69	2.02	1.40			5.40E-04
2.80	5.65	2.02	1.39			5.42E-04

2.53	5.12	2.02	1.25	1.02	0.01	3.75E-02
2.49	5.05	2.01	1.24	1.01	0.01	3.71E-02
2.47	5.01	2.00	1.23	1.00	0.01	3.69E-02
2.48	5.02	2.00	1.24	1.01	0.01	3.69E-02
2.42	4.90	1.99	1.22	0.99	0.01	3.44E-02
2.44	4.95	1.97	1.24	1.01	0.01	3.53E-02

2.42	4.91	1.96	1.24			3.40E-02
2.46	5.00	2.01	1.22			3.41E-02
2.48	5.04	2.02	1.23			3.39E-02
2.46	5.00	2.02	1.22			3.40E-02
			1.23			

2.38	4.84	2.02	1.18			3.40E-02

2.36	4.80	2.02	1.17			3.38E-02
2.39	4.85	2.02	1.18			3.38E-02
2.38	4.84	2.02	1.18			3.37E-02
2.36	4.79	2.01	1.17			3.48E-02
2.36	4.79	2.01	1.17			3.38E-02
2.42	4.90	2.01	1.20	1.03	0.03	3.40E-02
2.39	4.84	2.01	1.19	1.02	0.03	3.39E-02
2.42	4.90	2.01	1.20	1.03	0.03	3.40E-02
2.41	4.88	2.02	1.19	1.02	0.03	3.39E-02
2.40	4.86	2.01	1.19	1.02	0.03	3.37E-02
2.40	4.87	2.01	1.19	1.02	0.03	3.38E-02
2.41	4.88	2.01	1.20	1.03	0.03	3.41E-02
2.46	4.99	2.01	1.22	1.05	0.03	3.45E-02
2.41	4.90	2.01	1.20	1.03	0.03	3.45E-02
2.43	4.93	2.01	1.21	1.04	0.03	3.40E-02
2.42	4.92	2.01	1.21	1.04	0.03	3.41E-02
2.42	4.91	2.00	1.21	1.03	0.03	3.39E-02
2.25	4.57	2.00	1.12	0.97	0.03	3.36E-02
2.34	4.75	2.00	1.17	1.01	0.03	3.43E-02
2.32	4.70	1.99	1.16	1.00	0.03	3.41E-02
2.31	4.69	1.99	1.16	1.00	0.03	3.41E-02
2.30	4.67	1.99	1.16	1.00	0.03	3.44E-02
2.24	4.53	1.99	1.13	0.97	0.03	3.29E-02
2.25	4.55	1.99	1.13	0.97	0.03	3.31E-02
2.23	4.52	1.99	1.12	0.97	0.03	3.28E-02
2.25	4.55	1.99	1.13	0.97	0.03	3.30E-02

2.46	4.98	1.98	1.24	1.07	0.03	3.41E-02
2.57	5.20	1.98	1.30	1.11	0.03	3.82E-02
2.49	5.04	1.98	1.26	1.08	0.03	3.77E-02
2.46	4.98	1.98	1.24	1.07	0.03	3.69E-02
2.28	4.62	1.97	1.15			3.38E-02
2.31	4.70	1.97	1.17			3.45E-02
2.26	4.59	1.97	1.14			3.35E-02
2.24	4.56	1.98	1.14			3.34E-02
			1.16			
0.25	0.49	1.97	0.13	0.11	0.04	7.31E-02
2.35	4.73	1.97	1.19	1.02	0.04	3.56E-02
2.32	4.69	1.97	1.18	1.01	0.04	3.65E-02
2.23	4.51	1.97	1.13	0.97	0.04	3.44E-02
2.33	4.70	1.97	1.18	1.01	0.04	3.82E-02
2.31	4.67	1.97	1.17	1.01	0.04	3.45E-02
2.31	4.65	1.97	1.17	1.00	0.04	6.91E-02
2.24	4.53	1.96	1.14	0.98	0.04	6.51E-02
2.26	4.56	1.96	1.15	0.98	0.04	4.92E-02
2.33	4.70	1.96	1.19	1.02	0.04	4.78E-02
2.40	4.84	2.02	1.19	1.02	0.04	4.64E-02
2.42	4.90	2.04	1.19	1.02	0.04	4.52E-02
2.38	4.82	2.05	1.17	1.00	0.04	4.58E-02
2.42	4.90	2.05	1.18	1.01	0.04	4.36E-02
2.52	5.09	2.06	1.22	1.05	0.04	3.18E-02
2.52	5.10	2.05	1.23	1.05	0.04	3.56E-02
2.48	5.01	2.06	1.21	1.03	0.04	5.59E-02
2.52	5.10	2.06	1.23	1.05	0.04	3.94E-02

2.49	5.04	2.05	1.21	1.04	0.04	3.06E-02
2.48	5.02	2.05	1.21	1.03	0.04	3.04E-02
2.46	4.96	2.06	1.19	1.02	0.04	4.33E-02
2.50	5.05	2.05	1.22	1.04	0.04	3.20E-02
2.40	4.87	2.05	1.17	1.00	0.04	3.13E-02
2.49	5.03	2.05	1.21	1.04	0.04	3.89E-02
2.48	5.01	2.05	1.21	1.04	0.04	3.93E-02
2.47	5.00	2.04	1.21	1.04	0.04	3.08E-02
2.48	5.01	2.04	1.21	1.04	0.04	3.11E-02
2.49	5.03	2.05	1.22	1.04	0.04	3.06E-02
2.45	4.97	2.04	1.20	1.03	0.04	3.10E-02
2.47	5.00	2.04	1.21	1.04	0.04	3.15E-02

3.84	7.72	2.04	1.89			9.77E-04
3.82	7.67	2.04	1.87			9.55E-04
3.82	7.68	2.04	1.88			9.59E-04
3.70	7.44	2.04	1.81			1.06E-03
3.82	7.68	2.04	1.87			9.53E-04
						9.61E-04

2.39	4.85	2.02	1.19			3.49E-02
2.36	4.80	2.01	1.18			3.50E-02
2.37	4.82	2.01	1.18			3.49E-02
2.38	4.84	2.00	1.19			3.48E-02
			1.17			

4.38	8.80	2.31	1.90			1.06E-03
4.39	8.81	2.31	1.90			1.11E-03
4.36	8.77	2.30	1.89			1.18E-03
4.32	8.69	2.30	1.88			1.23E-03

2.84	5.75	2.29	1.24	3.18E-02
2.85	5.76	2.29	1.25	3.44E-02
2.78	5.63	2.28	1.22	3.65E-02
2.82	5.70	2.28	1.24	3.60E-02
4.28	8.61	2.27	1.89	1.09E-03
4.28	8.59	2.27	1.89	1.12E-03
4.27	8.57	2.27	1.88	1.19E-03
4.26	8.57	2.27	1.88	1.22E-03
4.26	8.55	2.26	1.88	1.18E-03
				1.15E-03
3.84	7.73	2.02	1.90	1.17E-03
3.85	7.74	2.02	1.90	1.26E-03
3.87	7.78	2.02	1.91	1.26E-03
3.84	7.73	2.02	1.90	1.28E-03
2.58	5.24	2.02	1.28	3.46E-02
2.55	5.19	2.02	1.26	3.48E-02
2.59	5.25	2.01	1.29	3.51E-02
2.52	5.12	2.01	1.26	3.50E-02
2.51	5.08	2.01	1.25	3.51E-02
2.51	5.10	2.00	1.25	3.49E-02
2.53	5.12	2.00	1.26	3.52E-02
2.53	5.13	2.00	1.27	3.51E-02

2.37	4.80	1.99	1.19	3.40E-02
2.38	4.81	1.99	1.19	3.42E-02
2.38	4.82	1.99	1.20	3.40E-02
2.38	4.81	1.99	1.20	3.40E-02
3.75	7.53	1.99	1.89	1.12E-03
3.68	7.40	1.98	1.86	1.15E-03
3.70	7.44	1.98	1.87	1.08E-03
3.72	7.47	1.97	1.89	1.09E-03
				1.17E-03
2.42	4.90	1.97	1.23	3.57E-02
2.40	4.88	1.96	1.22	3.55E-02
2.41	4.90	1.96	1.23	3.54E-02
2.41	4.89	1.96	1.23	3.53E-02
2.60	5.27	1.97	1.32	3.68E-02
2.63	5.32	1.97	1.34	3.73E-02
2.63	5.32	1.96	1.34	3.78E-02
2.62	5.30	1.96	1.34	3.70E-02
2.52	5.12	2.01	1.25	3.49E-02
2.52	5.12	2.02	1.25	3.51E-02
2.52	5.11	2.03	1.24	3.49E-02
2.54	5.15	2.04	1.24	3.48E-02

3.85	7.73	2.04	1.88	1.05E-03
3.89	7.82	2.04	1.91	1.05E-03
3.85	7.73	2.05	1.88	1.08E-03
3.85	7.74	2.05	1.88	1.09E-03
				1.09E-03

^{16}OH (cps)	$^{16}OH/^{16}O$ background corrected	2s $^{16}OH/^{16}O$	Date	Time	X	Y
7.60E+07	3.26E-02	6.10E-05	10/19/20	1:20:00 PM	-979	470
8.11E+07	3.28E-02	6.10E-05	10/19/20	1:26:00 PM	-347	3835
8.09E+07	3.27E-02	6.10E-05	10/19/20	1:30:00 PM	-347	3835
8.01E+07	3.24E-02	6.10E-05	10/19/20	1:33:00 PM	-3224	169
8.19E+07	3.29E-02	6.10E-05	10/19/20	1:36:00 PM	-1389	-1299
8.24E+07	3.29E-02	6.10E-05	10/19/20	1:40:00 PM	-3031	-1288
8.56E+07	3.31E-02	6.10E-05	10/19/20	1:45:00 PM	-4004	-1480
8.42E+07	3.29E-02	6.10E-05	10/19/20	1:48:00 PM	-5225	-1595
8.62E+07	3.34E-02	6.10E-05	10/19/20	1:51:00 PM	-1027	-2390
8.43E+07	3.24E-02	6.10E-05	10/19/20	1:54:00 PM	-2606	-3195
8.40E+07	3.26E-02	6.10E-05	10/19/20	1:58:00 PM	-3400	-2558
8.37E+07	3.26E-02	6.10E-05	10/19/20	2:01:00 PM	-4542	-3083
8.20E+07	3.32E-02	6.10E-05	10/19/20	2:04:00 PM	-780	-3872
8.56E+07	3.33E-02	6.10E-05	10/19/20	2:09:00 PM	-1816	-4434
8.50E+07	3.32E-02	6.10E-05	10/19/20	2:13:00 PM	-271	-5158
8.50E+07	3.32E-02	6.10E-05	10/19/20	2:16:00 PM	-1323	-5244
8.19E+07	3.21E-02	6.10E-05	10/19/20	2:20:00 PM	139	-900
7.99E+07	3.21E-02	6.10E-05	10/19/20	2:23:00 PM	309	-1891
8.12E+07	3.22E-02	6.10E-05	10/19/20	2:26:00 PM	910	-2726
8.08E+07	3.21E-02	6.10E-05	10/19/20	2:29:00 PM	1502	-4569

7.74E+07	3.00E-02	6.10E-05	10/19/20	2:33:00 PM	1997	-2603
9.08E+07	3.56E-02	6.10E-05	10/19/20	2:37:00 PM	2044	-2521
7.34E+07	2.92E-02	6.10E-05	10/19/20	2:40:00 PM	2814	-2702
8.58E+07	3.38E-02	6.10E-05	10/19/20	2:43:00 PM	2672	-2875
7.31E+07	2.89E-02	6.10E-05	10/19/20	2:46:00 PM	2864	-3474
8.26E+07	3.21E-02	6.10E-05	10/19/20	2:51:00 PM	2580	-3515
7.76E+07	3.01E-02	6.10E-05	10/19/20	2:54:00 PM	1963	-3343
8.33E+07	3.28E-02	6.10E-05	10/19/20	3:02:00 PM	-997	516
8.26E+07	3.28E-02	6.10E-05	10/19/20	3:05:00 PM	-1589	-25
8.15E+07	3.24E-02	6.10E-05	10/19/20	3:08:00 PM	-3407	209
8.21E+07	3.29E-02	6.10E-05	10/19/20	3:11:00 PM	-3248	1122
9.27E+07	3.43E-02	6.10E-05	10/19/20	3:15:00 PM	1789	1954
9.48E+07	3.38E-02	6.10E-05	10/19/20	3:20:00 PM	2739	3150
9.51E+07	3.40E-02	6.10E-05	10/19/20	3:23:00 PM	3903	1951
9.37E+07	3.42E-02	6.10E-05	10/19/20	3:27:00 PM	4561	3250
8.24E+07	3.25E-02	6.10E-05	10/19/20	3:30:00 PM	527	3033
8.26E+07	3.29E-02	6.10E-05	10/19/20	3:33:00 PM	-124	3776
8.37E+07	3.33E-02	6.10E-05	10/19/20	3:37:00 PM	848	5793
8.11E+07	3.32E-02	6.10E-05	10/19/20	3:41:00 PM	3124	6503
8.05E+07	3.26E-02	6.10E-05	10/19/20	3:44:00 PM	460	2985
8.14E+07	3.32E-02	6.10E-05	10/19/20	3:48:00 PM	869	5396
1.08E+08	4.24E-02	6.10E-05	10/19/20	3:53:00 PM	-3248	2117
1.04E+08	4.06E-02	6.10E-05	10/19/20	3:56:00 PM	-3228	2117
1.07E+08	4.20E-02	6.10E-05	10/19/20	3:59:00 PM	-3228	2097
9.86E+07	3.88E-02	6.10E-05	10/19/20	4:02:00 PM	-3248	2097

4.42E+06			10/19/20	4:09:00 PM	597	1364
4.49E+06			10/19/20	4:12:00 PM	617	1364
4.63E+06			10/19/20	4:15:00 PM	623	1343
4.50E+06			10/19/20	4:18:00 PM	643	1343
1.53E+06			10/19/20	4:21:00 PM	1878	1445
1.51E+06			10/19/20	4:24:00 PM	2050	1380
1.52E+06			10/19/20	4:31:00 PM	1893	1210
1.52E+06			10/19/20	4:34:00 PM	1955	1102
9.48E+07	3.63E-02	6.10E-05	10/19/20	4:37:00 PM	3336	-2921
9.26E+07	3.59E-02	6.10E-05	10/19/20	4:40:00 PM	3536	-3729
9.12E+07	3.57E-02	6.10E-05	10/19/20	4:43:00 PM	3964	-4195
9.15E+07	3.57E-02	6.10E-05	10/19/20	4:47:00 PM	2384	-4315
8.33E+07	3.33E-02	6.10E-05	10/19/20	4:51:00 PM	4793	-3872
8.63E+07	3.42E-02	6.10E-05	10/19/20	4:55:00 PM	2138	-3510
8.21E+07	3.28E-02	6.10E-05	10/19/20	5:01:00 PM	-988	553
8.40E+07	3.29E-02	6.10E-05	10/19/20	5:06:00 PM	-1665	-120
8.40E+07	3.27E-02	6.10E-05	10/19/20	5:08:00 PM	-3376	112
8.37E+07	3.29E-02	6.10E-05	10/19/20	5:11:00 PM	-3270	1160
8.09E+07	3.30E-02	2.13E-05	10/24/20	2:07:00 PM	-268	-2030

7.99E+07	3.29E-02	2.13E-05	10/24/20	2:10:00 PM	-125	-2014
8.06E+07	3.28E-02	2.13E-05	10/24/20	2:13:00 PM	11	-1980
8.03E+07	3.28E-02	2.13E-05	10/24/20	2:17:00 PM	-55	-1860
8.22E+07	3.38E-02	2.13E-05	10/24/20	2:20:00 PM	-350	-1877
7.96E+07	3.28E-02	2.13E-05	10/24/20	2:23:00 PM	-433	-1967
8.20E+07	3.30E-02	2.13E-05	10/24/20	2:27:00 PM	1219	-1612
8.08E+07	3.29E-02	2.13E-05	10/24/20	2:30:00 PM	1919	-1671
8.21E+07	3.30E-02	2.13E-05	10/24/20	2:33:00 PM	1427	-2358
8.15E+07	3.29E-02	2.13E-05	10/24/20	2:36:00 PM	1597	-3087
8.08E+07	3.28E-02	2.13E-05	10/24/20	2:39:00 PM	1409	-4303
8.11E+07	3.28E-02	2.13E-05	10/24/20	2:43:00 PM	1314	-1407
8.21E+07	3.32E-02	2.13E-05	10/24/20	2:46:00 PM	1462	-2361
8.48E+07	3.36E-02	2.13E-05	10/24/20	2:50:00 PM	2678	-478
8.33E+07	3.36E-02	2.13E-05	10/24/20	2:53:00 PM	2854	-1486
8.26E+07	3.31E-02	2.13E-05	10/24/20	2:56:00 PM	3166	-2199
8.25E+07	3.31E-02	2.13E-05	10/24/20	3:00:00 PM	2987	-3319
8.18E+07	3.29E-02	2.13E-05	10/24/20	3:03:00 PM	3104	-4420
7.57E+07	3.26E-02	2.13E-05	10/24/20	3:07:00 PM	4414	58
8.02E+07	3.33E-02	2.13E-05	10/24/20	3:10:00 PM	4219	-1765
7.89E+07	3.31E-02	2.13E-05	10/24/20	3:14:00 PM	5095	-2686
7.90E+07	3.32E-02	2.13E-05	10/24/20	3:17:00 PM	4991	-695
7.92E+07	3.34E-02	2.13E-05	10/24/20	3:20:00 PM	5843	-1514
7.38E+07	3.20E-02	2.13E-05	10/24/20	3:24:00 PM	3582	1259
7.45E+07	3.22E-02	2.13E-05	10/24/20	3:28:00 PM	4916	1005
7.33E+07	3.19E-02	2.13E-05	10/24/20	3:31:00 PM	4421	2402
7.41E+07	3.20E-02	2.13E-05	10/24/20	3:34:00 PM	5563	2248

8.40E+07	3.31E-02	2.13E-05	10/24/20	3:38:00 PM	-670	2230
9.81E+07	3.72E-02	2.13E-05	10/24/20	3:42:00 PM	-287	3182
9.38E+07	3.67E-02	2.13E-05	10/24/20	3:45:00 PM	-1875	3261
9.08E+07	3.59E-02	2.13E-05	10/24/20	3:48:00 PM	-1040	3718
7.69E+07	3.28E-02	2.13E-05	10/24/20	3:52:00 PM	-262	-2106
7.99E+07	3.36E-02	2.13E-05	10/24/20	3:55:00 PM	-188	-2138
7.57E+07	3.26E-02	2.13E-05	10/24/20	3:58:00 PM	-141	-2199
7.51E+07	3.25E-02	2.13E-05	10/24/20	4:02:00 PM	-275	-2223
1.81E+07	7.21E-02	2.13E-05	10/24/20	4:07:00 PM	-2074	2408
8.34E+07	3.46E-02	2.13E-05	10/24/20	4:10:00 PM	-2280	2314
8.48E+07	3.56E-02	2.13E-05	10/24/20	4:13:00 PM	-2252	1086
7.69E+07	3.35E-02	2.13E-05	10/24/20	4:17:00 PM	-5163	1574
8.89E+07	3.72E-02	2.13E-05	10/24/20	4:20:00 PM	-4114	2282
7.97E+07	3.35E-02	2.13E-05	10/24/20	4:23:00 PM	-3579	3154
1.59E+08	6.82E-02	2.13E-05	10/24/20	4:28:00 PM	-3832	26
1.46E+08	6.42E-02	2.13E-05	10/24/20	4:31:00 PM	-3813	1
1.11E+08	4.82E-02	2.13E-05	10/24/20	4:34:00 PM	-3759	61
1.11E+08	4.68E-02	2.13E-05	10/24/20	4:37:00 PM	-3743	-42
1.11E+08	4.54E-02	2.13E-05	10/24/20	4:42:00 PM	-3444	-1180
1.09E+08	4.42E-02	2.13E-05	10/24/20	4:45:00 PM	-3424	-1180
1.09E+08	4.48E-02	2.13E-05	10/24/20	4:48:00 PM	-3424	-1200
1.06E+08	4.27E-02	2.13E-05	10/24/20	4:51:00 PM	-3444	-1200
8.02E+07	3.09E-02	2.13E-05	10/24/20	4:55:00 PM	2230	4346
8.98E+07	3.47E-02	2.13E-05	10/24/20	4:58:00 PM	1611	4764
1.39E+08	5.49E-02	2.13E-05	10/24/20	5:02:00 PM	4511	4568
9.93E+07	3.84E-02	2.13E-05	10/24/20	5:05:00 PM	3687	5215

7.63E+07	2.97E-02	2.13E-05	10/24/20	5:08:00 PM	2631	5806
7.53E+07	2.94E-02	2.13E-05	10/24/20	5:11:00 PM	2661	5731
1.06E+08	4.24E-02	2.13E-05	10/24/20	5:15:00 PM	1790	5690
7.99E+07	3.10E-02	2.13E-05	10/24/20	5:18:00 PM	2218	4324
7.51E+07	3.03E-02	2.13E-05	10/24/20	5:21:00 PM	2204	4383
9.68E+07	3.79E-02	2.13E-05	10/24/20	5:25:00 PM	3693	5235
9.73E+07	3.83E-02	2.13E-05	10/24/20	5:28:00 PM	3712	5256
7.61E+07	2.98E-02	2.13E-05	10/24/20	5:32:00 PM	2659	5829
7.72E+07	3.02E-02	2.13E-05	10/24/20	5:35:00 PM	2607	5818
7.61E+07	2.96E-02	2.13E-05	10/24/20	5:38:00 PM	2612	5784
7.62E+07	3.01E-02	2.13E-05	10/24/20	5:41:00 PM	2703	5775
7.79E+07	3.05E-02	2.13E-05	10/24/20	5:44:00 PM	2583	5821
3.75E+06			10/24/20	5:49:00 PM	-458	-95
3.65E+06			10/24/20	5:52:00 PM	-462	48
3.66E+06			10/24/20	6:00:00 PM	-653	-83
3.91E+06			10/24/20	6:03:00 PM	-686	-251
3.64E+06			10/24/20	6:06:00 PM	-627	-488
8.33E+07	3.39E-02	2.13E-05	10/24/20	6:11:00 PM	-329	-2084
8.27E+07	3.40E-02	2.13E-05	10/24/20	6:14:00 PM	-360	-2066
8.27E+07	3.39E-02	2.13E-05	10/24/20	6:17:00 PM	-443	-2010
8.30E+07	3.39E-02	2.13E-05	10/24/20	6:20:00 PM	-427	-1943
4.66E+06			10/27/20	9:34:00 AM	-66	819
4.89E+06			10/27/20	9:37:00 AM	-46	819
5.17E+06			10/27/20	9:40:00 AM	-46	799
5.30E+06			10/27/20	9:43:00 AM	-66	799

9.04E+07	3.07E-02	1.13E-04	10/27/20	9:47:00 AM	-2097	-63
9.79E+07	3.32E-02	1.13E-04	10/27/20	9:50:00 AM	-1292	-64
1.01E+08	3.53E-02	1.13E-04	10/27/20	9:53:00 AM	-293	-14
1.02E+08	3.49E-02	1.13E-04	10/27/20	9:57:00 AM	-620	-753
4.68E+06			10/27/20	##########	-56	719
4.80E+06			10/27/20	##########	-36	719
5.07E+06			10/27/20	##########	-54	717
5.19E+06			10/27/20	##########	-56	699
5.04E+06			10/27/20	##########	-25	727
4.51E+06			10/27/20	1:53:00 PM	-9	825
4.84E+06			10/27/20	1:56:00 PM	-9	805
4.88E+06			10/27/20	1:59:00 PM	-9	785
4.92E+06			10/27/20	2:02:00 PM	-9	765
8.94E+07	3.35E-02	1.62E-04	10/27/20	2:05:00 PM	3287	5114
8.89E+07	3.37E-02	1.62E-04	10/27/20	2:08:00 PM	4554	5145
9.07E+07	3.39E-02	1.62E-04	10/27/20	2:11:00 PM	6060	5041
8.83E+07	3.38E-02	1.62E-04	10/27/20	2:14:00 PM	2222	6373
8.79E+07	3.39E-02	1.62E-04	10/27/20	2:17:00 PM	650	2439
8.78E+07	3.38E-02	1.62E-04	10/27/20	2:20:00 PM	1783	2231
8.90E+07	3.41E-02	1.62E-04	10/27/20	2:23:00 PM	2750	2352
8.87E+07	3.39E-02	1.62E-04	10/27/20	2:26:00 PM	4955	2582

8.09E+07	3.29E-02	1.62E-04	10/27/20	2:29:00 PM	-806	1751
8.13E+07	3.30E-02	1.62E-04	10/27/20	2:32:00 PM	522	1590
8.10E+07	3.29E-02	1.62E-04	10/27/20	2:34:00 PM	1726	1444
8.08E+07	3.28E-02	1.62E-04	10/27/20	2:37:00 PM	3022	1216
4.18E+06			10/27/20	2:40:00 PM	-140	724
4.23E+06			10/27/20	2:43:00 PM	-142	766
3.99E+06			10/27/20	2:46:00 PM	-274	777
4.05E+06			10/27/20	2:49:00 PM	-311	772
8.62E+07	3.46E-02	6.33E-05	10/27/20	2:52:00 PM	3533	-406
8.53E+07	3.44E-02	6.33E-05	10/27/20	2:55:00 PM	4906	-431
8.55E+07	3.43E-02	6.33E-05	10/27/20	2:58:00 PM	4526	-1450
8.51E+07	3.42E-02	6.33E-05	10/27/20	3:01:00 PM	5435	-1469
9.57E+07	3.57E-02	6.33E-05	10/27/20	3:04:00 PM	-1643	-3723
9.82E+07	3.62E-02	6.33E-05	10/27/20	3:07:00 PM	-1433	-4581
9.94E+07	3.67E-02	6.33E-05	10/27/20	3:10:00 PM	-1403	-5614
9.67E+07	3.59E-02	6.33E-05	10/27/20	3:13:00 PM	-1407	-6221
8.80E+07	3.38E-02	6.33E-05	10/27/20	3:18:00 PM	2485	-1168
8.84E+07	3.40E-02	6.33E-05	10/27/20	3:21:00 PM	2084	-2158
8.79E+07	3.38E-02	6.33E-05	10/27/20	3:24:00 PM	1322	-1710
8.82E+07	3.37E-02	6.33E-05	10/27/20	3:27:00 PM	1637	-176

4.04E+06	10/27/20	3:30:00 PM	-253	681
4.11E+06	10/27/20	3:33:00 PM	-260	643
4.15E+06	10/27/20	3:36:00 PM	-197	657
4.19E+06	10/27/20	3:39:00 PM	-210	626

DTFA-X	DTFA-Y	Mass	L2p-bkg	H1-bkg	Sample Name	Chamber Pressure
-7	1	899155	850190	87932	Al-mesh/#1	3.50E-08
-6	1	899155	850190	87932	Al-mesh/#1	3.40E-08
-6	0	899155	850190	87932	Al-mesh/#1	3.50E-08
-5	0	899155	850190	87932	Al-mesh/#1	3.40E-08
-7	-1	899155	850190	87932	Al-mesh/#1	3.40E-08
-7	0	899155	850190	87932	Al-mesh/#1	3.40E-08
-5	2	899155	850190	87932	Al-mesh/#1	3.40E-08
-1	2	899155	850190	87932	Al-mesh/#1	3.40E-08
-7	-1	899155	850190	87932	Al-mesh/#1	3.40E-08
-8	-1	899155	850190	87932	Al-mesh/#1	3.40E-08
-7	0	899155	850190	87932	Al-mesh/#1	3.40E-08
-6	1	899155	850190	87932	Al-mesh/#1	3.40E-08
-8	-3	899155	850190	87932	Al-mesh/#1	3.40E-08
-8	-3	899155	850190	87932	Al-mesh/#1	3.40E-08
-8	-6	899155	850190	87932	Al-mesh/#1	3.30E-08
-9	-5	899155	850190	87932	Al-mesh/#1	3.40E-08
-7	-2	899155	850190	87932	Al-mesh/#1	3.30E-08
-6	-2	899155	850190	87932	Al-mesh/#1	3.40E-08
-8	-3	899155	850190	87932	Al-mesh/#1	3.40E-08
-8	-4	899155	850190	87932	Al-mesh/#1	3.40E-08

-5	-4	899155	850190	87932	Al-mesh/#1	3.40E-08
-6	-4	899155	850190	87932	Al-mesh/#1	3.40E-08
-5	-3	899155	850190	87932	Al-mesh/#1	3.40E-08
-7	-2	899155	850190	87932	Al-mesh/#1	3.40E-08
-6	-2	899155	850190	87932	Al-mesh/#1	3.40E-08
-6	-3	899155	850190	87932	Al-mesh/#1	3.40E-08
-6	-3	899155	850190	87932	Al-mesh/#1	3.30E-08
-7	0	899155	850190	87932	Al-mesh/#1	3.40E-08
-6	0	899155	850190	87932	Al-mesh/#1	3.40E-08
-5	1	899155	850190	87932	Al-mesh/#1	3.40E-08
-5	2	899155	850190	87932	Al-mesh/#1	3.30E-08
-7	1	899155	850190	87932	Al-mesh/#1	3.40E-08
-6	0	899155	850190	87932	Al-mesh/#1	3.40E-08
-6	1	899155	850190	87932	Al-mesh/#1	3.40E-08
-5	0	899155	850190	87932	Al-mesh/#1	3.40E-08
-6	1	899155	850190	87932	Al-mesh/#1	3.30E-08
-5	3	899155	850190	87932	Al-mesh/#1	3.30E-08
-4	4	899155	850190	87932	Al-mesh/#1	3.40E-08
-1	3	899155	850190	87932	Al-mesh/#1	3.30E-08
-7	1	899155	850190	87932	Al-mesh/#1	3.30E-08
-4	4	899155	850190	87932	Al-mesh/#1	3.30E-08
-2	3	899155	850190	87932	Al-mesh/#1	3.30E-08
-2	3	899155	850190	87932	Al-mesh/#1	3.30E-08
-2	3	899155	850190	87932	Al-mesh/#1	3.30E-08
-2	3	899155	850190	87932	Al-mesh/#1	3.30E-08

-6	0	899155	850190	87932	Al-mesh/#1	3.40E-08
-6	0	899155	850190	87932	Al-mesh/#1	3.40E-08
-6	0	899155	850190	87932	Al-mesh/#1	3.40E-08
-5	0	899155	850190	87932	Al-mesh/#1	3.40E-08
-8	3	899155	850190	87932	Al-mesh/#1	3.30E-08
-8	3	899155	850190	87932	Al-mesh/#1	3.30E-08
-8	2	899155	850190	87932	Al-mesh/#1	3.30E-08
-9	2	899155	850190	87932	Al-mesh/#1	3.30E-08
-5	-2	899155	850190	87932	Al-mesh/#1	3.40E-08
-5	-1	899155	850190	87932	Al-mesh/#1	3.30E-08
-3	-2	899155	850190	87932	Al-mesh/#1	3.30E-08
-5	-3	899155	850190	87932	Al-mesh/#1	3.30E-08
-5	0	899155	850190	87932	Al-mesh/#1	3.40E-08
-6	-2	899155	850190	87932	Al-mesh/#1	3.30E-08
-7	2	899155	850190	87932	Al-mesh/#1	3.30E-08
-6	1	899155	850190	87932	Al-mesh/#1	3.30E-08
-5	1	899155	850190	87932	Al-mesh/#1	3.30E-08
-5	3	899155	850190	87932	Al-mesh/#1	3.30E-08
-14	14	899152	860662	87430	Al-mesh/#1	6.30E-08

-16	15	899152	860662	87430	Al-mesh/#1	6.30E-08
-15	13	899152	860662	87430	Al-mesh/#1	6.20E-08
-14	14	899152	860662	87430	Al-mesh/#1	6.20E-08
-11	14	899152	860662	87430	Al-mesh/#1	6.10E-08
-14	14	899152	860662	87430	Al-mesh/#1	6.00E-08
-16	14	899152	860662	87430	Al-mesh/#1	5.90E-08
-17	14	899152	860662	87430	Al-mesh/#1	5.90E-08
-19	14	899152	860662	87430	Al-mesh/#1	5.80E-08
-20	14	899152	860662	87430	Al-mesh/#1	5.80E-08
-19	12	899152	860662	87430	Al-mesh/#1	5.70E-08
-16	13	899152	860662	87430	Al-mesh/#1	5.60E-08
-19	15	899152	860662	87430	Al-mesh/#1	5.50E-08
-13	14	899152	860662	87430	Al-mesh/#1	5.50E-08
-19	15	899152	860662	87430	Al-mesh/#1	5.50E-08
-20	15	899152	860662	87430	Al-mesh/#1	5.50E-08
-21	16	899152	860662	87430	Al-mesh/#1	5.40E-08
-23	15	899152	860662	87430	Al-mesh/#1	5.40E-08
-18	16	899152	860662	87430	Al-mesh/#1	5.30E-08
-21	16	899152	860662	87430	Al-mesh/#1	5.20E-08
-17	16	899152	860662	87430	Al-mesh/#1	5.20E-08
-13	16	899152	860662	87430	Al-mesh/#1	5.20E-08
-16	16	899152	860662	87430	Al-mesh/#1	5.10E-08
-6	15	899152	860662	87430	Al-mesh/#1	5.00E-08
-9	15	899152	860662	87430	Al-mesh/#1	5.00E-08
-5	15	899152	860662	87430	Al-mesh/#1	5.00E-08
-7	14	899152	860662	87430	Al-mesh/#1	5.00E-08

-4	16	899152	860662	87430	Al-mesh/#1	4.90E-08
1	17	899152	860662	87430	Al-mesh/#1	4.80E-08
-2	14	899152	860662	87430	Al-mesh/#1	4.80E-08
-3	15	899152	860662	87430	Al-mesh/#1	4.80E-08
0	15	899152	860662	87430	Al-mesh/#1	4.70E-08
4	15	899152	860662	87430	Al-mesh/#1	4.70E-08
-2	15	899152	860662	87430	Al-mesh/#1	4.70E-08
-1	14	899152	860662	87430	Al-mesh/#1	4.60E-08
-19	11	899152	860662	87430	Al-mesh/#1	4.60E-08
-14	15	899152	860662	87430	Al-mesh/#1	4.50E-08
-16	16	899152	860662	87430	Al-mesh/#1	4.50E-08
-9	13	899152	860662	87430	Al-mesh/#1	4.50E-08
-12	13	899152	860662	87430	Al-mesh/#1	4.50E-08
-7	13	899152	860662	87430	Al-mesh/#1	4.40E-08
-15	14	899152	860662	87430	Al-mesh/#1	4.50E-08
-15	14	899152	860662	87430	Al-mesh/#1	4.50E-08
-16	14	899152	860662	87430	Al-mesh/#1	4.50E-08
-16	15	899152	860662	87430	Al-mesh/#1	4.50E-08
-6	16	899152	860662	87430	Al-mesh/#1	4.40E-08
-8	16	899152	860662	87430	Al-mesh/#1	4.40E-08
-7	15	899152	860662	87430	Al-mesh/#1	4.30E-08
-8	15	899152	860662	87430	Al-mesh/#1	4.40E-08
-7	18	899152	860662	87430	Al-mesh/#1	4.30E-08
-6	17	899152	860662	87430	Al-mesh/#1	4.30E-08
-8	15	899152	860662	87430	Al-mesh/#1	4.20E-08
-7	14	899152	860662	87430	Al-mesh/#1	4.20E-08

-1	17	899152	860662	87430	Al-mesh/#1	4.20E-08
-4	17	899152	860662	87430	Al-mesh/#1	4.20E-08
3	18	899152	860662	87430	Al-mesh/#1	4.20E-08
-6	18	899152	860662	87430	Al-mesh/#1	4.10E-08
-5	19	899152	860662	87430	Al-mesh/#1	4.10E-08
-5	15	899152	860662	87430	Al-mesh/#1	4.10E-08
-6	15	899152	860662	87430	Al-mesh/#1	4.10E-08
-3	15	899152	860662	87430	Al-mesh/#1	4.00E-08
-3	16	899152	860662	87430	Al-mesh/#1	4.00E-08
-3	15	899152	860662	87430	Al-mesh/#1	4.00E-08
-4	15	899152	860662	87430	Al-mesh/#1	4.00E-08
0	16	899152	860662	87430	Al-mesh/#1	4.00E-08
-11	16	899152	860662	87430	Al-mesh/#1	4.00E-08
-12	16	899152	860662	87430	Al-mesh/#1	3.90E-08
-7	17	899152	860662	87430	Al-mesh/#1	3.90E-08
-12	17	899152	860662	87430	Al-mesh/#1	3.90E-08
-9	17	899152	860662	87430	Al-mesh/#1	3.90E-08
-7	16	899152	860662	87430	Al-mesh/#1	3.80E-08
-6	16	899152	860662	87430	Al-mesh/#1	3.80E-08
-3	16	899152	860662	87430	Al-mesh/#1	3.80E-08
-8	16	899152	860662	87430	Al-mesh/#1	3.70E-08
3	4	899159	878790	87501	Al-mesh/#1	3.70E-08
3	2	899159	878790	87501	Al-mesh/#1	3.60E-08
2	1	899159	878790	87501	Al-mesh/#1	3.60E-08
2	1	899159	878790	87501	Al-mesh/#1	3.60E-08

8	1	899159	878790	87501	Al-mesh/#1	3.60E-08
6	-1	899159	878790	87501	Al-mesh/#1	3.60E-08
3	0	899159	878790	87501	Al-mesh/#1	3.60E-08
4	2	899159	878790	87501	Al-mesh/#1	3.50E-08
1	0	899159	878790	87501	Al-mesh/#1	3.60E-08
1	1	899159	878790	87501	Al-mesh/#1	3.60E-08
1	0	899159	878790	87501	Al-mesh/#1	3.60E-08
-1	-1	899159	878790	87501	Al-mesh/#1	3.60E-08
1	0	899159	878790	87501	Al-mesh/#1	3.50E-08
-7	2	899159	878790	87501	Al-mesh/#1	3.40E-08
-7	1	899159	878790	87501	Al-mesh/#1	3.40E-08
-6	0	899159	878790	87501	Al-mesh/#1	3.50E-08
-6	0	899159	878790	87501	Al-mesh/#1	3.40E-08
-12	-2	899159	878790	87501	Al-mesh/#1	3.40E-08
-12	-4	899159	878790	87501	Al-mesh/#1	3.30E-08
-13	-9	899159	878790	87501	Al-mesh/#1	3.40E-08
-9	1	899159	878790	87501	Al-mesh/#1	3.30E-08
-8	0	899159	878790	87501	Al-mesh/#1	3.30E-08
-10	1	899159	878790	87501	Al-mesh/#1	3.30E-08
-11	0	899159	878790	87501	Al-mesh/#1	3.30E-08
-17	0	899159	878790	87501	Al-mesh/#1	3.30E-08

-6	0	899159	878790	87501	Al-mesh/#1	3.30E-08
-9	1	899159	878790	87501	Al-mesh/#1	3.30E-08
-11	1	899159	878790	87501	Al-mesh/#1	3.30E-08
-13	1	899159	878790	87501	Al-mesh/#1	3.30E-08
-7	1	899159	878790	87501	Al-mesh/#1	3.30E-08
-8	0	899159	878790	87501	Al-mesh/#1	3.30E-08
-8	0	899159	878790	87501	Al-mesh/#1	3.30E-08
-7	1	899159	878790	87501	Al-mesh/#1	3.30E-08
-16	2	899159	878790	87501	Al-mesh/#1	3.30E-08
-20	4	899159	878790	87501	Al-mesh/#1	3.30E-08
-18	2	899159	878790	87501	Al-mesh/#1	3.30E-08
-19	4	899159	878790	87501	Al-mesh/#1	3.30E-08
-8	5	899159	878790	87501	Al-mesh/#1	3.30E-08
-9	4	899159	878790	87501	Al-mesh/#1	3.30E-08
-11	4	899159	878790	87501	Al-mesh/#1	3.30E-08
-11	4	899159	878790	87501	Al-mesh/#1	3.30E-08
-13	0	899159	878790	87501	Al-mesh/#1	3.30E-08
-13	3	899159	878790	87501	Al-mesh/#1	3.30E-08
-13	0	899159	878790	87501	Al-mesh/#1	3.30E-08
-12	-2	899159	878790	87501	Al-mesh/#1	3.30E-08

-7	-1	899159	878790	87501	Al-mesh/#1	3.20E-08
-7	-2	899159	878790	87501	Al-mesh/#1	3.20E-08
-7	-2	899159	878790	87501	Al-mesh/#1	3.20E-08
-7	-2	899159	878790	87501	Al-mesh/#1	3.20E-08

Comment

larger 2SE

larger OH

crack

larger 2SE

larger 2SE

larger 2SE

larger 2SE

epoxy

larger OH

weird grain, larger OH
weird grain, larger OH
weird grain
weird grain

larger OH
larger OH
larger OH

larger OH

lower cps
larger OH
larger OH

larger 2SE, lower cps, larger OH

Calculation of matrix bias effects in antigorite RMs

RM	Serpentine	Mg# (mole %)	LF $\delta^{18}O_{V\text{-}SMOW}$ (‰)	LF 2 SE (‰)
Serpentine				
UWSrp-8	Atg	77.5	6.45	0.11
UWSrp-5	Atg	90.4	8.88	0.05
UWSrp-4	Atg	91.9	7.52	0.12
UWSrp-1 (normalizing)	**Atg**	**94.8**	**8.38**	**0.04**
UWSrp-9	Atg	98.3	2.36	0.11
UWSrp-6	Atg	97.8	5.59	0.19
UWSrp-7	Atg	99.5	3.69	0.18
SSE				
RMSE				
MSWD				

Reference values of standards used to standardize laser fluorination analyses of serpentine refe

RM	Mineral	LF $\delta^{18}O_{V\text{-}SMOW}$ (‰)	LF 2 SE (‰)	Lab
UWG-2	Grt	5.80	0.01	
UWC-3	Cal	12.49	0.02	UW-Madison
NBS-28	Qtz	9.51	0.09	

Fitting parameters	a	b	SSE	R-square
WI-STD-97	0.096764	-9.3793	0.21	0.94
UWSrp-GGR2020	0.116913	-11.2253	0.12	0.97
Srp STD 1b	0.095328	-9.0816	0.42	0.87

Calculation of matrix bias effects in the lizardite and chrysotile RM

RM	Serpentine	Mg# (mole %)	LF $\delta^{18}O_{V\text{-}SMOW}$ (‰)	LF 2 SE (‰)
L3431	Lz	98.3	5.32	0.10

C22908	Ctl	98.05	4.66	0.02
Working RM				
UWSrp-1	Atg	94.8	8.38	0.04
UWC-3				

bias* (UWSrp-1)	2 SE	WI-STD- 2σ (‰)
-1.83	0.10	0.20
-0.70	0.10	0.17
-0.71	0.06	0.19
0.00	**0.09**	**0.13**
-0.10	0.19	0.25
0.32	0.17	0.29
0.27	0.20	0.30
-0.39		

ence materials.

Analyzed serpentine samples
all serpentine samples
only samples bracketed by UWC-3
all serpentine samples

Adjusted R-square	2 RMSE	MSWD
0.91	0.41	2.99
0.96	0.31	2.93
0.78	0.65	3.17

average $\delta^{18}O$ RAW (‰)	bias bracket UWSrp-1 (‰)	bias(x) (‰)
9.55	4.89	5.03

8.70	5.03	5.14

-97 (S1)

fit	residuals	weighted residuals	bias* (UWSrp-1)
-1.88	0.00	11.08	-2.17
-0.63	0.00	0.34	-0.59
-0.49	0.05	0.05	-0.67
-0.21	0.04	0.26	**0.00**
0.13	0.05	1.08	0.18
0.08	0.06	0.78	0.41
0.25	0.00	1.38	0.28
	0.21		-0.37
	0.20		
		2.99	

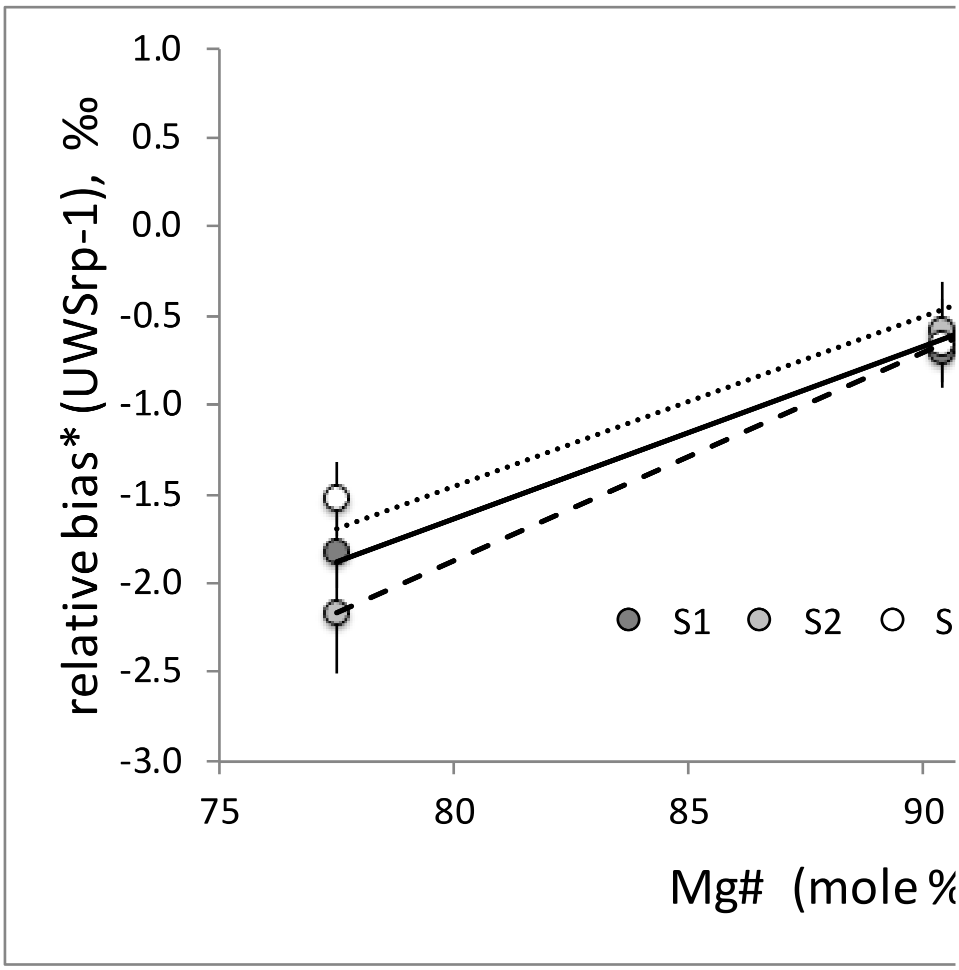

WI-STD-97 (S1)

δ^{18}O VSMOW relative to UWSrp-1 (‰)	bias(*x*) (‰)	2SE	2σ (‰)
4.50	-0.81	0.19	0.48

3.54	-1.11	0.21	0.47
		0.10	
		0.07	

	UWSrp-GGR2020 (S2)	
2 SE	**2σ (‰)**	**fit**
0.27	0.34	-2.16
0.22	0.28	-0.66
0.35	0.40	-0.48
0.13	**0.17**	-0.14
0.25	0.32	0.27
0.18	0.31	0.21
0.15	0.29	0.41

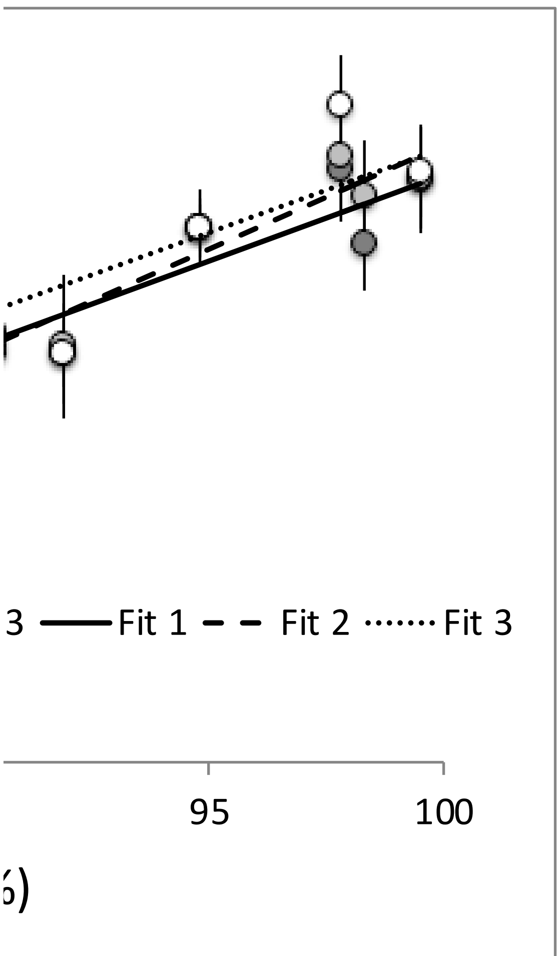

average δ^{18}O RAW (‰)	bias bracket UWSrp-1 (‰)	bias(x) (‰)
8.79	4.73	5.00

8.78	4.73	4.97

residuals	weighted residuals	bias* (UWSrp-1)	2 SE
0.00	9.60	-1.53	0.06
0.00	0.30	-0.65	0.18
0.03	0.03	-0.71	0.19
0.02	0.30	**0.00**	**0.13**
0.01	1.27		
0.04	1.06	0.69	0.13
0.02	2.10	0.32	0.09
0.12		-0.31	
0.16			
	2.93		

UWSrp-GGR2020 (S2)

$\delta^{18}O$ VSMOW relative to UWSrp-1 (‰)	bias(*x*) (‰)	2SE	2σ (‰)
3.77	-1.54	0.22	0.44

3.79	-0.86	0.30	0.47
		0.15	

	Srp STD 1b (S3)	
2σ (‰)	**fit**	**residuals**
0.21	-1.69	0.03
0.25	-0.46	0.04
0.28	-0.32	0.15
0.22	-0.04	0.00
	0.29	
0.28	0.24	0.20
0.26	0.40	0.01
		0.42
		0.32

average δ[18]O RAW (‰)	**bias bracket UWC-3 (‰)**	**bias UWC-3/UWSrp-1 (‰)**
8.88	-10.29	-14.78

weighted residuals
9.18
0.09
0.00
0.33
1.09
1.98

3.17

Srp STD 1b (S3)

bias(x) (‰)	δ^{18}O VSMOW relative to UWSrp-1 (‰)	bias(x) (‰)	2SE
4.85	4.02	-1.29	0.14

0.15

0.10
0.09

2σ (‰)
0.71

SIMS session	Mount I.D.	File	Analysis I.D.	$\delta^{18}O$ ‰ (RAW)	2SE (int.)
S1 (28 September 2018)					
	UW-Talc				
	Talc RM				
		20180928(	UWC3-1	2.27	0.48
		20180928(	UWC3-2	2.63	0.54
		20180928(	UWC3-3	2.59	0.51
		20180928(	UWC3-4	2.67	0.45
		20180928(	UWT1-gr1	9.26	0.15
		20180928(	UWT1-gr2	5.57	1.50
		20180928(	UWT1-gr3	8.34	0.16
		20180928(	UWT1-gr4	8.89	0.17
		20180928(	UWT1-gr5	8.87	0.14
		20180928(	UWT1-gr6	8.54	0.21
		20180928(	UWT1-gr7	9.04	0.20
		20180928(	UWT1-gr8	8.81	0.18
		20180928(	UWT1-gr9	8.59	0.11
		20180928(	UWT1-gr10	8.76	0.22
		20180928(	UWC3-5	2.78	0.47
		20180928(	UWC3-6	2.71	0.52
		20180928(	UWC3-7	2.56	0.47
		20180928(	UWC3-8	2.73	0.50
			average and 2SD	2.70	0.19
			bracket average and 2SD	**2.62**	**0.32**
			2SE		**0.11**
		20180928(	UWT1-gr11	8.88	0.15
		20180928(	UWT1-gr12	8.47	0.12
		20180928(	UWT1-gr13	9.43	0.18
		20180928(	UWT1-gr14	9.56	0.10
		20180928(	UWT1-gr15	6.33	0.77
		20180928(	UWT1-gr15b	7.61	0.27
		20180928(	UWT1-gr17	9.12	0.14
		20180928(	UWT1-gr1b	8.98	0.16
		20180928(	UWT1-gr2b	8.47	0.18
		20180928(	UWT1-gr3b	8.85	0.12
		20180928(	UWC3-9	2.76	0.52
		20180928(	UWC3-9	2.57	0.55

20180928(	UWC3-9	2.61	0.45
20180928(	UWC3-9	2.82	0.51
	average and 2SD	2.69	0.23
	bracket average and 2SD	**2.69**	**0.20**
	2SE		**0.07**
20180928(	UWT1-gr4b	8.90	0.16
20180928(	UWT1-gr5b	8.85	0.15
20180928(	UWT1-gr8b	8.80	0.10
20180928(	UWT1-gr7b	9.03	0.21
20180928(	UWT1-gr9b	5.40	0.57
20180928(	UWT1-gr10b	8.70	0.14
20180928(	UWT1-gr11b	8.47	0.21
20180928(	UWT1-gr16	8.91	0.15
20180928(	UWT1-gr16b	9.02	0.13
20180928(	UWT1-gr14b	8.64	0.14
	average and 2SD	**8.81**	**0.75**
	2SE		**0.14**
20180928(	UWC3-10	2.92	0.50
20180928(	UWC3-10	2.67	0.53
20180928(	UWC3-10	2.87	0.51
20180928(	UWC3-10	2.65	0.47
	average and 2SD	2.78	0.28
	bracket average and 2SD	**2.73**	**0.26**
	2SE		**0.09**

S2 (10 December 2018)

Talc STD 1b

Talc RM

20181208(	UWC3-5	2.63	0.47
20181208(	UWC3-6	2.53	0.42
20181208(	UWC3-7	2.44	0.46
20181208(	UWC3-8	2.56	0.47
20181208(	UWT1-1	8.63	0.14
20181208(	UWT1-2	8.31	0.18
20181208(	UWT1-3	8.35	0.14
20181208(	UWT1-4	8.24	0.15
20181208(	UWT1-5	8.27	0.15

20181208(	UWT1-6	7.79	0.16
20181208(	UWT1-7	7.27	0.13
20181208(	UWT1-8	7.88	0.21
20181208(	UWT1-9	8.31	0.17
20181208(	UWT1-10	7.48	0.15
20181208(	UWC3-9	2.81	0.53
20181208(	UWC3-10	2.79	0.43
20181208(	UWC3-11	2.75	0.53
20181208(	UWC3-12	2.83	0.51
	average and 2SD	2.80	0.07
	bracket average and 2SD	**2.67**	**0.30**
	2SE		**0.10**
20181208(	UWT1-11	8.10	0.20
20181208(	UWT1-12	8.42	0.10
20181208(	UWT1-13	8.31	0.11
20181208(	UWT1-14	8.23	0.20
20181208(	UWT1-15	8.31	0.13
20181208(	UWT1-16	7.56	0.16
20181208(	UWT1-17	3.93	0.25
20181208(	UWT1-18	7.73	0.17
20181208(	UWT1-19	7.26	0.16
20181208(	UWT1-20	7.68	0.16
	average and 2SD (perpendicular)	**8.32**	**0.27**
	average and 2SD (parallel)	**7.66**	**0.65**
	orientation effect		
	2SE (perpendicular)		**0.09**
	2SE (parallel)		**0.22**
20181208(	UWC3-13	2.62	0.48
20181208(	UWC3-14	2.78	0.49
20181208(	UWC3-15	2.78	0.48
20181208(	UWC3-16	2.44	0.46
	average and 2SD	2.65	0.33
	bracket average and 2SD	**2.72**	**0.27**
	2SE		**0.09**

S3 (19 October 2020)

Talc STD 1b

Talc RM

20201019(	Tlc STD 1b-UWC-3-gr1	3.04	0.61
20201019(	Tlc STD 1b-UWC-3-gr1	3.30	0.51
20201019(	Tlc STD 1b-UWC-3-gr1	3.44	0.52
20201019(	Tlc STD 1b-UWC-3-gr1	3.22	0.52
20201019(	Tlc STD 1b-UWT-1-gr3	8.62	0.16
20201019(	Tlc STD 1b-UWT-1-gr3	8.11	0.19
20201019(	Tlc STD 1b-UWT-1-gr4	8.60	0.19
20201019(	Tlc STD 1b-UWT-1-gr4	9.02	0.19
20201019(	Tlc STD 1b-UWT-1-gr6	7.60	0.15
20201019(	Tlc STD 1b-UWT-1-gr3	7.61	0.14
20201019(	Tlc STD 1b-UWT-1-gr4	8.61	0.16
	average and 2SD (parallel)	**8.43**	**0.99**
	bias*(UWC-3)		
	2SE		**0.40**
20201019(	Tlc STD 1b-UWT-1-gr7	8.80	0.19
20201019(	Tlc STD 1b-UWT-1-gr7	9.56	0.18
20201019(	Tlc STD 1b-UWT-1-gr8	9.20	0.12
20201019(	Tlc STD 1b-UWT-1-gr8	8.90	0.17
20201019(	Tlc STD 1b-UWT-1-gr10	11.24	0.12
20201019(	Tlc STD 1b-UWT-1-gr10	8.98	0.15
20201019(	Tlc STD 1b-UWT-1-gr11b	10.87	0.11
20201019(	Tlc STD 1b-UWT-1-gr11	9.10	0.18
20201019(	Tlc STD 1b-UWT-1-gr11b	11.58	0.16
	average and 2SD (perpendicular)	**9.09**	**0.54**
	bias*(UWC-3)		
	orientation effect		
	average bias*(UWC-3)		
	2SE		**0.22**
20201019(	Tlc STD 1b-UWC-3-gr1	3.02	0.55
20201019(	Tlc STD 1b-UWC-3-gr1	3.29	0.54
20201019(	Tlc STD 1b-UWC-3-gr1	2.76	0.49
20201019(	Tlc STD 1b-UWC-3-gr1	3.20	0.56
	average and 2SD	3.07	0.47
	bracket average and 2SD	**3.16**	**0.42**
	2SE		**0.15**

S4 (24 October 2020)

Talc STD 1b

Talc RM

20201019(	Tlc STD 1b-UWC-3-gr1	2.53	0.47
20201019(	Tlc STD 1b-UWC-3-gr1	2.42	0.43

20201019(	Tlc STD 1b-UWC-3-gr1	2.42	0.48
20201019(	Tlc STD 1b-UWC-3-gr1	2.35	0.47
20201019(	Tlc STD 1b-UWT-1-gr3	7.68	0.15
20201019(	Tlc STD 1b-UWT-1-gr4	8.07	0.17
20201019(	Tlc STD 1b-UWT-1-gr6	7.65	0.17
20201019(	Tlc STD 1b-UWT-1-gr5	7.73	0.15
20201019(	Tlc STD 1b-UWT-1-gr2	8.17	0.17
20201019(	Tlc STD 1b-UWT-1-gr1	7.93	0.13
	average and 2SD (parallel)	**7.87**	**0.43**
	bias*(UWC-3)		
	2SE		**0.18**
20201019(	Tlc STD 1b-UWT-1-gr7	8.62	0.14
20201019(	Tlc STD 1b-UWT-1-gr8	8.63	0.15
20201019(	Tlc STD 1b-UWT-1-gr10	8.55	0.16
20201019(	Tlc STD 1b-UWT-1-gr10	8.32	0.22
20201019(	Tlc STD 1b-UWT-1-gr11	8.46	0.16
20201019(	Tlc STD 1b-UWT-1-gr11(b)	10.94	0.21
20201019(	Tlc STD 1b-UWT-1-gr8	8.19	0.18
20201019(	Tlc STD 1b-UWT-1-gr10(b)	11.10	0.17
	average and 2SD (perpendicular)	**8.46**	**0.35**
	bias*(UWC-3)		
	orientation effect		
	average bias*(UWC-3)		
	2SE		**0.14**
20201019(	Tlc STD 1b-UWC-3-gr1	2.51	0.38
20201019(	Tlc STD 1b-UWC-3-gr1	2.11	0.45
20201019(	Tlc STD 1b-UWC-3-gr1	2.87	0.44
20201019(	Tlc STD 1b-UWC-3-gr1	2.10	0.48
20201019(	Tlc STD 1b-UWC-3-gr1	2.26	0.39
	average and 2SD	2.24	0.39
	bracket average and 2SD	**2.34**	**0.34**
	2SE		**0.12**

Bias (‰)	$\delta^{18}O$ ‰ (V-SMOW)	2s (ext.)	2σ ‰	^{16}O (Gcps)	^{18}O (Mcps)	IP (nA)	Yield (Gcps/nA)
				4.23		1.91	2.21
				4.22		1.91	2.20
				4.23		1.91	2.21
				4.21		1.92	2.19
				2.54		1.92	1.32
				1.93		1.94	1.00
				2.55		1.92	1.32
				2.53		1.93	1.31
				2.53		1.91	1.32
				2.57		1.91	1.34
				2.57		1.87	1.38
				2.47		1.86	1.33
				2.46		1.91	1.29
				2.46		1.91	1.28
				4.17		1.90	2.20
				4.19		1.90	2.20
				4.19		1.90	2.21
				4.13		1.88	2.20
-9.75	**12.49**						
				2.48		1.87	1.33
				2.40		1.86	1.29
				2.36		1.82	1.29
				2.40		1.84	1.31
				2.09		1.82	1.15
				2.43		1.82	1.34
				2.48		1.80	1.37
				2.45		1.84	1.33
				2.37		1.84	1.29
				2.45		1.83	1.33
				4.04		1.82	2.22
				4.05		1.82	2.22

		4.04	1.82	2.22
		4.04	1.83	2.21
-9.68	**12.49**			
		2.42	1.82	1.33
		2.36	1.81	1.30
		2.35	1.86	1.26
		2.54	1.82	1.40
		2.16	1.84	1.17
		2.38	1.86	1.28
		2.42	1.86	1.30
		2.44	1.87	1.30
		2.43	1.86	1.30
		2.42	1.85	1.31
0.80	**8.00**			
		4.05	1.84	2.21
		4.06	1.84	2.21
		4.07	1.84	2.21
		4.06	1.84	2.20
-9.64	**12.49**			
		4.07	2.07	1.97
		4.07	2.06	1.98
		4.05	2.06	1.97
		3.99	2.04	1.95
		2.51	2.02	1.24
		2.52	2.02	1.24
		2.51	2.03	1.24
		2.50	2.02	1.24
		2.48	2.00	1.24

		2.23	1.95	1.14
		2.17	1.95	1.12
		2.25	1.91	1.18
		2.05	1.94	1.06
		2.19	1.93	1.13
		3.81	1.92	1.98
		3.83	1.93	1.98
		3.84	1.93	1.98
		3.81	1.94	1.97
-9.70	**12.49**			
		2.40	1.93	1.24
		2.38	1.93	1.23
		2.38	1.93	1.23
		2.37	1.92	1.23
		2.35	1.91	1.23
		2.22	1.89	1.17
		2.16	1.88	1.15
		2.20	1.91	1.15
		2.13	1.92	1.11
		2.26	1.95	1.16
0.31	**8.00**			**1.24**
-0.33				**1.13**
0.65				
		3.90	1.97	1.98
		3.88	1.97	1.97
		3.89	1.98	1.97
		3.89	1.97	1.97
-9.65	**12.49**			

		3.81	7.66	1.98	1.93
		3.77	7.59	1.97	1.92
		3.81	7.66	1.96	1.94
		3.94	7.93	2.02	1.95
		2.44	4.94	2.02	1.21
		2.47	5.00	2.01	1.23
		2.37	4.79	2.01	1.18
		2.47	5.00	1.99	1.24
		2.30	4.65	1.98	1.16
		2.37	4.79	1.96	1.21
		2.58	5.21	2.02	1.28
0.43	**8.00**				**1.22**
0.43					
		2.51	5.07	2.01	1.24
		2.49	5.03	2.01	1.23
		2.49	5.04	2.01	1.24
		2.47	5.00	2.01	1.23
		2.43	4.92	1.99	1.22
		2.43	4.92	1.98	1.23
		2.46	5.00	1.98	1.24
		2.39	4.83	1.98	1.21
		2.46	4.99	1.97	1.25
1.08	**8.00**				**1.23**
1.08					
0.66					
0.75					
		3.78	7.61	1.95	1.94
		3.93	7.90	2.01	1.96
		3.98	8.01	2.02	1.97
		3.91	7.87	2.02	1.93
-9.22	**12.49**				
		3.77	7.58	2.00	1.88
		3.84	7.71	2.00	1.92

		3.82	7.67	2.00	1.91
		3.83	7.69	2.00	1.91
		2.42	4.89	1.98	1.22
		2.34	4.73	1.97	1.19
		2.32	4.69	1.96	1.18
		2.33	4.71	1.96	1.19
		2.37	4.79	1.95	1.21
		2.51	5.07	2.01	1.25
-0.13	**8.00**				**1.21**
-0.13					
		2.48	5.01	2.03	1.22
		2.48	5.02	2.03	1.22
		2.44	4.93	2.03	1.20
		2.46	4.98	2.03	1.21
		2.53	5.12	2.03	1.25
		2.42	4.91	2.02	1.20
		2.47	5.00	2.03	1.22
		2.45	4.96	2.03	1.21
0.46	**8.00**				**1.22**
0.46					
0.59					
0.17					
		3.93	7.90	2.02	1.94
		3.80	7.64	2.02	1.88
		3.83	7.71	2.02	1.90
		3.85	7.74	2.02	1.91
		3.86	7.77	2.02	1.92
-10.03	**12.49**				

$^{16}OH/^{16}O$	^{16}OH (cps)	$^{16}OH/^{16}O$ background corrected	2s $^{16}OH/^{16}O$	Date	Time	X
1.44E-03	6.09E+06			9/28/18	########	-386
1.44E-03	6.09E+06			9/28/18	########	-355
1.44E-03	6.09E+06			9/28/18	########	-328
1.44E-03	6.05E+06			9/28/18	########	-302
1.01E-02	2.57E+07	8.61E-03	3.21E-04	9/28/18	########	165
1.33E-02	2.58E+07	1.18E-02	3.21E-04	9/28/18	########	1238
1.04E-02	2.65E+07	8.86E-03	3.21E-04	9/28/18	########	2505
1.01E-02	2.54E+07	8.52E-03	3.21E-04	9/28/18	########	1378
1.01E-02	2.56E+07	8.60E-03	3.21E-04	9/28/18	########	1649
1.01E-02	2.60E+07	8.59E-03	3.21E-04	9/28/18	########	2032
1.03E-02	2.65E+07	8.77E-03	3.21E-04	9/28/18	########	3823
1.01E-02	2.50E+07	8.56E-03	3.21E-04	9/28/18	########	3857
9.98E-03	2.45E+07	8.44E-03	3.21E-04	9/28/18	########	3966
9.88E-03	2.43E+07	8.35E-03	3.21E-04	9/28/18	########	2839
1.90E-03	7.91E+06			9/28/18	########	-368
1.48E-03	6.22E+06			9/28/18	########	-341
1.49E-03	6.23E+06			9/28/18	########	-313
1.63E-03	6.75E+06			9/28/18	########	-374
1.53E-03						
9.97E-03	2.47E+07	8.36E-03	3.35E-04	9/28/18	########	1923
1.01E-02	2.41E+07	8.46E-03	3.35E-04	9/28/18	########	4017
9.64E-03	2.28E+07	8.03E-03	3.35E-04	9/28/18	########	5929
9.68E-03	2.32E+07	8.07E-03	3.35E-04	9/28/18	########	3274
1.12E-02	2.34E+07	9.58E-03	3.35E-04	9/28/18	########	3058
1.08E-02	2.62E+07	9.15E-03	3.35E-04	9/28/18	########	2802
1.01E-02	2.52E+07	8.53E-03	3.35E-04	9/28/18	########	1696
1.01E-02	2.46E+07	8.47E-03	3.35E-04	9/28/18	########	274
9.93E-03	2.36E+07	8.33E-03	3.35E-04	9/28/18	########	1137
9.95E-03	2.43E+07	8.35E-03	3.35E-04	9/28/18	########	1810
1.83E-03	7.41E+06			9/28/18	########	-337
1.52E-03	6.17E+06			9/28/18	########	-317

1.51E-03	6.11E+06			9/28/18	########	-297
1.49E-03	6.00E+06			9/28/18	########	-277

1.61E-03

1.03E-02	2.49E+07	8.82E-03	3.03E-04	9/28/18	########	1693
9.92E-03	2.34E+07	8.43E-03	3.03E-04	9/28/18	########	2259
1.00E-02	2.36E+07	8.56E-03	3.03E-04	9/28/18	########	3678
1.03E-02	2.63E+07	8.83E-03	3.03E-04	9/28/18	########	4311
1.28E-02	2.78E+07	1.14E-02	3.03E-04	9/28/18	########	4499
9.88E-03	2.35E+07	8.39E-03	3.03E-04	9/28/18	########	2963
9.91E-03	2.40E+07	8.42E-03	3.03E-04	9/28/18	########	1976
1.01E-02	2.45E+07	8.58E-03	3.03E-04	9/28/18	########	2248
1.01E-02	2.44E+07	8.57E-03	3.03E-04	9/28/18	########	2299
1.00E-02	2.42E+07	8.52E-03	3.03E-04	9/28/18	########	3684

1.36E-03	5.53E+06			9/28/18	########	-393
1.39E-03	5.63E+06			9/28/18	########	-373
1.40E-03	5.70E+06			9/28/18	########	-353
1.42E-03	5.75E+06			9/28/18	########	-333

1.49E-03

2.51E-04	1.02E+06			12/10/18	########	504
2.57E-04	1.05E+06			12/10/18	########	481
2.57E-04	1.04E+06			12/10/18	########	489
2.74E-04	1.09E+06			12/10/18	########	496

9.51E-03	2.39E+07	9.24E-03	5.28E-05	12/10/18	########	-1015
9.58E-03	2.41E+07	9.31E-03	5.28E-05	12/10/18	########	-1010
9.52E-03	2.39E+07	9.25E-03	5.28E-05	12/10/18	########	-1006
9.54E-03	2.39E+07	9.27E-03	5.28E-05	12/10/18	########	-998
9.54E-03	2.37E+07	9.27E-03	5.28E-05	12/10/18	########	-993

9.41E-03	2.10E+07	9.14E-03	5.28E-05	12/10/18	########	-2828
9.51E-03	2.07E+07	9.24E-03	5.28E-05	12/10/18	########	-2590
9.55E-03	2.15E+07	9.28E-03	5.28E-05	12/10/18	########	-2248
9.50E-03	1.94E+07	9.23E-03	5.28E-05	12/10/18	########	-1811
9.61E-03	2.11E+07	9.34E-03	5.28E-05	12/10/18	########	-2000
3.34E-04	1.27E+06			12/10/18	########	534
2.66E-04	1.02E+06			12/10/18	########	554
2.66E-04	1.02E+06			12/10/18	########	573
2.66E-04	1.01E+06			12/10/18	########	619
2.71E-04						
9.52E-03	2.28E+07	9.25E-03	4.89E-05	12/10/18	########	-2283
9.45E-03	2.25E+07	9.18E-03	4.89E-05	12/10/18	########	-2267
9.56E-03	2.27E+07	9.28E-03	4.89E-05	12/10/18	########	-2177
9.58E-03	2.27E+07	9.31E-03	4.89E-05	12/10/18	########	-2156
9.51E-03	2.23E+07	9.24E-03	4.89E-05	12/10/18	########	-2077
9.64E-03	2.14E+07	9.37E-03	4.89E-05	12/10/18	########	-4400
1.24E-02	2.68E+07	1.21E-02	4.89E-05	12/10/18	########	-4825
9.42E-03	2.07E+07	9.15E-03	4.89E-05	12/10/18	########	-5581
9.42E-03	2.00E+07	9.15E-03	4.89E-05	12/10/18	########	-4642
9.50E-03	2.15E+07	9.23E-03	4.89E-05	12/10/18	########	-4511
2.64E-04	1.03E+06			12/10/18	########	672
2.67E-04	1.04E+06			12/10/18	########	656
2.66E-04	1.04E+06			12/10/18	########	661
2.64E-04	1.03E+06			12/10/18	########	719
2.74E-04						

2.80E-03	1.07E+07			10/19/20	########	802
1.01E-03	3.82E+06			10/19/20	########	822
1.04E-03	3.96E+06			10/19/20	########	822
1.12E-03	4.40E+06			10/19/20	########	802
9.94E-03	2.43E+07	9.94E-03	1.29E-03	10/19/20	########	-5570
9.98E-03	2.47E+07	9.98E-03	1.29E-03	10/19/20	########	-6139
9.94E-03	2.36E+07	9.94E-03	1.29E-03	10/19/20	########	-4440
1.02E-02	2.51E+07	1.02E-02	1.29E-03	10/19/20	########	-4126
9.99E-03	2.30E+07	9.99E-03	1.29E-03	10/19/20	########	-1321
9.91E-03	2.35E+07	9.91E-03	1.29E-03	10/19/20	########	-6294
9.99E-03	2.57E+07	9.99E-03	1.29E-03	10/19/20	########	-5066
		9.99E-03				
1.02E-02	2.55E+07	1.02E-02	1.29E-03	10/19/20	########	2426
1.01E-02	2.52E+07	1.01E-02	1.29E-03	10/19/20	########	3257
1.01E-02	2.51E+07	1.01E-02	1.29E-03	10/19/20	########	1817
1.01E-02	2.50E+07	1.01E-02	1.29E-03	10/19/20	########	2347
3.20E-02	7.76E+07	3.20E-02	1.29E-03	10/19/20	########	2600
1.02E-02	2.47E+07	1.02E-02	1.29E-03	10/19/20	########	2663
3.16E-02	7.78E+07	3.16E-02	1.29E-03	10/19/20	########	6437
1.02E-02	2.43E+07	1.02E-02	1.29E-03	10/19/20	########	6344
3.14E-02	7.73E+07	3.14E-02	1.29E-03	10/19/20	########	6494
		1.01E-02				
9.49E-04	3.59E+06			10/19/20	########	829
9.29E-04	3.65E+06			10/19/20	########	773
9.23E-04	3.68E+06			10/19/20	########	926
9.28E-04	3.63E+06			10/19/20	########	940
1.21E-03						
2.25E-03	8.49E+06			10/24/20	########	706
2.54E-03	9.75E+06			10/24/20	########	681

2.02E-03	7.73E+06			10/24/20	########	635
2.05E-03	7.83E+06			10/24/20	########	676
1.08E-02	2.61E+07	1.08E-02	6.19E-04	10/24/20	########	-6883
1.05E-02	2.45E+07	1.05E-02	6.19E-04	10/24/20	########	-6347
1.03E-02	2.40E+07	1.03E-02	6.19E-04	10/24/20	########	-3929
1.06E-02	2.47E+07	1.06E-02	6.19E-04	10/24/20	########	-4529
1.05E-02	2.49E+07	1.05E-02	6.19E-04	10/24/20	########	-4621
1.07E-02	2.69E+07	1.07E-02	6.19E-04	10/24/20	########	-1694
1.06E-02	2.63E+07	1.06E-02	6.19E-04	10/24/20	########	379
1.07E-02	2.65E+07	1.07E-02	6.19E-04	10/24/20	########	1184
1.05E-02	2.56E+07	1.05E-02	6.19E-04	10/24/20	########	-164
1.05E-02	2.58E+07	1.05E-02	6.19E-04	10/24/20	########	-253
1.05E-02	2.65E+07	1.05E-02	6.19E-04	10/24/20	########	4784
3.22E-02	7.80E+07	3.22E-02	6.19E-04	10/24/20	########	4904
1.06E-02	2.62E+07	1.06E-02	6.19E-04	10/24/20	########	1118
3.23E-02	7.90E+07	3.23E-02	6.19E-04	10/24/20	########	449
2.30E-03	9.03E+06			10/24/20	########	787
1.66E-03	6.32E+06			10/24/20	########	740
1.73E-03	6.65E+06			10/24/20	########	701
1.73E-03	6.64E+06			10/24/20	########	559
1.78E-03	6.90E+06			10/24/20	########	608

2.04E-03

Y	DTFA-X	DTFA-Y	Mass	L2p-bkg	H1-bkg	Sample Name	Chamber Pressure
656	-3	-4	899142	-1662739	93397	Si-mesh/#1	4.30E-08
657	-4	-7	899142	-1662739	93397	Si-mesh/#1	4.30E-08
658	-4	-7	899142	-1662739	93397	Si-mesh/#1	4.30E-08
660	-3	-7	899142	-1662739	93397	Si-mesh/#1	4.30E-08
3523	10	-12	899142	-1662739	93397	Si-mesh/#1	4.30E-08
4556	-9	-13	899142	-1662739	93397	Si-mesh/#1	4.30E-08
3745	-2	-8	899142	-1662739	93397	Si-mesh/#1	4.30E-08
3199	-16	-5	899142	-1662739	93397	Si-mesh/#1	4.30E-08
2109	-6	-8	899142	-1662739	93397	Si-mesh/#1	4.30E-08
912	-15	-6	899142	-1662739	93397	Si-mesh/#1	4.30E-08
3153	-3	-16	899142	-1662739	93397	Si-mesh/#1	4.30E-08
2077	3	-18	899142	-1662739	93397	Si-mesh/#1	4.30E-08
1102	-5	-6	899142	-1662739	93397	Si-mesh/#1	4.30E-08
-412	-21	-1	899142	-1662739	93397	Si-mesh/#1	4.20E-08
624	1	-6	899142	-1662739	93397	Si-mesh/#1	4.20E-08
624	1	-7	899142	-1662739	93397	Si-mesh/#1	4.20E-08
624	1	-7	899142	-1662739	93397	Si-mesh/#1	4.20E-08
593	0	-7	899142	-1662739	93397	Si-mesh/#1	4.20E-08
-395	-25	-8	899142	-1662739	93397	Si-mesh/#1	4.20E-08
-495	-9	-8	899142	-1662739	93397	Si-mesh/#1	4.20E-08
-2264	1	-17	899142	-1662739	93397	Si-mesh/#1	4.20E-08
-1594	-5	-22	899142	-1662739	93397	Si-mesh/#1	4.10E-08
-3457	-12	-9	899142	-1662739	93397	Si-mesh/#1	4.20E-08
-3294	-8	-12	899142	-1662739	93397	Si-mesh/#1	4.20E-08
-3451	-4	-7	899142	-1662739	93397	Si-mesh/#1	4.20E-08
2636	-9	-4	899142	-1662739	93397	Si-mesh/#1	4.20E-08
4522	-10	-9	899142	-1662739	93397	Si-mesh/#1	4.20E-08
4055	-17	-4	899142	-1662739	93397	Si-mesh/#1	4.30E-08
592	-5	-5	899142	-1662739	93397	Si-mesh/#1	4.30E-08
592	-5	-5	899142	-1662739	93397	Si-mesh/#1	4.20E-08

592	-5	-5	899142	-1662739	93397	Si-mesh/#1	4.30E-08
592	-5	-5	899142	-1662739	93397	Si-mesh/#1	4.30E-08
3204	1	-12	899142	-1662739	93397	Si-mesh/#1	4.30E-08
2236	10	-10	899142	-1662739	93397	Si-mesh/#1	4.20E-08
1728	-8	2	899142	-1662739	93397	Si-mesh/#1	4.30E-08
3357	-7	-17	899142	-1662739	93397	Si-mesh/#1	4.30E-08
907	0	-5	899142	-1662739	93397	Si-mesh/#1	4.10E-08
-786	-20	6	899142	-1662739	93397	Si-mesh/#1	4.20E-08
-192	-10	-11	899142	-1662739	93397	Si-mesh/#1	4.20E-08
-2422	-1	-1	899142	-1662739	93397	Si-mesh/#1	4.20E-08
-2618	-6	3	899142	-1662739	93397	Si-mesh/#1	4.20E-08
-2894	-12	3	899142	-1662739	93397	Si-mesh/#1	4.20E-08
521	-1	-4	899142	-1662739	93397	Si-mesh/#1	4.10E-08
521	-1	-4	899142	-1662739	93397	Si-mesh/#1	4.10E-08
521	-2	-5	899142	-1662739	93397	Si-mesh/#1	4.10E-08
521	-1	-4	899142	-1662739	93397	Si-mesh/#1	4.10E-08
-180	0	8	899124	-1896732	93071	/#1	9.60E-09
-211	0	8	899124	-1896732	93071	/#1	9.70E-09
-245	1	9	899124	-1896732	93071	/#1	9.60E-09
-272	0	8	899124	-1896732	93071	/#1	9.80E-09
2071	-6	12	899124	-1896732	93071	/#1	9.60E-09
2008	-6	12	899124	-1896732	93071	/#1	9.70E-09
1962	-6	12	899124	-1896732	93071	/#1	9.60E-09
1932	-6	13	899124	-1896732	93071	/#1	9.90E-09
1872	-6	13	899124	-1896732	93071	/#1	9.80E-09

-5724	-14	-6	899124	-1896732	93071	/#1	1.00E-08
-5930	-6	-3	899124	-1896732	93071	/#1	9.90E-09
-6068	-6	-6	899124	-1896732	93071	/#1	9.70E-09
-6493	11	8	899124	-1896732	93071	/#1	9.90E-09
-6410	3	7	899124	-1896732	93071	/#1	9.80E-09
-298	-4	9	899124	-1896732	93071	/#1	9.90E-09
-342	-4	9	899124	-1896732	93071	/#1	9.70E-09
-208	-3	9	899124	-1896732	93071	/#1	9.80E-09
-187	-4	8	899124	-1896732	93071	/#1	9.70E-09
2083	3	14	899124	-1896732	93071	/#1	9.90E-09
2021	2	14	899124	-1896732	93071	/#1	9.90E-09
2028	3	12	899124	-1896732	93071	/#1	9.70E-09
1930	2	12	899124	-1896732	93071	/#1	9.70E-09
1637	1	16	899124	-1896732	93071	/#1	9.70E-09
-5087	2	12	899124	-1896732	93071	/#1	9.70E-09
-4773	1	8	899124	-1896732	93071	/#1	9.80E-09
-4548	-14	12	899124	-1896732	93071	/#1	9.70E-09
-2267	-1	11	899124	-1896732	93071	/#1	9.70E-09
-2138	4	7	899124	-1896732	93071	/#1	9.60E-09
-197	-4	10	899124	-1896732	93071	/#1	9.80E-09
-252	-4	9	899124	-1896732	93071	/#1	9.70E-09
-293	-4	9	899124	-1896732	93071	/#1	9.70E-09
-342	-4	9	899124	-1896732	93071	/#1	9.70E-09

-222	-14	7	899155	850190	87932	Al-mesh/#1	3.00E-08
-222	-14	8	899155	850190	87932	Al-mesh/#1	3.00E-08
-242	-15	1	899155	850190	87932	Al-mesh/#1	2.90E-08
-242	-15	0	899155	850190	87932	Al-mesh/#1	3.00E-08
3426	-23	-13	899155	850190	87932	Al-mesh/#1	2.90E-08
2865	-30	-1	899155	850190	87932	Al-mesh/#1	2.90E-08
5891	-28	-9	899155	850190	87932	Al-mesh/#1	2.90E-08
5818	-26	-5	899155	850190	87932	Al-mesh/#1	2.90E-08
4880	-20	8	899155	850190	87932	Al-mesh/#1	2.90E-08
3036	-36	-7	899155	850190	87932	Al-mesh/#1	2.90E-08
5424	-38	0	899155	850190	87932	Al-mesh/#1	3.00E-08
1381	-18	-1	899155	850190	87932	Al-mesh/#1	2.90E-08
1343	-20	1	899155	850190	87932	Al-mesh/#1	3.00E-08
2573	-17	1	899155	850190	87932	Al-mesh/#1	3.00E-08
2696	-18	2	899155	850190	87932	Al-mesh/#1	3.00E-08
5501	-12	2	899155	850190	87932	Al-mesh/#1	3.00E-08
5425	-13	1	899155	850190	87932	Al-mesh/#1	3.00E-08
2160	-16	-7	899155	850190	87932	Al-mesh/#1	3.00E-08
1802	-20	-5	899155	850190	87932	Al-mesh/#1	3.00E-08
2026	-20	-5	899155	850190	87932	Al-mesh/#1	3.00E-08
-336	-18	1	899155	850190	87932	Al-mesh/#1	3.00E-08
-355	-18	1	899155	850190	87932	Al-mesh/#1	2.90E-08
-96	-17	1	899155	850190	87932	Al-mesh/#1	2.90E-08
-68	-17	2	899155	850190	87932	Al-mesh/#1	2.90E-08
-419	-9	0	899152	860662	87430	Al-mesh/#1	8.30E-08
-370	-9	-1	899152	860662	87430	Al-mesh/#1	8.10E-08

-537	-7	-1	899152	860662	87430	Al-mesh/#1	8.00E-08
-560	-13	-2	899152	860662	87430	Al-mesh/#1	8.10E-08
-188	-12	8	899152	860662	87430	Al-mesh/#1	7.70E-08
3336	-8	-23	899152	860662	87430	Al-mesh/#1	7.70E-08
3572	-22	-14	899152	860662	87430	Al-mesh/#1	7.50E-08
5090	-20	-6	899152	860662	87430	Al-mesh/#1	7.40E-08
531	-15	0	899152	860662	87430	Al-mesh/#1	7.40E-08
1622	-2	-10	899152	860662	87430	Al-mesh/#1	7.10E-08
1139	-12	-2	899152	860662	87430	Al-mesh/#1	7.10E-08
2903	-14	2	899152	860662	87430	Al-mesh/#1	6.90E-08
5434	-9	0	899152	860662	87430	Al-mesh/#1	6.80E-08
5276	-11	-1	899152	860662	87430	Al-mesh/#1	6.70E-08
3783	-13	-4	899152	860662	87430	Al-mesh/#1	6.70E-08
3807	-11	-6	899152	860662	87430	Al-mesh/#1	6.60E-08
2872	-13	3	899152	860662	87430	Al-mesh/#1	6.50E-08
5612	-11	-1	899152	860662	87430	Al-mesh/#1	6.50E-08
-487	-14	-1	899152	860662	87430	Al-mesh/#1	6.30E-08
-510	-11	-1	899152	860662	87430	Al-mesh/#1	6.20E-08
-540	-13	-2	899152	860662	87430	Al-mesh/#1	6.10E-08
-644	-10	-1	899152	860662	87430	Al-mesh/#1	6.00E-08
-541	-10	-2	899152	860662	87430	Al-mesh/#1	6.00E-08

Comment

UWT-1b
large 2SE
UWT-1a
UWT-1a
UWT-1b
UWT-1b
UWT-1b
UWT-1a
UWT-1a
UWT-1a

UWT-1a
UWT-1a
UWT-1b
UWT-1b
large 2SE
UWT-1a
UWT-1b
UWT-1b
UWT-1a
UWT-1a

UWT-1a
UWT-1b
UWT-1a
UWT-1b
large 2SE
UWT-1a
UWT-1a
UWT-1a
UWT-1a
UWT-1b

UWT-1b, perpendicular
UWT-1b, perpendicular
UWT-1b, perpendicular
UWT-1b, perpendicular
UWT-1b, perpendicular

UWT-1b, parallel
UWT-1b, parallel
UWT-1b, parallel
UWT-1b, parallel
UWT-1b, parallel

UWT-1b, perpendicular
UWT-1b, perpendicular
UWT-1b, perpendicular
UWT-1b, perpendicular
UWT-1b, perpendicular
UWT-1b, parallel
larger OH (chlorite)
UWT-1b, parallel
UWT-1b, parallel
UWT-1b, parallel

UWT-1b, parallel
UWT-1b, parallel
UWT-1b, parallel
UWT-1b, parallel

UWT-1b, parallel
UWT-1b, parallel

chlorite

chlorite

chlorite

chlorite, larger OH

chlorite, larger OH

CALCULATIONS OF SERPENTINE-WATER FRACTIONATION

Calcite-water calibrations

A	B	C	*T* range (°C)
2.78	0	-2.89	0-500
2.75	0	-3.06	0-500
0	18.03	-32.42	10-40

Sample ID	**OM13-13**	**OM13-17A**	**OM13-14A**
Δ^{18}O(calcite-serpentine), ‰	*13.25*	*16.61*	*15.05*
T (°C)	*25*	*41*	*44*
T (K)	*298.15*	*314.15*	*317.15*
1000 ln α(Cc-water)	28.38	25.28	24.75
1000 ln α(Cc-water)	27.88	24.80	24.28
1000 ln α(Cc-water)	28.05	24.97	24.43
average/sample	**28.10**	**25.02**	**24.49**
2sd/sample	**0.52**	**0.48**	**0.48**
2SE/sample	**0.30**	**0.28**	**0.28**

Sample ID	**OM13-13**	**OM13-17A**	**OM13-14A**
Δ^{18}O(calcite-serpentine), ‰	*13.25*	*16.61*	*15.05*
T (°C)	*25*	*41*	*44*
T (K)	*298.15*	*314.15*	*317.15*
1000 ln α(Srp-water)	14.94	8.53	9.56
1000 ln α(Srp-water)	14.43	8.06	9.10
1000 ln α(Srp-water)	14.61	8.23	9.24
average/sample	**14.66**	**8.27**	**9.30**
2sd/sample	**0.51**	**0.47**	**0.47**
2SE/sample	**0.29**	**0.27**	**0.27**

Sample ID	**OM13-13**	**OM13-17A**	**OM13-14A**
Δ^{18}O(calcite-serpentine), ‰	*13.25*	*16.61*	*15.05*
T (°C)	*25*	*41*	*44*
T (K)	*298.15*	*314.15*	*317.15*
A-factor (Srp-water)	1.33	0.84	0.96
A-factor (Srp-water)	1.28	0.80	0.91
A-factor (Srp-water)	1.30	0.81	0.93

average/sample	**1.30**	**0.82**	**0.94**
2sd/sample	**0.05**	**0.05**	**0.05**
2SE/sample	**0.03**	**0.03**	**0.03**

Quartz-water calibrations

A	B	C	*T* range (°C)
4.48	-4.77	1.71	0-1200
3.34	0	-3.31	250-500
3.55	0	-2.57	195-573
3.38	0	-2.9	200-500
3.306	0	-2.71	180-550
2.91	0	0	250
3.05	0	-2.09	265-465
4.20	-3.30	0	*250-800*
4.28	-3.50	0	*0-800*
2.35	0.00	1.16	*400-750*

Sample ID	**OM09-12**	
Δ^{18}O(quartz-serpentine), ‰	*14.99*	*(measured by SIMS, see Tabl*
T (°C)	*100*	*(clumped isotope temperature*
T (K)	*373.15*	
1000 ln α(Qtz-water)	21.10	*Zheng, Y.F. (1993) Calculati*
1000 ln α(Qtz-water)	20.68	*Matsuhisa et al. (1979) Oxyg*
1000 ln α(Qtz-water)	22.93	*Friedman and O'Neil (1977)*
1000 ln α(Qtz-water)	21.37	*Clayton et al. (1972) Oxygen*
1000 ln α(Qtz-water)	21.03	*Ligang et al. (1989) Oxygen*
1000 ln α(Qtz-water)	20.90	*Pollington et al. (2016) Expe*
1000 ln α(Qtz-water)	19.81	*Matthews and Backinsale (19*
1000 ln α(Qtz-water)	21.32	*Sharp et al. (2016) A calibra*
1000 ln α(Qtz-water)	21.36	*Sharp et al. (2016) A calibra*
1000 ln α(Qtz-water)	18.04	*Hu and Clayton (2003) Oxyg*
average/sample	**20.85**	
2sd/sample	**2.51**	
2SE/sample	**0.79**	

Sample ID	**OM09-12**	
Δ^{18}O(quartz-serpentine), ‰	*14.99*	*(measured by SIMS, see Tabl*

T (°C)	*100*	*(clumped isotope temperature*
T (K)	*373.15*	
1000 ln α(Srp-water)	6.02	*Zheng, Y.F. (1993) Calculati*
1000 ln α(Srp-water)	5.60	*Matsuhisa et al. (1979) Oxyg*
1000 ln α(Srp-water)	7.82	*Friedman and O'Neil (1977)*
1000 ln α(Srp-water)	6.29	*Clayton et al. (1972) Oxygen*
1000 ln α(Srp-water)	5.95	*Ligang et al. (1989) Oxygen*
1000 ln α(Srp-water)	5.82	*Pollington et al. (2016) Expe*
1000 ln α(Srp-water)	4.75	*Matthews and Backinsale (19*
1000 ln α(Srp-water)	6.23	*Sharp et al. (2016) A calibra*
1000 ln α(Srp-water)	6.27	*Sharp et al. (2016) A calibra*
1000 ln α(Srp-water)	3.00	*Hu and Clayton (2003) Oxyg*
average/sample	**5.78**	
2sd/sample	**2.47**	
2SE/sample	**0.78**	

Sample ID	**OM09-12**	
$\Delta^{18}O$(quartz-serpentine), ‰	*14.99*	*(measured by SIMS, see Table*
T (°C)	*100*	*(clumped isotope temperature*
T (K)	*373.15*	
A-factor (Srp-water)	0.84	*Zheng, Y.F. (1993) Calculati*
A-factor (Srp-water)	0.78	*Matsuhisa et al. (1979) Oxyg*
A-factor (Srp-water)	1.09	*Friedman and O'Neil (1977)*
A-factor (Srp-water)	0.88	*Clayton et al. (1972) Oxygen*
A-factor (Srp-water)	0.83	*Ligang et al. (1989) Oxygen*
A-factor (Srp-water)	0.81	*Pollington et al. (2016) Expe*
A-factor (Srp-water)	0.66	*Matthews and Backinsale (19*
A-factor (Srp-water)	0.87	*Sharp et al. (2016) A calibra*
A-factor (Srp-water)	0.87	*Sharp et al. (2016) A calibra*
A-factor (Srp-water)	0.42	*Hu and Clayton (2003) Oxyg*
average/sample	**0.80**	
2sd/sample	**0.34**	
2SE/sample	**0.11**	

Talc-water calibrations

A	**B**	**C**	***T* range (°C)**
2.11	2.49	-8.24	

4.2	-7.04	2.14	0-1200

Sample ID	**OM10-02**	
Δ^{18}O(talc-serpentine), ‰	*3.85*	*(measured by SIMS, see Tabl*
T (°C)	*100*	*(clumped isotope temperature*
T (K)	*373.15*	
1000 ln α(Tlc-water)	13.59	*Savin and Lee (1988) Isotopi*
1000 ln α(Tlc-water)	13.44	*Zheng, Y.F. (1993) Calculati*
average/sample	**13.51**	
2sd/sample	**0.21**	
2SE/sample	**0.15**	

Sample ID	**OM10-02**	
Δ^{18}O(talc-serpentine), ‰	*3.85*	*(measured by SIMS, see Tabl*
T (°C)	*90*	*(clumped isotope temperature*
T (K)	*363.15*	
1000 ln α(Srp-water)	9.70	*Savin and Lee (1988) Isotopi*
1001 ln α(Srp-water)	9.55	*Zheng, Y.F. (1993) Calculati*
average/sample	**9.63**	
2sd/sample	**0.21**	
2SE/sample	**0.15**	

Sample ID	**OM10-02**	
Δ^{18}O(talc-serpentine), ‰	*3.85*	*(measured by SIMS, see Tabl*
T (°C)	*90*	*(clumped isotope temperature*
T (K)	*363.15*	
A-factor (Srp-water)	1.28	*Savin and Lee (1988) Isotopi*
A-factor (Srp-water)	1.26	*Zheng, Y.F. (1993) Calculati*
average/sample	**1.27**	
2sd/sample	**0.03**	
2SE/sample	**0.02**	

Summary

Sample ID	**T (°C)**	**T (K)**	**$1/T^2$ (K)**
OM13-13	25	298.2	1.12E-05

OM13-13	25	298.2	1.12E-05
OM13-13	25	298.2	1.12E-05
OM13-17A	41	314.2	1.01E-05
OM13-17A	41	314.2	1.01E-05
OM13-17A	41	314.2	1.01E-05
OM13-14A	44	317.2	9.94E-06
OM13-14A	44	317.2	9.94E-06
OM13-14A	44	317.2	9.94E-06
OM13-11	50	323.2	9.58E-06
OM13-11	50	323.2	9.58E-06
OM13-11	50	323.2	9.58E-06
OM09-12	100	373.2	7.18E-06
OM09-12	100	373.2	7.18E-06
OM09-12	100	373.2	7.18E-06
OM09-12	100	373.2	7.18E-06
OM09-12	100	373.2	7.18E-06
OM09-12	100	373.2	7.18E-06
OM09-12	100	373.2	7.18E-06
OM09-12	100	373.2	7.18E-06
OM09-12	100	373.2	7.18E-06
OM09-12	100	373.2	7.18E-06
OM10-02	100	373.2	7.18E-06
OM10-02	100	373.2	7.18E-06

Serpentine-water calibrations

A	B	C	Reference
1.51	0.00	-4.57	*Früh-Green et a*
3.99	-8.12	2.35	*Zheng (1993)*
1.56	0.00	-4.70	*Wenner and Tay*
0.58	8.90	-17.80	*Savin and Lee (*
3.49	0.00	-9.48	*Saccocia et al. (*
1.04	**0.00**	**0.00**	***This study***

T (°C)	0	10	25
T (K)	273	283	298

$10^6/T^2$	13.4	12.5	11.2
1000 ln α(Srp-water)	15.67	14.26	12.42
1000 ln α(Srp-water)	26.10	23.44	20.00
1000 ln α(Srp-water)	16.21	14.76	12.85
1000 ln α(Srp-water)	22.56	20.87	18.58
1000 ln α(Srp-water)	37.30	34.05	29.78
1000 ln α(Srp-water)	13.97	13.00	11.73

FACTORS

Type	**Reference**
experimental	*O'Neil et al. (1969) Oxygen isotope fractionation in div*
experimental	*Golyshev et al. (1981) Fractionation of stable isotopes*
experimental	*Kim and O´Neil (1997) Equilibrium and nonequilibrium*
OM13-11	
13.58	*(measured by SIMS, see Table 1)*
50	*(clumped isotope temperatures, see de Obeso and Kelen*
323.15	
23.73	*O'Neil et al. (1969) Oxygen isotope fractionation in div*
23.27	*Golyshev et al. (1981) Fractionation of stable isotopes*
23.37	*Kim and O´Neil (1997) Equilibrium and nonequilibrium*
23.46	
0.48	
0.28	
OM13-11	
13.58	*(measured by SIMS, see Table 1)*
50	*(clumped isotope temperatures, see de Obeso and Kelen*
323.15	
10.02	*O'Neil et al. (1969) Oxygen isotope fractionation in div*
9.57	*Golyshev et al. (1981) Fractionation of stable isotopes*
9.67	*Kim and O´Neil (1997) Equilibrium and nonequilibrium*
9.75	
0.47	
0.27	
OM13-11	
13.58	*(measured by SIMS, see Table 1)*
50	*(clumped isotope temperatures, see de Obeso and Kelen*
323.15	
1.05	*O'Neil et al. (1969) Oxygen isotope fractionation in div*
1.00	*Golyshev et al. (1981) Fractionation of stable isotopes*
1.01	*Kim and O´Neil (1997) Equilibrium and nonequilibrium*

1.02
0.05
0.03

Type	**Reference**
increment	*Zheng, Y.F. (1993) Calculation of oxygen isotope fracti*
experimental	*Matsuhisa et al. (1979) Oxygen isotopic fractionation i*
theoretical	*Friedman and O'Neil (1977) Compilation of stable isot*
experimental	*Clayton et al. (1972) Oxygen isotope exchange between*
experimental	*Ligang et al. (1989) Oxygen isotope fractionation in th*
experimental	*Pollington et al. (2016) Experimental calibration of sil*
experimental	*Matthews and Backinsale (1979) Oxygen isotope equili*
experimental	*Sharp et al. (2016) A calibration of the triple oxygen is*
experimental+empirical	*Sharp et al. (2016) A calibration of the triple oxygen is*
experimental	*Hu and Clayton (2003) Oxygen isotope salt effects at hi*

e 1)
s, see Kelemen et al., 2022)

on of oxygen isotope fractionation in anhydrous silicate minerals; Geochim. Cosm
en isotopic fractionation in the system quartz-albite-anorthite-water; Geochim. Co
Compilation of stable isotope fractionation factors of geochemical interest; U.S. G
isotope exchange between quartz and water; J. Geophys. Res. 77, 3057–3067
isotope fractionation in the quartz-water-salt system; Economic Geology 84(6), 16
rimental calibration of silicon and oxygen isotope fractionationsbetween quartz an
79) Oxygen isotope equilibration systematics between quartz and water; Am. Mine
tion of the triple oxygen isotope fractionation in the SiO_2–H_2O system and applic
tion of the triple oxygen isotope fractionation in the SiO_2–H_2O system and applic
en isotope salt effects at high pressure and high temperature and the calibration of

e 1)

s, see Kelemen et al., 2022)

on of oxygen isotope fractionation in anhydrous silicate minerals; Geochim. Cosm
en isotopic fractionation in the system quartz-albite-anorthite-water; Geochim. Co
Compilation of stable isotope fractionation factors of geochemical interest; U.S. G
isotope exchange between quartz and water; J. Geophys. Res. 77, 3057–3067
isotope fractionation in the quartz-water-salt system; Economic Geology 84(6), 16
rimental calibration of silicon and oxygen isotope fractionationsbetween quartz an
79) Oxygen isotope equilibration systematics between quartz and water; Am. Mine
tion of the triple oxygen isotope fractionation in the SiO_2–H_2O *system and applic*
tion of the triple oxygen isotope fractionation in the SiO_2–H_2O *system and applic*
en isotope salt effects at high pressure and high temperature and the calibration of

e 1)
s, see Kelemen et al., 2022)

on of oxygen isotope fractionation in anhydrous silicate minerals; Geochim. Cosm
en isotopic fractionation in the system quartz-albite-anorthite-water; Geochim. Co
Compilation of stable isotope fractionation factors of geochemical interest; U.S. G
isotope exchange between quartz and water; J. Geophys. Res. 77, 3057–3067
isotope fractionation in the quartz-water-salt system; Economic Geology 84(6), 16
rimental calibration of silicon and oxygen isotope fractionationsbetween quartz an
79) Oxygen isotope equilibration systematics between quartz and water; Am. Mine
tion of the triple oxygen isotope fractionation in the SiO_2–H_2O *system and applic*
tion of the triple oxygen isotope fractionation in the SiO_2–H_2O *system and applic*
en isotope salt effects at high pressure and high temperature and the calibration of

Type	**Reference**
theoretical	*Savin and Lee (1988) Isotopic studies of hydrous phyllo*

theoretical *Zheng, Y.F. (1993) Calculation of oxygen isotope fracti*

e 1)
s, see Kelemen et al., 2022)

c studies of hydrous phyllosilicates. In Hydrous Phyllosilicates (exclusive of micas)
on of oxygen isotope fractionation in hydroxyl-bearing silicates; Earth. Plan. Sci.

e 1)
s, see Kelemen et al., 2022)

c studies of hydrous phyllosilicates. In Hydrous Phyllosilicates (exclusive of micas)
on of oxygen isotope fractionation in hydroxyl-bearing silicates; Earth. Plan. Sci.

e 1)
s, see Kelemen et al., 2022)

c studies of hydrous phyllosilicates. In Hydrous Phyllosilicates (exclusive of micas)
on of oxygen isotope fractionation in hydroxyl-bearing silicates; Earth. Plan. Sci.

1000 ln α(Srp-water)	**1000 ln α(Srp-water) average**	**A-factor**	**A-factor average**	**2s**
14.94		1.33	1.3	0.05

14.43	14.7	1.28		
14.61		1.30		
8.53		0.84	0.8	0.05
8.06	8.3	0.80		
8.23		0.81		
9.56		0.96	0.9	0.05
9.10	9.3	0.91		
9.24		0.93		
10.02		1.05	1.0	0.05
9.57	9.8	1.00		
9.67		1.01		
6.02		0.84	0.8	0.34
5.60		0.78		
7.82		1.09		
6.29		0.88		
5.95	5.8	0.83		
5.82		0.81		
4.75		0.66		
6.23		0.87		
6.27		0.87		
3.00		0.42		
9.70	9.6	1.28	1.3	0.03
9.55		1.26		
			0.4	**2s**
			0.2	**2SE**

l. (1996)

lor (1971)

1988)

(2009)

30	40	50	60	70
303	313	323	333	343

10.9	10.2	9.6	9.0	8.5
11.86	10.83	9.89	9.03	8.25
18.98	17.11	15.43	13.93	12.57
12.27	11.21	10.24	9.36	8.55
17.87	16.54	15.30	14.14	13.06
28.50	26.11	23.94	21.96	20.16
11.34	10.63	9.98	9.39	8.85

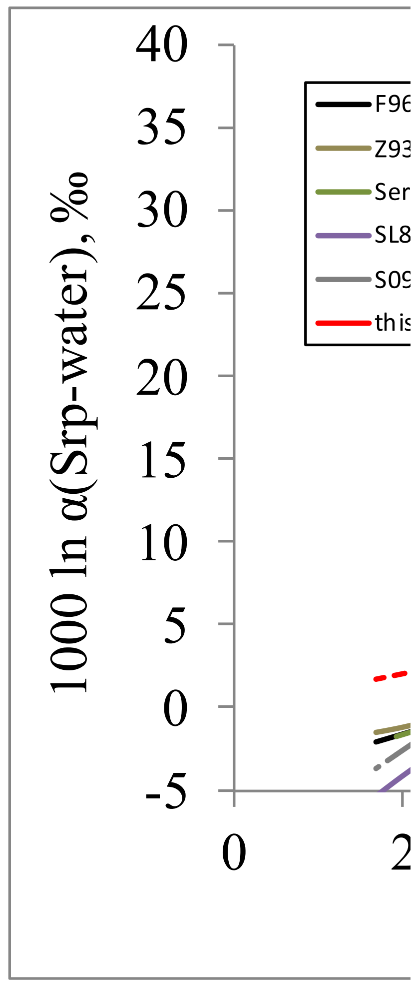

alent metal carbonates; J. Chem. Phys. 51(12), 5547–5558 NOTE: as i
in carbonate systems; Geochem. Int'l. 18, 85–99
n oxygen isotope effects in synthetic carbonates; Geoch. Cosmoc. Acta 6

ıen, 2018)

alent metal carbonates; J. Chem. Phys. 51(12), 5547–5558
in carbonate systems; Geochem. Int'l. 18, 85–99
n oxygen isotope effects in synthetic carbonates; Geoch. Cosmoc. Acta 6

ıen, 2018)

alent metal carbonates; J. Chem. Phys. 51(12), 5547–5558
in carbonate systems; Geochem. Int'l. 18, 85–99
n oxygen isotope effects in synthetic carbonates; Geoch. Cosmoc. Acta 6

ıen, 2018)

alent metal carbonates; J. Chem. Phys. 51(12), 5547–5558
in carbonate systems; Geochem. Int'l. 18, 85–99
n oxygen isotope effects in synthetic carbonates; Geoch. Cosmoc. Acta 6

ionation in anhydrous silicate minerals; Geochim. Cosmochim. Acta 57,
n the system quartz-albite-anorthite-water; Geochim. Cosmochim. Acta
ope fractionation factors of geochemical interest; U.S. Geol. Surv. Prof.
quartz and water; J. Geophys. Res. 77, 3057–3067
e quartz-water-salt system; Economic Geology 84(6), 1643–1650
icon and oxygen isotope fractionationsbetween quartz and water at 250
bration systematics between quartz and water; Am. Mineral. 64(1–2),23
otope fractionation in the SiO_2–H_2O system and applications to natura
otope fractionation in the SiO_2–H_2O system and applications to natura
igh pressure and high temperature and the calibration ofoxygen isotope

ochim. Acta 57, 1079–1091
smochim. Acta 43, 1131–1140
Geol. Surv. Prof. Paper 440–KK, Washington, D.C. (67 pp.)

43–1650
d water at 250 °C by in situ microanalysis ofexperimental products and
eral. 64(1–2),232–240
ations to natural samples; Geoch. Cosmoch. Acta 186, 105–119
ations to natural samples; Geoch. Cosmoch. Acta 186, 105–119
foxygen isotope geothermometers; Geoch. Cosmoch. Acta 67(17), 3227–

ochim. Acta 57, 1079–1091
smochim. Acta 43, 1131–1140
Geol. Surv. Prof. Paper 440–KK, Washington, D.C. (67 pp.)

43–1650
d water at 250 °C by in situ microanalysis ofexperimental products and
ral. 64(1–2),232–240
ations to natural samples; Geoch. Cosmoch. Acta 186, 105–119
ations to natural samples; Geoch. Cosmoch. Acta 186, 105–119
oxygen isotope geothermometers; Geoch. Cosmoch. Acta 67(17), 3227–

ochim. Acta 57, 1079–1091
smochim. Acta 43, 1131–1140
Geol. Surv. Prof. Paper 440–KK, Washington, D.C. (67 pp.)

43–1650
d water at 250 °C by in situ microanalysis ofexperimental products and
ral. 64(1–2),232–240
ations to natural samples; Geoch. Cosmoch. Acta 186, 105–119
ations to natural samples; Geoch. Cosmoch. Acta 186, 105–119
oxygen isotope geothermometers; Geoch. Cosmoch. Acta 67(17), 3227–

silicates. In Hydrous Phyllosilicates (exclusive of micas). S.W. Bailey E *ionation in hydroxyl-bearing silicates; Earth. Plan. Sci. Lett. 120, 247–*

. S.W. Bailey Ed. Rev. Mineral. 19, 189–233
Lett. 120, 247–263

. S.W. Bailey Ed. Rev. Mineral. 19, 189–233
Lett. 120, 247–263

. S.W. Bailey Ed. Rev. Mineral. 19, 189–233
Lett. 120, 247–263

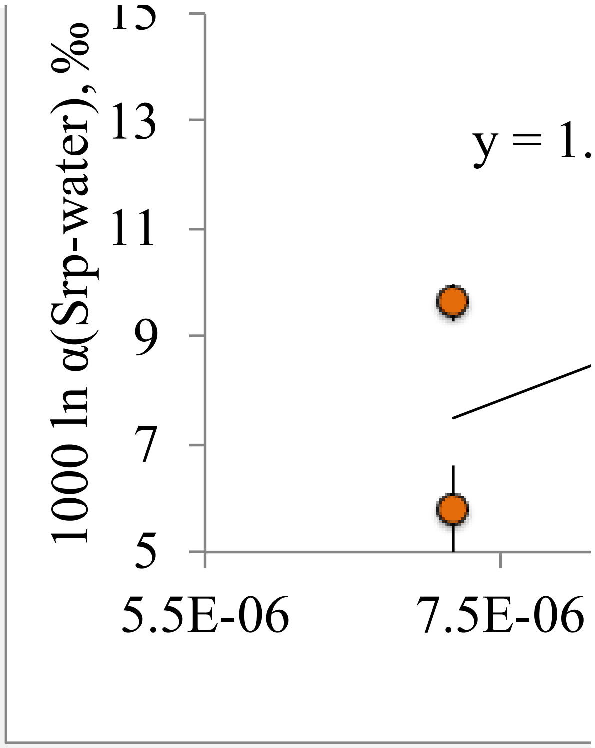

$1/T^2$ (K)
1.12E-05
1.01E-05
9.94E-06
9.58E-06
7.18E-06
7.18E-06

80	90	100	150	200	250
353	363	373	423	473	523

8.0	7.6	7.2	5.6	4.5	3.7
7.54	6.88	6.27	3.86	2.17	0.95
11.35	10.25	9.24	5.44	3.01	1.41
7.81	7.13	6.50	4.01	2.27	1.00
12.05	11.11	10.22	6.47	3.60	1.33
18.50	16.98	15.58	10.01	6.11	3.27
8.36	7.91	7.49	5.82	4.66	3.81

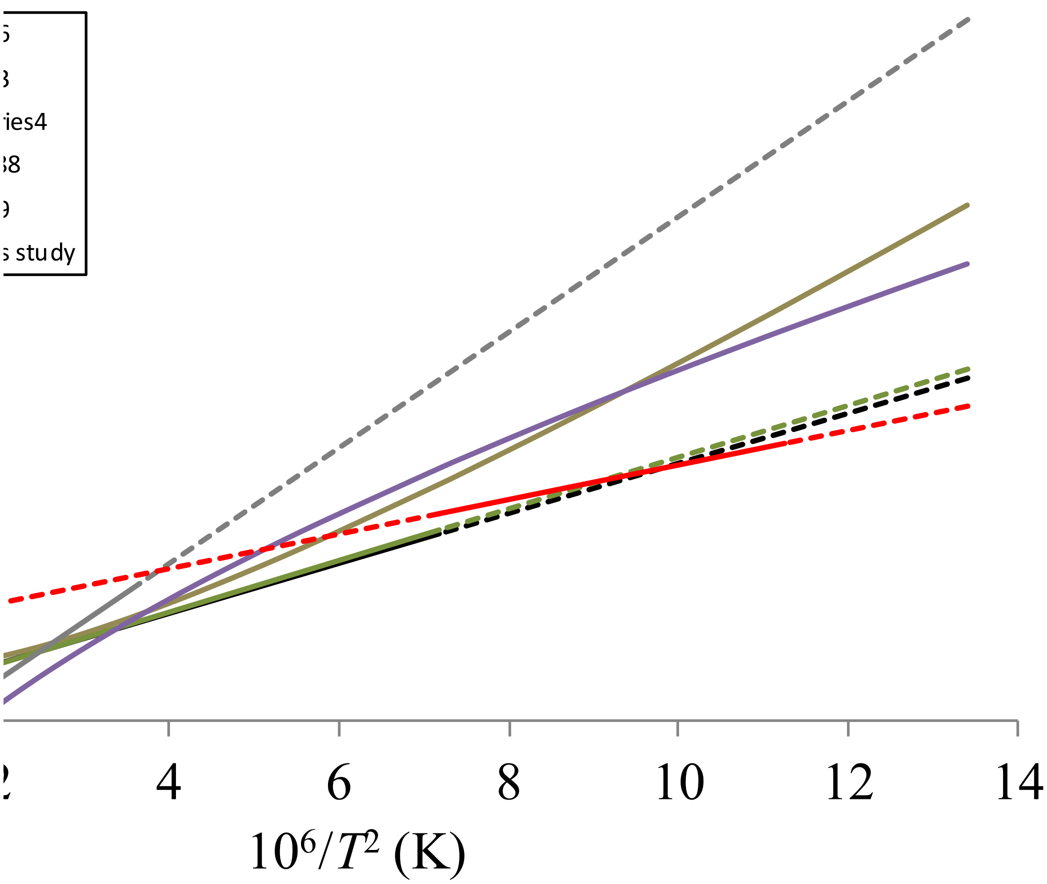

n Friedman and O´Neil (1977)

51, 3461–3475

51, 3461–3475

51, 3461–3475

51, 3461–3475

1079–1091
43, 1131–1140
Paper 440–KK, Washington, D.C. (67 pp.)

°C by in situ microanalysis ofexperimental products and application to zoned low δ
2–240
al samples; Geoch. Cosmoch. Acta 186, 105–119
al samples; Geoch. Cosmoch. Acta 186, 105–119
geothermometers; Geoch. Cosmoch. Acta 67(17), 3227–3246

application to zoned low δ^{30}Si quartzovergrowths; Chemical Geology 421, 127–

-3246

application to zoned low δ ^{30}Si quartzovergrowths; Chemical Geology 421, 127–

-3246

application to zoned low δ ^{30}Si quartzovergrowths; Chemical Geology 421, 127–

-3246

Ed. Rev. Mineral. 19, 189–233

-263

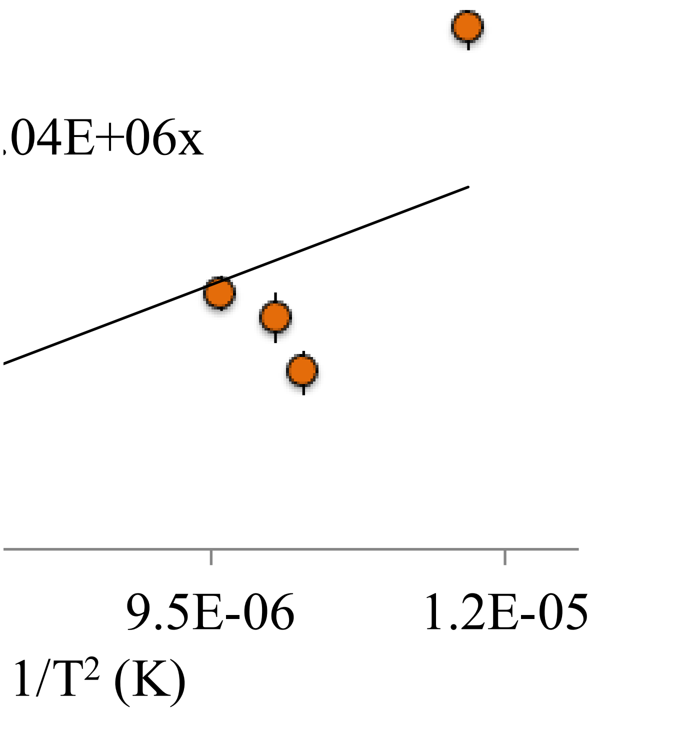

1000 ln α(Srp-water)	
average	2SE (Table 1)
14.66	0.40
8.27	0.41
9.30	0.47
9.75	0.33
5.78	0.83
9.63	0.34

300	350	400	450	500
573	623	673	723	773

3.0	2.6	2.2	1.9	1.7
0.03	-0.68	-1.24	-1.68	-2.04
0.33	-0.41	-0.91	-1.25	-1.48
0.05	-0.68	-1.26	-1.72	-2.09
-0.51	-2.02	-3.30	-4.38	-5.32
1.14	-0.49	-1.78	-2.81	-3.64
3.17	2.68	2.30	1.99	1.74

δ ^{30}Si quartzovergrowths; Chemical Geology 421, 127–142

-142

142

142

Früh-Green et al. (1996)
Zheng (1993)
Wenner and Taylor (1971)
Savin and Lee (1988)
Saccocia et al. (2009)
This study